PREPARATION AND CHARACTERIZATIONS OF DOPED ZnO (Fe, Ag, Mg) AND CO-DOPED ZnO (Fe, Ag) NANOPARTICLES FOR EFFICIENT PHOTOCATALYTIC DEGRADATION



A thesis submitted to the

BHARATHIDASAN UNIVERSITY, TIRUCHIRAPPALLI

in partial fulfillment of the requirements for the award of the Degree of

DOCTOR OF PHILOSOPHY IN PHYSICS

By

Mr. M. SENTHIL KUMAR, M.Sc., M.Phil., (Ref. No: 31498/Ph.D. K2/ Physics/Part-Time/ October 2015)

Research Supervisor

Dr. C. ARUNAGIRI, M.Sc., M.Phil., B.Ed., Ph.D.,



POST GRADUATE AND RESEARCH DEPARTMENT OF PHYSICS THANTHAI PERIYAR GOVERNMENT ARTS AND SCIENCE COLLEGE (AUTONOMOUS)

(Formerly Periyar E.V.R College)
(Affiliated to Bharathidasan University)
TIRUCHURAPPALLI – 620 023
TAMIL NADU, INDIA.

MARCH 2022



Dr. C. ARUNAGIRI, M. Sc., M. Phil., B. Ed., Ph.D.

Assistant Professor & Research Supervisor PG & Research Department of Physics

Thanthai Periyar Government Arts & Science College (Autonomous)

(Formerly Periya E.V.R College)

Tiruchappalli – 620 023, Tamil Nadu, India. Telephone: 0431-2420079; Fax: 0431-2332010

Mobile: +9196262-76982

Web: www.periyarevrcollege.ac.in

E-mail: pevrarunphyics@gmail.com; arunasuba03@yahoo.com

CERTIFICATE

This is to certify that the thesis entitled "PREPARATION AND CHARACTERIZATIONS OF DOPED ZnO (Fe, Ag, Mg) AND CO-DOPED ZnO (Fe, Ag) NANOPARTICLES FOR EFFICIENT PHOTOCATALYTIC DEGRADATION" is a record of independent research work done by Mr. M. SENTHIL KUMAR, under my supervision at the Thanthai Periyar Government Arts and Science College (Autonomous), Tiruchirappalli - 620 023 and that the thesis has not previously formed the basis for the award of any Degree, Diploma, Associateship, Fellowship or any other similar title.

Research Supervisor

DECLARATION

I, M. SENTHIL KUMAR hereby declare that the thesis entitled

"PREPARATION AND CHARACTERIZATIONS OF DOPED ZnO (Fe, Ag, Mg)

AND CO-DOPED ZnO (Fe, Ag) NANOPARTICLES FOR EFFICIENT

PHOTOCATALYTIC DEGRADATION" Submitted to Bharathidasan University,

Tiruchirappalli in partial fulfilment of the requirement for the award of the degree of

DOCTOR OF PHILOSOPHY IN PHYSICS is a original work done by me under

the supervision and guidance of Dr. C. ARUNAGIRI, M. Sc., M. Phil., B. Ed.,

Ph. D. Assistant Professor, Department of Physics, Thanthai Periyar Government

Arts and Science College (Autonomous), Trichy-23 and it has not formed the basis for

the award of any Degree/Diploma/Associateship/Fellowship or other similar title to

any candidate in any University.

Place:

Signature of the candidate

Date:



P.G. & RESEARCH DEPARTMENT OF PHYSICS THANTHAI PERIYAR ARTS AND SCIENCE COLLEGE (AUTONOMOUS) (Foremerly Periyar E.V.R College) TIRUCHIRAPPALLI-23

(Affiliated to Bharathidasan University, Tiruchirappalli-24)

CERTIFICATE OF PLAGIARISM CHECK

1.	Name of the Scholar	M. SENTHIL KUMAR
2.	Course of Study	Ph. D., PHYSICS (Part-Time)
3.	Title of the Thesis	PREPARATION AND CHARACTERIZATIONS OF DOPED ZnO (Fe, Ag, Mg) AND CO-DOPED ZnO (Fe, Ag) NANOPARTICLES FOR EFFICIENT PHOTOCATALYTIC DEGRADATION
4.	Name of the Research Supervisor	Dr. C. ARUNAGIRI
5	Department/Institution/Research center	PG & Research Department of Physics Thanthai Periyar Government Arts and Science College (Autonomous), Tiruchirappalli -23
6	Acceptable Maximum Limit	10%
7	Percentage of Similarity of Content Identified	2%
8	Software Used	Ouriginal
9	Date of Verification	28.02.2022

Report on plagiarism check, Item with % of similarity is attached

Signature of the candidate

Signature of the research supervisor



Document Information

Analyzed document M.Senthil Kumar (Physics).pdf (D129002206)

Submitted 2022-02-28T06:36:00.0000000

Submitted by Srinivasa ragavan S

Submitter email bdulib@gmail.com

Similarity 2%

Analysis address bdulib.bdu@analysis.urkund.com

Sources included in the report

Jour	ses included in the report		
W	URL: https://www.researchgate.net/publication/256831898_Synthesis_characterization_photocataly tic_and_antibacterial_activities_of_Ag-doped_ZnO_powders_modified_with_a_diblock_copolymer Fetched: 2019-12-11T17:40:02.4100000	<u></u>	2
W	URL: https://www.mdpi.com/2079-4991/11/4/1059/pdf Fetched: 2021-08-17T06:15:05.6870000	88	2
W	URL: https://www.researchgate.net/publication/315474018_Photocatalytic_efficiencies_of_Ni_Mn_F e_and_Ag_doped_ZnO_nanostructures_synthesized_by_hydrothermal_method_The_synergisticant agonistic_effect_between_ZnO_and_metals Fetched: 2020-03-10T06:17:16.8600000	88	2
W	URL: http://www.mater-rep.com/EN/10.11896/cldb.201906006 Fetched: 2020-12-02T13:12:25.9600000	88	1
W	URL: https://www.researchgate.net/publication/333084187_Investigations_on_the_ZnOand_Cr-doped_ZnO_powders Fetched: 2019-10-22T08:22:34.5470000		1
W	URL: https://link.springer.com/article/10.1007/s10853-020-05453-1 Fetched: 2021-12-09T10:40:15.5230000	88	3
W	URL: https://www.researchgate.net/publication/237016815_Photocatalytic_degradation_of_methyle ne_blue_with_Fe_doped_ZnS_nanoparticles Fetched: 2021-06-22T08:14:01.2030000	88	1
W	URL: https://www.researchgate.net/publication/265387230_The_effect_of_Ce4_incorporation_on_structural_morphological_and_photocatalytic_characters_of_ZnO_nanoparticles Fetched: 2020-09-14T08:24:45.9730000	88	3
W	URL: https://link.springer.com/article/10.1007/s10854-020-04968-2 Fetched: 2021-09-09T11:59:06.9600000	88	1
W	URL: https://iopscience.iop.org/article/10.1088/2632-959X/ab7a43 Fetched: 2020-05-14T10:10:07.2600000	88	1
W	URL: http://www.orientjchem.org/vol37no3/exploration-of-methylene-blue-degradation-over-zno-nanorods-mechanism-using-scavenging-reagents/ Fetched: 2021-07-22T11:49:20.7470000	88	1

ACKNOWLEDGEMENT

With everlasting memories

Words would not be sufficient to express my sincere gratitude I feel towards my research supervisor **Dr. C. Arunagiri, M. Sc. M. Phil., B. Ed., Ph. D., Assistant Professor, Department of Physics, Thanthai Periyar Government Arts and Science College (Autonomous), Trichy-23 for his instructive and informative suggestions, expert guidance, persistent attention, amiable treatment and manifold help bestowed throughout the progress of my research work. In real words, he acted more than a teacher towards me as part of family and paved path for the successful completion of my research programme.**

I express my profound thanks to **Dr. J. Suganthi,** Principal, Thanthai Periyar Government Arts and Science College (Autonomous), Trichy-23 for having permitted me to carryout Ph.D. Research Programme in this esteemed institution.

I express my thanks to **Dr. T. Balakrishnan**, Head of the Department of Physics, Thanthai Periyar Government Arts and Science College (Autonomous), Trichy-23 for his constant encouragement and support during the course of study.

I am obliged to express my sincere gratitude to **Doctoral committee members** of **Dr. A. Sakthivelu and Dr. S. Muruganantham,** Assistant Professor of Physics, Thanthai Periyar Government Arts and Science College (Autonomous), Trichy-23 and National College (Autonomous), Trichy-01 for his consent and motivation in my academic career.

I sincerely thank to all the **faculty members of Physics**, Thanthai Periyar Government Arts and Science College (Autonomous), Trichy for their kind cooperation during the period of my research study

I sincerely thank to all the faculty members of Physics, Government Arts and Science College, Ariyalur for their kind co-operation during the period of my research study.

My warm thanks to Dr. N. Vetrivelan, Principal, Prof. G. Ravi, Vice-Principal, Dr. P. Senthilnathan, Head of the Department of Tamil, Dr. D. Mahesh, Director of Management Studies, Dr. R. Kumaresan Deaen-Research and other Faculties, Srinivasan College of Arts & Science, Perambalur for their kind co-operation during the period of my research study.

I express my thanks to the **Librarian**, Periyar University, Salem, Bharathiar University, Coimbatore, Bharthidasan University, Tiruchirappalli, University of Madras, Chennai, IIT Madras, Chennai, Alagappa University, Karaikudi.

I express my thanks to my Co-Research Scholars Mr. Karthikeyan, Ms. Anitha, Mr. Selvakumar, Mr. Kabilan for their support and help during my research work.

I would like to express my gratitude to my Father Theivathiru.

M. Murugesan, Mother Smt. M. Pappathi, Wife Smt. Uma Senthil Kumar,

My Lovable Kids and also my thanks to my brother Mr. M. Karthikeyan, for their understanding, help and support. I also extend my deep love and affection to my friends who have been very co-operative during the period of my study.

The acknowledgement made are surely incomplete as there have been a number of invisible hands which have been extending motivation, encouragement support and care for the completion of the research project my special thanks to everyone.

Finally, I thank the Almighty who made this everything a reality.

M. SENTHIL KUMAR

CONTENTS

S.No		Title	Page Number
	i)	List of Tables	vi
	ii)	List of Figures	vii
	iii)	List of Abbreviations	xii
	iv)	List of Symbols	xiii
	v)	Abstract	xiv
1		INTRODUCTION TO METAL DOPED ZnO NANOPARTICLES AND LITERATURE REVIEW	
	1.1	Introduction	1
	1.2	Zinc Oxide	3
		1.2.1 Crystal Structure	3
		1.2.2 Electronic Structure	5
	1.3	Applications of ZnO	5
		1.3.1 Photocatalytic degradation	5
		1.3.2 Mechanism of Degradation	6
	1.4	Literature Survey	8
	1.5	Objectives of the Present Work	18
		References	20
2		PREPARATION AND CHARACTERIZATION TECHNIQUES	
	2.1	Introduction	23
	2.2	Chemical Methods	24
		2.2.1 Chemical Vapour Deposition (CVD)	24
		2.2.2 Sol-gel Method	25
		2.2.3 Solvothermal Method	26
		2.2.4 Hydrothermal Method	26
		2.2.5 Co-precipitation Method	27
	2.3	Characterization Techniques	29
		2.3.1 X – Ray Diffraction Techniques	29

		2.3.2 Scanning Electron Microscope (SEM)	31
		2.3.3 Energy dispersive X-ray spectroscopy (EDX)	34
		2.3.4 Fourier transforms infra-red spectroscopy (FT-IR)	35
		2.3.5 UV-Visible Double Beam Spectrophotometer	37
		2.3.6 I-V Characteristics	39
		2.3.6.1Temperature dependence of conductivity	39
		2.3.7 Photocatalytic Activity Setup	40
		References	42
3	EI	FFICIENT PHOTOCATALYTIC DEGRADATION OF ORGANIC DYES USING Fe-DOPED ZnO NANOPARTICLES	
	3.1	Introduction	43
	3.2	Synthesis of pure ZnO, Fe-Doped ZnO (ZnO-Fex, $X \approx 0.05, 0.075$ and 0.1%) Nanoparticles	45
		3.2.1 Materials	45
		3.2.2 Preparation of pure ZnO Nanoparticles	46
		3.2.3 Preparation of Fe-doped ZnO (ZnO-Fex, $x \approx 0.05, 0.075$ and 0.1%) Nanoparticles	46
	3.3	Characterization Techniques	47
		3.3.1 XRD Analysis	48
		3.3.2 SEM Analysis	51
		3.3.3 EDX Analysis	51
		3.3.4 UV-Visible Absorption Spectra	53
		3.3.5 FT-IR Analysis	55
		3.3.6 I-V Characteristics	56
	3.4	Photocatalytic Degradation of MB and MO	58
		3.4.1 Influence of Ph	58
		3.4.2 Influence of catalyst concentration	60
		3.4.3 Influence of UV irradiation time of MB	60
		3.4.4 Influence of UV irradiation time of MO	62
	3.5	Conclusion	64
		References	65

4	EFFICIENT PHOTOCATALYTIC DEGRADATION OF 4 ORGANIC DYES WITH Ag DOPED ZnO NANOPARTICLES UNDER UV LIGHT IRRADIATION				
	4.1	Introduction	69		
	4.2	Synthesis of pure ZnO, Ag-Doped ZnO (ZnO - Agx,	71		
		$x \approx 0.05, 0.075$ and 0.1%) Nanoparticles			
		4.2.1 Materials	71		
		4.2.2 Preparation of pure ZnO Nanoparticles	71		
		4.2.3 Preparation of Ag-doped ZnO (ZnO - Agx, $x \approx 0.05$, 0.075 and 0.1%) Nanoparticles	72		
	4.3	Structural Optical and Electrical Properties of pure and Ag -Doped ZnO Nanoparticl	72		
		4.3.1 XRD Analysis	72		
		4.3.2 SEM with EDX Analysis	75		
		4.3.3 UV-Visible Absorption Spectra	78		
		4.3.4 FT-IR Analysis	79		
		4.3.5 I-V Characteristics	80		
		4.3.6 Photocatalytic Activity	81		
		4.3.6.1 Optimized Factors to the Catalytic Activity	81		
		4.3.6.2 Impact of UV irradiation on Degradation of MB and MO	82		
	4.4	Conclusion	86		
		References	87		
5		EPARATION AND CHARACTERIZATION OF PURE AND Mg- DOPED ZnO NANOPARTICLES FOR PHOTOCATALYTIC DEGRADATION			
	5.1	Introduction	90		
	5.2	Synthesis of pure ZnO, Mg-Doped ZnO (ZnO - Mgx,	91		
		$x \approx 0.05$, 0.075 and 0.1%) Nanoparticles			
		5.2.1 Materials	91		
		5.2.2 Preparation of pure ZnO Nanoparticles	92		
		5.2.3 Preparation of Mg-doped ZnO (ZnO - Mgx, $x \approx 0.05, 0.075$ and 0.1%) Nanoparticles	92		

	5.3	Results and Discussion	93
		5.3.1 XRD Analysis	93
		5.3.2 SEM Analysis	95
		5.3.3 EDX Analysis	97
		5.3.4 UV-Visible Absorption Spectra	98
		5.3.5 FT-IR Analysis	99
		5.3.6 I-V Characteristics	100
		5.3.7 Photocatalytic Activity	102
		5.3.7.1 Optimized Factors to the Catalytic Activity	102
		5.3.7.2 Impact of UV irradiation on Degradation of MB and MO	103
	5.4	Conclusion	107
		References	108
6		HIGHLY ENHANCED PHOTOCATALYTIC DEGRADATION OF CO-DOPED ZnO (Fe,Ag) NANOPARTICLES	
	6.1	Introduction	111
	6.2	Synthesis of pure ZnO, Co-Doped ZnO (Fe,Ag) (ZnO-Fe-Agx, $n \approx 0.075\%$, $x \approx 0.01$, 0.02 And 0.03%) Nanoparticles	114
		6.2.1 Materials	114
		6.2.2 Preparation of pure ZnO Nanoparticles	114
		6.2.3 Preparation of co-doped ZnO (Fe,Ag) (ZnO-Fen-Agx, n \approx 0.075%, x \approx 0.01, 0.02 and 0.03%) Nanoparticles	114
	6.3	Structural, Optical and Electrical Properties of pure ZnO and Co-Doped ZnO(Fe,Ag) Nanoparticles	116
		6.3.1 XRD Analysis	116
		6.3.2 SEM Analysis	118
		6.3.3 EDX Analysis	119
		6.3.4 UV-Vis Absorption Analysis	121
		6.3.5 FT-IR Analysis	123
		6.3.6 I-V Characteristics	124
		6.3.7 Photocatalytic Activity	126

	6.3.7.1 Influence of optimized parameters	126
	6.3.7.2 Photocatalytic performance of MB	128
6.4	Photocatalytic performance of MO	130
6.5	Degradation Mechanism of MB and MO	132
6.6	Conclusion	134
	References	135
SUM	IMARY AND SUGGESTIONS FOR FUTURE WORK	
	Summary	140
	Suggestion for Future Work	144
	LIST OF PUBLICATIONS	

LIST OF TABLES

S. No.	Table No.	Title	Page No.
01	1.1	Important Parameters of ZnO	3
02	3.1	The Lattice Parameters & average crystallite size of ZnO $-\operatorname{Fe}_x$ nanoparticles	49
03	4.1	Lattice parameters and crystallite size of Pure and Agdoped ZnO nanoparticles.	75
04	5.1	Lattice parameters and crystallite size of Pure and Mgdoped ZnO nanoparticles.	95
05	6.1	The structural parameters for Pure and AFZ nanoparticles	118
06	6.2	Phase Composition of Pure and AFZ nanoparticles	121

LIST OF FIGURES

S. No.	Figure No.	Title	Page No.
01	1.1	Molecular structure of Methylene blue dye	2
02	1.2	Crystal structure of ZnO (a) Wurtzite and (b) cubic zincblende	4
03	1.3	Various crystal planes of the ZnO hexagonal structure	4
04	1.4	Photo-degradation mechanism of the MB and MO dye in presence of (Ag, Fe) co-doped ZnO nanocomposites	7
05	2.1	Schematic diagram of Top-down and bottom-up approaches	23
06	2.2	The typical Teflon-lined autoclave apparatus	27
07	2.3	Schematic diagram of XRD apparatus and (b) photograph of XRD apparatus.	30
08	2.4	Schematic diagram of a SEM and (b) photograph image of a SEM-JEOL JS-6390 apparatus set up	33
09	2.5	Principle of EDX analysis	35
10	2.6	Schematic diagram of a FT-IR and (b) photograph image of a FT-IR JASCO 410 apparatus set up.	36
11	2.7	Schematic diagram of UV-Visible analysis (b) Photograph image of a UV2700 apparatus set up.	38
12	2.8	Photograph of a keithley electrometer 2400 model	40
13	2.9	Photograph of a photodegradation experimental setup	41
14	3.1	Flow chart depicting the preparation of the pure and Fe-doped ZnO nanoparticles	47
15	3.2	XRD patterns of (a) Pure ZnO and Fe-doped ZnO nanoparticles (b) Fe concentration dependent shift in primary diffraction peaks.	50

16	3.3	SEM images of (a) Pure ZnO (b) 0.05, (c) 0.075 and (d) 0.1 mol.% Fe-doped ZnO nanoparticles	52
17	3.4	EDS images of (a) Pure ZnO (b) 0.05, (c) 0.075 and (d) 0.1 mol.% Fe-doped ZnO nanoparticles	53
18	3.5	UV-Vis absorbance spectra of (a) Pure ZnO (b) 0.05, (c) 0.075 and (d) 0.1 mol.% Fe-doped ZnO nanoparticles	54
19	3.6	FT-IR spectra of (a) Pure ZnO and (b) 0.1% Fe-doped ZnO nanoparticles	55
20	3.7	I-V characteristics of (a) Pure ZnO and (b) 0.1% Fe-doped ZnO nanoparticles	57
21	3.8	(a) Influence of pH and (b) catalyst concentration on the photodegradation of MB and MO	59
22	3.9	UV-Vis absorption spectra of MB dye degradation of (a) Pure ZnO (b) 0.05, (c) 0.075 and (d) 0.1 mol.% Fe-doped ZnO nanoparticles and (e) influence on the photodegradation of MB.	61
23	3.10	UV–Vis absorption spectra of MO dye degradation of (a) Pure ZnO, (b) 0.05, (c) 0.075 and (d) 0.1 mol.% Fe-doped ZnO nanoparticles and (e) influence on the photodegradation of MO.	63
24	4.1	(a) XRD patterns of un-doped and Ag-doped ZnO nanoparticles(b) expanded view of XRD patterns shift.	73
25	4.2	SEM images of (a) Pure ZnO (b) 0.05, (c) 0.075 and (d) 0.1 mol.% Ag-doped ZnO nanoparticles	76
26	4.3	EDX images of (a) pure ZnO (b) 0.1 mol.% Ag-doped ZnO nanoparticles	77
27	4.4	UV-Vis absorbance spectra of (a) Pure ZnO (b) 0.05, (c) 0.075 and (d) 0.1 mol.% Ag-doped ZnO nanoparticles	78

284.5FT-IR spectra of (a) Pure ZnO and (b) 0.1% Ag-doped ZnO nanoparticles79294.6I-V characteristics of (a) Pure ZnO and (b) 0.1% Ag-doped ZnO nanoparticles80304.7MB dye degradation of (a) Pure (b) 0.05, (c) 0.075, (d) 0.1 mol.% Ag-doped ZnO nanoparticles (MB dye:10 ppm, catalyst dose:10 mg, pH=6) and (e) effect of irradiation time of UV on MB photo-degradation85314.8MO dye degradation of (a) Pure (b) 0.05, (c) 0.075, (d) 0.1 mol.% Ag-doped ZnO nanoparticles (MB dye:10 ppm, catalyst dose:10 mg, pH=6) and (e) effect of irradiation time of UV on MO photo-degradation94325.1(a) XRD patterns of pure and Mg-doped ZnO nanoparticles (b) expanded view of XRD patterns shift.94335.2SEM images of (a) Pure ZnO (b) 0.05, (c) 0.075 and (d) 0.1 mol.% Mg-doped ZnO nanoparticles96345.3EDX images of (a) no ZnO (b) 0.1 mol.% Mg-doped ZnO nanoparticles97355.4UV-Vis absorbance spectra of (a) Pure ZnO (b) 0.05, (c) 0.075 and (d) 0.1 mol.% Mg-doped ZnO nanoparticles99365.5FT-IR spectra of (a) Pure ZnO and (b) 0.1% Mg-doped ZnO nanoparticles100375.6I-V characteristics of (a) Pure ZnO and (b) 0.1% Mg-doped ZnO nanoparticles101				
ZnO nanoparticles 30 4.7 MB dye degradation of (a) Pure (b) 0.05, (c) 0.075, (d) 0.1 83 mol.% Ag-doped ZnO nanoparticles (MB dye:10 ppm, catalyst dose:10 mg, pH=6) and (e) effect of irradiation time of UV on MB photo-degradation 31 4.8 MO dye degradation of (a) Pure (b) 0.05, (c) 0.075, (d) 0.1 85 mol.% Ag-doped ZnO nanoparticles (MB dye:10 ppm, catalyst dose:10 mg, pH=6) and (e) effect of irradiation time of UV on MO photo-degradation 32 5.1 (a) XRD patterns of pure and Mg-doped ZnO nanoparticles (b) 94 expanded view of XRD patterns shift. 33 5.2 SEM images of (a) Pure ZnO (b) 0.05, (c) 0.075 and (d) 0.1 96 mol.% Mg-doped ZnO nanoparticles 34 5.3 EDX images of (a) no ZnO (b) 0.1 mol.% Mg-doped ZnO 97 nanoparticles 35 5.4 UV-Vis absorbance spectra of (a) Pure ZnO (b) 0.05, (c) 0.075 99 and (d) 0.1 mol.% Mg-doped ZnO nanoparticles 36 5.5 FT-IR spectra of (a) Pure ZnO and (b) 0.1% Mg-doped ZnO 100 nanoparticles	28	4.5		79
mol.% Ag-doped ZnO nanoparticles (MB dye:10 ppm, catalyst dose:10 mg, pH=6) and (e) effect of irradiation time of UV on MB photo-degradation 31	29	4.6		80
mol.% Ag-doped ZnO nanoparticles (MB dye:10 ppm, catalyst dose:10 mg, pH=6) and (e) effect of irradiation time of UV on MO photo-degradation 32 5.1 (a) XRD patterns of pure and Mg-doped ZnO nanoparticles (b) 94 expanded view of XRD patterns shift. 33 5.2 SEM images of (a) Pure ZnO (b) 0.05, (c) 0.075 and (d) 0.1 96 mol.% Mg-doped ZnO nanoparticles 34 5.3 EDX images of (a) no ZnO (b) 0.1 mol.% Mg-doped ZnO 97 nanoparticles 35 5.4 UV-Vis absorbance spectra of (a) Pure ZnO (b) 0.05, (c) 0.075 99 and (d) 0.1 mol.% Mg-doped ZnO nanoparticles 36 5.5 FT-IR spectra of (a) Pure ZnO and (b) 0.1% Mg-doped ZnO 100 nanoparticles 37 5.6 I-V characteristics of (a) Pure ZnO and (b) 0.1% Mg-doped 101	30	4.7	mol.% Ag-doped ZnO nanoparticles (MB dye:10 ppm, catalyst dose:10 mg, pH=6) and (e) effect of irradiation time of UV on	83
expanded view of XRD patterns shift. 33 5.2 SEM images of (a) Pure ZnO (b) 0.05, (c) 0.075 and (d) 0.1 96 mol.% Mg-doped ZnO nanoparticles 34 5.3 EDX images of (a) no ZnO (b) 0.1 mol.% Mg-doped ZnO 97 nanoparticles 35 5.4 UV-Vis absorbance spectra of (a) Pure ZnO (b) 0.05, (c) 0.075 99 and (d) 0.1 mol.% Mg-doped ZnO nanoparticles 36 5.5 FT-IR spectra of (a) Pure ZnO and (b) 0.1% Mg-doped ZnO 100 nanoparticles 37 5.6 I-V characteristics of (a) Pure ZnO and (b) 0.1% Mg-doped 101	31	4.8	mol.% Ag-doped ZnO nanoparticles (MB dye:10 ppm, catalyst dose:10 mg, pH=6) and (e) effect of irradiation time of	85
mol.% Mg-doped ZnO nanoparticles 34 5.3 EDX images of (a) no ZnO (b) 0.1 mol.% Mg-doped ZnO 97 nanoparticles 35 5.4 UV-Vis absorbance spectra of (a) Pure ZnO (b) 0.05, (c) 0.075 99 and (d) 0.1 mol.% Mg-doped ZnO nanoparticles 36 5.5 FT-IR spectra of (a) Pure ZnO and (b) 0.1% Mg-doped ZnO 100 nanoparticles 37 5.6 I-V characteristics of (a) Pure ZnO and (b) 0.1% Mg-doped 101	32	5.1		94
nanoparticles 35 5.4 UV-Vis absorbance spectra of (a) Pure ZnO (b) 0.05, (c) 0.075 99 and (d) 0.1 mol.% Mg-doped ZnO nanoparticles 36 5.5 FT-IR spectra of (a) Pure ZnO and (b) 0.1% Mg-doped ZnO 100 nanoparticles 37 5.6 I-V characteristics of (a) Pure ZnO and (b) 0.1% Mg-doped 101	33	5.2		96
and (d) 0.1 mol.% Mg-doped ZnO nanoparticles 36 5.5 FT-IR spectra of (a) Pure ZnO and (b) 0.1% Mg-doped ZnO nanoparticles 37 5.6 I-V characteristics of (a) Pure ZnO and (b) 0.1% Mg-doped 101	34	5.3		97
nanoparticles 37 5.6 I-V characteristics of (a) Pure ZnO and (b) 0.1% Mg-doped 101	35	5.4		99
	36	5.5		100
	37	5.6		101

38	5.7	MB dye degradation of (a) Pure (b) 0.05, (c) 0.075, (d) 0.1 mol.% Mg-doped ZnO nanoparticles (MB dye:10 ppm, catalyst dose:10 mg, pH=6) and (e) effect of irradiation time of UV on MB photo-degradation	104
39	5.8	MO dye degradation of (a) Pure (b) 0.05, (c) 0.075, (d) 0.1 mol.% Mg-doped ZnO nanoparticles (MB dye:10 ppm, catalyst dose:10 mg, pH=6) and (e) effect of irradiation time of UV on MO photo-degradation	106
40	6.1	Schematic diagram of synthesizing the pure and co-doped (Fe,Ag) ZnO nanoparticles	115
41	6.2	(a) XRD patterns of pure ZnO and AFZ-1, AFZ-2 and AFZ-3 nanoparticles (b) expanded view of primary XRD patterns	117
42	6.3	SEM Images of (a) Pure ZnO (b) AFZ-1, (c) AFZ-2 and (d) AFZ-3 nanoparticles	119
43	6.4	EDX Images of (a) Pure ZnO (b) AFZ-1, (c) AFZ-2 and (d) AFZ-3 nanoparticles	120
44	6.5	(a) UV-Vis Absorbance Spectra of pure and AFZ Photocatalysts, (b) The Plot of (αhν)2 vs. Photoenergy	122
45	6.6	FT-IR spectra of (a) Pure ZnO and (b) AFZ-3 nanoparticles	123
46	6.7	I-V characteristics of (a) Pure ZnO and (b) AFZ-3 nanoparticles	125
47	6.8	(a) Influence of pH and (b) catalyst concentration and (c) dye PPM on the photodegradation of MB and MO	127
48	6.9	UV-visible spectra of MB (dye conc.=10 ppm, pH = 6 and catalyst dosage =20 mg) at different time intervals in presence of (a) Pure ZnO (b) AFZ-1, (c) AFZ-2, and (d) AFZ-3 nanoparticles and (e) comparison of photocatalytic efficiency of MB	129

49	6.10	UV-visible Spectra of MO (dye conc.=10 ppm, pH = 6 and catalyst dosage =20 mg) at Different Time Intervals in Presence of (a) Pure ZnO (b) AFZ-1, (c) AFZ-2, and (d) AFZ-3 nanoparticles and (e) Comparison of Photocatalytic Efficiency of MO	131
50	6.11	Photodegradation mechanism of the MB and MO dye in the presence AFZ photocatalysts	133

ABBREVIATIONS USED

ZnO - Zinc Oxide

Fe - Iron

Ag - Silver

MB - Methyl Blue

DDW - Double Distilled Water

MO - Methyl Orange

UV - Ultra Violet Light

CB - Conduction Band

VB - Valance Band

XRD - X-Ray Diffraction

SEM - Scanning Electron Microscope

TEM - Transmission Electron Microscope

FESEM - Field Emission Scanning Electron Microscope

HRTEM - High Resolution Transmission Electron Microscope

XPS - X-ray Photoelectron Spectroscopy

EDS or EDX - Electron Dispersive X-ray Spectroscopy

FT-IR - Fourier Transform Infrared Spectroscopy

PL - Photo Luminescence Spectroscopy

PVD - Physical Vapour Deposition

CVD - Chemical Vapour Deposition

AFZ-1 - Silver (Ag) Co-doped Iorn (Fe) Zinc (ZnO) (0.1%)

AFZ-2 - Silver (Ag) Co-doped Iorn (Fe) Zinc (ZnO) (0.2%)

AFZ-3 - Silver (Ag) Co-doped Iorn (Fe) Zinc (ZnO) (0.3%)

JCPDS - Join Committee on Powder Diffraction Standards

SYMBOLS USED

Symbol	Meaning	Unit
λ	Wavelength	μm or Å
A	Optical absorption coefficient	cm ⁻¹
β	Full width half maximum	Degree
t	Thickness	Nm
D	Crystalline size	Nm
R	Reflectance	Degree
E_{g}	Energy band gap	electron volt (eV)
ρ	Resistivity	'ncm
k	Boltzmann Constant	JK ⁻¹
T	Temperature	K
n	Refractive Index	No unit

ABSTRACT

ZnO based photocatalyst is a promising solution for efficient photocatalytic degradation of organic dyes. ZnO nanoparticles have been prepared using zinc nitrate hexahydrate and sodium hydroxide as precursor by co-precipitation method. Fe, Ag, Mg-doped ZnO nanoparticles were synthesized by wet-chemical based co-precipitation method with different doping concentrations such as 0.05, 0.075 & 0.1 mol.%., respectively. For Ag co-doped Fe-ZnO nanoparticles were synthesized using various concentrations Ag (0.01, 0.02, and 0.03%) of silver nitrate hexahydrate used as a source material.

All the prepared nanoparticles are annealed at 450 °C for 1h. The prepared nanoparticles were characterized by X-ray diffraction (XRD), scanning electron microscopy (SEM) with energy-dispersive X-ray analysis (EDX), UV–Visible spectra (UV-Vis), Fourier Transform Infrared (FT-IR) spectra and I-V analysis. XRD patterns reveal that all the crystal phases are hexagonal wurtzite structure of ZnO. It also clearly indicates that the primary peak position shifted towards to higher angles. This minor shift is mainly happened due to doped (Fe³⁺, Ag⁺ & Mg²⁺,) ions substitute for ZnO matrix cause the reduction in average crystallite size and lattice parameters.

The SEM image of synthesized samples indicates that the dopant material changes the irregular spherical structure into various morphology. EDX and FTIR spectra of prepared samples reveal that the presence of elemental presentation and chemical functional groups, respectively. By using the UV-VIS absorption spectra, the decrease of band gap from 3.60 to 3.27 eV is red-shift due to the incorporation of Ag/Fe/Mg into ZnO lattice. The increases in electrical conductivity value by

increasing temperature from 30 to 130 °C. This phenomenon of increase in conductivity can be explained on the basis of the increase in the charge carrier's mobility.

All the synthesized nanoparticles have been used to investigate the methylene blue (MB) and methyl orange (MO) dye degradation at pH = 2, 4 & 6 for different UV light irradiation time intervals. The influence of photodegradation parameters maximum at pH=6 and catalyst concentration=10 mg accepted as an ideal for the all the samples. The possible mechanism for the enhanced photocatalytic activity of prepared samples under UV light irradiation is also tentatively proposed.

Fe, Ag, Mg (0.05, 0.075, and 0.1%)-doped ZnO shows higher photocatalytic activity than that of undoped ZnO. Ag (0.01%, 0.02% & 0.03%) co-doped Fe-ZnO nanoparticles shows enhanced dye degradation efficiency compared with undoped ZnO.

The chapter I of the thesis gives the introductory and present investigation has been dedicated to explain briefly.

The chapter II covers the importance of various characterization techniques and instruments used in the present study.

The chapter III briefly explains the variation of various properties and photocatalytic decolourization of Fe doped ZnO nanoparticles from simple co-precipitation method.

The Chapter IV and V discussed about:

Synthesis of high crystalline and different mole ratios of Ag, Mg doped
 ZnO nanoparticles using co-precipitation method.

- Characterization of synthesized Ag, Mg doped ZnO nanoparticles using XRD, SEM with EDX, UV-Vis spectra, FT-IR and IV techniques.
- Photocatalytic activity of all the synthesized nanoparticles for the treatment of organic dyes and their degradation performance testing under UV light.

The Chapter VI briefly explains the variation of various properties and photocatalytic decolourization of co-doped (Fe, Ag) ZnO nanoparticles from simple co-precipitation method.

Discussed the various Characterization techniques such as XRD, SEM,
 EDX, FT-IR, UV Vis Spectroscopy I-V Characteristics and photo degradation.

CHAPTER – I

CHAPTER - I

Introduction to Metal Doped ZnO Nanoparticles and Literature Review

1.1 Introduction

Now a days, the world facing several pollution problems, each and every day, 7×10^5 tons of harmful organic pollutants are discharged into the environment from varies industries. Among them approximately 10,000 different types of dyes and pigments were included. Organic dyes play a vital role owing to their great demand in textile, cosmetic and food industries. These dyes are not only chemically stable, it will produce deep colour with bad smell to the water and also highly carcinogenic in nature [1]. To protect our environment from this chemical pollution, various water treatment techniques have been contributed. Among them semiconductor photocatalysis has a great potential to contribute the waste water treatment. Since the mechanism of photodegradation of ZnO was proved to be same as TiO₂ [2].

Among the various solution routes, sol-gel via co-precipitation method is a very attractive and popular method because it can be used to prepare on large area, handy in nature, synthesis is carried out at room temperature and it is easy to control the parameters. It is also permit tailoring of certain desired structural characteristics such as compositional homogeneity, grain size, particle morphology and porosity. Preparation of transition metal-doped ZnO nanoparticles by sol-gel via co-precipitation method, characterization and investigation of their photocatalytic activity have been reported in recent literature [3, 4].

Methylene blue (MB) is a cationic dye, generally used for coloring the papers, hair colorant, dyeing the fabrics and ability to cause some harmful effects [5]. The molecular structure of the dye is given in Fig. 1.1. Strong exposure can increase heart rate and induce vomiting, cyanosis, jaundice and tissue necrosis in Human [6].

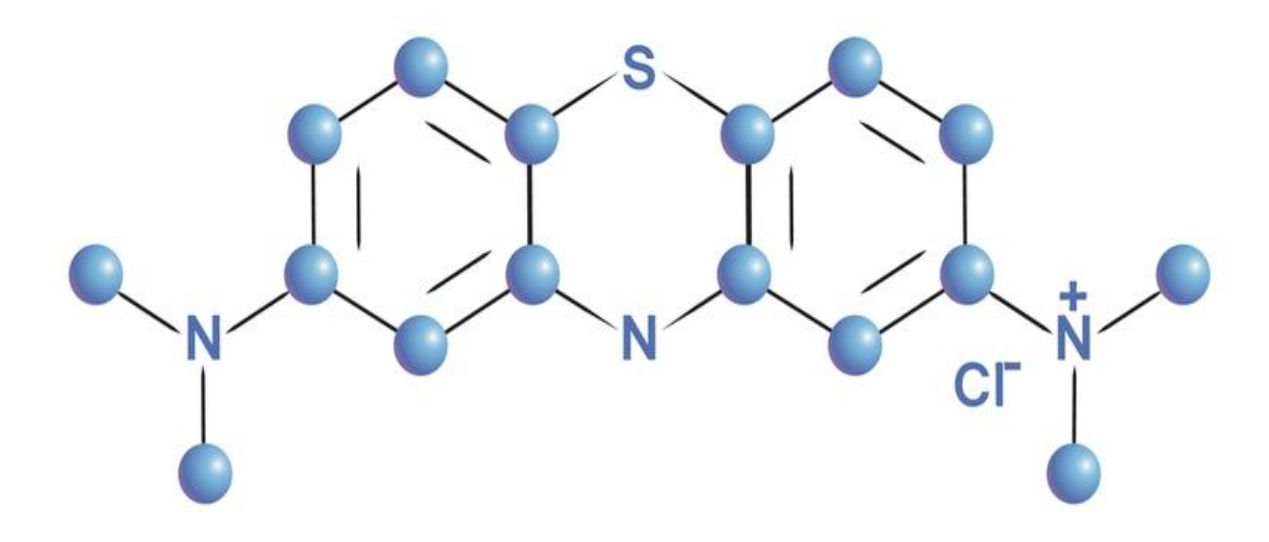


Fig. 1.1: Molecular structure of Methylene blue dye

The photocatalytic activity of the photocatalyst was evaluated by using MB or MO as a model pollutant. In the present work, the photocatalytic activity of M/ZnO [M= Fe, Ag, Mg], for the degradation of MB under visible light irradiation was investigated. An optimization of the photocatalytic process was attempted through tuning a series of reaction parameters such as pH, catalyst concentration and dye concentration. Intense research work on the preparation and characterization of undoped and co-doped ZnO has been carried out by achieving higher efficiencies. The work also includes the preparation and characterization of new class of (Ag, Fe & Mg) co-doped ZnO nanoparticles based photocatalysts.

1.2 Zinc Oxide

Zinc Oxide (ZnO) is an inorganic wide bandgap (3.3 eV) semiconductor and it belongs to II-VI group of transition elements. Compared with all other materials it shows higher electron mobility. In this section, the general properties of the ZnO material including crystal structure and electronic structure are given in detail. It also shows attracted features with excellent optoelectronic and piezoelectric properties [7, 8]. The important structural and physical parameters were given in Table 1.1.

Table 1.1 Important parameters of ZnO

Chemical Formula	ZnO
Appearance	White Solid
Molar Mass	81.38 g/mol
Melting and Boiling point	1,975 °C
Solubility in water	Insoluble
Bandgap	3.3 eV
Crystal structure	Hexagonal Wurtzite
Space group	C ⁴ _{6v} -P6 ₃ mc

1.2.1 Crystal Structure

At room temperature ZnO shows hexagonal-shaped wurtzite crystal structure. In addition to this it also exists in the cubic rock salt and cubic zinc-blende forms [9-10]. In ZnO crystal structure, each Zn ion is surrounded by four oxygen ions, and vice versa. The structure with tetrahedral configuration and its unit cell structure are shown in Fig. 1.2. The Zn²⁺ and O₂- ions in grey and yellow colour, respectively. The lattice parameters are a =b= 0.32498 nm and c = 0.52066 nm. The volume of the ZnO unit cell with a wurtzite structure is 23.8×10^{-3} nm³ [11].

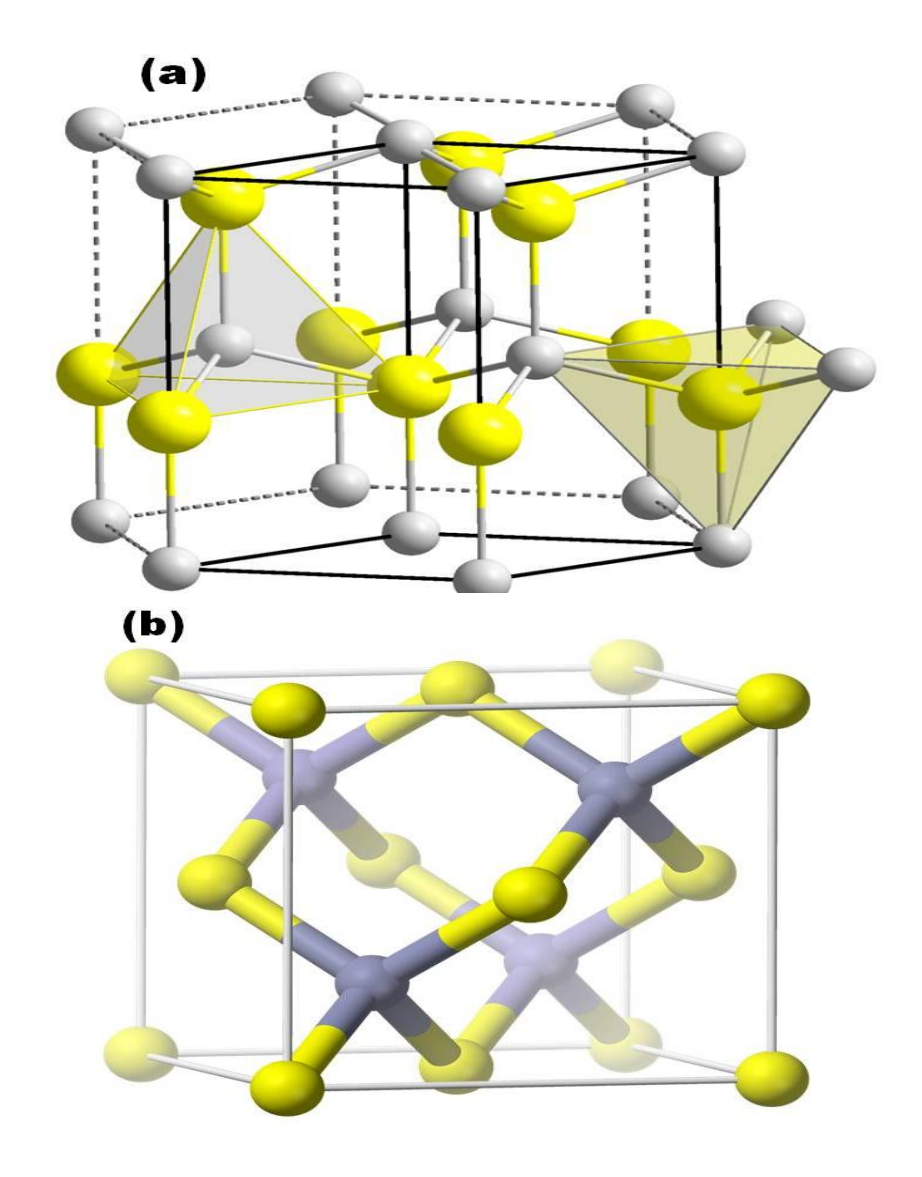


Fig. 1.2: Crystal structure of ZnO (a) Wurtzite and (b) cubic zincblende

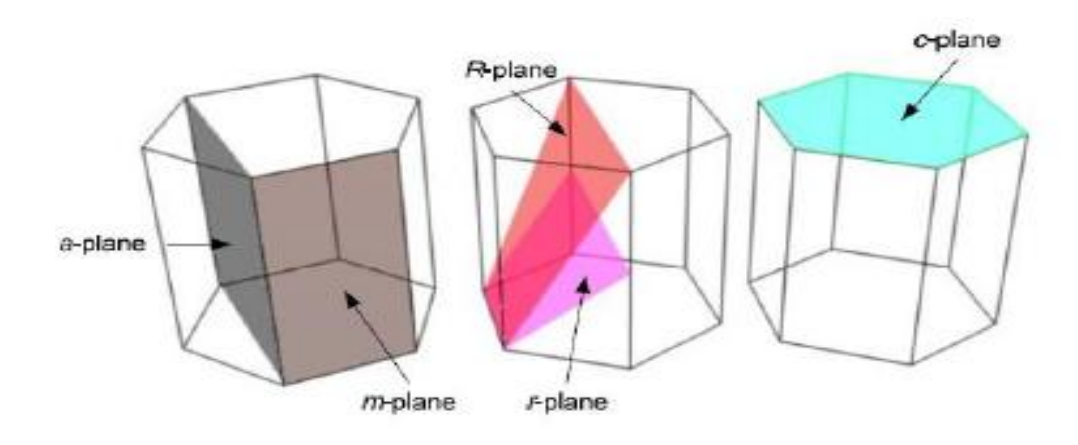


Fig. 1.3: Various crystal planes of the ZnO hexagonal structure

1.2.2 Electronic Structure

Zinc (Zn) metal has the outer shell electronic configuration of 3d¹⁰ 4s² while oxygen (O) has the outer shell electronic configuration of 2s² 2p⁴. Since 'O' has greater electro negativity than 'Zn', this enables to draw the outer shell electrons of Zn 4s shell into unequal bonds with O. All the experimental studies show that the 3d electrons of Zn have an influence on the valence band electrons of Zn and O such as Zn-4s and O-2p [12, 13]. Additionally, hybrid orbital's strongly influence the Zn-4s and O-2p electrons. Due to the existence of conduction band minimum and valence band maximum in phase the band gap is high. In addition to this its wave functions/k-vector values are the same.

1.3 Applications of ZnO

ZnO nanoparticles are widely used in various fields like optoelectronic devices, solar cell application, LED, photodetectors, optical switches, Super capacitor application and photocatalytic application. Among this photocatalytic application is very important for our healthy life, due to this the effect of various parameters are analysed in the present research work.

1.3.1 Photocatalytic Degradation

An especially designed photocatalytic reactor system made of wooden chamber was used for photodegradation experiments, which contain 10 ml of MB dye (20 mg/l) solution and 6 mg of undoped and (Ag, Fe) co-doped ZnO catalysts. Before the UV-irradiation, the solution was stirred in the dark (15 min) to permit stability of the system. Irradiation was maintained out using UV table lamp of 15 W having wavelength 365 nm was reserved inside the wooden chamber. The distance between

photoreactor and light sources was 20 cm. During the UV-irradiation and MB or MO solution were 2-3 ml was withdrawn and centrifuged to separate the catalyst. The enhanced photocatalytic degradation of MB or MO dye was observed by evaluating the absorbance using a UV-Vis double beam spectrophotometer (Shimadzu-AU-2707) at ~664 or ~464 nm wavelength. The photocatalytic degradation (%) of MB in each sample was calculated using the Eq. (1) [14].

Degradation percentage =
$$[(A_0 A_t)/A_0] \times 100 (\%)$$
 ... (1)

Where 'A₀' is the absorbance of initial sample (t = 0 min) at ~664 or ~464 nm, 'A_t' is the absorbance at the same wavelength of the UV irradiated solution (t = t min). Similar stages were repeated for pure ZnO and other three samples of (Ag, Fe) codoped ZnO nanocomposites. The photocatalytic degradation percentage calculations were made according to above Eq. (1).

1.3.2 Mechanism of Degradation

Fig.1.4. displays a mechanism of the charge separation and photocatalytic degradation for (Ag, Fe) co-doped ZnO nanocomposites based photocatalyst. When heterogeneous semiconductor is irradiated by UV light, a valence band electron (VB) goes to the conduction band (CB), exit a hole in the valence band. Mostly, recombination of electron-holes reduces the photocatalytic degradation of heterogeneous semiconductors. However, the presence of 'Ag' and 'Fe' hold the electron from CB of ZnO, suppressing the electron-hole recombination [15, 16]. Moreover, Ag acts as a sink of the electrons from CB of ZnO and after that silver (Ag) is oxidized by the absorption of oxygen to produce reactive oxygen species (O₂). The reactive oxygen species (O₂) is then further reduced to form hydroxyl radical (·OH).

On the other hand, the holes combine with water to form hydroxyl (·OH) radical and these hydroxyl radicals (·OH) break down the dye molecules in order to degrade the dye. 'Fe' doping also overwhelms recombination of electron and positive holes by electron trapping.

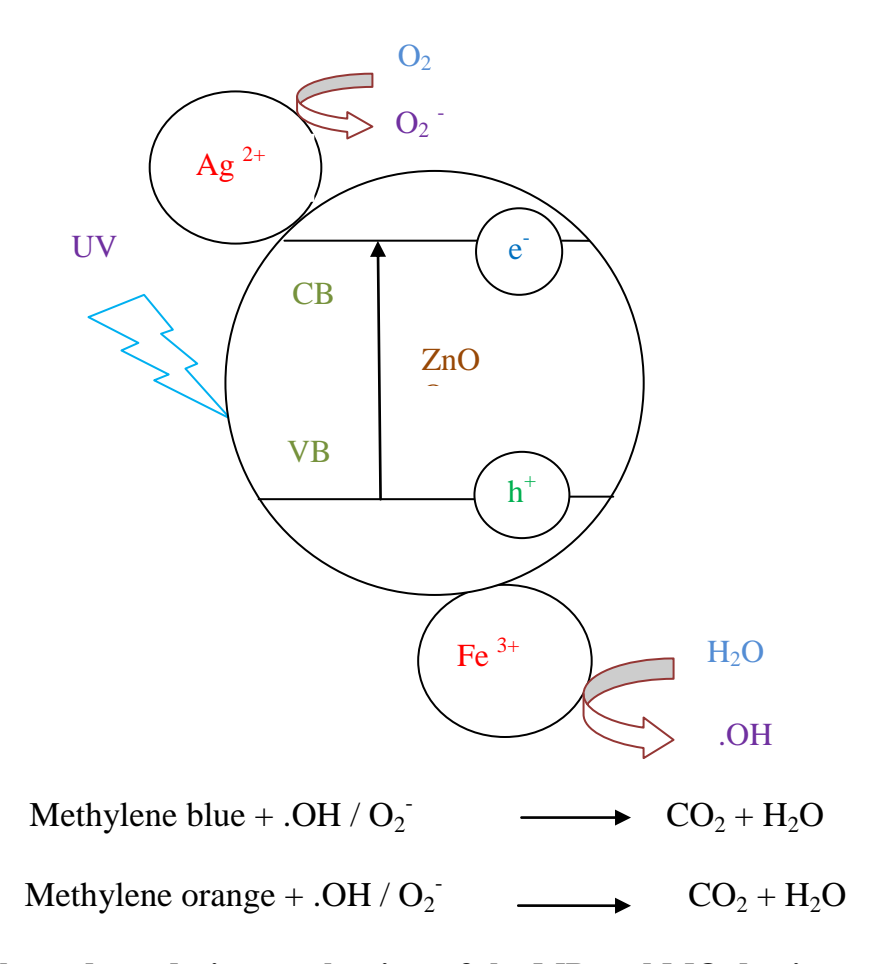


Fig.1.4: Photo-degradation mechanism of the MB and MO dye in presence of (Ag, Fe) co-doped ZnO nanocomposites

It is shown that the photocatalytic degradation of (Ag, Fe) co-doped ZnO nanocomposites based photocatalyst is higher than that of all other semiconductor photocatalysts. The trapping nature of Ag and Fe produced more superoxide radical anion, and at the same time VB holes of ZnO react with water to produce highly reactive hydroxyl radical (·OH). The superoxide radical anion and hydroxyl radical are used for degradation of dye.

1.4 Literature Survey

Zhang *et al.* [17] have reported the synthesis of ZnO nanoparticles by simple chemical method. The structural and optical properties of the prepared ZnO nanoparticles have been confirmed by using TEM, XRD and UV-VIS spectroscopy. The synthesized nanoparticle shows lattice contraction due to high attractive electrostatic interaction between Zn²⁺ and O₂⁻ ions. Band gap energy of ZnO nanoparticle is 3.4 eV, obtained from the UV-Visible reflectance spectra, which is higher than that of the bulk. Absorption peak of the prepared sample is 262nm which is highly blue shifted as compared to the bulk (360 nm). Large band gap energy and highly blue shifted absorption edge confirm that the prepared ZnO nanoparticle exhibit strong quantum confinement effect. The average sizes of the sample have also been determined to be 5 to 8 nm from the peak absorbance wavelength and using the equation derived from the effective mass model. As temperature increases the particle size of the sample is found to be increases.

Abinaya *et al.* [18] have synthesized ZnO nanoplates with a low temperature and aqueous solution-based method without a calcination process. This method was also found to be easy and simple approach for the incorporation of Cu and Ag dopants into ZnO. X-Ray diffraction (XRD) studies confirmed that the synthesized samples were in hexagonal wurtzite structure. From the FESEM images it is observed that although the morphology does not change with dopants it has increased antibacterial activity compared to pure ZnO. The absence of impurities and the presence of Cu and Ag were evidenced by EDX. HRTEM images also confirmed the morphology as nanoplates. UV-Visible absorption analysis shows characteristic absorption peak of

ZnO nanoparticles. The most interesting observation was found that the Ag doped ZnO has MIC values against *E.coli*, *S.aureus and S.typhi* comparable to commercial antibiotics, which has the mechanism for bactericide. The XPS results revealed the oxidation state of Ag as metallic silver. The photo activation of ZnO and the metallic Ag were the main cause for the enhanced activity.

Madras *et al.* [19] synthesized hexagonal wurtzite ZnO was carried having BET surface area of 16.8 m²/g. A modification to ZnO was performed by Ag substitution and impregnation bearing surface area of 14.2m²/g and 12.4m²/g, respectively. The XPS results revealed the Substitution and impregnation of silver as Ag+ ion. The photocatalytic tests showed that Ag impregnated ZnO exhibits excellent bacterial inactivation. The porous and open structure of ZnO favored the effective inactivation by increasing the number of active sites and effective charge separation observed in presence of Ag. Ag acts as an electron sink and hole as hydroxyl radical former for the photochemical killing of bacteria.

Tripathi *et al.* [20] have reported the photocatalytic activity of pure and Agdoped TiO₂ photocatalyst was examined by performing the photodegradation of methylene blue dye. The experimental result exhibited that Ag-doped TiO₂ photocatalyst can effectively degrade MB under visible light irradiation and 4.0 mole % Ag-doped TiO₂ showed the highest photocatalytic activity among all the samples synthesized by sol-gel route. The antibacterial activity was tested against bacterial strain such as Escherichia Coli, Pseudomonas aeruginosa, Klebsiella pneumoniae and Enterobacter Cloacae. Parallel analysis by various characterization tools (XRD, Raman, SEM, EDS, TEM, UV- visible, FTIR and PL) also demonstrated that the Ag-

doped TiO₂ photocatalyst showed enhanced photocatalytic and antibacterial activity. TEM analysis confirms the presence of anatase phase structure without any other impurity phases. SEM images showed the uniform morphology in the form of tiny crystals. EDX spectrum revealed the presence of Ag, along with to Ti and O. UV-visible spectroscopy shows a systematic variation in absorption edge with increasing Ag substitution.

Chauhan *et al.* [21] were synthesized Ag-doped ZnO nanoellipsoids by simple solution process at low-temperature and used as effective photocatalyst. X-Ray diffraction (XRD) studies confirmed that the as-synthesized nanoellipsoids are well-crystalline, possessing wurtzite hexagonal phase and grown in very high density. The as-synthesized Ag-doped ZnO nanoellipsoids were used as photocatalysts and series of photocatalytic experiments revealed that the photocatalytic degradation efficiency was enhanced with increasing the amount of Ag-doped ZnO nanoellipsoids up to certain extent and after that the reduction in degradation was observed. Under optimized conditions, ~99.5% photo-degradation of MO was achieved in 240 minutes. Further, the fabricated Ag-doped ZnO NEs based hydrazine sensor exhibited a high sensitivity of ~9.46 μA/cm².μM and detection limit of 0.07 μM in a short response time of < 10s. The presented work demonstrates that simply prepared Ag-doped ZnO nanoellipsoids are efficient photocatalyst and electron mediator for the fabrication of highly sensitive chemical sensors.

Manjari *et al.* [22] were synthesized the Cu, and Ag NPs and Cu,ZnO and Ag@ZnO nanocomposite using aqueous bark extract of *A.* Analysis by various characterization characterized using UV–Vis Spectra, XRD, Raman spectra, TEM,

SAED, EDAX, and FTIR. The characterization reveals the formation of Cu and Ag nanoparticles with an average size 18 and 12 nm, immobilized over surface of ZnO. The synergetic effect between metal and porous material exhibited enhanced catalytic and recyclable activity than pure Cu and Ag NPs in both liquid and solid phase. As compared to Ag/ZnO, Cu/ZnO has exhibited eminently high heterogeneous catalytic activity in the reduction of p-NP. Finally, immobilization of metal nanoparticles over surface of porous material exhibited more stability and activity by easily dispersion of catalyst in reaction solutions.

Yanhong Lin et al. [23] synthesized a series of Fe/ZnO photocatalysts by a simple and rapid facile hydrothermal method. The difference in the transfer pathway of photogenerated electrons results in the different photocatalytic activity under the irradiation of UV and visible light because of the coexistence of Fe³⁺ and Fe²⁺ in the ZnO host. When the samples are irradiated by UV light, the Fe ions may act as traps for the photogenerated electrons and holes and promote the recombination; thus, the Fe/ZnO photoactivity is reduced. Whereas, in the presence of visible light, the existence of Fe³⁺/Fe²⁺can facilitate separation, and hider recombination photogenerated electron-hole pairs from excited RhB.

Faheem Ahmed *et al.* [24] have reported different water samples, the Fe–Ag co-doped TiO₂ NPs were found to be an excellent decontaminating catalyst for flumioxazin. The compound persists for several days in the absence of a catalyst. The mobile phase, acetonitrile, and HPLC water have shown good separation and resolution, and the time required to analyze three different types of buffers for chromatographic determination is a very short run time. Photocatalytic studies of

flumioxazin at various conditions such as acidic, basic, and neutral revealed that the activity was enormously increased with Fe–Ag co-doped TiO₂ NPs as the time frame is fixed for a stipulated number of hours, whereas the activity was not found without addition of Fe–Ag co-doped TiO₂ NPs, even though experiments were carried out over several days.

Esmaeil Babanezhad et al. [25] were prepared to improve the photocatalytic efficiency under visible light irradiation, Ag/Fe₂O₃ doped ZnO nanostructures by a facile co-precipitation method. XRD and EDX reveal the presence of Ag and Fe₂O₃ in ZnO matrix with a hexagonal structure growth in 101 directions. FESEM images show agglomeration of NPs irregularly shaped, decreasing with increasing doped concentration, also appearing of scattered of Nanorod, Nanosheet, and small single NPs. The optical Characterisation shows Ag/Fe₂O₃ doped ZnO has increased absorption in the visible light region when compared to undoped ZnO. This three component Nano junction (ZnO/Ag/Fe₂O₃) system showed enhanced photocatalytic activities for the degradation of MB dye. The degradation efficiency of undoped ZnO and doped ZnO enhanced using coprecipitation due to high aspect ratio of ZnO and the effects of a doped nanostructure. The photocatalytic activity enhanced almost attributed to the excellent separation of photo generated charge carriers.

Mariani A. Ciciliati *et al.* [26] were synthesized nanostructured zinc oxide and iron doped zinc oxide by a simple modified sol–gel method. The ZnO could be doped with 1mo 1% of Fe ions. Results indicate that, most probably, with more than 2 mol% of Fe, Fe₂O₃ phase segregation occurs. The average crystallite size of the samples decreased with an increase in the Fe doping amount. Then a noparticles showed a near

hexagonal shape. A decrease in the band gap energy was observed from 3.1eV (ZnO) to 2.3eV (Fe₁₀ Zn₉₀), and the surface area increased from 18 (Zn 100) to 55 m² g⁻¹ (Fe₅-Zn₉₅).

S. Malghe *et al.* [27] we reported synthesis of visible light activated N-doped ZnO nanospheres using microemulsion method. Through UV analysis clearly shows red shift in the absorption spectra due to N-doping. The photocatalytic degradation of MG follows pseudo first order kinetics over pure and N-doped ZnO catalysts. N-doped ZnO sample prepared at 500 °C showed excellent visible light photocatalytic activity. Photocatalytic degradation rate for pure is 1.29×10^{-2} min⁻¹ and N-doped ZnO is 2.6×10^{-2} min⁻¹. This was due to the significantly enhanced absorption ability of N-doped ZnO in the visible region, small crystal size, and larger surface area. The catalyst is highly stable and can be used repeatedly.

Roya Mohammadzadeh Kakhki1 *et al.* [28] were prepared ZnO and Ag doped ZnO based visible light photocatalysts developed by using a new method. low cost, high production and excellent performance of the resulting products. Various mol% of highly active silver modified and unmodified ZnO photocatalysts were prepared. The structural and optical properties of the resultant materials were characterized by UV–Vis, XRD, PL, FTIR, FESEM and EDS. Photocatalytic activity of all samples was determined by analyzing the degradation of methylene blue in the presence of the pure ZnO and Ag doped ZnO nanoparticles. Silver modification caused the material to show significant improvement in the photocatalytic activity. 0.5 mol% silver was considered as the optimum concentration. Also, the effect of initial MB concentration, the amount of catalyst and the pH of solution on photo degradation of MB was

investigated. The mechanism of photocatalytic activity was studied and it was found that the presence of silver facilitates the interfacial charge transfer processes.

Thi Kieu Xuan Huynh *et al.* [29] In this study, ZnO nanoparticles was modified with AgNO₃, KF by thermal shock method. The experimental results show that all modified ZnO catalysts exhibited higher photocatalytic activity than unmodified ZnO sample. The enhanced activity of Ag-ZnO is attributed to silver species (Ag⁰ and Ag⁺) on its surface, which is able to create the absorption in the visible region and suppress the charge recombination whereas the improved activity of F-ZnO is assigned to the increase of surface hydroxyl groups and the formation of zinc vacancies, which can promote the generation of hydroxyl radicals and enhance the mobility of photogenerated holes.

Rosari Saleh *et al.* [30] have deposited Fe-doped ZnO nanoparticles with various dopant concentrations using co-precipitation method. The structural, morphological, optical and magnetic properties as well as the photocatalytic activity under UV irradiation have been performed. The effect of pH on the photocatalytic activity was investigated. The results indicated that an acidic medium is appropriate for the degradation of MO, while the degradation of MB is enhanced in an alkaline medium. However, in general, Fe-doped ZnO nanoparticles are better catalysts for the degradation of methyl orange under UV irradiation than for the degradation of methylene blue. The results also revealed that the addition of a dopant atom significantly improved the photocatalytic activity. The optimum conditions for the photocatalytic activity were obtained at a Fe doping concentration of 21 at. %, an

initial dye concentration of 20 mg/L, a catalyst dose of 0.6 gr/L and a pH of 4 for MO and 13 for MB.

L. John Kennedy et al. [31] were synthesized ZnO and Co²⁺ doped ZnO by coprecipitation method dried at 200 °C for 1 h followed by annealing at 500 °C for 3 h. Nano sized particles with various nanostructures were synthesized and it was found that as Co²⁺ concentration increases, the crystallites size decreases. The lattice is subjected to strain due to the substitution of dopant. Secondary phases corresponding to Co₃O₄ were observed for higher concentration of Co²⁺ doping. It was observed that the band gap of pure ZnO decreases as Co²⁺ dopant increases. UV emission in pure ZnO was identified along with defect states. As Co²⁺ concentration increases, UV emission completely vanishes and only defect states corresponding to violet emission, blue emission, green emission, emission were identified. For undoped and Co²⁺ doped ZnO powders, the absorption peak at around 428 cm⁻¹, confirms the formation of ZnO by the FTIR spectra. Different morphologies such as nano hollow rods, nano rods, nano sheets with pores, nano spheres were identified. The BMP model is the more probable mechanism responsible for RTFM due to the presence of defects and oxygen vacancies which led to the formation of BMPs.

Arthoba Nayaka *et al.* [32] synthesized pure ZnO and Cr-doped ZnO nanoparticles by a simple microwave combustion method. The effect of Cr doping on the structure, optical and electrical properties of ZnO were studied. The particle size of the synthesized nanoparticles was found to be ~30 to 66 nm. The SEM and TEM analyses were showed that the crystal structure of ZnO and Cr-ZnO. The UV analysis of synthesized nanoparticles was studied by measuring of band gap energy. This

reveals that with increasing the doping concentration of Cr up to 8 wt%, the band gap edge shifted to longer wavelength region. I-V characteristics of the ZnO and Cr doped ZnO films in dark and under UV-illumination showed that, the band gap of ZnO found to be decreased with increase in Cr content up to 8 wt%.

Auttasit Tubtimtae *et al.* [33] ZnO nanorods were prepared by a simple low-temperature aqueous solution technique on undoped and indium-doped ZnO films. The undoped film consists of nascent nanorods, but doping changes the surface morphology of the film. Nanorods grown on the undoped film are single-crystalline and vertically aligned to the substrate and become branch-like structures after 2 wt% doped in the film. PL spectra reveal the good optical properties of the nanorods and indicate that being ZnO. Doping with 2 wt% indium results in the largest increase in electrical conductance in the ZnO film and yields the best power conversion efficiency.

Rosari Saleh *et al.* [34] were synthesized Zinc oxide nanoparticles doped with manganese and cobalt by a coprecipitation method and were used as a catalyst in the process of photodegradation of methyl orange as a dye model. Doping of ZnO with manganese and cobalt results in an enhanced photo degradation efficiency. The photodegradation efficiency was influenced by different reaction parameters such as the type of dopant, the amount of dopant and the pH values. The maximum photodegradation efficiency for methyl orange was obtained with a catalyst ZnO loading of 12 at.% of Mn and a pH value of 4.

Anandan *et al.* [35] synthesized La-doped ZnO nanoparticles with different La contents and were characterized by various sophisticated techniques such as XRD,

UV-Visible, AFM, XPS, and HR-SEM. The XRD results revealed that La³⁺ is uniformly dispersed on ZnO nano particles in the form of small La₂O₃ cluster. It was found that the particle size of La-doped ZnO is much smaller as compared to that of pure ZnO and decreases with increasing La loading. Rough and high porous surface of La-doped ZnO was observed by AFM, which is critical for enhancing the photocatalytic activity. The photocatalytic activity of La-doped ZnO in the degradation of monocrotophos (MCP) was studied. The effects of the adsorption of MCP, lights of wavelength, and the solution pH on the photocatalytic activity of La⁻ doped ZnO with different La loading were studied and the results were compared with pure ZnO and pure TiO₂. It was observed that the rate of degradation of MCP over La⁻ doped ZnO increases with increasing La loading up to 0.8 wt% and then decreases. It was found that the doping of La in ZnO helps to achieve complete mineralization of MCP within a short irradiation time. Among the catalyst studied, the 0.8 wt% La⁻ doped ZnO was the most active, showing high relative photonic efficiencies and high photo-catalytic activity for the degradation of MCP.

M. Shanthi *et al.* [36] was synthesized Ce-co-doped Ag–ZnO by a simple solvo thermal method. The presence of Ce and Ag in the catalyst has been revealed by XRD, FE-SEM images, EDS, DRS, PL, CV and BET surface area measurements. Co-dopants shift the absorption of ZnO to the entire visible region. Ce–Ag–ZnO shows lower reflectance in the visible region than ZnO, and shifting of the absorption edge to the visible region when compared to ZnO. The lower reflectance led to a higher absorption visible region. The PL spectra reveal the suppression of recombination of photo generated electron–hole pairs by Ce and Ag loading on ZnO. 'Ag' and Ce⁴⁺ trap

the photo-excited electrons, so that the recombination rate of the electron-hole pairs decreases. Ce–Ag–ZnO is found to be more efficient than Ag–ZnO, Ce–ZnO, bare ZnO, commercial ZnO, TiO₂-P₂₅ and TiO₂ (Merck) for degradation of NBB degradation under solar light. The optimum pH and catalyst dosage for efficient removal of dye are found to be 9 and 3 g/l, respectively. COD measurements confirm the complete mineralization of the NBB molecule. A mechanism involving electron trapping by Ag and Ce is proposed to explain the higher photocatalytic activity of the catalyst. The catalyst was found to be reusable.

1.5 Objectives of the Present Work

The primary objective of present research is to progress an organized study on the preparation of undoped, Fe, Ag, Mg doped ZnO and Ag co-doped Fe-ZnO nanoparticles for photocatalytic applications.

The following is an overview of the thesis structure:

The chapter 1 of the thesis gives the introductory and present investigation has been dedicated to explain briefly.

The chapter 2 covers the importance of various characterization techniques and instruments used in the present study.

The chapter 3 briefly explains the variation of various properties and photocatalytic decolourization of Fe doped ZnO nanoparticles from simple co-precipitation method.

The Chapter 4 and 5 discussed about:

 Synthesis of high crystalline and different mole ratios of Ag, Mg doped ZnO and using co-precipitation method.

- Characterization of synthesized Ag, Mg doped ZnO nanoparticles using XRD, SEM with EDX, UV-Vis spectra, FT-IR and IV techniques.
- Photocatalytic activity of all the synthesized nanoparticles for the treatment of organic dyes and their degradation performance testing under UV light.
- The Chapter 6 briefly explains Synthesis, Characterizations of Synthesized nanoparticles and photo-catalytic decolourization of Ag codoped Fe -ZnO nanoparticles from simple co-precipitation method.
- Finally the conclusion and perspectives of the research work in which important points of the results were summarized.

References

- [1] K. Vignesh, R. Priyanka, R. Hariharan, M. Rajarajan, A. Suganthi, J. Ind. Eng. Chem. 20 (2014) 435–443.
- [2] M. Swaminathan, N. Shobana, J. Separ. Puri. Techn. 56 (2007) 101–107.
- [3] Muneer M. Ba-Abbad, Abdul Amir H. Kadhum, Abu Bakar Mohamad, Mohd S. Takriff, Kamaruzzaman Sopian, Chemosphere, 91 (2013) 1604–1611
- [4] C. Aydın, M.S. Abd El-sadek, KaiboZheng, I.S. Yahia, F. Yakuphanoglu, Optics & Laser Technology, 48 (2013) 447–452.
- [5] N. M. Ganesan, N. Muthukumarasamy, R. Balasundaraprabhu, T. S. Senthil, Optoelect. Adv. Mater. – Rapid Commun. 8 (2014) 581 – 586.
- [6] J. Li, C. Hu, Y. Zhou, M. Li, F. Xue, H. Li, J. Health Sci. 55 (2009) 619–624.
- [7] Y. F Zhu, A. H. Fan, W. Z. Shen A, J. Phys. Chem. C 112 (2008) 10402–10406.
- [8] S. K. Panda, A. Dev, S. Chaudhuri, J. Phys. Chem. C 111 (2007) 5039–5043.
- [9] P. Yang, X. Xiao, Y. Li, Y. Ding, P. Qiang, X. Tan, W. Mai, Z. Lin, W. Wu, T. Li, [10] H. Jin, P. Liu, J. Zhou, C.P. Wong, Z.L. Wang, ACS Nano 7 (2013) 2617–2626.
- [10] X. Xia, J. Tu, Y. Zhang, X. Wang, C. Gu, X.-B. Zhao, H.J. Fan, ACS Nano 6 (2012) 5531–5538.
- [11] Z. L. Wang, R. Guo, G.-R. Li, L.-X. Ding, Y.-N. Ou, Y.-X. Tong, RSC Adv. 1 (2011) 48–51.
- [12] J. P. Richters, T. Voss, D.S. Kim, R. Scholz, M. Zacharias, Nanotech. 19 (2008) 305–202.
- [13] C.Y. Chen, C.A. Lin, M.J. Chen, G.R. Lin, J.H. H, Nanotech. 20 (2009) 185605.

- [14] S. Yu, L. Ding, H. Zheng, C. Xue, L. Chen, and W. Zhang, Thin Solid Films 540, (2013), 146.
- [15] C. Abinaya, M. Marikkannan, M. Manikandan, J. Mayandi, P. Suresh,
 V. Shanmugaiah, C. Ekstrum, J. M. Pearce, Mater. Chem. Phys. 184 (2016) 172–
 182
- [16] Sangeeta Adhikari, Aditi Banerjee, Neerugatti KrishnaRao Eswar, Debasish Sarkar, Giridhar Madras, RSC Advances 63 (2015).
- [17] T. Ali, Ateeq Ahmed, Umair Alam, Imran Uddin, P. Tripathi and M. Muneer, Mater. Chem. Phys. 212 (2018) 325–335.
- [18] G. Manjari, S. Saran, Suja P, Devipriya, A. Vijaya Bhaskara Rao, Cataly. Lett. 148 (2018).
- [19] Shasha Yi Jiabao Cui Shuo Li Lijing Zhang Dejun Wang Yanhong Lin, Applied Surface Sciecne 319 (2014) 230–236.
- [20] Tentu Nageswara Rao, Y. Prashanthi, Faheem Ahmed, Shalendra Kumar, Nishat Arshi, G. Rajasekhar Reddy and Tentu Manohra Naidu, "Frontiers in Nanotechnology (2021).
- [21] Esmaeil Babanezhad, Seyedeh Fatemeh Mosavi Tarsia, Hossein Abbastabar Ahangar, Ag-Fe-codoped ZnO nanoparticles for photocatalytic decolorization of Direct blue 78 (2015) 11.
- [22] Mariani A.Ciciliati a,n, MarcelaF.Silva a, DanielaM.Fernandes a, MauricioA.C.deMelo b, Ana AdelinaW.Hechenleitner a, Edgardo A.G.Pineda Mater Letters 159 (2015) 84–86.

- [23] B Atul .S Lavand, Yuvraj . Malghe, Journal of Asian Ceramic Societies 3 (2015) 221–368.
- [24] Roya Mohammadzadeh Kakhki, Reza Tayebee, Fatemeh Ahsani, J. Mater. Sci.: Mater. Electro. 28 (2017).
- [25] Huu Thinh Pham Nguyen, Thi Minh Tram Nguyen, Chau Ngoc Hoang, Tien Khoa Le, Torben Lund, Huu Khanh Hung Nguyen, Thi Kieu Xuan Huynh, Arabian Journal of Chemistry, 13(1) (2018) 1837–1847.
- [26] Rosari Saleh, Nadia Febiana Djaja, Superlattices and Microstructures 74 (2014) 217–233.
- [27] S. Fabbiyola, L. John Kennedy, Udaya Aruldoss, M. Bououdina, A.A. Dakhel, J. Judith Vijaya. Powder Technology 286 (2015) 757–765.
- [28] R.O. Yathisha, Y. Arthoba Nayaka, C.C. Vidyasagar, Materials Chemistry and Physics 181 (2016).
- [29] Auttasit Tubtimtae, Ming-Way Lee, Superlattices and Microstructures 52 (2012) 987–996.
- [30] Rosari Saleh, Nadia Febiana Djaja, Spectrochimica Acta 130 (2014) 581–590.
- [31] S. Anandan, A. Vinu, , K. L. P. Sheeja Lovely, N. Gokulakrishnan, P. Srinivasu,
 T. Mori, V. Murugesan, V. Sivamurugan, K. Ariga, J. Mol. Cataly. A:
 Chemical 266 (2007) 149–157.
- [32] S. Raad, J. Sabry, W. I. Aziz, M. Rahmah, Materials Technology (2019).

CHAPTER – II

CHAPTER - II

Preparation and Characterization Methods

2.1 Introduction

In this chapter, the preparation of nanoparticles is discussed in detail. The nanoparticle synthesis is one of the most active research in modern manufacturing of new materials due to their fascinating properties at the nanoscale level. In general, nanomaterials can be synthesized in two fundamentally different approaches namely, top-down and bottom-up approaches. In top-down approach, the bulk materials are divided into microparticles and further in the order of nanometers. On the other hand, bottom-up approach the nanostructured materials are synthesized from atomic level and is shown in Fig.2.1.

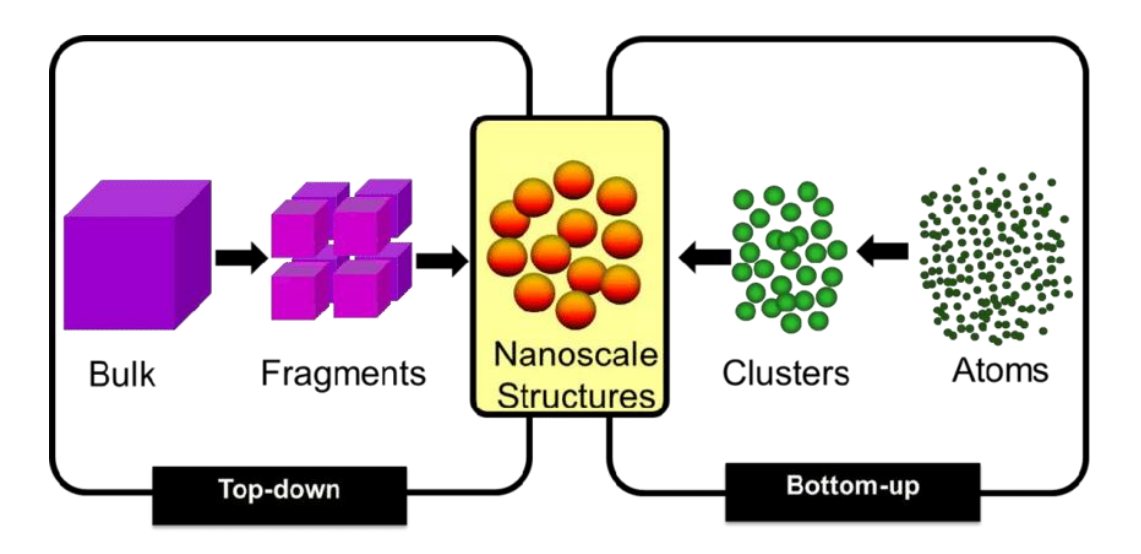


Fig.2.1: Schematic diagram of Top-down and bottom-up approaches

However, it is subdivided into two types such as physical and chemical methods. In the physical method, nanoparticles are prepared from a top-down approach. Laser ablation, radiolysis, vaporization, physical vapor deposition (PVD), are the example for some physical processing methods. Other methods like ball

milling and high melting mixing are the example for mechanical processing methods. In chemical methods, nanomaterials are synthesized in terms of bottom-up approach such as chemical vapour deposition (CVD), sol-gel method, solvothermal method, hydrothermal method, co-precipitation method, templating and chemical reduction methods, etc. Among these methods, the present research focuses on co-precipitation method. Because it is simple and cost-effective technique which has been used by many researchers for the synthesis of semiconducting nanoparticles. This chapter contains a brief description of the chemical routes to prepare and investigate the semiconducting nanoparticle.

2.2 Chemical Methods

There are various chemical methods have been developed to prepare doped ZnO (Fe, Ag, Mg) and co-doped ZnO (Fe, Ag) nanoparticles, among them the most common methods are discussed below.

2.2.1 Chemical Vapour Deposition (CVD)

Chemical Vapour Deposition (CVD) is an excellent method, which is utilized to control the crystallinity, particle size, shape and chemical compositions. CVD process is used to obtain high-purity and performance nanomaterial based thin films. CVD technique involves chemical reaction between organo-metallic precursor and a carrier gas. The quality of the deposited materials strongly depends on the concentration of the precursors and the reaction temperature [1]. It also includes trichloride, metal-organic and hydride chemical vapor deposition method. In a typical CVD process, the atoms or molecules which are in the gaseous state are either allowed to react homogeneously or heterogeneously depending on applications. In

homogeneous CVD, the atoms or molecules in the gas phase are diffused towards the cold surface owing to the thermophoric phases. The diffused particles collected from cold surface to give nanopowders or deposited onto a substrate film. In heterogeneous CVD, a dense film of nanoparticles is obtained on the substrate surface. The advantages of this method include the uniform coating of nanofilms. This process has some restrictions that include it is hard to scale up and the highest annealing temperatures reported by Sudarshan [2]. In some of the processes, the chemical reaction may be activated through an external agency, such as, application of heat, rf field, light or X-rays, an electric or glow discharge or electron bombardment.

2.2.2 Sol-gel Method

Sol-gel technique is a flexible synthesis approach that can be used to incorporate the creation of inorganic colloidal suspension in a liquid (sol) turned into continuous network (gel) phase. The sol-gel method is based on poly condensation reactions of metal chlorides/alkoxides precursors with precise stoichiometric ratio to produce nano materials. When the polymerization is complete and the solvent has evaporated, the sol forms a gel. The crystallite size and shape are controlled by the sol-gel transitions. A gel is not static during aging but can continue to undergo hydrolysis process and condensation chemical reaction is given in Equation 2.1 & 2.2.

$$M-O-R + H_2O \rightarrow M-OH + R-OH (Hydrolysis)$$
 ... (2.1)

$$M-O-H + R-O-M \rightarrow M-O-M + R-OH$$
 (Condensation) ... (2.2)

The precursor sol can be further processed to obtain the substrate in a film, either by dip or spin coating, or cast into a container with desired shape or powders by calcinations. The sol-gel method is an interesting, cheap and low temperature

technique, which is used to produce a range of nanoparticles with controlled chemical compositions. In aero gel, the final material can be designed to have interconnected nanoscale porosity and hence a high surface area. The sol-gel derived nanoparticles are used in wide range applications like optics, electronics, energy, space, bio-sensors and drug delivery.

2.2.3 Solvothermal Method

The solvothermal method is similar to the hydrothermal method, with the exception that the variety of solvents other than water (non-aqueous) can be used for this process. Solvothermal process involves the use of a solvent under moderate to high pressure (typically between 1 and 10,000 atm) and temperature (typically between 100 and 1000 °C) that allows the interaction of precursors during synthesis. Organic solvents with high boiling point are possible to achieve much higher temperatures [3]. This method versatile nature has better control of the crystallinity, size and shape distributions than the hydrothermal method. A wide variety of ZnO nanoparticles or nanorods with/without using the surfactants are prepared from this technique.

2.2.4 Hydrothermal Method

Hydrothermal method is promoted by an inorganic formation in a pressurized vessel called an autoclave under elevated pressure and temperature in the presence of water. A hydrothermal method can be described as "a chemical reaction in a closed system in the occurrence of a solvent (non-aqueous and aqueous solution) at a temperature greater than the boiling point of a solvent". Temperature in the autoclave can be raised above the boiling point of water, which reaches the pressure of vapour

concentration. The hydrothermal method has been widely used to control the crystallite size, phase and surface morphology through regulation of the solution composition, response temperature, pressure, additives, solvent properties and aging time [4]. The typical Teflon-lined autoclave apparatus is shown in Fig. 2.2.



Fig.2.2: Autoclave apparatus

2.2.5 Co-precipitation Method

The Co-precipitation is a wet-chemical technique used to produce nano crystalline materials with high specific surface area, superior homogeneity, purity, better micro structural control of metallic particles, narrow pore size and uniform particle distribution. Co-precipitation method also offers several other advantages, like low temperature processing, possibility of coating on large area substrates and most importantly cost effective.

Co-precipitation method is more suitable to prepare optical materials as it permits molecular-level mixing, processing of raw materials, and preparation of precursors at relatively lower temperature, produces nano-structured bulk powders and thin films. This method is an efficient pre-concentration technique for tracing heavy metal ions. In addition, the shape and size of the particles can be controlled by altering pH of the medium. This method is often used to produce metal oxide nano materials at low-cost.

There are three main mechanisms of co-precipitation: inclusion, occlusion and adsorption. An inclusion occurs when the impurity occupies a lattice site in the crystal structure of the carrier, resulting in a crystallographic defect; this can happen when the ionic atoms and charge of the impurity are similar to those of the carrier. An occlusion occurs when an absorbed impurity gets physically trapped inside the crystal as it grows. An adsorbate is an impurity that is weekly bound to the surface of the precipitate.

Co-precipitation is also potentially important to many environmental issues closely related to water resources, including acid mine drainage, radio nuclide migration in fouled waste repositories, metal contaminant transport at industrial and defense sites, metal concentrations in aquatic systems, wastewater treatment technology and also used as a method of magnetic nano particle synthesis.

A detailed study has been made about the various methods available for preparation of ZnO nano particles. In the present study co-precipitation method has been used for the preparation of undoped, Fe, Ag doped ZnO and codoped (Fe,Ag) ZnO nanoparticles.

2.3 Characterization Medthods

To identify the structure, surface morphology, chemical composition, optical and electrical properties of the prepared samples are characterized using various characterization techniques. All the equipment setup, characterization tools and working principle are explained in detail in this section.

2.3.1 X-Ray Diffraction Technique (XRD)

The physical characteristics of nanoparticles are extremely affected by structure. X-ray diffraction, neutron diffraction technique, and Raman spectroscopy were uniquely used to identify the structure of samples. Among these, XRD technique have dominant role in the characterization due to its simplicity, quantitative and more reliability.

X-ray diffraction technique is a versatile, non-contact and non-destructive technique used to analyze the crystal structure and the schematic diagram of X-ray diffraction is shown in Fig. 2.3(a). It also provides valuable insight about the crystalline quality, lattice planes and unit cell dimensions, etc. X-rays are produced by a CRT, filtered to generate monochromatic radiation, collide to concentrate and then directed towards the sample. Generally, when X-ray beam incident on a sample, interacts with the electrons and it scattered out by the sample atoms. However, the XRD technique works only for the scattered elastic X-ray waves, they are partially coherent may interfere with the incident waves under certain conditions. Therefore, crystal information can be obtained from the elastic scattered X-ray waves. The interaction of the X-rays with the sample produces constructive interference based on Bragg's law reported by Rousseau [5],

$$2d_{hkl}\sin\theta = n\lambda \qquad ... (2.3)$$

Where, 'd_{hkl}' is the distance between adjacent planes, ' θ ' is the scattering angle of incident X-ray, 'n' is the order of diffraction and ' $\lambda = 1.5406$ Å' is the wavelength of the X-ray. The lattice parameters 'a' and 'c' of hexagonal wurtzite structure can be calculated by using the following equation 2.4 [6],

$$\frac{1}{d_{hkl}^2} = \frac{4}{3} \left(\frac{h^2 + hk + k^2}{a^2} \right) + \frac{1^2}{c^2} \qquad \dots (2.4)$$

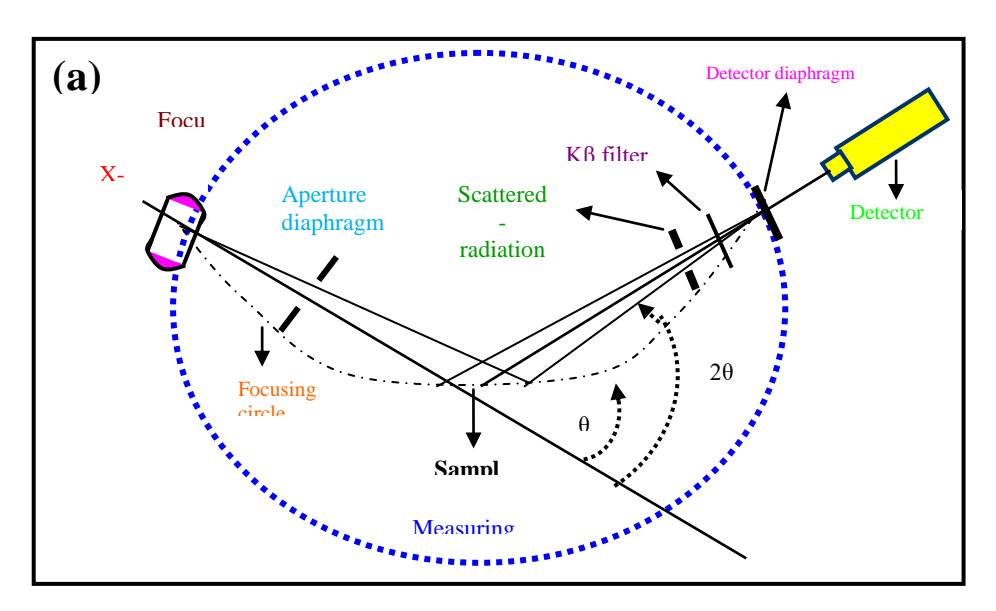




Fig.2.3: (a) Schematic diagram of XRD apparatus and (b) Photograph of XRD apparatus

Where, a and c are the lattice constants of the unit cell.

For (002) plane
$$d_{002} = c/2$$
 and

For (100) plane
$$d_{100} = 0.86 \times a$$

The average crystalline size (D) of the samples can be calculated from the full width at half maximum (FWHM) using Scherrer's formula [7].

$$D = \frac{k\lambda}{\beta \cos \theta} \qquad ... (2.5)$$

Here 'k' is the shape factor ≈ 0.94 , ' λ ' is the wavelength of X-rays used, ' β ' is the FWHM and ' θ ' is the Bragg's angle [8]. In the present work the prepared undoped and doped ZnO samples are analyzed by using PANalytical X-ray diffractometer [Fig.2.3(b)] with CuK α (λ =1.5406Å) radiation. The scanning of the sample lies in the range of 10–80° and step size is 0.02/sec.

2.3.2 Scanning Electron Microscope (SEM)

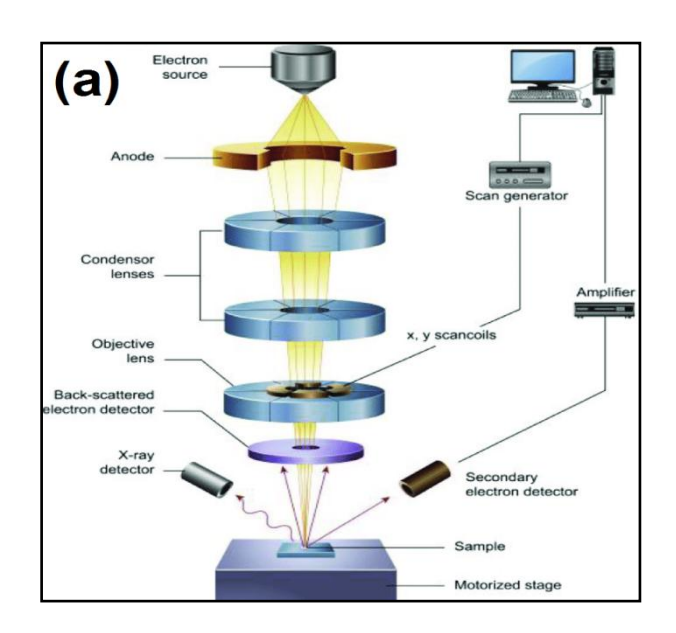
The Scanning Electron Microscope (SEM) is used to investigate the surface morphology of the prepared samples. SEM image was produced by scanning the sample with a high energy beam of electrons, emitted by the secondary or scattered electrons. Various interactions may occur with the high energetic electrons. These interactions cause the emission of the secondary electrons, backscattered electrons, characteristic X-rays, Auger electrons and cathode-luminescence emission on the top side of the sample. The emitted electrons collected by a suitable device and translated into signals that contain information about the sample's topography, surface morphology and composition of the sample. In the most standard detection mode, signals are covert into image of the sample on a CRT.

The schematic diagram of the typical SEM apparatus is shown in Fig. 2.4(a). The SEM used in this work consists of two column chambers under vacuum. The upper chamber containing the electron gun column acting as an electron source, which can be either a tungsten filament made of lanthanum hexaphoride (LaB₆) crystal acts as a thermionic emitter. The lower chamber with sample holder and stage control without breaking vacuum is done by using various pumping techniques with pressure control holes. The beam is passing through a pair of scanning coil which deflect the beam in the x-y axes so it scans in a rectangular area of the sample surface. There are two magnetic condenser lenses and apertures are used to focus the electron stream of about 0.4 nm to 5 nm in diameter and also to eliminate the high-angle electrons from the beam. The objective lens focuses the scanning beam onto the sample. There are suitable detectors to detect the secondary electron emission after the interaction with the sample. The process was repeated until the whole area of the sample and it has been scanned over the CRT screen.

The ejected secondary electrons and backscattered electrons have energy in the range of few 100eV to 40 keV. This sufficient energy stimulates a scintillator and then emitted light amplified using a photomultiplier tube and converted into a digital image. The amount of emitted secondary electrons increases with the angle between the surface and the incoming electron beam. The acceleration voltage between the cathode and the anode is ~0.5 to 30 kV magnitudes under vacuum (~ 10⁻⁶ Pa) in the column of the microscope. SEM image can produce very high-resolution images of the sample, revealing the details ranging from 1 to 5 nm. In scanning electron microscope, a wide range of image is magnified in the range from x25 to x250, 000.

These images have a very large depth of field yielding a characteristic 3D appearance useful for understanding the surface structure of the sample. In SEM analysis, sample preparation is the only requirement and the sample must be conductive to undergo SEM analysis.

In the present study, the surface morphological image of the prepared samples has been studied using SEM-JEOL JS-6390 series scanning electron microscope and is shown in Fig.2.4 (b).



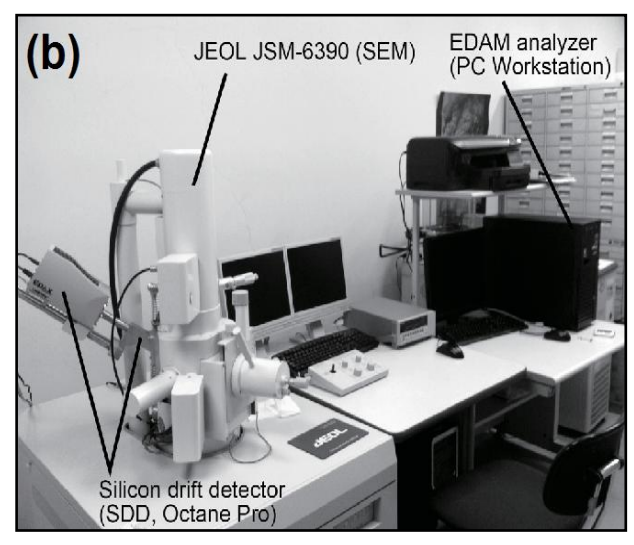


Fig.2.4: (a) Schematic diagram of a SEM and (b) photograph image of a SEM-JEOL JS-6390 apparatus set up

2.3.3 Energy dispersive X-ray spectroscopy (EDX)

Energy dispersive X-ray spectroscopy (EDX, EDS, EDAX or XEDS) is an analytical technique used to identifying the elemental analysis or chemical compositional variation of a sample. The basic principle of EDX characterization relies that each element has a unique atomic structure allowing X-rays to identify each other and it is due to the electromagnetic emission spectrum. EDX works as an energy-resolving device and it present such as a multichannel analyzer, shown in Fig.2.4 (b). EDX also provides the stoichiometry information of the composite material under investigation.

In this technique, the high energy beam of charged particles, such as electrons or protons, or the X-ray beam, is focused into the sample to induce the characteristic X-ray emission from a sample. The ejected electrons during the interactions lead to a second detectable signal (X-ray excitation). Some of the secondary electrons emitted leave behind an inner shell hole of a surface atom and these holes are recombine with electrons. The energy difference between the higher energy and the lower energy orbital shells of the atoms may be released in the form of X-rays as shown in the Fig.2.5. The produced characteristic X-rays are analyzed by two dispersion methods. There are Wavelength Dispersion (WD) and Energy Dispersion (ED) methods. The energy of the X-rays emitted from a sample can be measured by an energy dispersive (ED) spectrometer. In ED system, a lithium drifted silicon detector is placed close to the sample to receive the X-rays. Compared with WD, the ED is fast and convenient in scanning. The whole range of X-rays can be collected and analyzed to allow identification of the element in the region. The EDX pattern displays the different

peaks corresponding to the elements present. This allows the concentration of the elements present in the sample to be measured.

In the present investigation, the presence of elements in the synthesized sample have been identified using energy dispersive X-ray analysis (EDAX, Thermo-Noran system Six) system attached with JEOL JS-6390 scanning electron microscope.

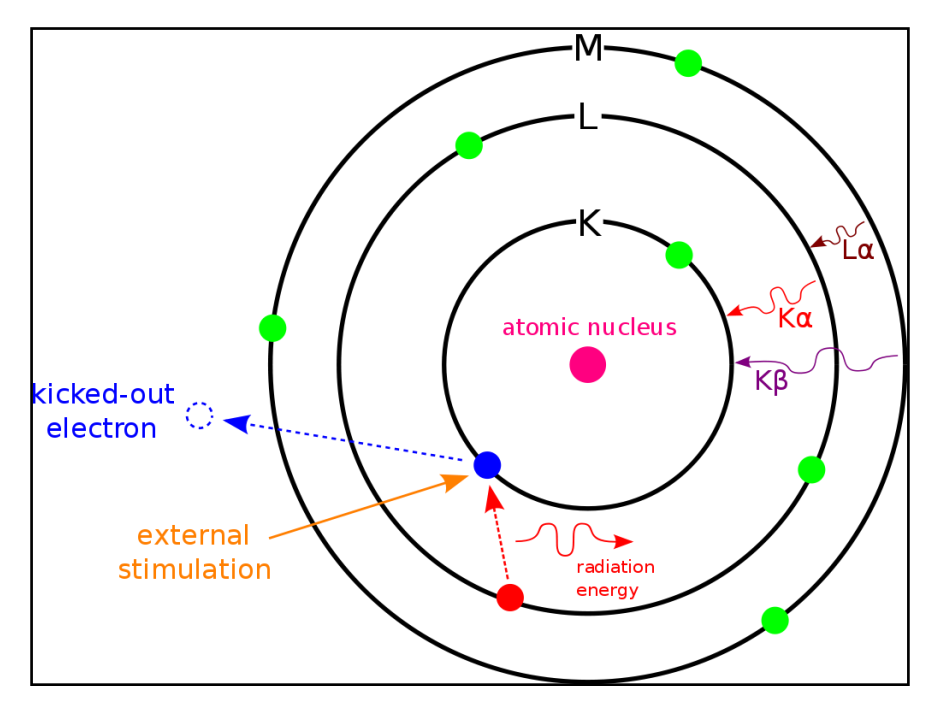


Fig. 2.5: Principle of EDX analysis

2.3.4 Fourier transforms infra-red spectroscopy (FT-IR)

Fourier transform infrared spectroscopy (FT-IR) has become the standard technique, provides specific information about the chemical characterization. IR spectroscopy is a non-destructive technique for identifying chemicals that are organic or inorganic. FTIR can be applied to the analysis of solid, liquids and gases. FTIR spectrometer collects all the wavelengths simultaneously and digitizes the inter-ferro gram, performs the FT function and converted from an interference pattern to displays the spectrum. FTIR is the most powerful tool for identifying the chemicals from paints, polymers, coatings, drugs and contaminants types and chemical bonds

(functional groups). By understanding the IR absorption spectrum, the chemical bonds in a molecule can be determined. FTIR spectrum of undoped sample is typically so unique that they are like a molecular "fingerprint". To identify the organic compounds IR was used, the inorganic compounds are usually identified using these simple spectra. For most common materials the spectrum of an unknown can be identified by comparison to a library of known compounds. To identify few common materials, IR will need to be combined with NMR, emission spectroscopy, mass spectrometry and X-ray diffraction techniques.

FT-IR is typically based on a Michelson interferometer with a movable mirror as shown in Fig. 2.6(a). It consists of a beam splitter, a fixed mirror and a mirror that propagates back and forth, very precisely. The beam splitter is made of a special material that strikes half of the radiation and reflects the other half. Radiation from the source strikes the beam splitter and separates into two beams.

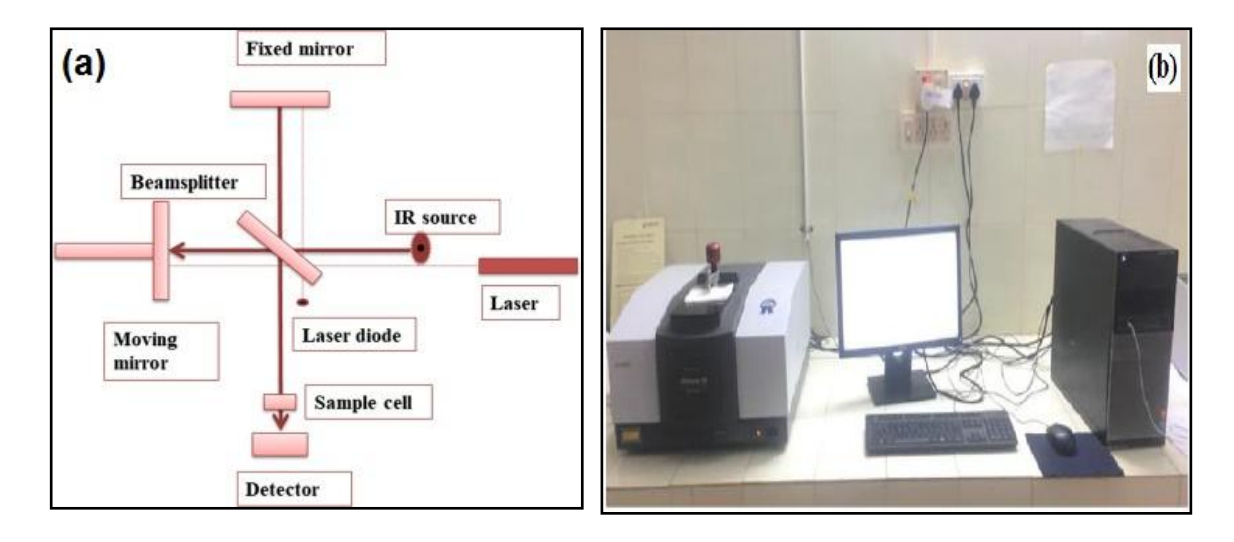


Fig.2.6: (a) Schematic diagram of a FT-IR and (b) photograph image of a FT-IR JASCO 410 apparatus set up

One beam is transmitted to the fixed beam through the beam splitter and the second beam is reflected off the beam splitter to the moving mirror. The fixed and

moving mirrors reflect the radiation back to the beam splitter. Again, half of this reflected radiation is transmitted and half is reflected back at the beam splitter, resulting in one beam passing to the detector and the second back to the source. The frequency of molecular bonds vibration depends on the types of bonds and elements present in the material. For a given specific bond, it can vibrate with a specific frequency and the frequency of vibration corresponds to various high frequency excited state and low frequency ground state. In the present work, samples were analyzed using the JASCO FTIR-410 instrument, shown in Fig. 2.6(b).

2.3.5 UV-Visible Double Beam Spectrophotometer

To study the optical properties, a total wavelength range has been recorded from 190 nm to 1100 nm wavelength. The spectrophotometer is equipped with two light sources, a deuterium arc lamp for ultraviolet (UV) light and a tungsten-halogen lamp for visible and infrared (IR) light as shown in Fig. 2.7 (a). After wards, the light beam passes through a monochromator and is then incident on a sample. With the help of various optical elements, the incident light is directed to the sample and gets absorbed or transmitted it can be collected by a detector. In the present investigation, the optical absorbance spectra of the prepared samples have been recorded using UV-VIS double beam spectrophotometer (SYSTRONICS: AU-2707) at room temperature [Fig.2.7 (b)]. According to the UV-visible spectra, the band gap energy of the sample can be calculated using Tauc's Equation.

$$(\alpha h \upsilon)^{n} = B(h \upsilon - Eg) \qquad ... (2.6)$$

Where α is the absorption co-efficient, h ν is the energy of the incident photon, B is the constant, E_g is the optical band gap energy and n is two different values that characterizes the band gap transition process (n = 2 for direct or n = 1/2 for indirect allowed transition). The electronic transitions between the valence band and conduction band can be direct or indirect.

The value of the band gap (E_g) is obtained by extrapolating the linear portion of the graph to intercept the photon energy axis. The optical method provides a very simple way of finding the band gap as compared to the electrical method using the thermal excitation. Here the excitation is less reliable because of the fact that the effective mass of electron and holes also influence most of the electrical properties.

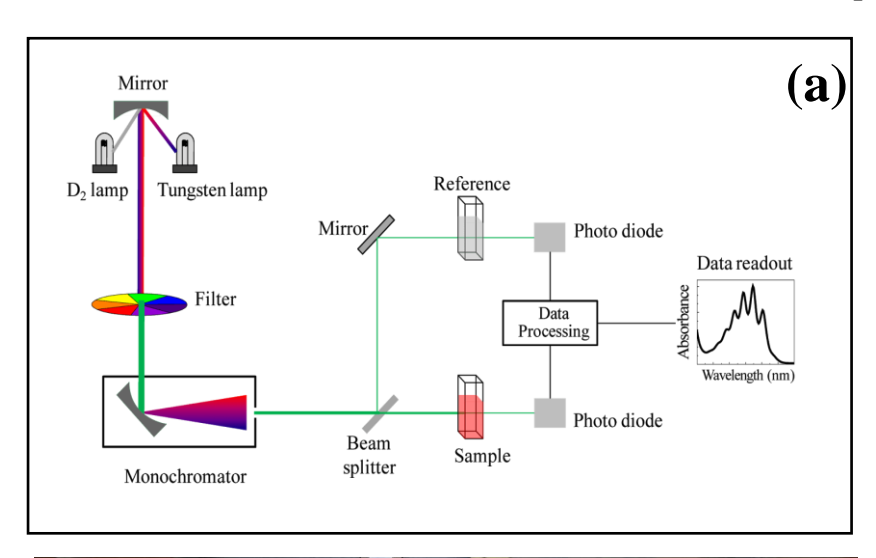




Fig. 2.7: (a) Schematic diagram of UV-Visible analysis (b) Photograph image of a UV2700 apparatus set up

2.3.6 I-V Characteristics

The I-V characteristics were recorded for the samples using a constant DC power supply and Keithley electrometer. The current was recorded as a function of the changing applied potential across the two terminals. DC conductivity was estimated using the Equation 2.7.

$$\sigma_{\rm dc} = \frac{1}{\rho_{\rm dc}} = \left(\frac{1}{R}\right) \times \left(\frac{L}{A}\right) \qquad \dots (2.7)$$

Where R is the resistance, L is the thickness, A is the cross-sectional area, σ is the conductivity, and ρ is the resistivity of the sample. In samples, sheet resistance was calculated using the Equation 2.8,

$$R_{S}=4.532\times\left(\frac{L}{A}\right) \qquad \dots (2.8)$$

Where, 'V' is the measuring voltage and 'I' is the applied current. For resistivity was calculated using the Equation 2.9,

$$\rho = R_S \times t$$
 ...(2.9)

where 't' is the thickness of the sample. The conductivity was calculated using the Equation 2.10,

$$\sigma = \frac{1}{\rho} \qquad \dots (2.10)$$

2.3.6.1 Temperature dependence of conductivity

The temperature dependence of conductivity was determined by placing the pellet in a suitably designed apparatus. The pellet used in this measurement is a sandwich type cell, and it is placed in between two platinum electrodes, which were connected to the two terminals of the keithley electrometer as shown in Fig.2.8.

The apparatus consists of a sample holder, which was enclosed in an electromagnetic shielded cell and it was mounted inside a glass jacket. The entire setup was sealed and connected to a rotary vacuum pump. A small heater was mounted close to the pellet and using a suitable control device the temperature was controlled. A digital temperature indicator connected to a thermocouple was placed near the sample. The temperature was varied from room temperature to about 150 °C at a rate of 3 °C per minute. The change in resistivity with temperature was noted using an electrometer.



Fig.2.8: Photograph of a keithley electrometer 2400 model

2.3.7 Photocatalytic Activity Setup

A specially designed photocatalytic reactor system made of wooden chamber was used for photo degradation experiments. A UV lamp (Philips TUV-08) of 15 W having wavelength 365 nm was kept inside the wooden chamber. Undoped, Ag, Fe doped ZnO and Ag, co-doped Fe-ZnO samples prepared by co-precipitation method and used as a photocatalyst. The photocatalyst with undoped, Ag, Fe doped ZnO and Ag, co-doped Fe-ZnO samples were kept immersed in the methylene blue (MB) or methyl orange (MO) solution, the solution was stirred for 10 min, and then kept in the

dark for an hour to achieve adsorption equilibrium. When affixed onto the support, doped ZnO samples offer higher surface to volume ratio compared to undoped ZnO, allowing higher adsorption of the target molecules [9]. The sample was then transferred into the photo reactor for UV exposure and the lamp was turned on and approximately 5 ml mixture of photocatalyst and MB or MO solution. The dye-solution with the undoped, Ag, Fe doped ZnO and Ag, co-doped Fe-ZnO was exposed to light for 30 minutes interval at room temperature. The concentration of MB and MO in the solutions was ascertained by referring to the absorption concentration standard curve which was obtained by measuring the optical absorption of MB (λ =665 nm) and MO at (λ =464 nm) using UV–Vis double beam spectrometer. In the present work the undoped, Ag, Fe doped ZnO and Ag, co-doped Fe-ZnO samples were analyzed using the photodegradation experimental setup shown in Fig.2.9.

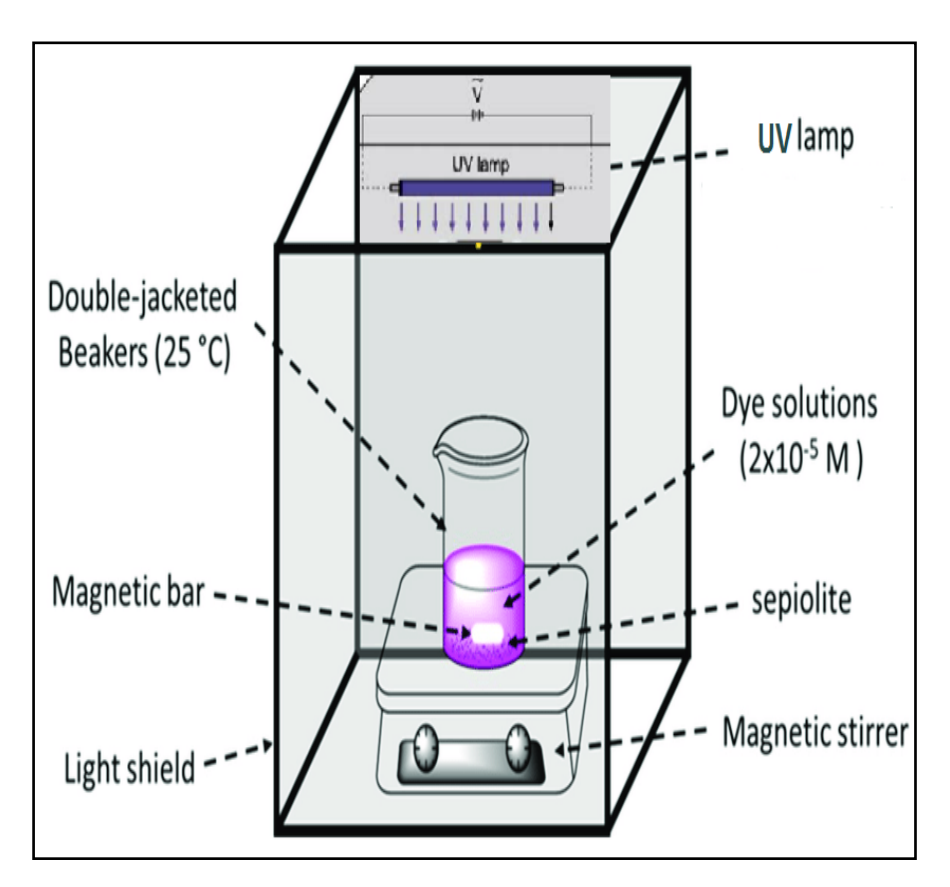


Fig. 2.9: Photograph of a photo degradation experimental setup.

References

- [1] CS Kim, K Okuyama, K Nakaso, M Shimada M. J. Chem. Eng. of Japan, 37, 11, (2004) 1379–1389.
- [2] TS Sudarshan, Advances in Surface Treatment: Research & Applications (ASTRA), Proceedings of the International Conference, Hyderabad, India, (2003) 412–422.
- [3] YW Wang, LZ Zhang, KJ Deng, XY Chen, ZG Zou. J. Phy. Chem. C, 111, (2007) 2709–2714.
- [4] O Carp, CL Huisman, A Reller, Prog. Solid State Chem. 32 (2004) 33–177.
- [5] J Rousseau, Basic Crystallography, Sussex: John Wiley & Son Ltd, 1998.
- [6] H Morkoç, U Özgür, Zinc Oxide- Fundamentals, Materials and Device Technology, Wiley: Germany, 2009.
- [7] K.P Biju, M.K Jain. Thin Solid Film, 516 (2008) 2175–2180.
- [8] BD Cullity, Stock, Elements of X-Ray Diffraction, 3rd ed., Prentice Hall, 2001.
- [9] S Baruah, RF Rafique, J Dutta. NANO 3 (2008) 399–407.

CHAPTER – III

CHAPTER – III

Efficient photocatalytic degradation of organic dyes using Fe-doped ZnO nanoparticles

3.1 Introduction

In recent years, many hazardous organic pollutants, such as toxic dyes and organic residuals released into the atmosphere from several industries [1, 2]. The degradation and full-mineralization process are vicious, because of merged structure of organic dyes. Among these organic dyes, methylene blue (MB:C₁₆H₁₈N₃SCl) and methyl orange (MO: C₁₄H₁₄N₃NaO₃S) are the most important dyes which are used in textile industries and very harmful to human. Because they cause increased heart rates, cyanosis, shock, sickness, injuries to tissue and various skin infections. They also highly harmful to the atmosphere, which then poses a threat to the health of cattle's and animals [3].

Industrial wastewater treatment and recycling are fundamental objectives to secure the worldwide biological system and improve the environment quality. Various techniques have been extensively utilized to suppress pollutants from contaminated water sources [4, 5]. Among them, photocatalysis has emerged to be a promising way to control the massive scale's current environmental pollution. The photocatalysts with semiconducting nanostructures have concerned much more attention due to their exceptional physico-chemical properties in the photocatalytic reaction [6-8].

Many researchers recently developed various photocatalysts using metal oxide semiconductor nanoparticles, including Bi₂O₃, TiO₂, ZnO, and WO₃. Among these transition metal oxides, zinc oxide (ZnO) is found very sensible in the photocatalytic

method due to their wide-bandgap, non-toxicity, and high photosensitivity [9-11]. ZnO is a wide-bandgap semiconductor with a direct energy bandgap (Eg≈3.37 eV) [12]. ZnO nanoparticles are especially attractive for many interesting nanotechnology applications such as transparent conductive coatings [13], photoanodes for dyesensitized solar cells (DSSCs) [14], gas sensors [15] and electro-photo luminescent materials [16]. Unfortunately, ZnO can only absorb UV light [17] and photocatalytic degradation efficiency was confined by the electron–hole charge carriers, low-adsorption, and low-reusability.

To rectify this problem, numerous reports focused on doping ZnO with transition metal (Fe, Co, Mn) ions [18], non-metal (N, C, S) ions [19] and noble metals loading (Ag, Au, Pd) [20] have been carried out. Wu *et al.* reported that compared with pure ZnO nanoparticles, ZnO based materials are potential photocatalysts, That can be used as the scaffold or the coating layer in various heterostructures [21–23]. Various techniques for the synthesis of pure ZnO and Fedoped ZnO nanoparticles are reported in the literature: hydrothermal method [24], combustion [25], and sol–gel method [26]. Among these synthesis methods, coprecipitation [27], is a flexible method for synthesizing the ZnO nanoparticles due to its low-cost, and easy to operate.

Several studies have been reported that the doping of ZnO with transition metal ions for visible light photocatalysts [28, 29]. It has been discovered that 2% Fe-doped ZnO degraded the methyl orange dye up to 80.8% within 210 min. under sun-light irradiation. The Fe doped ZnO degrades MB in 4h in sun light [30]. Zhang *et al.* investigated that Fe/ZnO nanowires is obviously superior to that of P25 against MO

[31]. Abbad *et al.* synthesized a Fe-doped ZnO nanoparticle and degraded 2-chlorophenol in aqueous solution under solar irradiation. The most significant photocatalytic action was accomplished with the optimized dopant centralization of 0.5 wt% Fe because of the small crystallite size and low bandgap with a low oxidation–reduction potential [32].

In the present chapter deals the various properties of an efficient Fe-doped ZnO nanoparticles for photocatalytic reaction. The effect of various dopant concentrations on structural, morphological, optical, and electrical properties of ZnO nanoparticles was investigated. Furthermore, the photocatalytic degradation of MB and MO dye under UV light irradiation was investigated in detail.

3.2 Synthesis of pure ZnO, Fe-doped ZnO (ZnO-Fe $_x$, x \approx 0.05, 0.075 and 0.1%) nanoparticles

In the present study pure ZnO and Fe-doped ZnO nanoparticles with various mol. % ($x \approx 0.05, 0.075$, and 0.1) were synthesized by using co-precipitation method.

3.2.1 Materials

All the chemicals used were analytical reagent (AR) grade obtained from Alfa Aesar chemicals, India. The chemicals such as zinc nitrate hexahydrate $[Zn(NO_3)_2 \cdot 6H_2O]$, ferric nitrate nonahydrate $[Fe(NO_3)_2 \cdot 9H_2O]$, sodium hydroxide [NaOH] methylene blue (MB) and methyl orange (MO) were used for the experimental process.

3.2.2 Preparation of Pure ZnO Nanoparticles

Zinc nitrate hexahydrate [Zn (NO₃)₂·6H₂O] and sodium hydroxide [NaOH] is taking as apparent materials to prepare pure ZnO nanoparticles. 10 g of zinc nitrate hexahydrate was dissolved into 20 ml of deionized water (DW) and stirred for 30 min. at room temperature in beaker. 8 g of sodium hydroxide was mixed with 100 ml of DW in another beaker. The sodium hydroxide was added drop by drop into the zinc nitrate hexahydrate under continuous stirring until to reach pH 11. The mixture solution was stirred for 2hr at room temperature. The obtained solutions were centrifuged, washed three times with DW and ethanol. After centrifugation, the precipitates are deposited in the beaker and dried in vacuum oven at 100 °C for 2hr [12]. The collected samples have been annealed at 450 °C for 1h using muffle furnace in silica crucible.

3.2.3 Preparation of Fe-doped ZnO (ZnO-Fex, $x \approx 0.05$, 0.075 and 0.1%) Nanoparticles

The ferric nitrate nonahydrate [Fe(NO₃)₂·9H₂O] was used as a precursor to prepare Fe doped ZnO nanoparticles. Various concentrations of ferric nitrate nonahydrate (0.05, 0.075 and 0.1 mol. %) was added into the zinc nitrate hexahydrate solution. Then sodium hydroxide was added drop wise to the above-mentioned solutions. The color was tuned around white to brownish color. After that the solutions were centrifuged and dried in a similar way as mentioned above. Finally, the obtained Fe-doped ZnO nanoparticles were annealed at 450 °C for 1h. Fig.3.1 depicts the detailed preparation procedure of pure and Fe-doped ZnO nanoparticles.

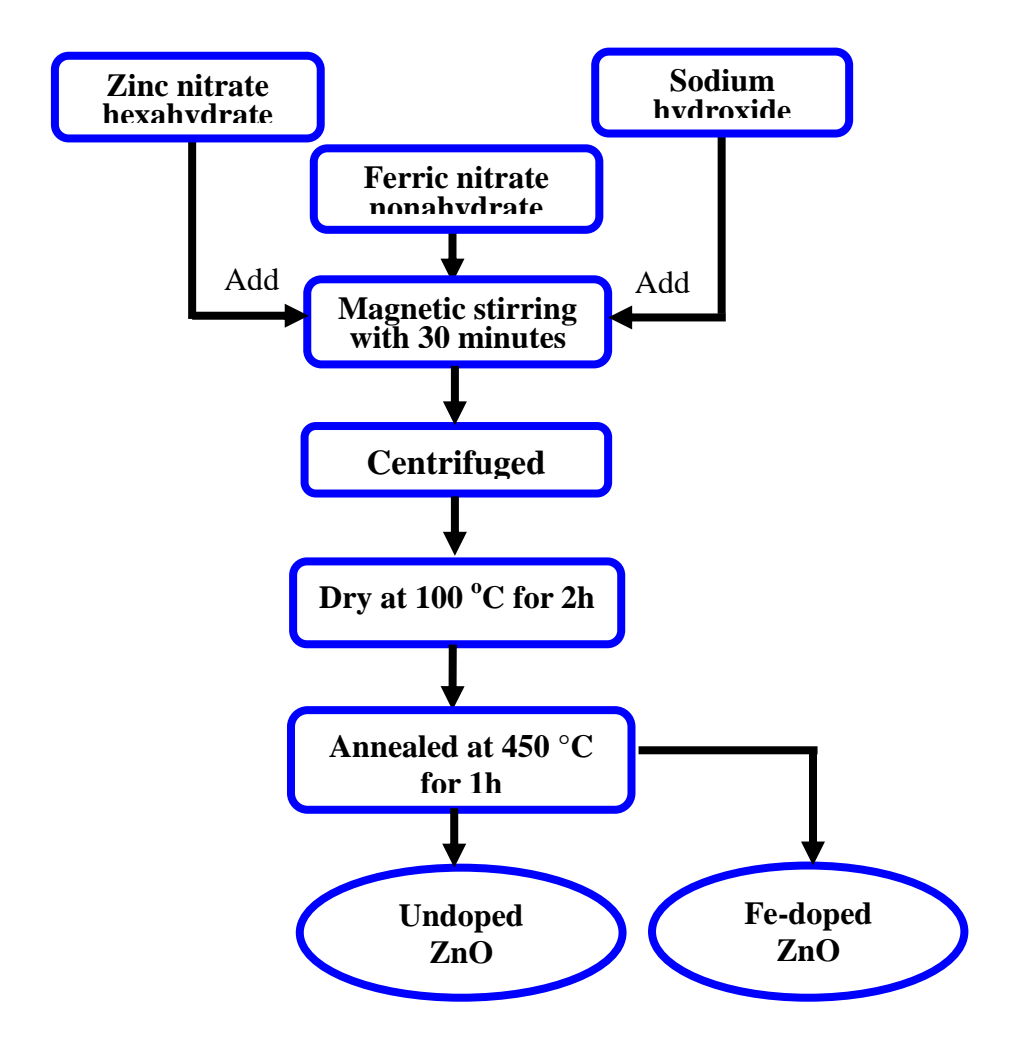


Fig.3.1: Flow chart depicting the preparation of the pure and Fe-doped ZnO nanoparticles

3.3 Characterization Techniques

Various important properties like structural, morphological, optical and photocatalytic activities of all the prepared samples were studied by X-ray diffraction technique (XRD), Scanning Electron Microscopy (SEM), FTIR, I-V and UV-Visible spectroscopy techniques. The obtained results of all the characterization techniques were briefly explained in the following chapters.

3.3.1 XRD Analysis

The crystal phase formation and structural properties of pure and ZnO-Fe_X nanoparticles were characterized by powder X-ray diffractometer (X'PERT PRO MPD) using CuK α radiation (λ = 0.15405 nm) operated at 40 kV voltage and 30 mA current with a scanning rate of 2° per min. The powder XRD characteristic patterns of ZnO-Fe_x (x \approx 0, 0.05, 0.075 and 0.1%) nanoparticles are shown in Fig. 3.2(a). All the XRD diffraction peaks are indexed to hexagonal structure of crystalline ZnO, further confirmed from the standard JCPDS No. 36-1451 (a = 0.325 nm and c = 0.5207 nm) [33, 34]. There are no characteristic peaks of Fe phases, or its oxides were not detected in samples.

Fig.3.2 (b) reveals that the magnification of primary peak at 31.8 (100), 34.3 (002) and 36.3° (101), it shows a minor shift in the 0.05, 0.075 and 0.1% Fe-doped ZnO. The ionic radii of Fe^{3+} and Zn^{2+} are different ($Fe^{3+} = 0.68$ Å and $Zn^{2+} = 0.74$ Å). This result suggests that the Fe ions substituting into the ZnO lattice [35]. The average crystalline sizes (D) of the ZnO-Fe_x was determined from the Debye–Scherrer equation (Eq. 1) [36]

$$D = 0.9\lambda/\beta \cos\theta \qquad \dots (2)$$

Where ' λ ' is the wavelength of the X-rays (1.5406 Å), β is the full width half maximum of the peak (FWHM), ' θ ' is the diffraction angle of the X-rays (1.5406 Å), respectively. The lattice parameters and average crystalline size of the samples are listed in Table 3.1.

Table: 3.1. The lattice parameters and average crystallite size of $ZnO-Fe_x$ nanoparticles

Fe Doping Concentration (mol. %)	Hkl	20 (degree)	a[Å]	c[Å]	Crystallite size (nm)
ZnO	(100)	31.77			
	(002)	34.40	3.24	5.20	23.53
	(101)	36.30			
ZnO-Fe _{0.05}	(100)	31.81			
	(002)	34.23	3.25	5.21	21.66
	(101)	36.37			
ZnO-Fe _{0.075}	(100)	31.71			
	(002)	34.43	3.25	5.20	16.23
	(101)	36.17			
ZnO- Fe _{0.1}	(100)	31.81			
	(002)	34.23	3.24	5.20	12.03
	(101)	36.23			

The average crystallite size (D) of ZnO – Fe_x calculated from XRD data are 23, 21, 16 and 12 nm, respectively. Furthermore, the increasing Fe content reduces the lattice parameters and average crystallite size. Previous reports reported by Jeyachitra *et al.* [12] in Fe-doped ZnO nanoparticles, Srinivasan *et al.* [37] in Mn-doped ZnO and Nahm *et al.* [38] in V₂O₅-doped ZnO ceramics are also similar to the obtained results.

The obtained result shows that there is no change in the peak positions of ZnO with the dopants. This result verifies that there is no additional phase formation due to the doping [12]. In addition to this, the high intensity peak of un-doped ZnO was linearly decreases with increase of dopant concentration and it is clearly observed in the XRD pattern.

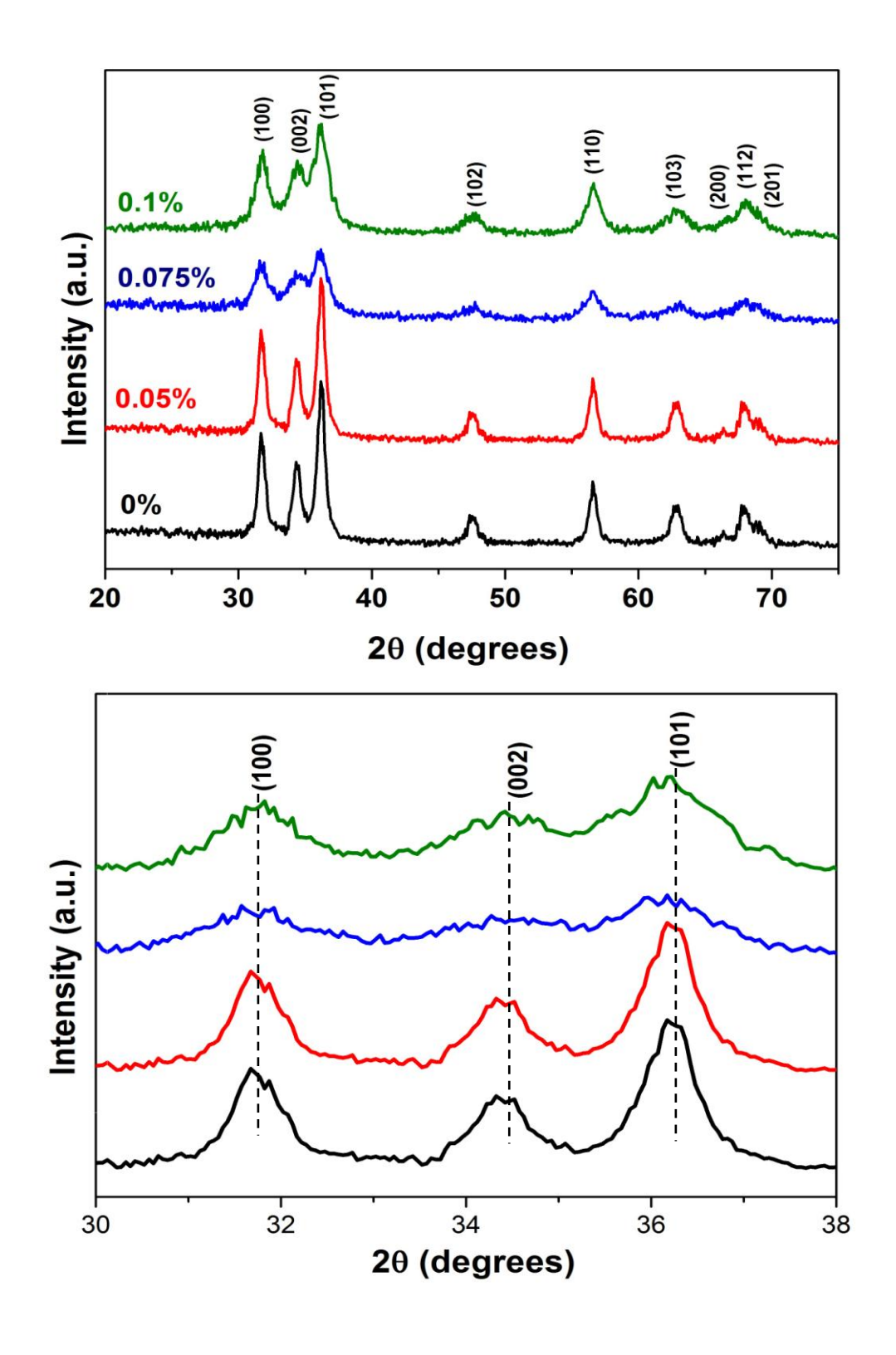


Fig.3.2: (a) XRD patterns of (a) pure ZnO and Fe-doped ZnO nanoparticles (b)

Fe concentration dependent shift in primary diffraction peaks

3.3.2 SEM Analysis

The surface morphology of pure and ZnO-Fe_X nanoparticles were analyzed by using by scanning electron microscope (SEM-JEOL JS-6390) with energy dispersive X-ray spectrometer (EDX) 21. SEM images of ZnO-Fe_x ($x\approx0$, 0.05, 0.075 and 0.1 mol. %) nanoparticles are given in Fig.3.3. Fig.3.3 (a) shows the surface morphology of pure ZnO with crystalline size of ~42-68 nm. Interestingly, when the Fe concentration was 0.05 mol.%, the ZnO nanoparticles are turned into spherical and it is shown in Fig.3.2(b). Fig.3.3(c-d) shows turning of needle and spherical like structures due to the doping of 0.075 to 0.1 mol. % of Fe-dopants in ZnO nanoparticles. Compared with pure ZnO, 0.1 mol. % of Fe-doped ZnO shows more information on the surface. The images clearly exposed that the surface morphology changed with the addition of Fe concentration, the agglomerated particles breaks and pores were created and then finally reduced into spherical nanoparticles. It can also be noticed that the size and morphology of ZnO-Fe_x nanoparticles enhanced with the dopant concentration. The reason for the variation of surface morphology with dopant concentration is due to the changes of alkalinity of the precursor solution and it varies the grain growth.

3.3.3 EDX Analysis

Fig.3.4 (a-d) shows the EDX analysis of the prepared samples and it was used to investigate the chemical composition of pure and ZnO - Fe_X nanoparticles. EDX spectrum of pure ZnO shows the existence of characteristic peaks of oxygen (O) and zinc (Zn) elements (Fig.3.4a). The atomic percentage of these elements found to be 49.5 and 50.5%, respectively. Fig.3.4 (b-d) shown the EDX spectra of ZnO- Fe_X nanoparticles also include elements such as O, D and D and D respectively. The inset of

EDX image $ZnO-Fe_x$ nanoparticles data was given in table format. The measured Fe concentration of 0.05, 0.075 and 0.1 mol. %, are about 2.71, 14.94 and 18.21%, respectively. The observed atomic percentage values almost match well with the samples.

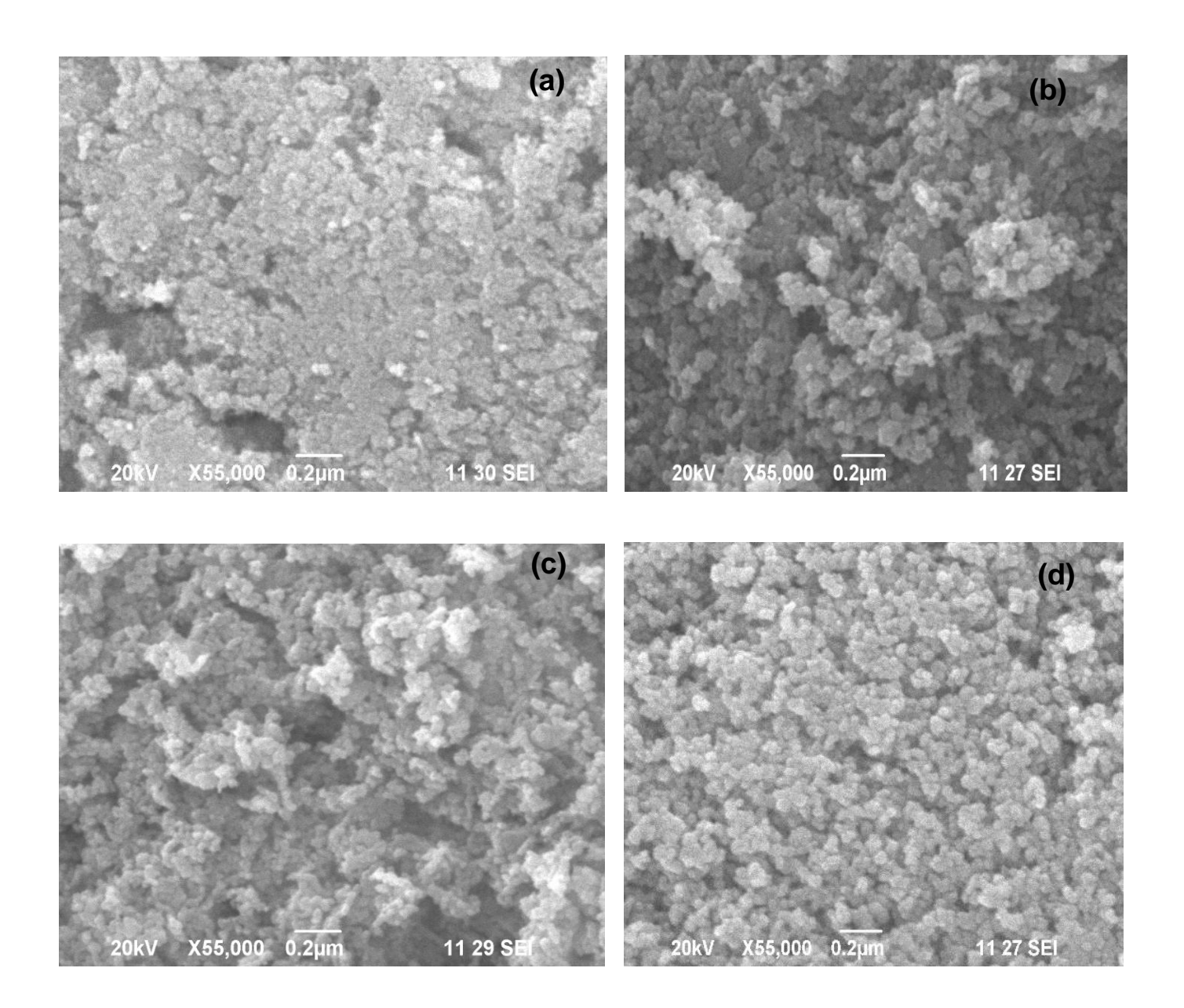


Fig.3.3: SEM images of (a) pure ZnO (b) 0.05, (c) 0.075 and (d) 0.1 mol. % Fedoped ZnO nanoparticles

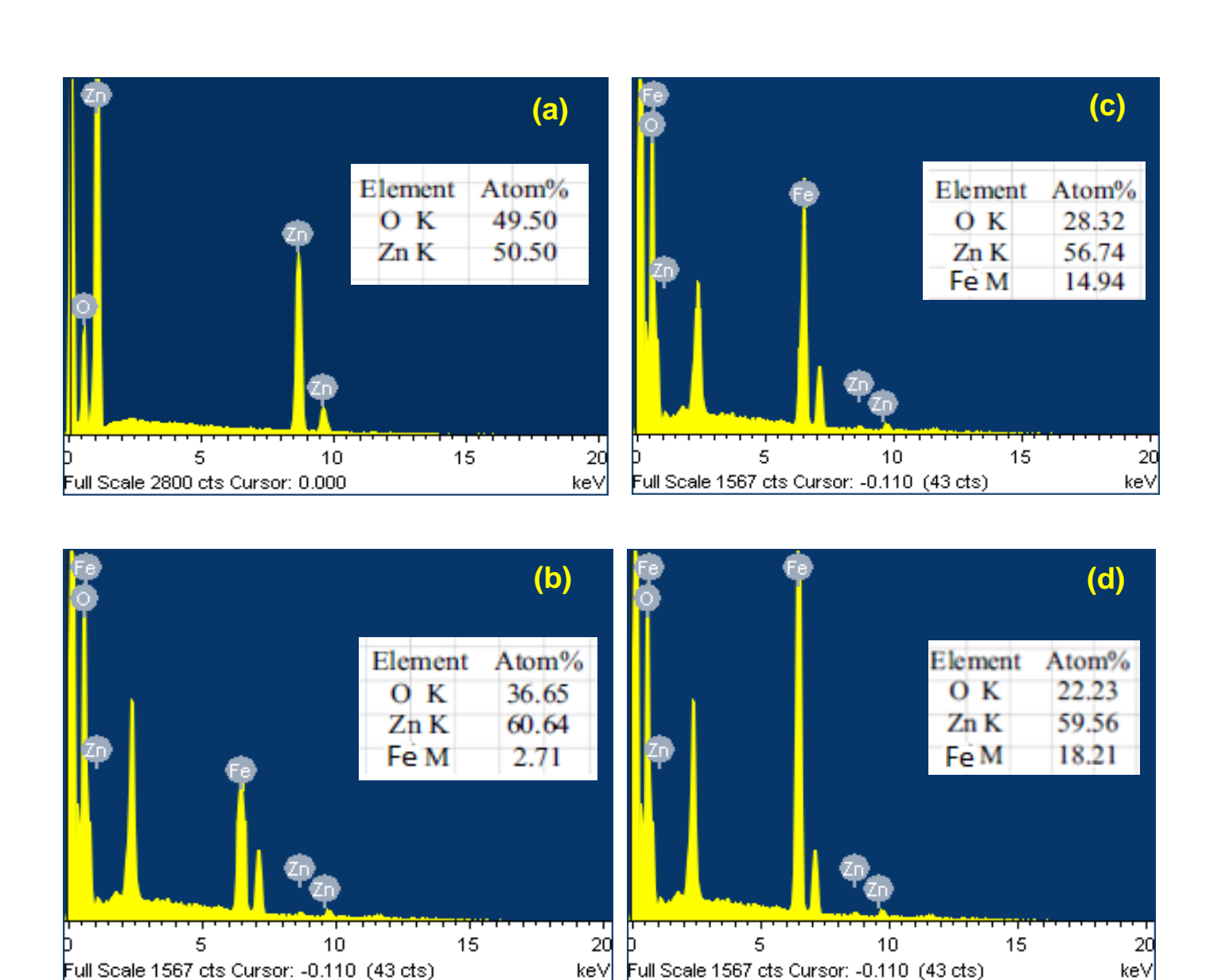


Fig.3.4: EDX images of (a) pure ZnO (b) 0.05, (c) 0.075 and (d) 0.1 mol.% Fedoped ZnO nanoparticles

3.3.4 UV-Visible Absorption Spectra

The optical properties of pure and ZnO-Fe $_X$ nanoparticles have been studied using UV-Vis double-beam spectrophotometer (Systronics: AU-2707). UV-absorption spectra of ZnO-Fe $_X$ (x \approx 0, 0.05, 0.075 and 0.1 mol. %) nanoparticles are shown in Fig.3.5 (a-d). The red-shift is due to the increase of crystallite size, and it was confirmed from the XRD results. The optical bandgap of ZnO and ZnO-Fe $_X$

nanoparticles was calculated using Tauc plot or from the formula Eg = hc/λ [39]. The calculated optical band gap values are 3.90, 3.89, 3.86 and 3.82 eV, which corresponds to pure ZnO and 0.05, 0.075 & 0.1 mol. % Fe-doped ZnO nanoparticles.

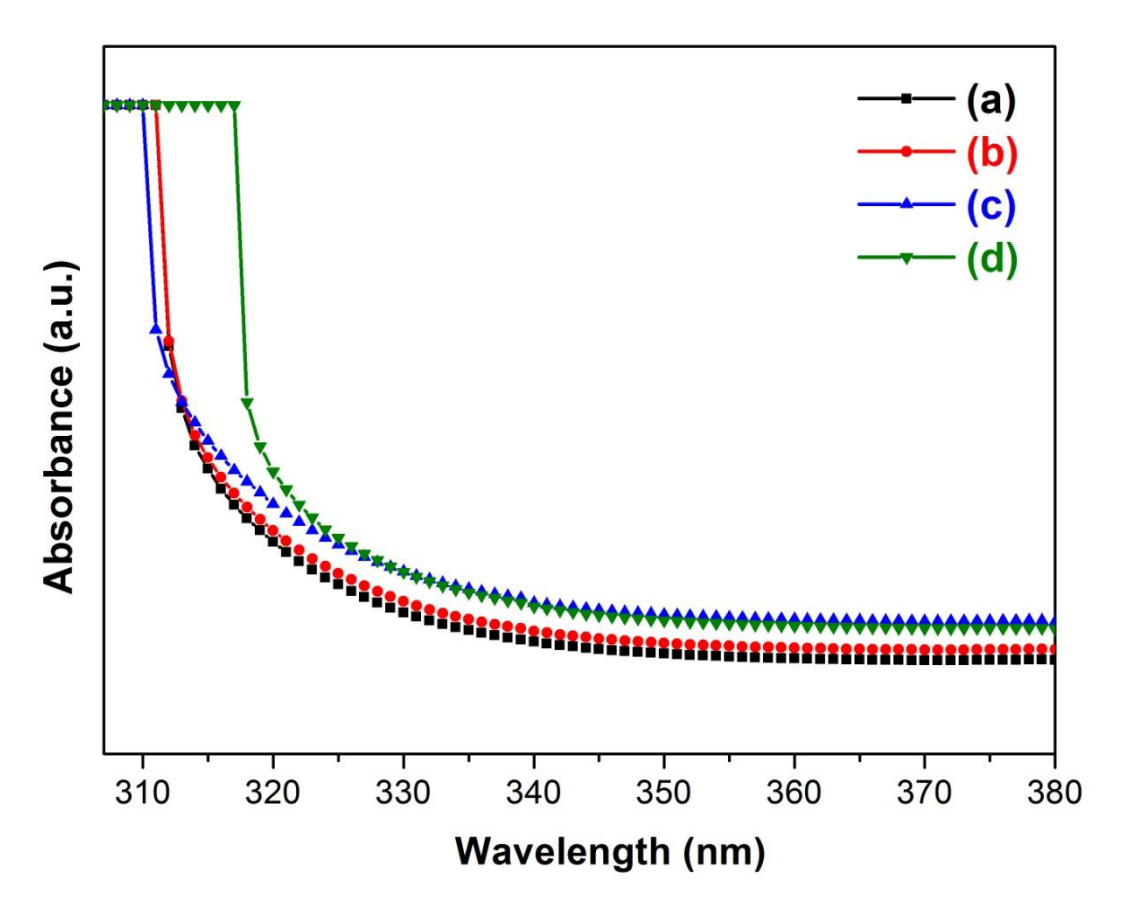


Fig.3.5: UV-Vis absorbance spectra of (a) pure ZnO (b) 0.05, (c) 0.075 and (d) 0.1 mol.% Fe-doped ZnO nanoparticles

The reduction of band gap is due to the formation of new defect states with dopant or the diffusion of dopants in the material. Similar result was also observed by Hassan et al. [40]. The substitute of Fe^{3+} with Zn^{2+} ions shares the oxygen with Zn atoms and reduces the band gap of the material.

The obtained absorbance spectrum clearly depicts the variation of absorbance from 310 to 350 nm. This variation is due to the intrinsic bandgap absorbance of ZnO or transitions of electrons from the valence band to conduction band.

3.3.5 FT-IR Analysis

Fourier Transform Infrared (FT-IR) spectra of prepared samples were recorded by using a FTIR Spectrometer (JASCO FTIR-410) in the range 400–4000 cm $^{-1}$ a resolution of 4 cm $^{-1}$ at room temperature using KBr disc. The FT-IR spectra of ZnO-Fe_X (x \approx 0 and 0.1 mol. %) nanoparticles in the range 4000–400 cm $^{-1}$ are presented in Fig.3.6 (a, b). The broad absorption band appearing in the range 3452–3446 cm $^{-1}$ corresponds to O–H stretching vibration, while the two peaks located at 1625 and 1591 cm $^{-1}$ is due to –OH bending vibration of the adsorbed H₂O molecules [41]. The bands lower intensity absorbed around 2380 cm $^{-1}$ which corresponds to the symmetric and asymmetric C–H bond.

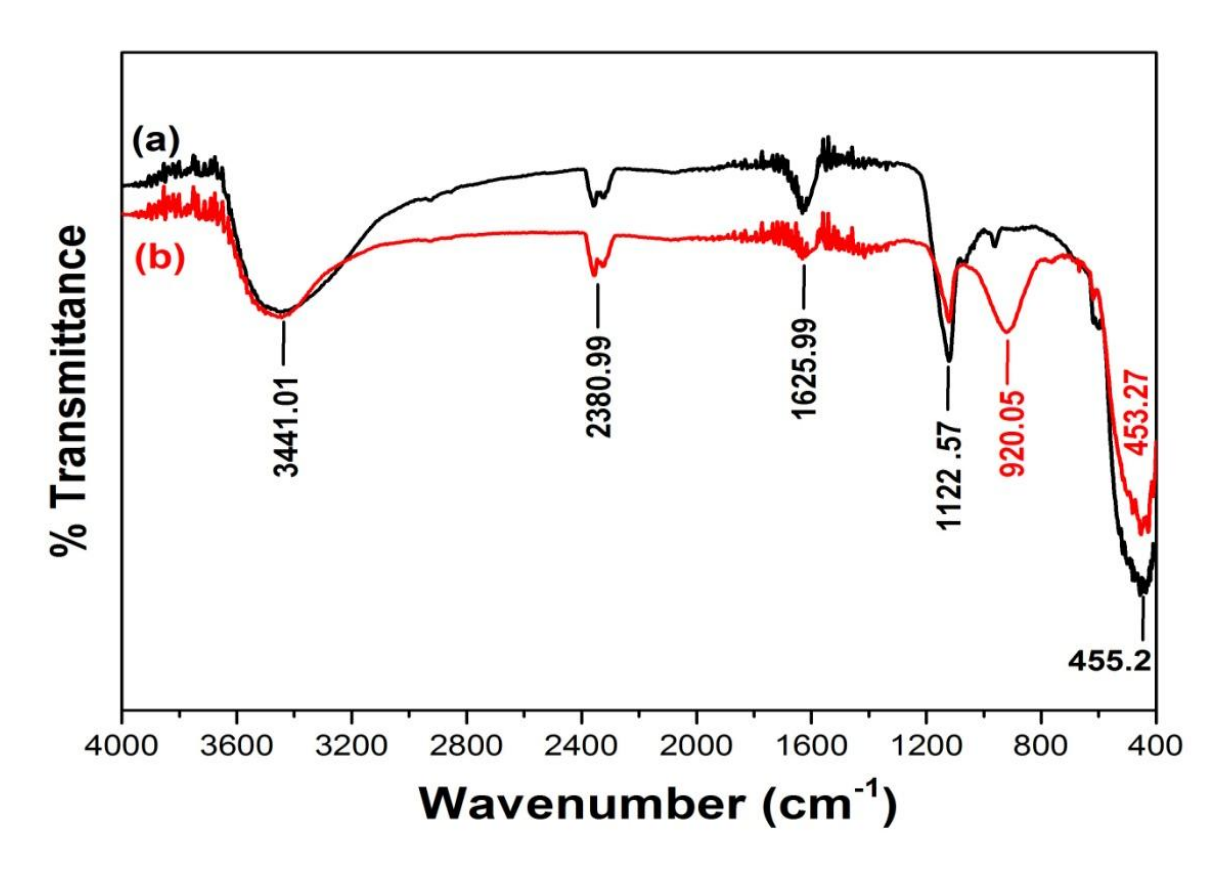
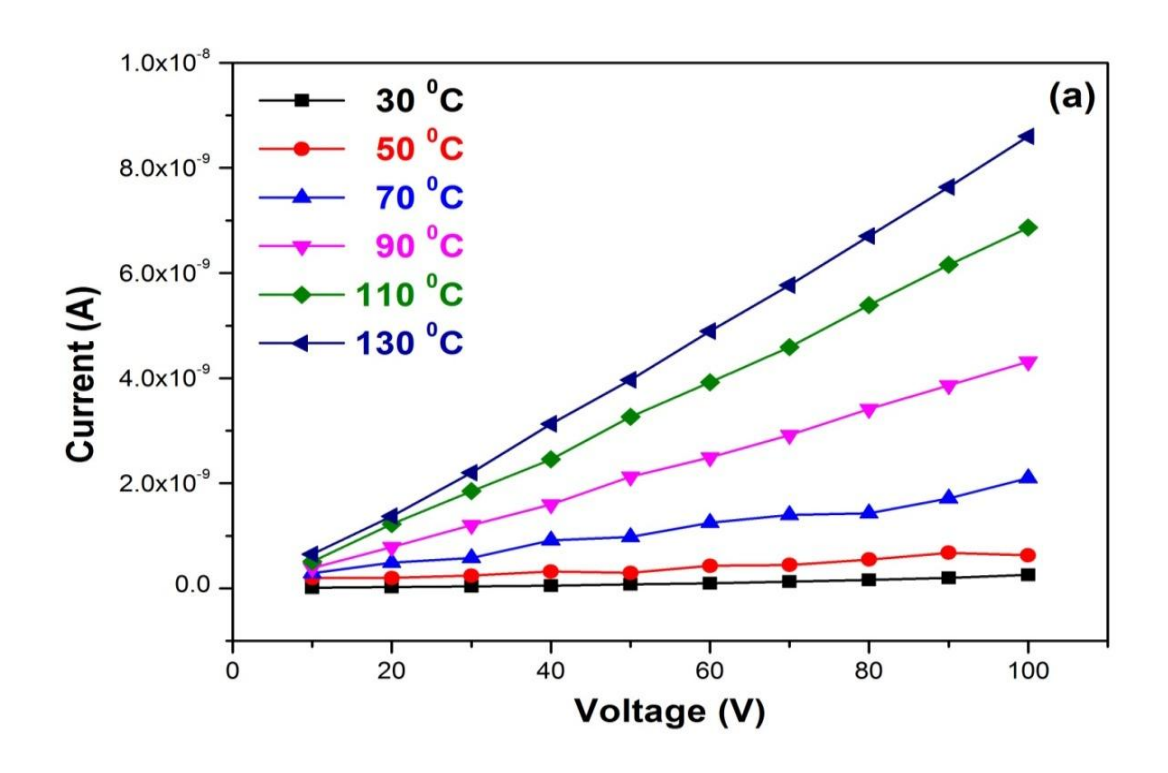


Fig.3.6: FT-IR spectra of (a) pure ZnO and (b) 0.1% Fe-doped ZnO nanoparticles

Two weak absorption peaks at 428 and 449 cm⁻¹ is due to Zn–O stretching mode for pure ZnO nanoparticles; similarly, for 0.1 mol.% Fe doped ZnO samples this is pointed out from absorption peaks in the range of 449 cm⁻¹ for pure and 0.1 mol.% Fe-doped ZnO sample may corresponds to Zn–O stretching mode. The absorption peaks located at 1120, 1122 and 800 cm⁻¹ attributed to the sulfate group, respectively [42]. Also, FTIR spectra of 0.1 mol. % Fe-doped ZnO shows that the small stretch observed at 601 cm⁻¹ corresponds to Fe–O stretch, as reported by Liu *et al.* [42]. Therefore, it might be due to Fe³⁺ ions substituted in Zn.

3.3.6 I-V Characteristics

The electrical properties of pure and ZnO-Fe_X nanoparticles has been confirmed by the study I-V analysis at different temperatures using Keithley electrometer (2400 model). I-V characteristics of ZnO-Fe_X ($x \approx 0$ and 0.1 mol. %) nanoparticles determined using Ag-paste for better electrical contact and the result is shown in Fig.3.7. From these curves, DC electrical conductivity measurement of ZnO-Fe_X ($x \approx 0$ and 0.1 mol. %) nanoparticles taken under varying temperatures of 30, 50, 70, 90, 110 and 130 °C (Increase of 20 °C). Thus, it increases the conductivity of 0.1% Fe-doped ZnO nanoparticles due to the increase in the mobility of charge carriers [43]. The remarkable increase in these samples may result in a higher advantage for optical device fabrication.



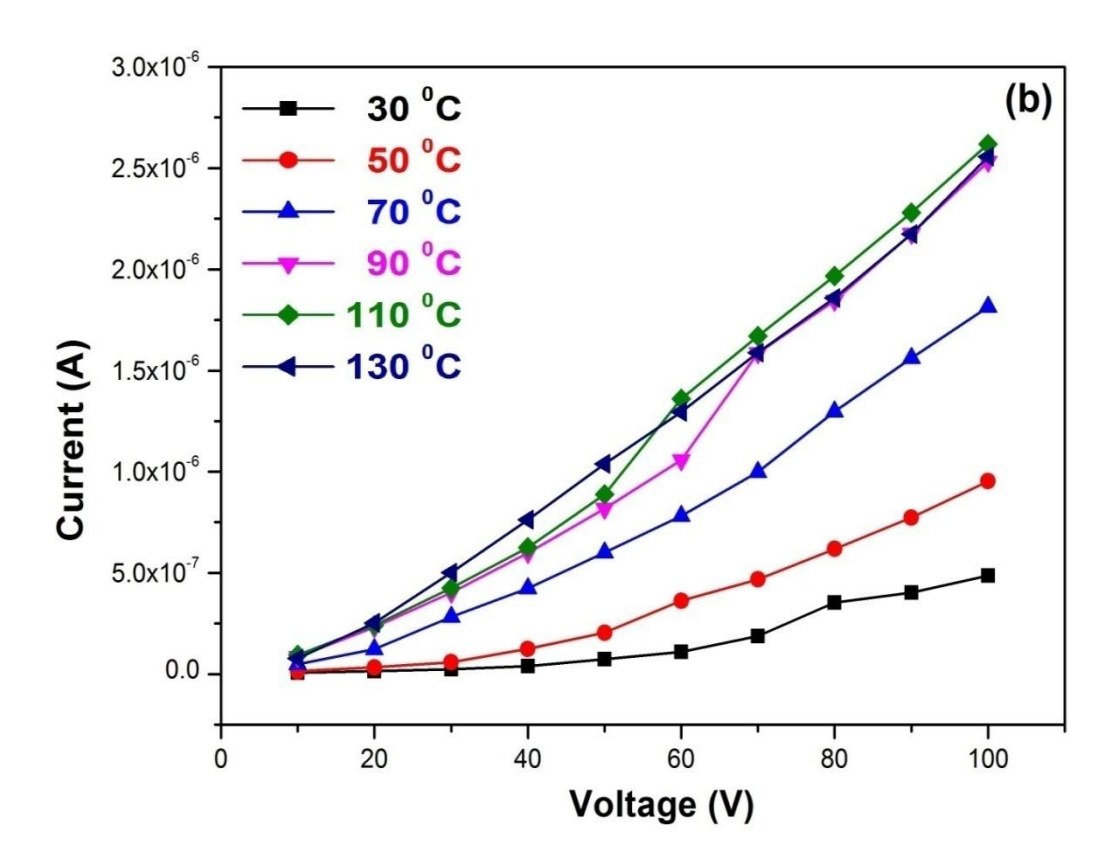


Fig.3.7: I-V characteristics of (a) pure ZnO and (b) 0.1% Fe-doped ZnO nanoparticles

3.4 Photocatalytic Degradation of MB and MO

The photocatalytic activity of pure and ZnO-Fe_X nanoparticles was evaluated by the degradation of MB and MO under UV light irradiation (8 W Philips). 20 mg of ZnO-Fe_x photocatalysts were dissolved in 20 ml aqueous MB and MO dye solution at various pH (2, 4, and 6). The dye solutions with ZnO-Fe_x photocatalysts were exposed to UV light from 0 to 180 min. at room temperature. Every 30 min, sampling out 2 ml of dye solution collected from samples for photocatalytic degradation test. The photocatalytic degradation of MB and MO was observed λ_{max} at ~664 and 464 nm respectively using a UV-visible spectrophotometer in the wavelength range 200–800 nm. Time dependent UV-vis spectra of both MB and MO dye degradation using undoped and Fe doped nanoparticles are shown in Fig.3.9 and 3.10. The rate of degradation was noted with reverence to the change in the intensity of absorption peak in the visible region.

3.4.1 Influence of pH

The adsorption of MB and MO dye molecules on pure ZnO nanoparticles strongly depends on the solution's pH and is displayed in Fig.3.8 (a). The influence of pH on the photodegradation of MB and MO dye was studied by varying the solution's pH from 2 to 6. The outcome shows that photodegradation was maximum in base medium. The degradation arrives at most extreme at pH 6 and decreases sensibly up to pH 2. Henceforth, the pH 6 was accepted as an ideal pH and utilized for additional investigation.

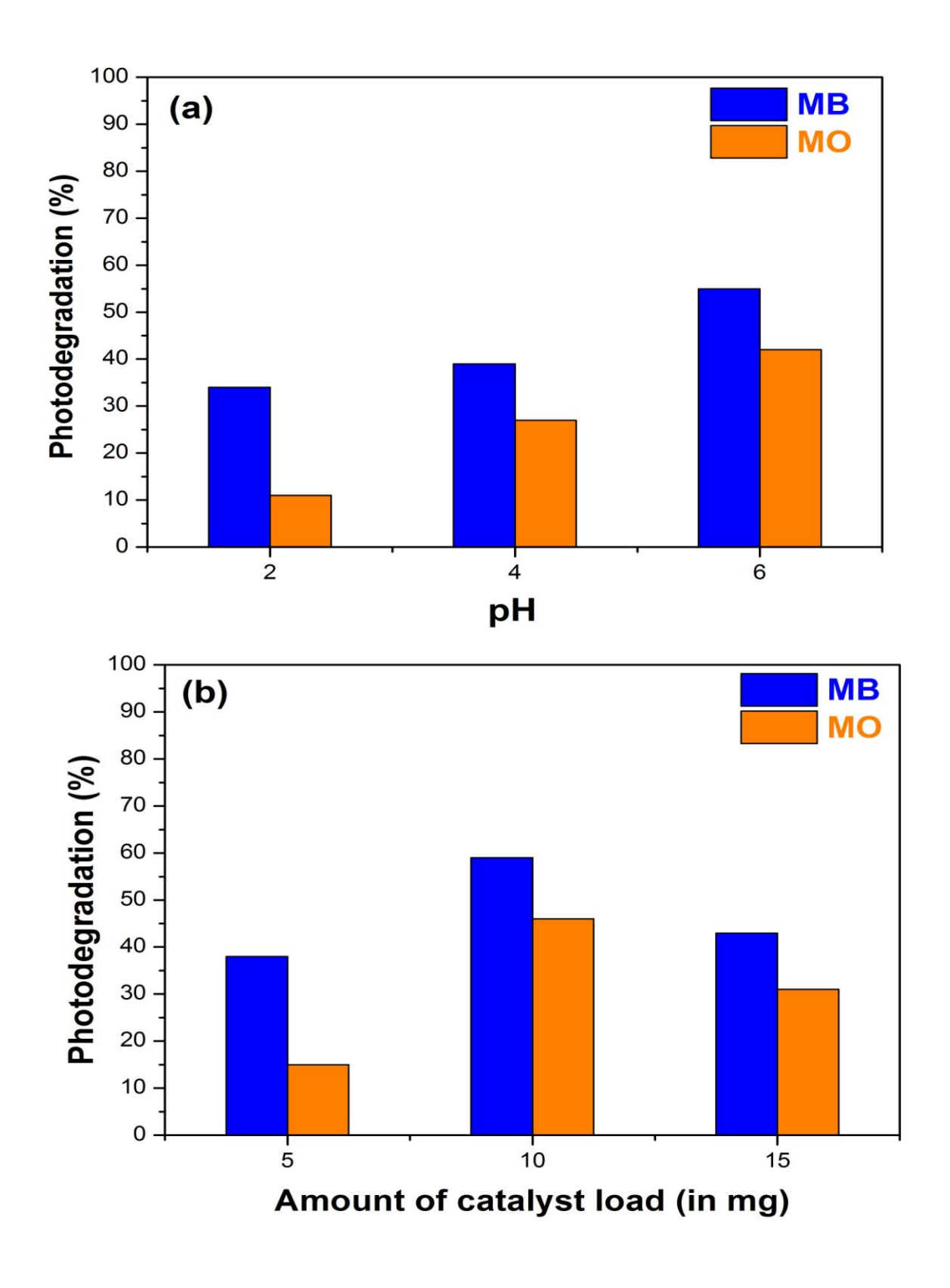


Fig.3.8: (a) Influence of pH and (b) catalyst concentration on the photodegradation of MB and MO

3.4.2 Influence of catalyst concentration

The influence of catalyst concentration on the photodegradation of MB and MO dye was verified using ZnO catalyst concentrations from 5 to 15 mg/30 ml in 10 ppm MB, and MO dye solution at pH 6 and it is displayed in Fig.3.8 (b). The variation in photodegradation can be clarified by accessibility of several surface-active sites and UV light radiation into dye solution. The photodegradation reaches maximum at 10 mg/30 ml. The reduced photodegradation at higher catalyst concentration (15 mg/30 ml) may be due to ZnO nanoparticles aggregation increases the scattering effect [44]. Consequently, 10 mg/30 ml ZnO photocatalyst was expected as an ideal catalyst weight.

3.4.3 Influence of UV irradiation time of MB

The photocatalytic activity was carried out with MB concentration of 2.0 mM, catalyst concentration of 10 mg, pH 6 and irradiation time up to 150 min. Fig.3.9 (a–d) show the variation in absorption spectra of MB illuminated to UV light for various irradiation times (0, 30, 60, 90, 120 and 150 min) in the presence of ZnO–Fe_x (x \approx 0, 0.05, 0.075, 0.1 mol. %) nanoparticles. The intensity of absorption peaks at 664 nm decreases gradually with irradiation time. MB dye was degraded under UV light from 0 to 150 min. in the presence of ZnO–Fe_x (x \approx 0, 0.05, 0.075, 0.1 mol.%) nanoparticles and is shown in Fig.3.9 (e). The result reveals that the Fe-doped ZnO shows higher photocatalytic activity than that of pure ZnO.

Fe (0.075%)-doped ZnO shows enhanced photocatalytic activity with a degradation efficiency of 68% for MB (pH 6) dye at 150 min. Fe (0.075%)-doped ZnO nanoparticles took less time to degrade the MB dye compared with other

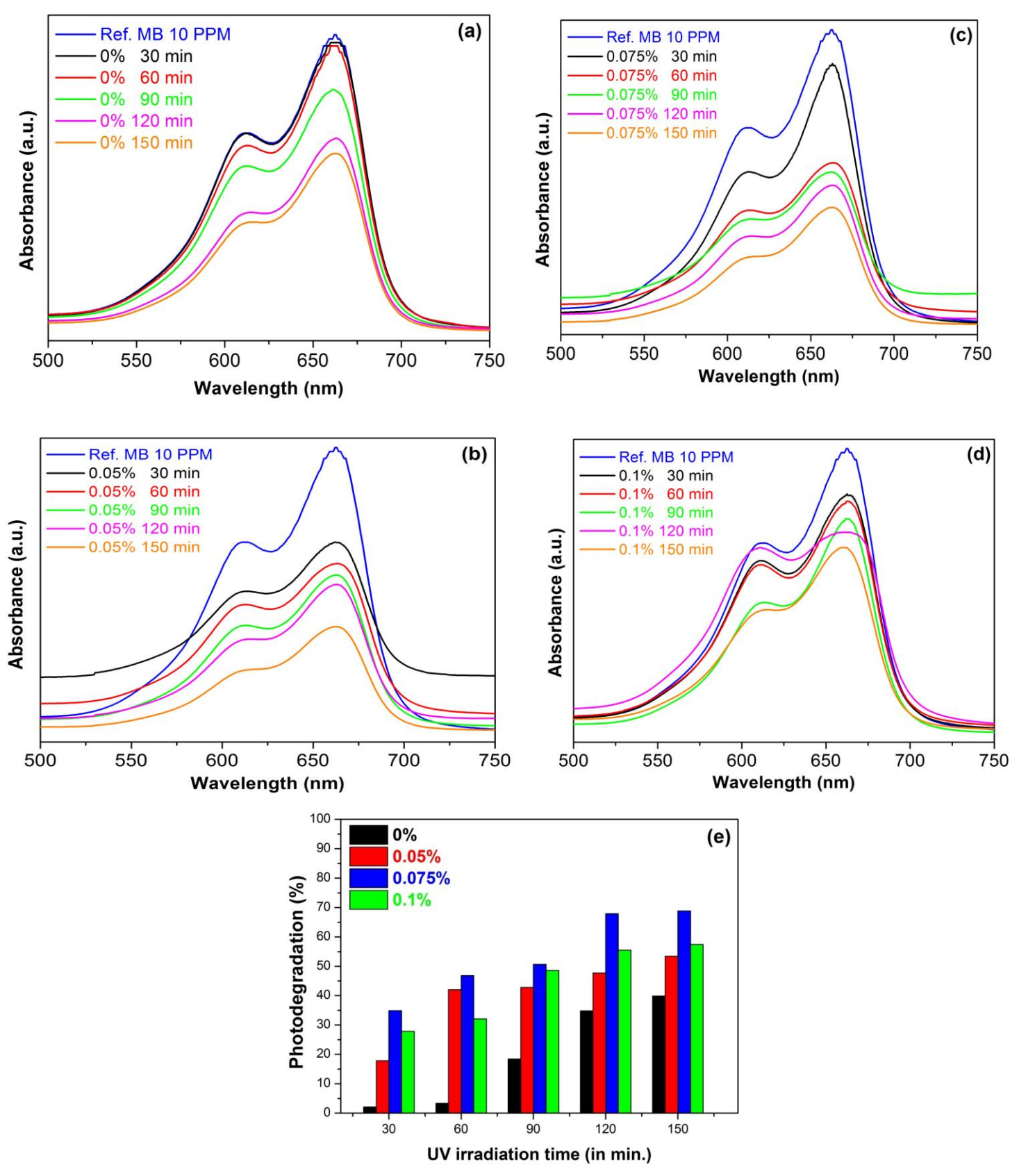


Fig.3.9: UV-Vis absorption spectra of MB dye degradation of (a) pure ZnO (b) 0.05, (c) 0.075 and (d) 0.1 mol.% Fe-doped ZnO nanoparticles and (e) influence on the photodegradation of MB

concentration of Fe. The reduction of photocatalytic activity at higher concentration Fe (0.1%)-doped ZnO may be due to photons' reduced path length [44].

Similar results are also observed by Suganthi and colleagues [45]. Another reason for the increase in the photocatalytic activity of Fe-doped ZnO nanoparticles, Fe ions substituted into ZnO surface may suppress the electron–hole pair recombination and enhance the dye degradation efficiency [46, 47]

3.4.4 Influence of UV irradiation time of MO

The photocatalytic activity was carried out with MO concentration of 3.0 mM, catalyst concentration of 10 mg, pH 6 and irradiation time up to 150 min. The variation in absorption spectra of MO showing to UV light for various irradiation times (0, 30, 60, 90, 120 and 150 min) in the presence of ZnO–Fe_x ($x \approx 0$, 0.05, 0.075, 0.1 mol. %) nanoparticles. The intensity of absorption peaks at 454 nm decreases gradually with the extension of irradiation time shown in Fig.3.10 (a–d). Fig.3.10 (e) shows the MO dye degradation under UV light from 0 to 150 min. in the presence of ZnO–Fe_x ($x \approx 0$, 0.05, 0.075, 0.1 mol.%) nanoparticles. The result reveals that the Fe (0.075%)-doped ZnO showed efficient photocatalytic activity with a degradation efficiency of 55% for MO (pH 6) dye at 150 min [48].

In this process, narrow semiconductors act as a sensitizer to improve the dye's photodegradation based on their electronic band structure. When the photocatalyst was illuminated with higher energy photons, it only allows the dye molecule oxidation [44].

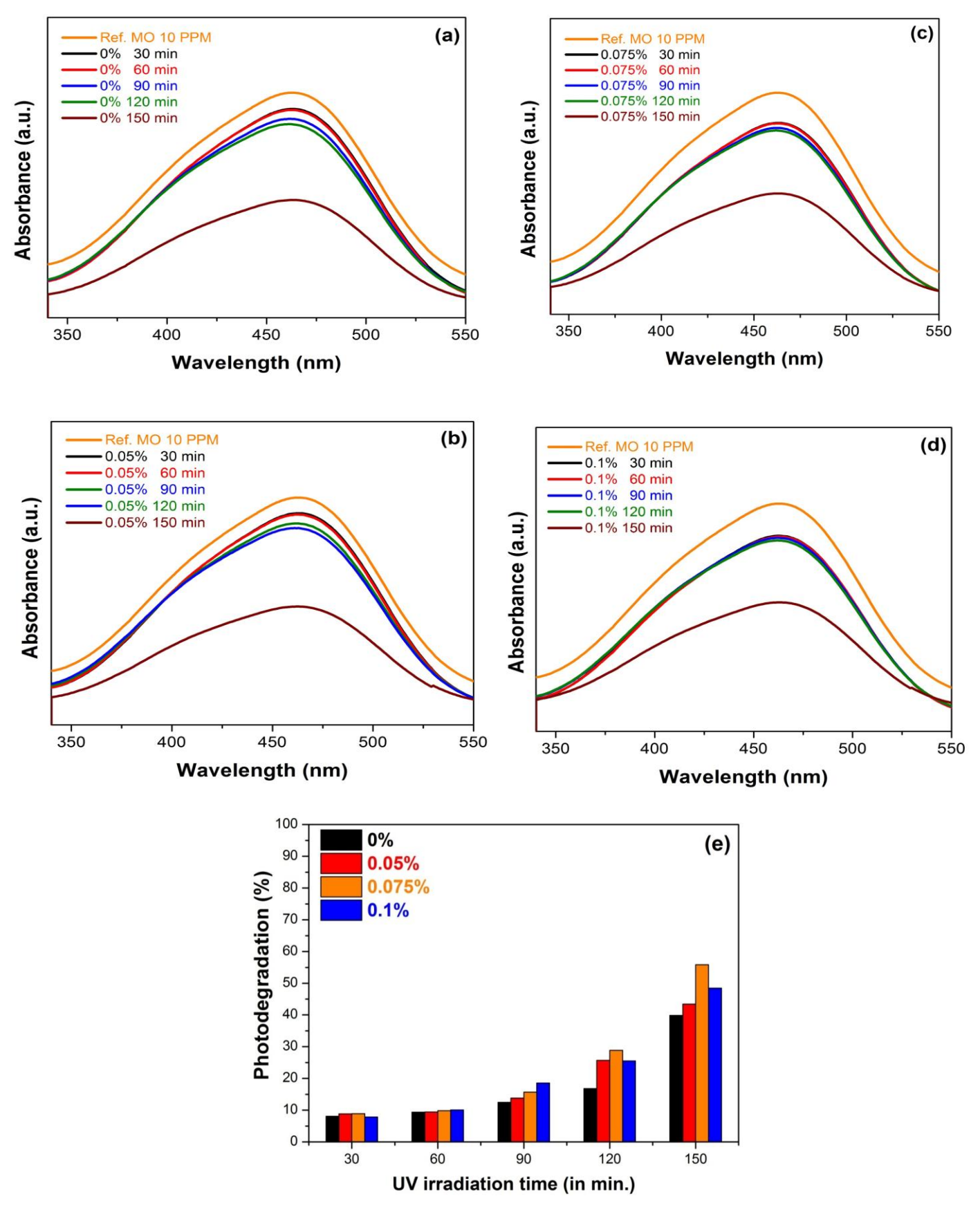


Fig.3.10: UV–Vis absorption spectra of MO dye degradation of (a) pure ZnO, (b) 0.05, (c) 0.075 and (d) 0.1 mol.% Fe-doped ZnO nanoparticles and (e) influence on the photodegradation of MO

We proposed a mechanism of $ZnO-Fe_x$ nanoparticles for efficient photocatalytic activity. It can be described as follows:

$$ZnO + h\gamma$$
 \longrightarrow $ZnO (h^{+}_{VB} + e^{-}_{CB})$... (2)

$$(h^{+}_{VB}) + dye$$
 \longrightarrow dye^{+}_{VB} \longrightarrow oxidation of dye molecule ... (3)

When ZnO is illuminated by visible light, holes (h^+_{VB}) and electrons (e^-_{CB}) are generated and passed through from valence to conduction band.

The photogenerated electrons and holes combine with Fe³⁺ ions, respectively.

$$Fe^{3+} + O_2 \longrightarrow Fe^{5+} + O_2^{\circ} - (electron release)$$
 ... (4)

$$Fe^{3+} + OH^{-} \longrightarrow Fe^{2+} + OH^{\circ}$$
 (hole release) ... (5)

These super oxide anion $(O_2^{\circ}-)$ and hydroxyl radicals (OH°) are strong oxidizing species, and it will degrade of MB and MO dye molecule (Eq. 6) [48]. From these results, novel Fe-doped ZnO nanoparticles have played a primary role in the degradation of organic dyes from wastewater.

3.5 Conclusion

Pure and different % of Fe-doped ZnO nanoparticles were prepared by using simple co-precipitation method. All the prepared samples are calcinated at 450 °C for 1h and they are characterized by X-ray diffraction technique, scanning electron microscope and UV-Vis spectroscopy analysis. The XRD result shows that when the doping concentration increases the particle size decreases. From the optical absorbance spectra, it should be noted that the band gap decreases with the dopant concentration. The effect of Fe doping on structural, optical and photocatalytic decolorization of MB and MO have been investigated. It has been observed that 0.075% Fe-doping the performance at higher pH values.

References

- [1] A. Nezamzadeh-Ejhieh, N. Moazzeni, J. Ind. Eng. Chem. 19, (2013) 1433–1442.
- [2] M. Safari, M. Nikazar, M. Dadvar, J. Ind. Eng. Chem. 19, (2013) 1697–1702.
- [3] Arques. A.M, Amat. A, Garcia, R. Vicente, J. Hazard. Mater. 146, (2007) 447.
- [4] V.K. Gupta, D. Pathania, S. Agarwal, P. Singh, J. Hazard. Mater. 243, (2012) 179.
- [5] B.K. Korbahti, K. Artut, C. Gecgel, A. Ozer, Chem. Eng. J. 173, (2011) 677.
- [6] J.B. Joo, I. Lee, M. Dahl, G.D. Moon, F. Zaera, Y. Yin, Adv. Funct. Mater. 23, (2013) 4246–4254.
- [7] T.H. Yu, W.Y. Cheng, K.J. Chao, S.Y. Lu, Nanoscale 5 (2013) 7356.
- [8] M. Lima, D. Fernandes, M. Silva, M. Baesso, A. Neto, G. de Morais et al., J. Sol-Gel Sci. Technol. 72, (2014) 301–309.
- [9] B. Cao, W. Cai, J. Phys. Chem. C 112, (2008) 680.
- [10] R. Saravanan, M.M. Khan, V.K. Gupta, E. Mosquera, F. Gracia, V. Narayanan,A. Stephen, RSC Adv. 5,(2015) 34645–34651.
- [11] R. Saravanan, N. Karthikeyan, V.K. Gupta, E. Thirumal, P. Thangadurai, V. Narayanan, A. Stephen, Mater. Sci. Eng., C 33, (2013) 2235–2244.
- [12] R. Jeyachitra, V. Senthilnathan, T.S. Senthil, J Mater Sci. Mater Electron 29, (2018) 1189–1197.
- [13] D. Rajesh, B. Varalakshmi, C.S. Sunandana, Phys. B 407, (2012) 4537–4539.
- [14] M. Arshad, M.M. Ansari, A.S. Ahmed, P. Tripathi, S.S.Z. Ashraf, A.H. Naqvi,A. Azam, J. Lumin. 161, (2015) 275–280.

- [15] L. Chow, O. Lupan, G. Chai, H. Khallaf, L.K. Ono, B.R. Cuenya, I.M. Tiginyan, V.V. Ursaki, V. Sontea, A. Schulte, Sens. Actuators A 189, (2013) 399–408.
- [16] Y.X. Liua, Y.C. Liua, D.Z. Shena, G.Z. Zhonga, X.W. Fana, X.G. Konga, R. Muc, D.O. Hendersonc, J. Cryst. Growth 240, (2002) 152–156.
- [17] T. Bak, J. Nowotny, M. Rekas, C. Sorrell, Int. J. Hydr. Energy 27, (2002) 991–1022.
- [18] Z. Han, L. Ren, Z. Cui, C. Chen, H. Pan, J. Chen, Appl. Catal. B Environ. 126, (2012) 298.
- [19] S.S. Shinde, C.H. Bhosale, K.Y. Rajpure, J. Photochem. Photobiol. B 113, (2012) 70.
- [20] Y. Min, K. Zhang, Y. Chen, Y. Zhang, W. Zhao, Sep. Purif. Technol. 92, (2012)115.
- [21] H. Wu, Z. Zheng, Y. Tang, N.M. Huang, R. Amal, H.N. Lim, Y.H. Ng, Sustain.
 Mater. Technol. 18, (2018) e.00075.
- [22] H. Wu, Z. Zheng, C.Y. Toe, X. Wen, J.N. Hart, R. Amal, Y.H. Ng, J. Mater. Chem. A 8, (2020) 5638–5646.
- [23] H. Wu, T.H. Tan, R. Liu, H.-Y. Hsu, Y.H. Ng J.Mater.Sci.32 (2021) 23007–23017.
- [24] A. Moulahi, F. Sediri, Ceram. Int. 40, (2014) 943–950.
- [25] N.L. Tarwal, P.R. Jadhav, S.A. Vanalakar, S.S. Kalagi, R.C. Pawar, J.S. Shaikh, Powder Technol. 208, (2011) 185–188
- [26] T. Ivanova, A. Harizanova, T. Koutzarova, B. Vertruyen, Mater. Lett. 64, (2010) 1147–114.

- [27] A. Rahmati, A.B. Sirgani, M. Molaei, M. Karimipour, Eur. Phys. J. Plus 129, (2014) 7.
- [28] P. Malathy, K. Vignesh, M. Rajarajan, A. Suganthi, Ceram. Int. 40, (2014) 101.
- [29] B.M. Rajbongshi, S.K. Samdarshi, Appl. Catal. B: Environ. 144, (2014) 435.
- [30] S. Dong, K. Xu, J. Liu, H. Cui, Phys. B 406, (2011) 3609.
- [31] Y. Zhang, M.K. Ram, E.K. Stefanalkos, D.Y. Goswami, Surf. Coat. Technol. 217, (2013) 119.
- [32] M.M. Ba-Abbad, A.A.H. Kadhum, A. Mohamad, M.S. Takriff, K. Sopian, Chemosphere 91, (2013) 1604–1611.
- [33] A.A. Ashkarran, A. Irajizad, S.M. Mahdavi, M.M. Ahadian, Mater. Chem. Phys. 118, (2009) 6–8.
- [34] J. Zhou, F. Zhao, Y. Wang, Y. Zhang, L. Yang, J. Lumin. 122–123, (2007) 195–197.
- [35] S. Bai, T. Guo, Y. Zhao, J. Sun, D. Li, A. Chen et al., Sens. Actuators B Chem. 195, (2014) 657–666.
- [36] M. Nasir, S. Bagwasi, Y. Jiao, F. Chen, B. Tian, J. Zhang, Chem. Eng. J. 236, 388 (2014)
- [37] G. Srinivasan, J. Kumar, Cryst. Growth 310, (2008) 1841.
- [38] C.W. Nahm, J. Mater. Sci. Mater. Electron. 24, (2013) 70.
- [39] T.G. Venkatesh, Y.A. Nayaka, R. Viswanatha, C.C. Vidyasagar, B.K. Chethana, Power Tech. 225, (2021) 232–238.
- [40] M.M. Hassan, W. Khan, A. Azam, A.H. Naqvi, J. Ind. Eng. Chem. 21, (2015) 283–291.

- [41] A. Mesaros, C.D. Ghitulica, M. Popa, R. Mereu, A. Popa, T. Petrisor Jr., M. Gabor, A.I. Cadis, B.S. Vasile, Ceram. Int. 40, (2014) 2835–2846.
- [42] C. Liu, D. Meng, H. Pang, X. Wua, J. Xie, X. Yu, L. Chen, X. Liu, J. Magn. Magn. Mater. 324, (2012) 3356.
- [43] S. Abed, H. Bougharraf, K. Bouchouit, Z. Sofiani, B. Derkowska-Zielinska, M.S. Aida, B. Sahraoui, Superlattice Microstruct. 85, (2015) 370.
- [44] S.V. Elangovan, V. Chandramohan, N. Sivakumar, T.S. Senthil, Desalin. Water Treat. 57, (2016) 9671–9678.
- [45] K. Vignesh, M. Rajarajan, A. Suganthi, J. Ind. Eng. Chem. 20, (2014) 3826–3833.
- [46] W. Bousslama, H. Elhouichet, M. Ferid, Optik 134, (2017) 88.
- [47] X. Yu, D. Meng, C. Li, U.K. Xu, J. Chen, C. Lu, Y. Wang, J. Mater. Sci. 25, (2014) 3920.
- [48] S.K. Kansal, M. Singh, D. Sud, J. Hazard. Mater. 141, (2007) 581–590.

CHAPTER – IV

CHAPTER - IV

Efficient photocatalytic degradation of organic dyes with Ag doped ZnO nanoparticles under UV light irradiation

4.1 Introduction

Economically growing countries like India are facing environmental pollution due to industrial developments. In particular, industrial effluents discharged from cosmetics, textile, paper and paint industries contain high levels of organic contaminants including toxic chemicals and heavy metals [1]. Untreated industrial effluents release into water system has become one of the most serious water pollutions that severely affect the ecosystem and human health. Appropriate treatment is essential for effective destruction of effluents before they are released into the ecosystem [2]. There are several techniques available for the wastewater treatment such as activated carbon adsorption, chemical oxidation, coagulation, ion exchange, reverse osmosis, electrodialysis and advanced oxidation processes (AOP) have been found to be ineffective for the mineralization of toxic organic compounds [3-7]. Among them, photocatalysis is an effective process that is used for heterogeneous photocatalytic degradation of organic effluents using a semiconductor as a photocatalyst [8]. Many researchers are recently focused in conversion of organic dyes into harmless chemicals using photo-catalysts. ZnO is a versatile multifunctional wide band gap semiconductor like TiO₂ and it has numerous superior properties such as high electron transport, light sensitive, thermal and chemically stable, non-toxic and sustainable with hydrogen environment [9, 10].

ZnO nanoparticles are effective photo-catalysts for degradation of toxic pollutants under UV irradiation. ZnO has better activity than TiO2 for photocatalytic degradation of some organic dyes [11, 12]. The photocatalytic efficiency of ZnO nanoparticles mainly depends on the ability of electron-holes (e⁻/h⁺) pair formation under light illumination. However, the rapid recombination of photo-excited electron holes (e⁻/h⁺), aggregation and low surface area of the bulk form are the main factors for the reduction of photocatalytic efficiency. Numerous methods, such as doping of metals and non-metals, combining with different semiconductors are used to overcome these drawbacks. The metal (Ag) doping of ZnO is most efficient way to improve its photocatalytic efficiency, because metal doping accelerates the charge carrier separation and change its physical and chemical properties [13-20]. ZnO has been prepared by a variety of techniques such as hydrothermal method [21], combustion [22], and sol-gel method [23]. Among these, co-precipitation [24] shows some advantages over the other methods.

The present work explains the effect of various concentrations of Ag dopant on the structural and photocatalytic activity of ZnO nanoparticles. Furthermore, the samples were characterized by XRD, SEM, FT-IR and UV-Vis spectrophotometer. To the best of our knowledge this is the first report of application of Ag-doped ZnO nanoparticles for the degradation of cationic dye (methylene blue) and anionic dye (methyl orange) in water.

4.2 Synthesis of pure ZnO, Ag-Doped ZnO (ZnO - Ag_x, X \approx 0.05, 0.075 and 0.1%) nanoparticles

To prepare pure ZnO and Ag-doped ZnO nanoparticles were synthesized using various mol.% ($x \approx 0.05, 0.075, \text{ and } 0.1$) using co-precipitation method.

4.2.1 Materials

All the chemical used in the experiments are analytical grade and were used without further purification. Zinc nitrate hexahydrate [Zn(NO₃)₂.6H₂O], silver nitrate Ag(NO₃), methylene blue (MB), methyl orange (MO) and sodium hydroxide [NaOH], were purchased from Alfa Aesar chemicals, India. Deionized water (DW) was used for all of the solutions.

4.2.2 Preparation of Pure ZnO Nanoparticles

In a typical synthesis, 10 g of Zn (NO₃)₂·6H₂O was dissolved into 20 ml of DW. In another container, 8 g of NaOH in 100 ml DW. Then NaOH added to the zinc nitrate solution. Both these solutions were added dropwise under continuous magnetic stirring until pH adjusted into 11. Then the above solution was heated in a vacuum oven at 150 °C for 1h. Afterwards, white color precipitates were separated by centrifugation and washed twice with DW followed by ethanol and dried at 100 °C for 2h. The dried participate was calcined at 450 °C for 1h and finally pure ZnO nanoparticles formed.

4.2.3 Preparation of Ag-doped ZnO (ZnO - Ag_x , $x \approx 0.05$, 0.075 and 0.1%) Nanoparticles

The silver nitrate precursor was used to prepare Ag-doped ZnO nanoparticles. For synthesis of Ag-doped ZnO nanoparticles containing various concentrations (mol% = 0.05, 0.075 and 0.1) of silver nitrate dissolved in water were added to the zinc nitrate solution with stirring. Then sodium hydroxide was added drop wise into the above-mentioned mixture solutions. The color was turned into white color. After that the solutions were centrifuged and annealed in a similar way as mentioned in the previous chapter. The co-precipitation method was selected based on available literature as described above [24]. Finally, all the obtained Ag-doped ZnO nanoparticles were used for further characterization.

4.3 Structural, Optical and Electrical Properties of Pure and Ag -Doped ZnO Nanoparticles

All the prepared nanoparticles have been characterized using XRD, SEM, EDX, UV-Visible, FTIR and I-V studies.

4.3.1 XRD Analysis

In order to investigate the crystal structure of pure ZnO and ZnO-Ag $_X$ nanoparticles were characterized by using a mini desktop X-ray diffractometer (X'PERT PRO MPD) operated at an accelerating potential of 40 kV and 30 mA filament current with CuKa radiation of wavelength 1.5406 A $^\circ$ with a scanning rate of 3/min. (from 2h = 10 to C) Fig.4.2 (a) depicts the PXRD patterns of pure ZnO and Ag-doped ZnO nanoparticles with different concentrations of Ag, i.e. 0.05, 0.075 and 0.1%. The XRD pattern of all

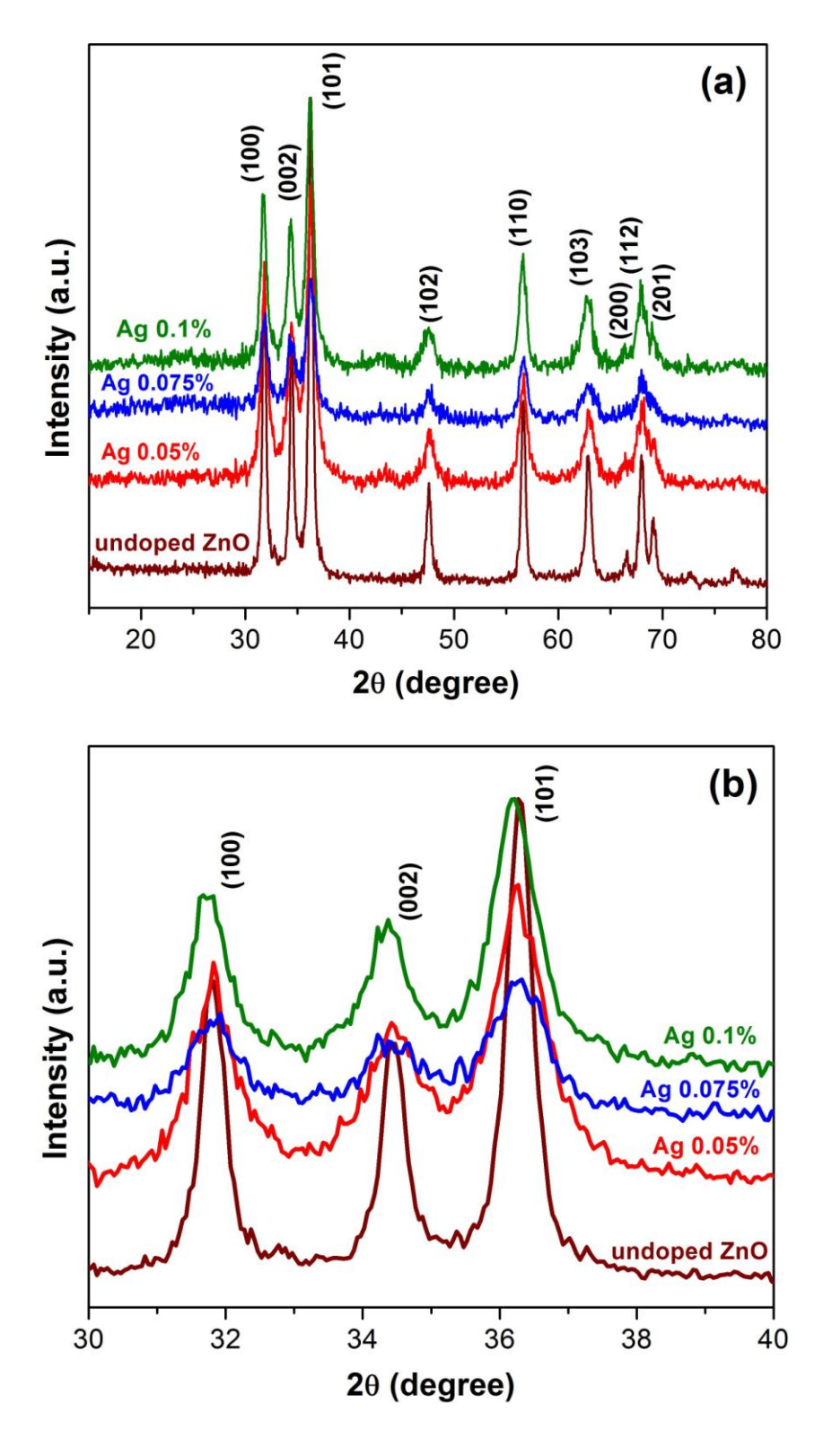


Fig.4.1: (a) XRD patterns of un-doped and Ag-doped ZnO nanoparticles (b) expanded view of XRD patterns shift

samples have strong diffraction peaks are assigned to (100), (002), (101), (102), (110), (103), (200), (112) and (201) planes of hexagonal wurtzite structure of ZnO in the Miller indices (JCPDS-36-1451) [26]. There are no extra peaks or other unidentified peaks correspond to Ag or its oxide phases in the XRD pattern.

Fig.4.1 (b) shows a magnification of the peak at 31.8° (100), 34.3° (002) and 36.3° (101) were a slight peak shift to lower angles observed in the 0.05, 0.075, and 0.1% Ag-doped ZnO nanoparticles. This result confirms that Ag impurity has been successfully incorporated into the ZnO lattice structure. The lattice constants and average crystallite size of major XRD peaks calculated for different samples are listed in Table 4.1. In our study, the effect of Ag doping on the average crystallite size (D) of was calculated for all samples by Debye–Scherrer's equation, and are found to be 23, 20, 19 and 18 nm, respectively [27].

These results indicate that the D value in the Ag-doped ZnO nanoparticles decreased as the doping concentration increased. Furthermore, the increasing Ag content decreases the lattice parameters and average crystallite size values. Other studies have found the same results were reported by Pal et al. [28] in Co-doped ZnO nanoparticles, Saravanan et al. [29] in Ag-doped ZnO nanoparticles and Udom et al. [30] in Ag-doped ZnO nanowires.

Table 4.1 Lattice parameters and crystallite size of pure and Ag-doped ZnO nanoparticles

Ag Doping Concentration (mol.%)	Hkl	a[Å]	c[Å]	c/a	Crystallite size (nm)
ZnO	(100) (002) (101)	3.2555	5.2184	1.6029	23
ZnO-Ag _{0.05}	(100) (002) (101)	3.2562	5.2190	1.6028	20
ZnO-Ag _{0.075}	(100) (002) (101)	3.2584	5.2210	1.6023	19
ZnO- Ag _{0.1}	(100) (002) (101)	3.2586	5.2240	1.6031	18

4.3.2 SEM and EDX Analysis

The surface morphology and chemical composition of the pure and ZnO-Ag_X nanoparticles were investigated by SEM with EDX of the samples were observed by scanning electron microscope (SEM-JEOL JS-6390) with energy dispersive X-ray spectrometer (EDX). SEM images of pure ZnO and Ag (0.05, 0.075 and 0.1 mol. %) doped ZnO nanoparticles are shown in Fig.4.3 (a-d). Fig.4.2 (a) shows the formation of irregular spherical morphology of the pure ZnO. From the Fig.4.2 (b-d), it was precisely discovered that well prepared samples are in nanometer size and the surface morphology changes with the silver concentration. The variation of surface

morphology with Ag dopant is due to the variation of number of nucleation sites [21]. The silver concentration reduces the particle size and it was confirmed from the XRD results. The obtained results are similar to the results reported by Pung et al. [31]

The EDX spectra for pure ZnO and Ag (0.1%)-doped ZnO nanoparticles are shown in Fig.4.4 (a, b). EDX spectrum of pure ZnO shows presence existence characteristic peaks of oxygen (O) and zinc (Zn) elements. The EDX pattern of Agdoped nanoparticles also includes elements such as existence of silver (Ag) together with Zn and O, indicating the successful doping of Ag in the ZnO matrix [31].

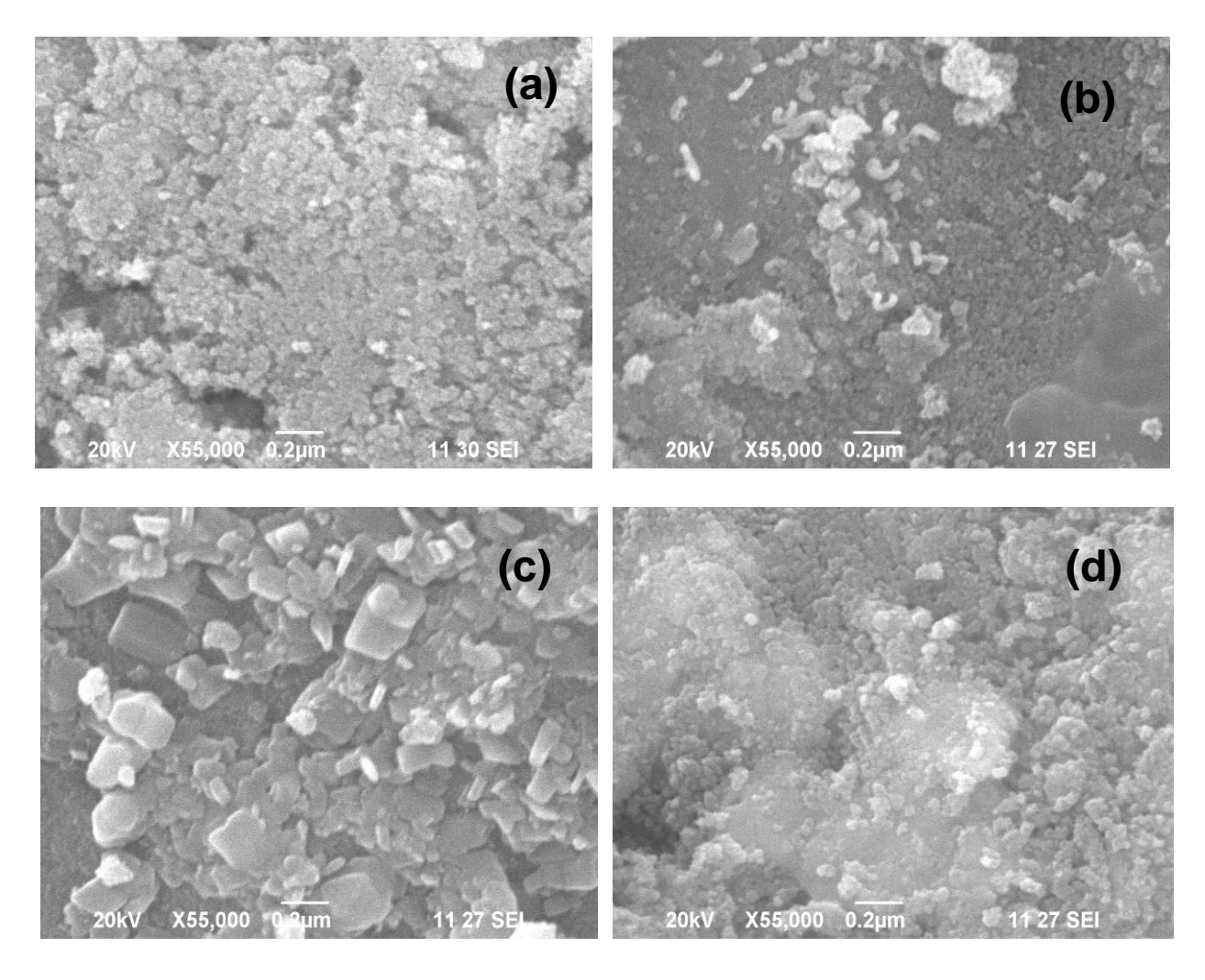
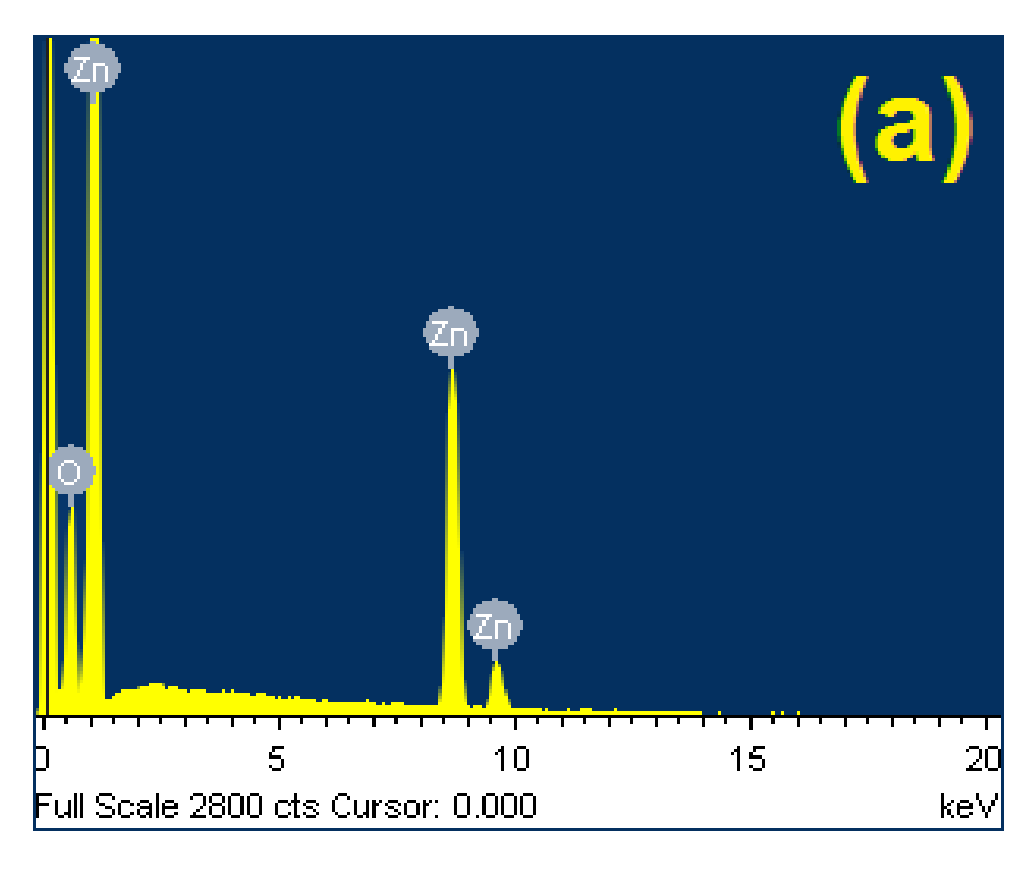


Fig.4.2: SEM images of (a) pure ZnO (b) 0.05, (c) 0.075 and (d) 0.1 mol.% Agdoped ZnO nanoparticles



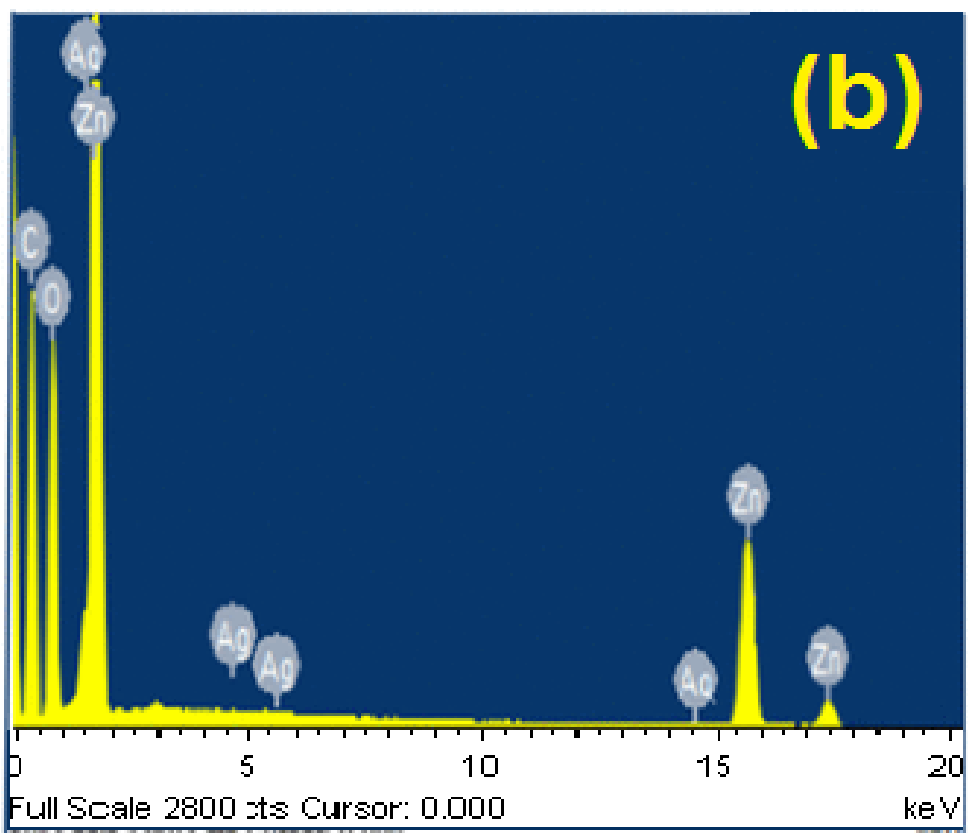


Fig.4.3: EDX images of (a) pure ZnO (b) 0.1 mol.% Ag-doped ZnO nanoparticles

4.3.3 UV-Visible Absorption Spectra

The band gaps and related optical properties of pure ZnO and Ag (0.05, 0.075 and 0.1 mol. %) doped ZnO nanoparticles were analysed from UV-visible spectra recorded using UV-Vis double-beam spectrophotometer (Systronics: AU-2707) and optical absorbance spectra have been studied. Fig.4.4 (a-d) shows the UV-Vis absorption spectra of pure ZnO and Ag (0.05, 0.075 and 0.1 mol. %) doped ZnO nanoparticles. Pure ZnO has an absorption cut-off edge was observed around 370 nm. The adsorption of Ag-doped ZnO nanoparticles was shifted to the longer wavelength from ZnO with the increase of the molar ratio of Ag (0.05, 0.075 and 0.1 mol. %). After Ag-doping display an additional hump absorption in the visible region observed at 373, 375 and 377 nm. The calculated optical band gap energies were 3.35, 3.33, 3.30 and 3.28 eV for un-doped ZnO and Ag-doped ZnO nanoparticles, respectively. According to some previous reports similar result was observed by Hassan et al. [32].

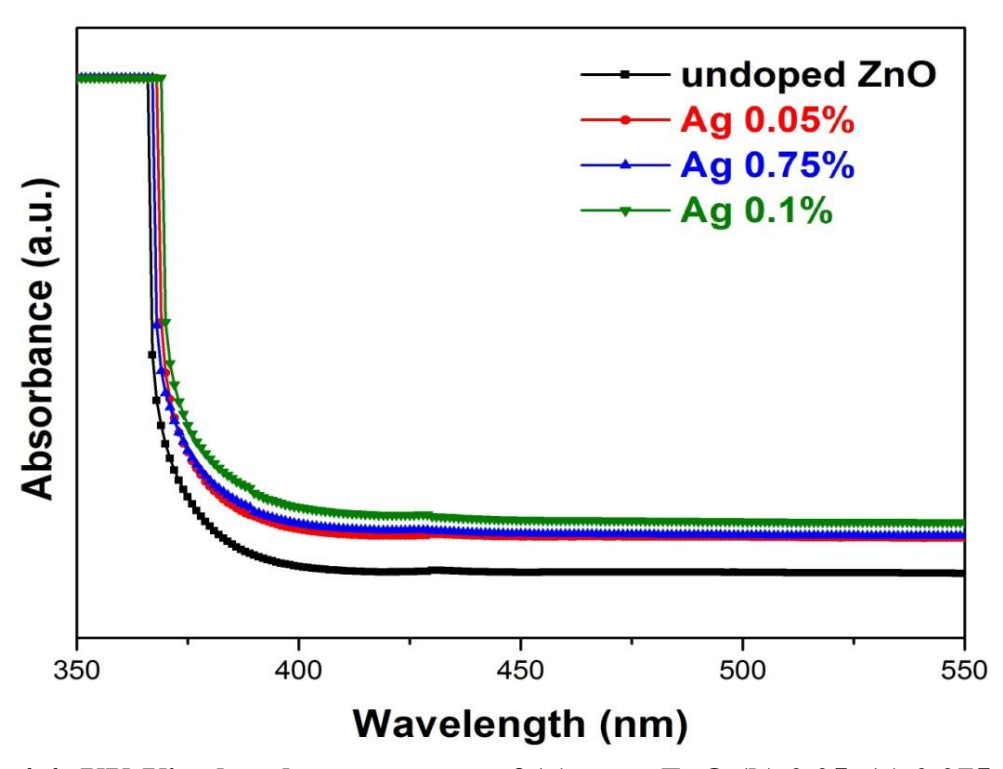


Fig.4.4: UV-Vis absorbance spectra of (a) pure ZnO (b) 0.05, (c) 0.075 and (d) 0.1 mol.% Ag-doped ZnO nanoparticles

4.3.4 FT-IR Analysis

The various functional groups formation of pure and ZnO-Ag_X nanoparticles were characterized by FT-IR spectra recorded by Perkin-Elmer spectrometer in the wavenumber range of 4000-400 cm⁻¹ using KBr pellet method. The FT-IR spectra of ZnO-Ag_X ($x \approx 0$ and 0.1 mol. %) nanoparticles are presented in Fig.4.5 (a, b). The absorption peaks present at 3441 and 1625 cm⁻¹ which corresponds to the -OH stretching and bending vibration of the water molecule [33]. The band at 2380 cm⁻¹ corresponds to symmetric and asymmetric C–H bond [34]. The observed FTIR spectrum exhibits several well-defined absorption bands at 1122 and 920 cm-1 and they are attributed to sulphate and C=C bonds, respectively [35]. The absorption peaks appear at 400 and 550 cm⁻¹ were assigned to the metal–oxygen (M–O) stretching mode [36] and the absorbance peak noticed in the spectra around 455 and 430 cm⁻¹ corresponds to the presence of Zn–O and Ag-O stretching bond, respectively.

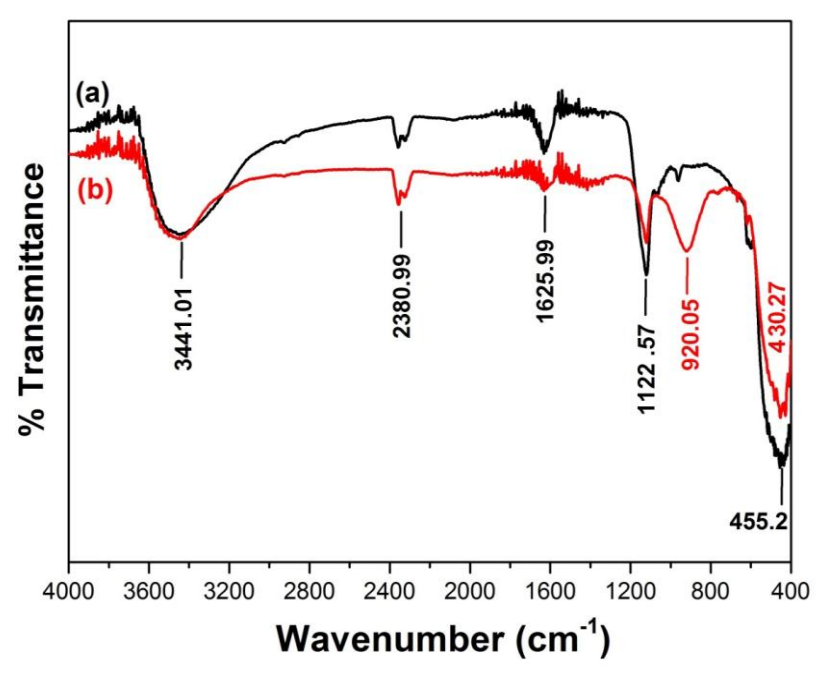


Fig.4.5: FT-IR spectra of (a) pure ZnO and (b) 0.1% Ag-doped ZnO nanoparticles

4.3.5 I-V Characteristics

Electrical properties of pure ZnO and Ag (0.1%)-doped ZnO nanoparticles was measured by using a Keithley electrometer 2400 model the I-V characteristics and it is presented in Fig.4.6(a, b). From IV curves, electrical conductivity of pure ZnO and Ag (0.1%)-doped ZnO taken under varying temperatures from 30 to 130 °C. This study reveals that (0.1%) Ag-doped ZnO nanoparticles shows better conductivity than the pure ZnO and it may due to the presence of more charge carrier's mobility [37].

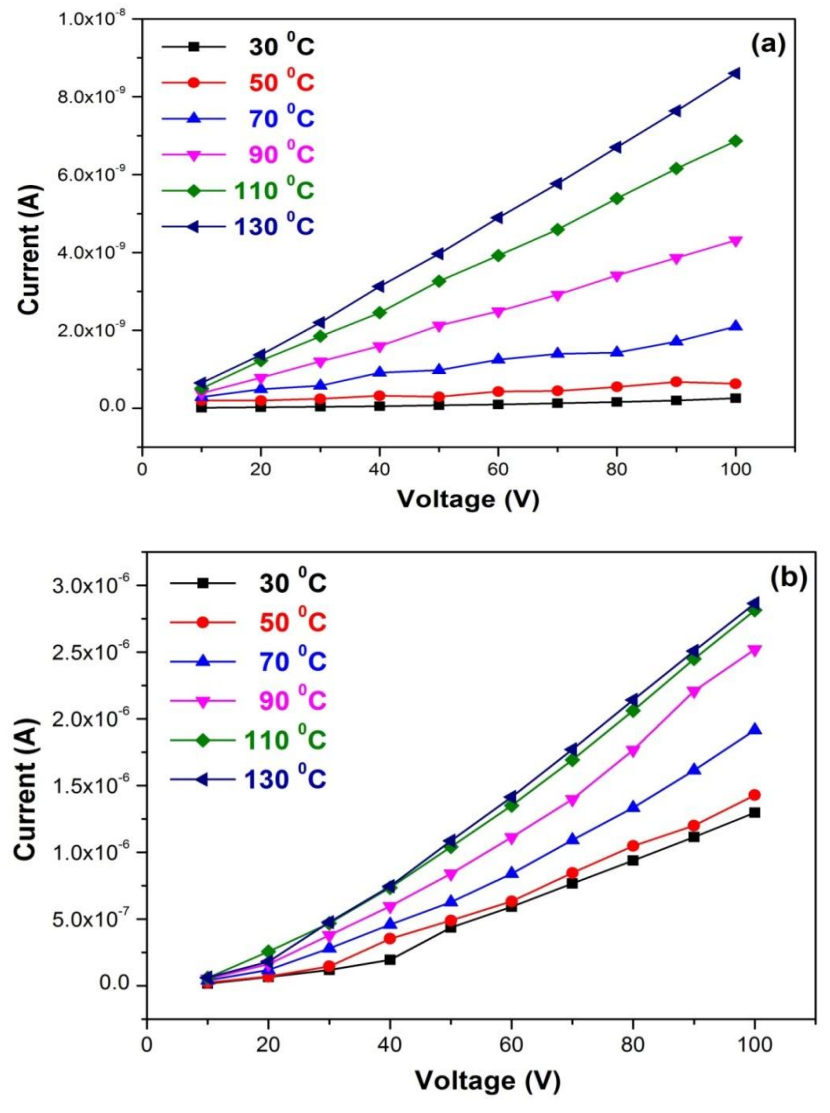


Fig.4.6: I-V characteristics of (a) pure ZnO and (b) 0.1% Ag-doped ZnO nanoparticles

4.3.6 Photocatalytic Activity

Photocatalytic activity of the pure and Ag-doped ZnO nanoparticles was evaluated for degradation of MB and MO dye solution under UV light irradiation. The photocatalytic procedure was conducted by adding 10 mg of photocatalyst in 50 ml, 10 ppm of MB and MO dye solution. The reaction mixture was stirred for 30 min. under a dark to reach adsorption–desorption equilibrium. After that the dye solution was irradiated with an 8 W UV lamp was switched on. At different time intervals (0, 15, 30, 45, 60 and 75 min.) samples were taken out and centrifuged to separate the catalyst and then the supernatant was analyzed in a UV-visible double beam spectrophotometer maximum wavelength (λ_{max}) observed at ~664 and 464 nm to study the photocatalytic degradation. The photo-degradation efficiency (D %) of the MB and MO dye was calculated using the equation [25]

$$(D \%) = [C-C_0/C_0] \times 100$$
 ... (1)

Where, C_0 and C are the initial and final degradation time of MB and MO (mg/l) dye solution used.

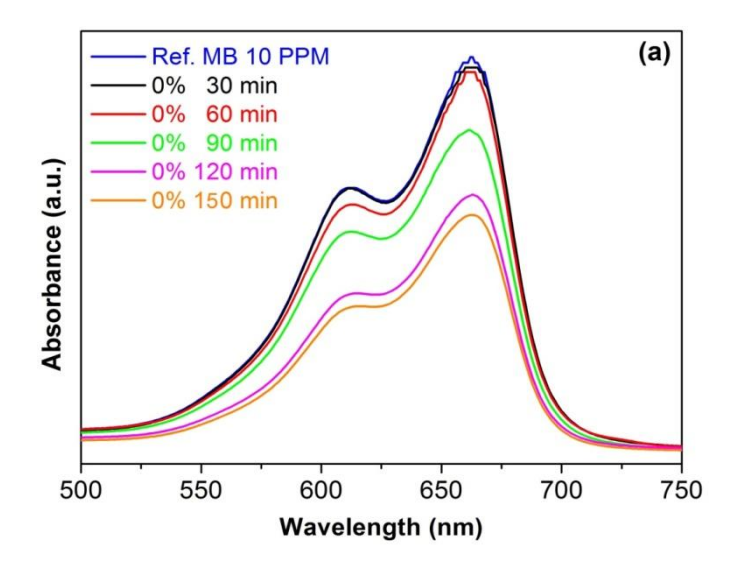
4.3.6.1 Optimized Factors to the Catalytic Activity

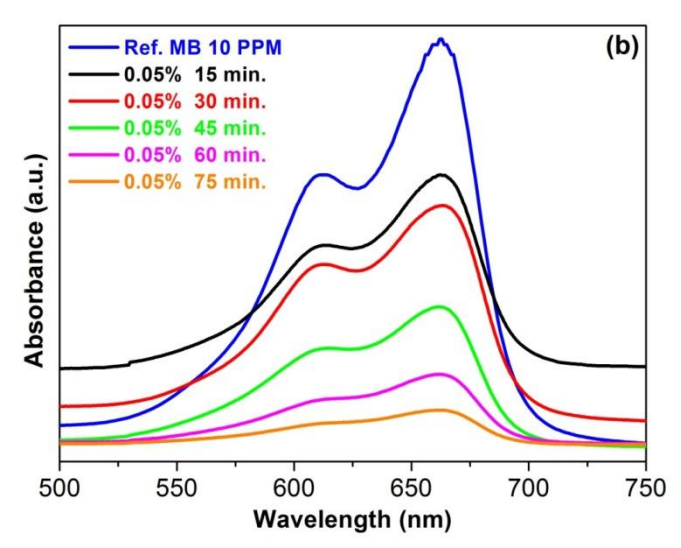
The photocatalytic degradation of pure ZnO and Ag-doped ZnO nanoparticles were selected for the evaluation of photocatalytic activity under UV-visible light. In order to study the effect of the UV light on the degradation of MB and MO dye. The dyes were prepared in various concentrations like acidic, neutral and alkaline medium. The photocatalytic activity was carried out and optimized for pure ZnO catalyst with MB and MO dye concentration of 10 ppm, catalyst concentration of 10 mg, pH = 6 and UV irradiation time up to 150 min.

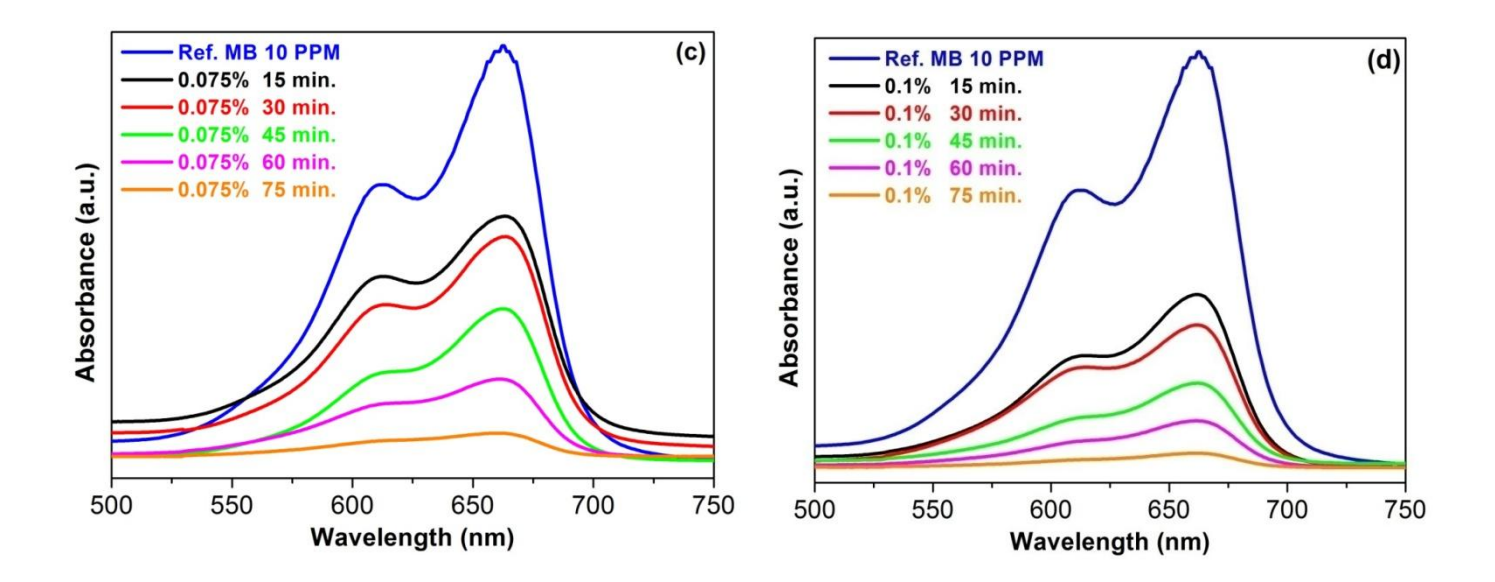
4.3.6.2 Impact of UV irradiation on Degradation of MB and MO

For the above-mentioned conditions, the photocatalytic degradation was carried out for Ag-doped ZnO nanoparticles. Fig.4.7 (a-d) shows the comparative spectra of degradation of MB dye with pure ZnO and Ag (mol% = 0.05, 0.075, 0.1)-doped ZnO nanoparticles with respect to time. The high intensity absorption peaks were observed at ~664 nm for MB dye. It was observed that the degradation of MB dye increases with increase of dopant concentration [24].

The effect of irradiation time of UV on MB dye degradation is shown in the above Fig.4.7 (e). The efficiency of pure and Ag-doped ZnO nanoparticles under UV light reaches 38, 90, 92 and 95% after 75 min light irradiation. Ag (0.1%)-doped ZnO nanoparticle shows the highest degradation efficiency of 95% under UV radiation for MB dye, while under similar conditions, a much lower efficiency (38%) was observed for pure ZnO nanoparticles under visible light radiation [24].







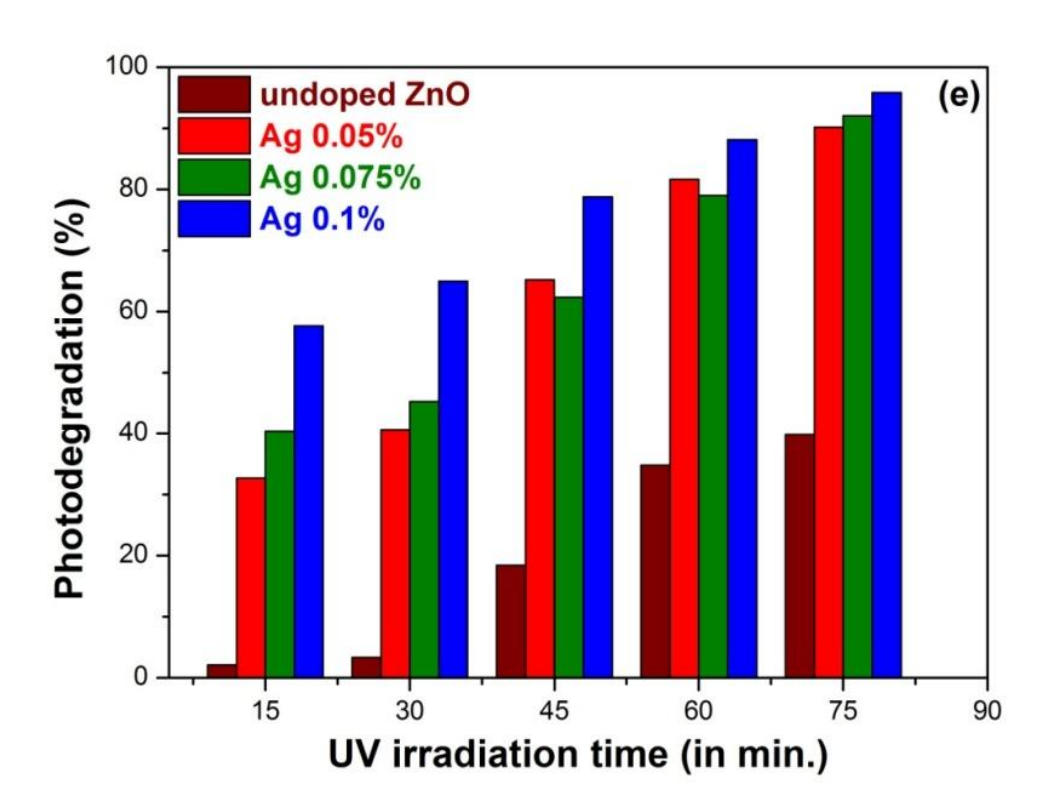


Fig.4.7: MB dye degradation of (a) pure (b) 0.05, (c) 0.075, (d) 0.1 mol.% Ag-doped ZnO nanoparticles (MB dye:10 ppm, catalyst dose:10 mg, pH=6) and (e) effect of irradiation time of UV on MB photo-degradation.

The comparative spectra for degradation MO dye with pure ZnO and Ag (mol% = 0.05, 0.075, 0.1)-doped ZnO nanoparticles with respect to time was presented in Fig.4.8(a-d). The high intensity absorption peaks of MO dye were observed at ~464 nm. The effect of irradiation time of UV on MO dye degradation is shown in Fig.4.8(e). The degradation efficiency increases with increase of dopant concentration and the obtained values are 36, 72, 92 and 76%, respectively for pure, 0.05, 0.075 and 0.1 mol.% Ag-doped ZnO nanoparticles. It can be seen that maximum degradation (92%) of MO dye was achieved for Ag (0.075%)-doped ZnO nanoparticles in 75 min. It should be noted that MB was degraded more faster than MO in the presence of the Ag-dopant.

The possible photocatalytic degradation mechanism of MB and MO on Agdoped ZnO nanoparticles under UV-visible light irradiation can be explained from the equation 2 to 7. During the catalytic process, photons can excite electrons in the valence band (VB) to be moved up to the conduct band (CB) and generate the same amount of electron-hole pair (e- and h⁺). The photo-excited electrons will be transferred from ZnO to Ag nanoparticles under the potential energy.

$$ZnO + h\gamma$$
 \longrightarrow $ZnO (h^+_{VB} + e^-_{CB})$... (2)

$$ZnO (e_{CB}^{-}) + Ag \longrightarrow ZnO + Ag (e_{CB}^{-})$$
 ... (3)

$$Ag (e_{CB}^-) + O_2 \longrightarrow O_2^- + Ag$$
 ... (4)

$$ZnO(h^{+}_{VB}) + H_2O \longrightarrow ZnO + H^{+} + OH \qquad ... (5)$$

$$(\cdot O_2^- + \cdot OH) + dye (MB \text{ or } MO) \longrightarrow degradation products ... (6)$$

$$(\cdot O_2^- + \cdot OH) + degradation products \longrightarrow CO_2 + H_2O$$
 ... (7)

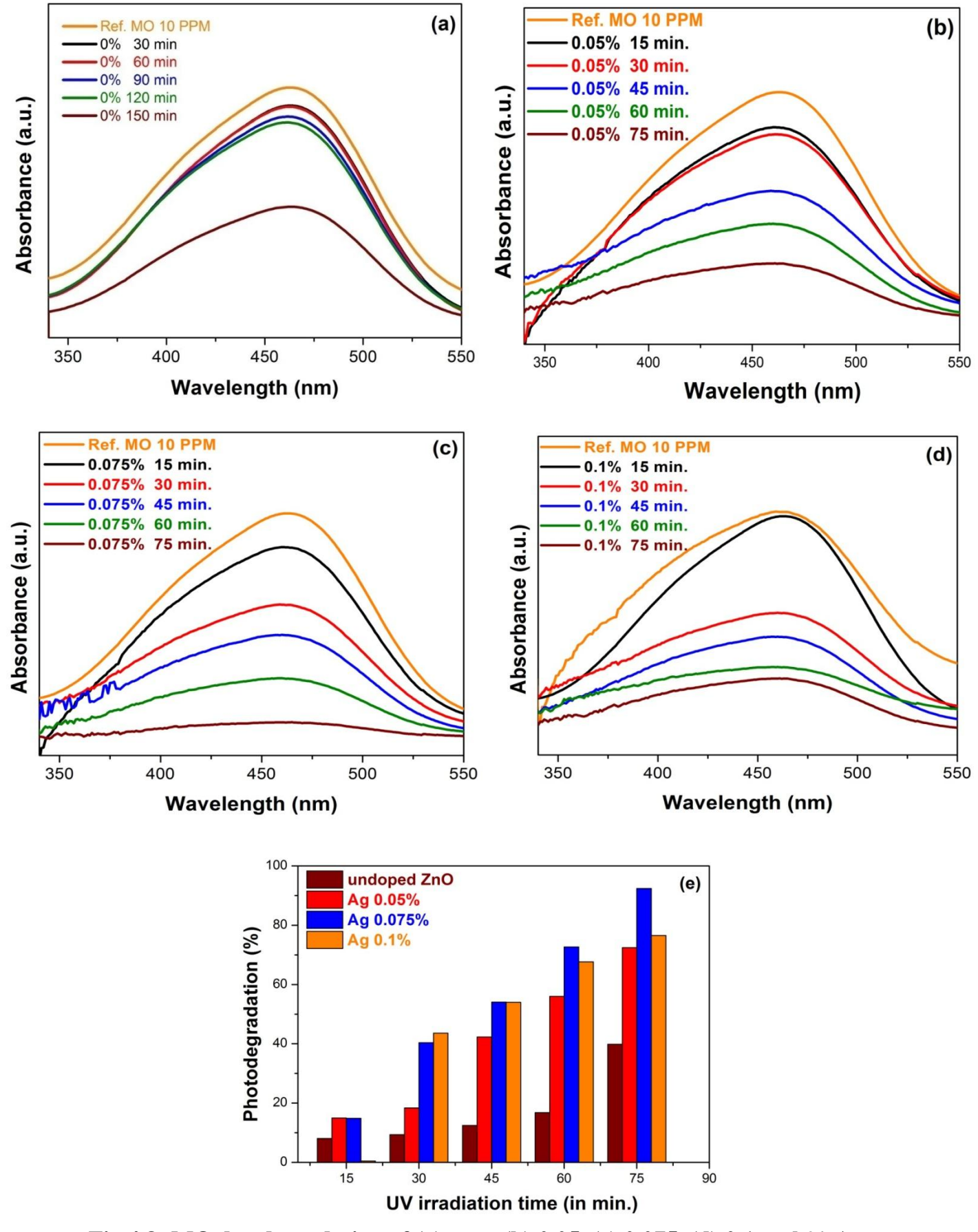


Fig.4.8: MO dye degradation of (a) pure (b) 0.05, (c) 0.075, (d) 0.1 mol.% Agdoped ZnO nanoparticles (MB dye:10 ppm, catalyst dose:10 mg, pH=6) and (e) effect of irradiation time of UV on MO photo-degradation

The photocatalytic activity is effective thereby preventing the recombination between electrons and holes on the surface of ZnO. Afterwards, the electron on Ag nanoparticles can produce the $\cdot O_2^-$ superoxide radical, while the holes in the VB can react with H_2O_2 to produce $\cdot OH$ hydroxyl radical [38]. These free radicals can degrade organic compounds to CO_2 and H_2O [31]. Till now, many studies have proven that electrons can transfer from Ag to the CB of ZnO. Then, they are scavenged by adsorbed O_2 molecules to yield superoxide radical anions $(\cdot O_2^-)$ to degrade dye molecules [38]. Therefore, the photocatalytic activity will be enhanced.

4.4 Conclusion

Pure and different % of Ag doped ZnO nanoparticles were prepared by using simple co-precipitation method. All the prepared samples are annealed at 450 °C for 1h and they are characterized by using various techniques like X-ray diffraction technique, scanning electron microscope and UV-Vis spectroscopy analysis. The XRD result shows that when the doping concentration increases the particle size decreases. From the optical absorbance spectra, it should be noted that the band gap decreases with the dopant concentration. The effect of Ag doping on structural, optical and photocatalytic decolorization of MB and Mo have been investigated. It has been observed that 0.075% Fe doping the performance at higher pH values.

References

- [1] RA Pereira, MFR Pereira, MM Alves,L Pereira. Appl Catal B. 144 (2014) 713-20.
- [2] A Umar, MS Akhtar, A Al-Hajry, MS Al-Assiri, GN Dar, M Saif Islam. Chem Eng J.262 (2015) 588-96.
- [3] B Gao, B Liu, T Chen, Yue Qinyan. J. Hazard. Mater. 187 (2011) 413-20.
- [4] A Szyguła, E Guibal, MA AriñoPalacín, M Ruiz, AM Sastre. J. Environ Manage. 90 (2009) 2979-86.
- [5] T-H Kim, Park Chulhwan, Kim Sangyong. J Clean Prod. 13 (2005) 779-86.
- [6] VK Gupta, D Pathania, S Agarwal, PJ Singh Hazard Mater, 243 (2012) 179-86.
- [7] BK Körbahti, K Artut, C Geçgel, A Özer. Chem Eng J. 173 (2011) 677-88.
- [8] A Umar, MS Akhtar, A Al-Hajry, MS Al-Assiri, NY Almehbad. Mater Res Bull. 047 (2012) 2407-14.
- [9] S Jagadhesan, N Senthilkumar, V Senthilnathan, TS Senthil. Mater Res Express. 5 (2) (2018) 025040.
- [10] VA Tu, VA Tuan. Viet J Chem. 56 (2018) 214-9.
- [11] A Shafaei, MM Nikazar, M Arami. 25 (1-3) 2010 8-16.
- [12] J Xie, Y Li, W Zhao, L Bian, Y Wei .207 (2011) 140-4.
- [13] B Subash, B Krishnakumar, M Swaminathan, M Shanthi 16 (2013) 1070-8.
- [14] ES Araújo, BP da Costa, RAP Oliveira, J Libardi, PM Faia, HP de Oliveira. J Environ Chem Eng. 4(3) (2016) 2820-9.
- [15] I Neelakanta Reddy, Ch Venkata Reddy, J Shim, B Akkinepally, M Cho, K Yoo, D Kim. Cat Today. 340 (2018) 277-85.

- [16] A Bera, D Basak. ACS Appl. Mater. Interfaces.2(2) (2010) 408-12.
- [17] BX Li, YF Wang. Facile 47(5) (2010) 615-23.
- [18] YZ Lei, GH Zhao, MC Liu, ZN Zhang, XL Tong, TC Cao. Fabrication, J. Phys. Chem. C. 133(44) (2009) 19067-76.
- [19] ZY Zhang, CL Shao, XH Li, CH Wang, MY Zhang, YC Liu. ACS Appl. Mater. Interfaces. 2(10) (2010) 2915-23.
- [20] Q Wang, BY Geng, SZ Wang. Environ Sci Technol.43(23) (2009) 8968-73.
- [21] N Sriharan, N Muthukumarasamy, M Thambidurai, TS Senthil. J Optoelectron. Adv. Mater.19 (9-10) (2017) 634-40.
- [22] NL Tarwal, PR Jadhav, SA Vanalakar, SS Kalagi, RC Pawar, JS Shaikh, SS Mali, DS Dalavi, PS Shinde, PS Patil. 208 (2011) 185-8.
- [23] Alireza Samadi Tabrizi. Int J Life Sci Pharma Res. 6(4) (2016) 1-11.
- [24] S Jagadhesan, V Senthilnathan, TS Senthil. J, Optoelectron, Adv, Mater. 20(2018) 188-95.
- [25] Davoud Balarak, Marzieh Baniasadi, Kethineni ChandrikaInt J. Life. Sci. Pharma. Res., 10 (2020) 17-22.
- [26] AA Ashkarran, A Irajizad, SM Mahdavi, MM Ahadian Mater. Chem. Phys. 118 (2009) 6-8.
- [27] M Nasir, S Bagwasi, Y Jiao, F Chen, B Tian, J Zhang. Chem. Eng. J. 236 (2014) 388-97.
- [28] B Pal, PK Giri. J. Nanosci. Nanotechnol. 11(10) (2011) 9167-74.
- [29] S Saravanan, M Silambarasan, T Soga. J.Appl. Phys.53(11S) (2011). 1.

- [30] I Udom, Y Zhang, MK Ram, EK Stefanakos, AF Hepp, R Elzein, R Schlaf, DY Goswami. Thin Solid Films. 564 (2014) 258-63.
- [31] SY Pung, WP Lee, A Aziz. Int. J. Inorg. Chem. (2012) 1-9
- [32] MM Mehedi Hassan, W Khan, A Azam, AH Naqvi. J. Ind. Eng. Chem. 21 (2021) 283-91.
- [33] AE Jiménez-González, JAS Soto Urueta, R Suárez-Parra. J. Cryst. Growth. 192 (3-4) (1998) 430-8.
- [34] D Ramimoghadam, MZB Hussein, YH Taufiq-Yap. J. 7(1) (2013) 71.
- [35] K Saoud, R Alsoubaihi, N Bensalah, T Bora, M Bertino. J. Mater. Res. Bull.63 (2015) 134-40.
- [36] M Srivastava, AK Ojha, S Chaubey, PK Sharma, AC Pandey .J Alloys. Compd. 494(1-2) (2014) 275-84.
- [37] S Abed, H Bougharraf, K Bouchouit, Z Sofiani, B Derkowska-Zielinska, MS Aida, B Sahraoui. Superlattices Microstruct. 85 (2015) 370-8.
- [38] M Mittal, M Sharma, OP Pandey. Sol. Energy. 110 (2014) 386-97. .

CHAPTER – V

CHAPTER – V

Preparation and Characterization of Pure and Mg-Doped ZnO Nanoparticles for Photocatalytic Degradation

5.1 Introduction

Since the mechanism of photodegradation of ZnO was proved to be same as TiO₂ [1]. ZnO is also a potential semiconductor with a wide band gap (3.37 eV) with large exciton binding energy of 60 meV, comparatively very soft material with high melting point [2, 3]. Zinc Oxide is also known as zincite, which seldom occurs in nature, normally in a crystalline form. Pure microcrystalline zinc oxide is white in colour, which is almost insoluble in water. The three different forms of crystalline zinc oxide are hexagonal wurtzite, cubic zinc blend and cubic rock salt. Among them wurtzite structure is most common because of its stability at ambient conditions and latter is most rarely found. Zinc oxide properties are always structure dependent. So, the properties vary with morphology, structure, particle size and shape. A large number of methods have been used to synthesize ZnO nanostructures, such as chemical vapor deposition, sol-gel method, sputtering deposition, and chemical solution deposition [4-7]. Comparing these methods, each method has some advantages and limitations, for example, control the growth of the ZnO nanostructures is not easy in the microwave and chemical vapor deposition due to the high reaction speed.

For ZnO nanostructures, the doping of selective elements is an important valuable technique to alter its electronic structure and then influence the optical, electrical, and magnetic properties, which are fundamental for their practical

applications. In particular, transition metal doped ZnO nanostructures reveal new physical and chemical properties, as long as the exciting opportunities for a wide range of applications in the areas of catalysis, gap sensors, solar cells, and so on [8]. The biocompatibility nature of ZnO is an important for medical application in medical as well as biological field [9]. Vinita et al. [10] have prepared sodium doped ZnO quantum dots and reported the biocompatibility and optical properties. Since, the urgent need for adveing the fabrics and ability to cause some harmful effects [13]. Strong exposure can increase heart rate and induce vomiting, cyanosis, jaundice and tissue necrosis in Human [14]. The photo- catalytic activity of the catalyst was evaluated by using methylene blue as a model pollutant. In order to achieve high photocatalytic activity, a series of experiments were carried out which includes effect of initial pH of dye solution, the effect of photocatalyst concentration and impact of UV irradiation. In this work, an attempt has been made to use pure and effect of various concentrations of Mg doped ZnO nanoparticles for degradation methylene blue and methyl orange in water.

5.2 Synthesis of pure ZnO, Mg-doped ZnO (ZnO-Mg_x, $x \approx 0.05,\, 0.075$ and 0.1%) nanoparticles

To prepare pure ZnO and Mg-doped ZnO nanoparticles were synthesized using various mol.% ($x \approx 0.05, 0.075, \text{ and } 0.1$) using co-precipitation method.

5.2.1 Materials

All the chemical used in the experiments are analytical grade and were used without further purification. Zinc nitrate hexahydrate [Zn(NO₃)₂.6H₂O], magnesium acetate tetrahydrate nitrate [Mg(CH₃COO)₂ .4H₂O], methylene blue (MB), methyl

orange (MO) and sodium hydroxide [NaOH], were purchased from Alfa Aesar chemicals, India. Deionized water (DW) was used for all of the solutions

5.2.2 Preparation of Pure ZnO Nanoparticles

In a typical synthesis, 10 g of Zn (NO₃)₂·6H₂O was dissolved into 20 ml of DW. In another container, 8 g of NaOH in 100 ml DW. Then NaOH added to the zinc nitrate solution. Both these solutions were added dropwise under continuous magnetic stirring until pH adjusted into 11. Then the above solution was heated in in a vacuum oven at 150 °C for 1h. Afterwards, white color precipitates were separated by centrifugation and washed twice with DW followed by ethanol and dried at 100 °C for 2h. The dried participate was calcined at 450 °C for 1h and finally pure ZnO nanoparticles formed.

5.2.3 Preparation of Mg-doped ZnO (ZnO-Ag_x, $x \approx 0.05$, 0.075 and 0.1%) Nanoparticles

The magnesium acetate tetrahydrate precursor was used to prepare Mg-doped ZnO nanoparticles. For synthesis of Mg-doped ZnO nanoparticles containing various concentrations (mol% = 0.05, 0.075 and 0.1) of magnesium acetate tetrahydrate dissolved in water were added to the zinc nitrate solution with stirring. Then sodium hydroxide was added drop wise into the above-mentioned mixture solutions. The color was turned into white color. After that the solutions were centrifuged and annealed in a similar way as mentioned in the previous chapter. The co-precipitation method was selected based on available literature as described above [16]. Finally, all the obtained Mg-doped ZnO nanoparticles were used for further characterization.

5.3 Results and Discussion

All the prepared nanoparticles have been characterized using XRD, SEM, EDX, UV-Visible, FTIR and I-V studies.

5.3.1 XRD Analysis

The crystalline phases of pure and Mg-doped ZnO nanoparticles were determined by powder X-ray diffractometer (X'PERT PRO MPD) using CuK α radiation (λ = 0.15405 nm) operated at 40 kV voltage and 30 mA current with a scanning rate of 2° per min. Fig.5.1 (a) depicts the XRD patterns of pure ZnO and Mg-doped ZnO nanoparticles with different concentrations of Mg, i.e. 0.05, 0.075 and 0.1%. The XRD pattern of all samples have strong and sharp diffraction peaks are assigned to (100), (002), (101), (102), (110), (103), (200), (112) and (201) planes of hexagonal wurtzite structure of ZnO in the Miller indices (JCPDS-36-1451) [18]. Interestingly the XRD pattern of Mg doped samples show much changes when compared with the pattern of pure ZnO, which confirms that there is no extra peaks or other unidentified peaks corresponds to Mg or its oxide phases in the XRD pattern.

Fig.5.1 (b) shows a magnification of the high intensity peaks at 31.8° (100), 34.3° (002) and 36.3° (101) displayed in Fig.5.1 (b) indicates that the preferential orientation for the sample is along the c-axis. were a slight peak shift to higher angles observed in the 0.05, 0.075, and 0.1% Mg-doped ZnO nanoparticles. The shift of peaks towards high angles corresponds to a lattice compression caused by replacement of Zn²⁺ by Mg²⁺ and this due to the difference in ionic radius of Zn and Mg. This result confirms that Mg impurity has been successfully incorporated into the ZnO lattice structure. Replacement of Mg in the Zn site introduces a change in 'd' and this

induces this type of angle shift [15]. The lattice constants and average crystallite size of major XRD peaks calculated for different samples are listed in Table 5.1. In our study, the effect of Mg doping on the average crystallite size (D) of was calculated for all samples by Debye–Scherrer's equation, and are found to be 23, 18, 16 and 15 nm, respectively.

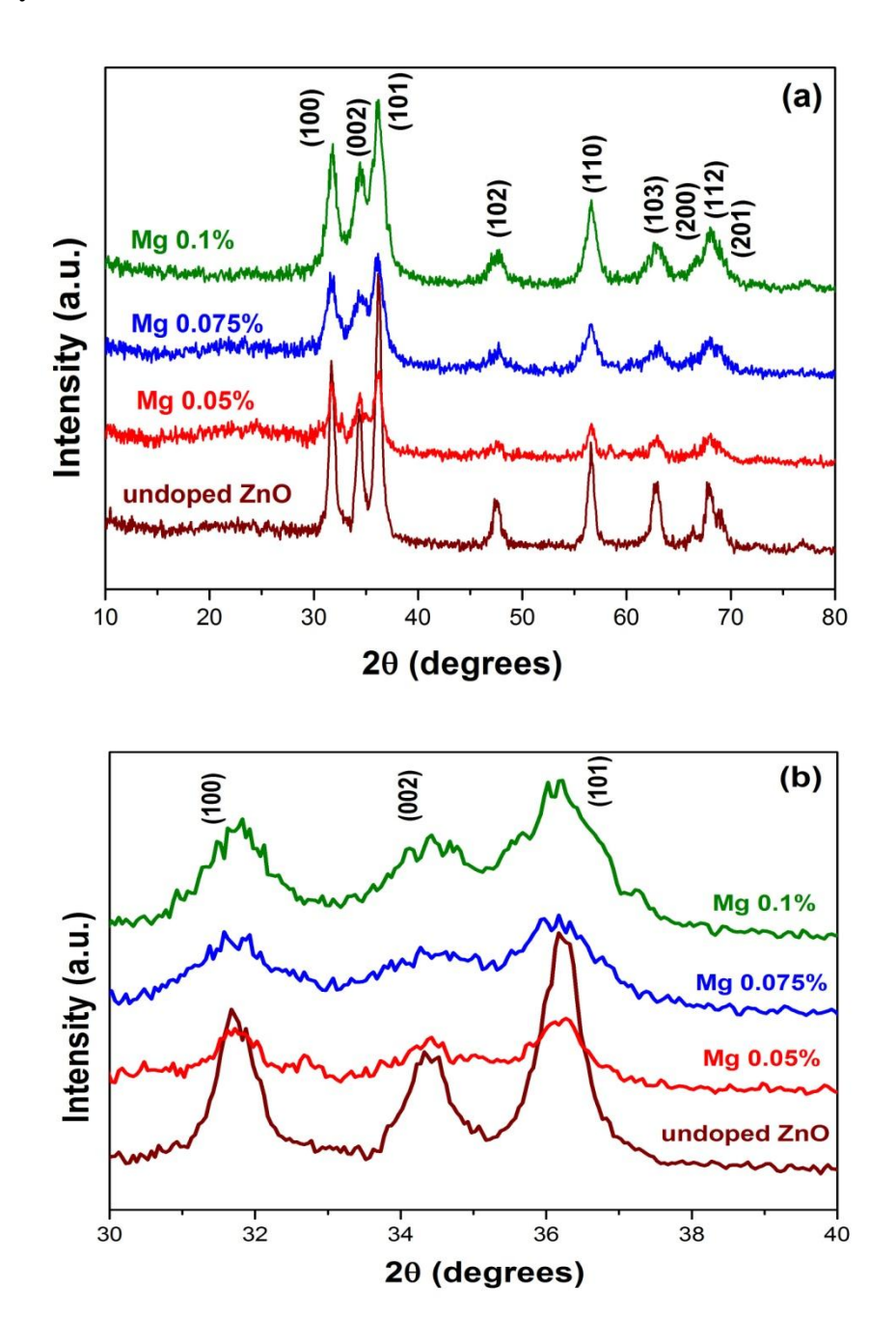


Fig. 5.1: (a) XRD patterns of un-doped and Mg-doped ZnO nanoparticles (b) expanded view of XRD patterns shift

These results indicate that the D value in the Mg-doped ZnO nanoparticles decreased as the doping concentration increased. Furthermore, the increasing Ag content decreases the lattice parameters and average crystallite size values. Based on review of literature found same results were reported by Saravanan et al. [19] in Mg-doped ZnO nanoparticles and Udom et al. [20] in Mg-doped ZnO nanowires.

Table 5.1 Lattice parameters and crystallite size of pure and Mg-doped ZnO nanoparticles

Mg Doping Concentration (mol.%)	Hkl	a[Å]	c[Å]	c/a	Crystallite size (nm)
ZnO	(100) (002) (101)	3.2555	5.2184	1.6029	23
ZnO-Mg _{0.05}	(100) (100) (002) (101)	3.2586	5.2240	1.6031	18
ZnO-Mg _{0.075}	(101) (100) (002) (101)	3.2562	5.2190	1.6027	16
ZnO- Mg _{0.1}	(100) (002) (101)	3.2556	5.1940	1.5954	15

5.3.2 SEM Analysis

The surface morphology of the pure and ZnO-Mg_X nanoparticles were investigated by scanning electron microscope (SEM-JEOL JS-6390) with energy dispersive X-ray spectrometer (EDX)21 SEM. SEM images of pure ZnO and Mg (0.05, 0.075 and 0.1 mol.%) doped ZnO nanoparticles are shown in Fig.5.2(a-d). Fig.5.2(a) shows the formation of irregular spherical morphology of the pure ZnO.

From the Fig.5.2 (b-d), it was clearly found that well prepared samples are in nanometer size and the surface morphology changes with the increase in addition of magnesium concentration. When the concentration of added magnesium increases the particles gets agglomerated and particle size increases for doped zinc oxide nanomaterials. The reason for the increase of particle size is the increase of alkalinity and it favors the grain growth. The increase of magnesium concentration increases the pH of the precursor solution and thereby enhances the crystal growth. Due to this the particle size of doped ZnO increases with increase of solution concentration.

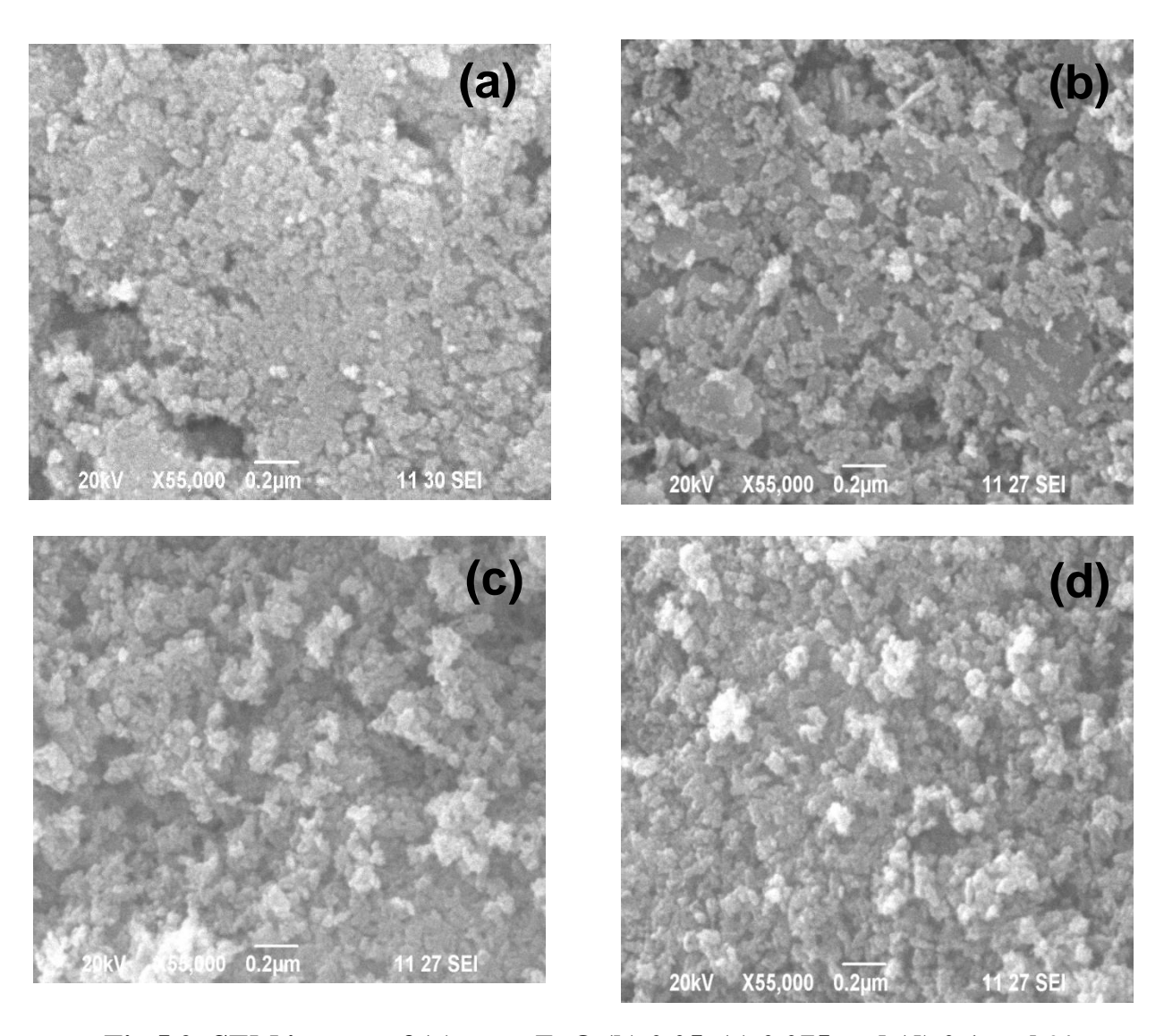


Fig.5.2: SEM images of (a) pure ZnO (b) 0.05, (c) 0.075 and (d) 0.1 mol.% Mg-doped ZnO nanoparticles

5.3.3 EDX Analysis

The elements present in the synthesized nanoparticles are analyzed using Energy Dispersive X-ray (EDX) meter. Energy Dispersive X-ray (EDX) analysis is based on the principle of unique atomic structure provides unique set of peaks on its X-ray spectrum for each element. The EDXA were recorded in the range of 0-20 keV binding energy region.

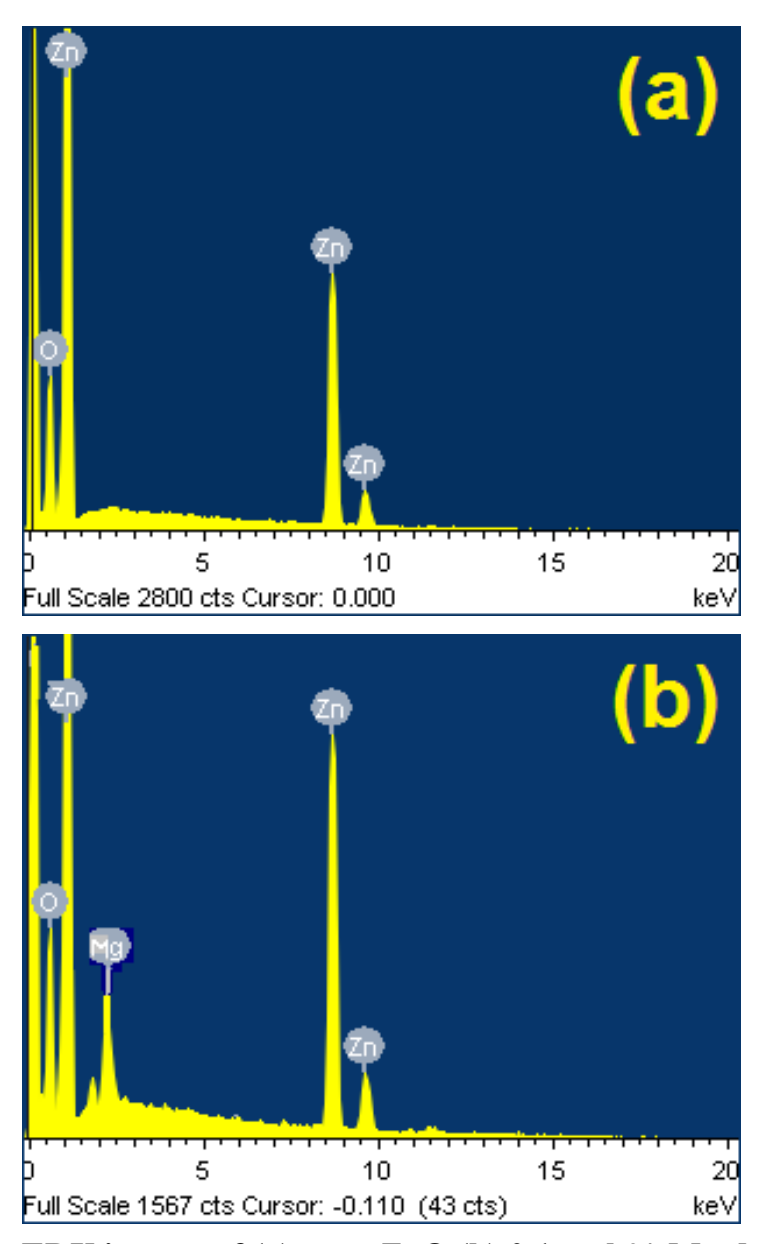


Fig.5.3: EDX images of (a) pure ZnO (b) 0.1 mol.% Mg-doped ZnO nanoparticles

The EDX spectra for pure ZnO and Mg (0.1%)-doped ZnO nanoparticles are shown in Fig.5.3 (a, b). EDX spectrum of pure ZnO sample contain only Zn and O elements no significant peaks for other elements were detected. The EDX pattern of Mg-doped nanoparticles also include elements such as existence of magnesium (Mg) composed with Zn and O, indicating the successful doping of Mg in the ZnO matrix.

5.3.4 UV-Visible Absorption Spectra

Band gap energies of the samples were analysed from UV-visible spectra recorded using UV-Vis double-beam spectrophotometer (Systronics: AU-2707). UV-Visible absorption spectra have been studied. The Fig.5.4 (a-d) shows the UV-Vis absorption spectra of pure ZnO and Mg (0.05, 0.075 and 0.1 mol. %) doped ZnO nanoparticles. Pure ZnO has an absorption cut-off edge was observed around 363 nm indicates the presence of good crystalline and impurity suppressed ZnO nanostructures. Substitution of Zn2+ by Mg2+ results in an increase in oxygen vacancies and electron concentration due to the electro negativity and ionic radius difference between Zn and Mg. Pure and Mg_x-doped ZnO (x = 0.05, 0.075 and 0.1%) shows the absorption peak at 363.71, 385.43, 396.28 and 404.97 nm respectively. The adsorption of Mg-doped ZnO nanoparticles was shifted to the longer wavelength from ZnO with the increase of the molar ratio of Mg (0.05, 0.075 and 0.1 mol. %). After Mg-doping display a small shift absorption in the visible region. The calculated optical band gap energies were 3.76, 3.64, 3.54 & 3.38 eV for pure and Mg-doped ZnO nanoparticles, respectively. According to some earlier reports similar result was observed by Hassan et al. [22].

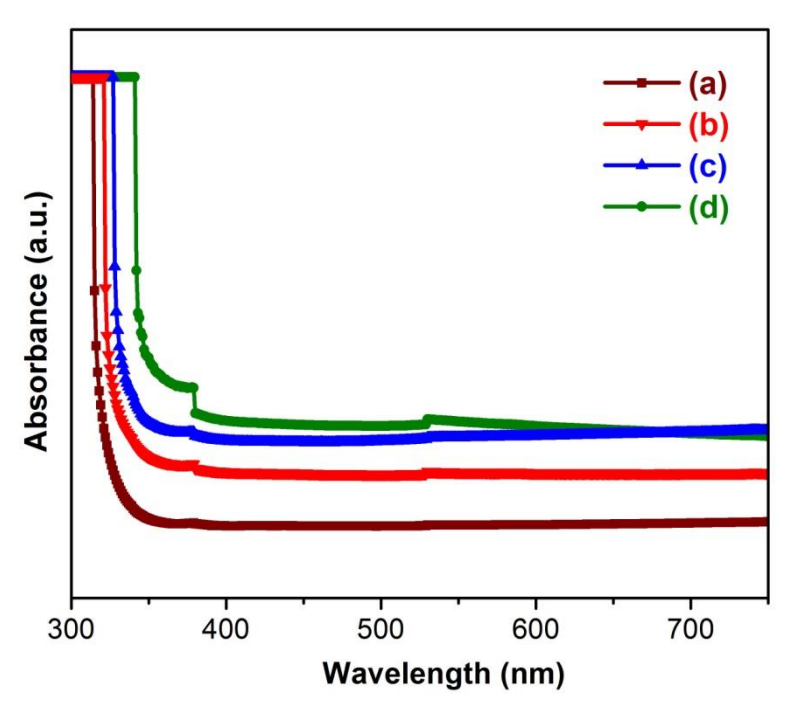


Fig.5.4: UV-Vis absorbance spectra of (a) pure ZnO (b) 0.05, (c) 0.075 and (d) 0.1 mol.% Mg-doped ZnO nanoparticles

5.3.5 FT-IR Analysis

The various functional groups of pure and ZnO-Mg_X nanoparticles were characterized by FT-IR transmittance spectra recorded by Perkin-Elmer spectrometer in the wavenumber range of 4000-400 cm⁻¹ using KBr pellet method. This spectral region encompasses several important stretch modes involving hydrogen bonded to carbon as well as to oxygen, and bonding between Zn–O is clearly observed. The FT-IR spectra of ZnO-Mg_X ($x \approx 0$ and 0.1 mol.%) nanoparticles are presented in Fig.5.5(a, b). Common bands exist at 3452 and 3441 and 1625 cm⁻¹ which corresponds to the -OH stretching and bending vibration of the water molecule [23]. The band at 2380 cm⁻¹ corresponds to symmetric and asymmetric C–H bond [24]. The observed FTIR spectrum exhibits several well-defined absorption bands at 1122, 1120 and 920 cm⁻¹ and they are attributed to sulphate and C=C bonds, respectively [25].

The absorption peaks appear at 400 and 550 cm⁻¹ were assigned to the metal—oxygen (M–O) stretching mode [26] and the absorbance peak noticed in the spectra around 455 and 453 cm⁻¹ corresponds to the presence of Zn–O and Mg-O stretching bond, respectively.

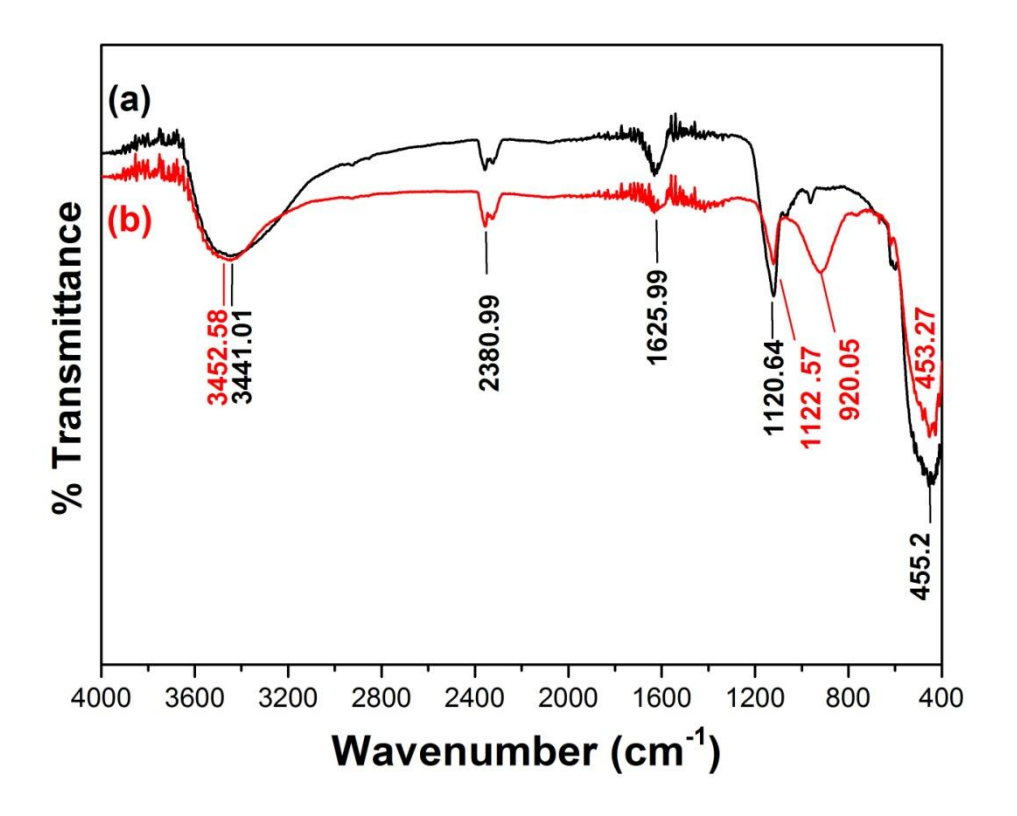


Fig.5.5: FT-IR spectra of (a) pure ZnO and (b) 0.1% Mg-doped ZnO nanoparticles

5.3.6 I-V Characteristics

Electrical characteristics (I-V) were carried out using a Keithley electrometer 2400 model of pure ZnO and Mg (0.1%)-doped ZnO nanoparticles was measured by using the I-V characteristics and it is presented in Fig.5.6 (a, b). From IV curves, electrical conductivity of pure ZnO and Mg (0.1%)-doped ZnO taken under varying temperatures from 30 to 130 °C. This study reveals that (0.1%) Mg-doped ZnO nanoparticles shows better conductivity than the pure ZnO and it may due to the presence of more charge carrier's mobility [27].

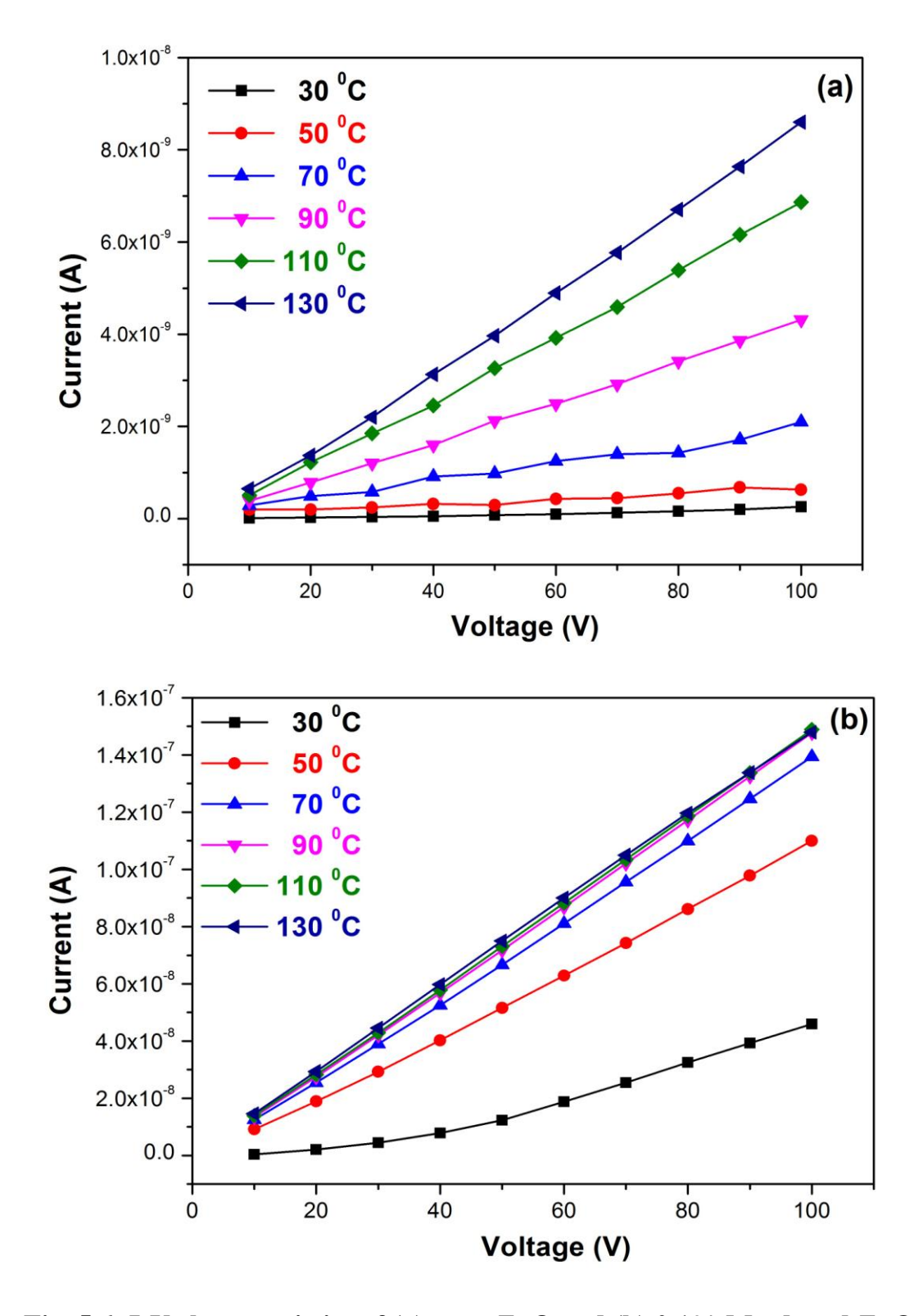


Fig. 5.6: I-V characteristics of (a) pure ZnO and (b) 0.1% Mg-doped ZnO nanoparticles

5.3.7 Photocatalytic Activity

Photocatalytic activity of the pure and Mg-doped ZnO nanoparticles was evaluated for degradation of MB and MO dye solution under UV light irradiation. The photocatalytic procedure was conducted by adding 10 mg of photocatalyst in 50 ml, 10 ppm of MB and MO dye solution. The reaction mixture was stirred for 30 min. under a dark to reach adsorption–desorption equilibrium. After that the dye solution was irradiated with an 8 W UV lamp was switched on. At different time intervals (0, 15, 30, 45, 60 and 75 min.) samples were taken out and centrifuged to separate the catalyst and then the supernatant was analyzed in a UV-visible double beam spectrophotometer maximum wavelength (λ_{max}) observed at ~664 and 464 nm to study the photocatalytic degradation. The photo-degradation efficiency (D%) of the MB and MO dye was calculated using the equation [17]

$$(D\%) = [A-A_0/A_0] \times 100$$
 ... (1)

Where, A_0 and A are the initial and final degradation time of MB and MO (mg/l) dye solution used.

5.3.7.1 Optimized factors to the photocatalytic activity

The photocatalytic degradation of pure and Mg-doped ZnO nanoparticles were selected for the evaluation of photocatalytic activity under UV-visible light. In order to study the effect of the UV light on the degradation of MB and MO dye. The dyes were prepared in various concentrations like acidic, neutral and alkaline medium. The photocatalytic activity was carried out and optimized for pure ZnO catalyst with MB and MO dye concentration of 10 ppm, catalyst concentration of 10 mg, pH = 6 and UV irradiation time up to 150 min

5.3.7.2 Impact of UV irradiation on degradation of MB and MO

For the above-mentioned conditions, the photocatalytic degradation was carried out for Mg-doped ZnO nanoparticles. Fig.5.7 & 5.8 depicts the absorbance spectra of the typical time dependent UV-Visible spectra of methylene blue dye during photo irradiation with Mg doped ZnO nanoparticles with pH = 2 and 4. The rate of degradation was recorded with respect to the change in the intensity of absorption peak in visible region. Fig.5.10(a-d) shows the comparative spectra of degradation of MB dye with pure ZnO and Mg (mol% = 0.05, 0.075, 0.1)-doped ZnO nanoparticles with respect to time at pH =6. The high intensity absorption peaks were observed at ~664 nm for MB dye. It was observed that the degradation of MB dye increases with increase of dopant concentration [16].

The effect of irradiation time of UV on MB dye degradation is shown in Fig.5.7(e). The efficiency of pure and Mg-doped ZnO nanoparticles under UV light reaches 40, 69, 68 and 57% after 75 min light irradiation. Mg (0.05%)-doped ZnO nanoparticle shows the highest degradation efficiency of 69% under UV radiation for MB dye, while under similar conditions, a much lower efficiency (40%) was observed for pure ZnO nanoparticles under visible light radiation [16].

The comparative spectra for degradation MO dye with pure ZnO and Mg (mol% = 0.05, 0.075, 0.1)-doped ZnO nanoparticles with respect to time was presented in Fig.5.8(a-d). The high intensity absorption peaks of MO dye were observed at ~464 nm. The effect of irradiation time of UV on MO dye degradation is shown in Fig.5.8(e). The degradation efficiency increases with increase of dopant concentration and the obtained values are 36, 72, 76 and 92%, respectively for pure,

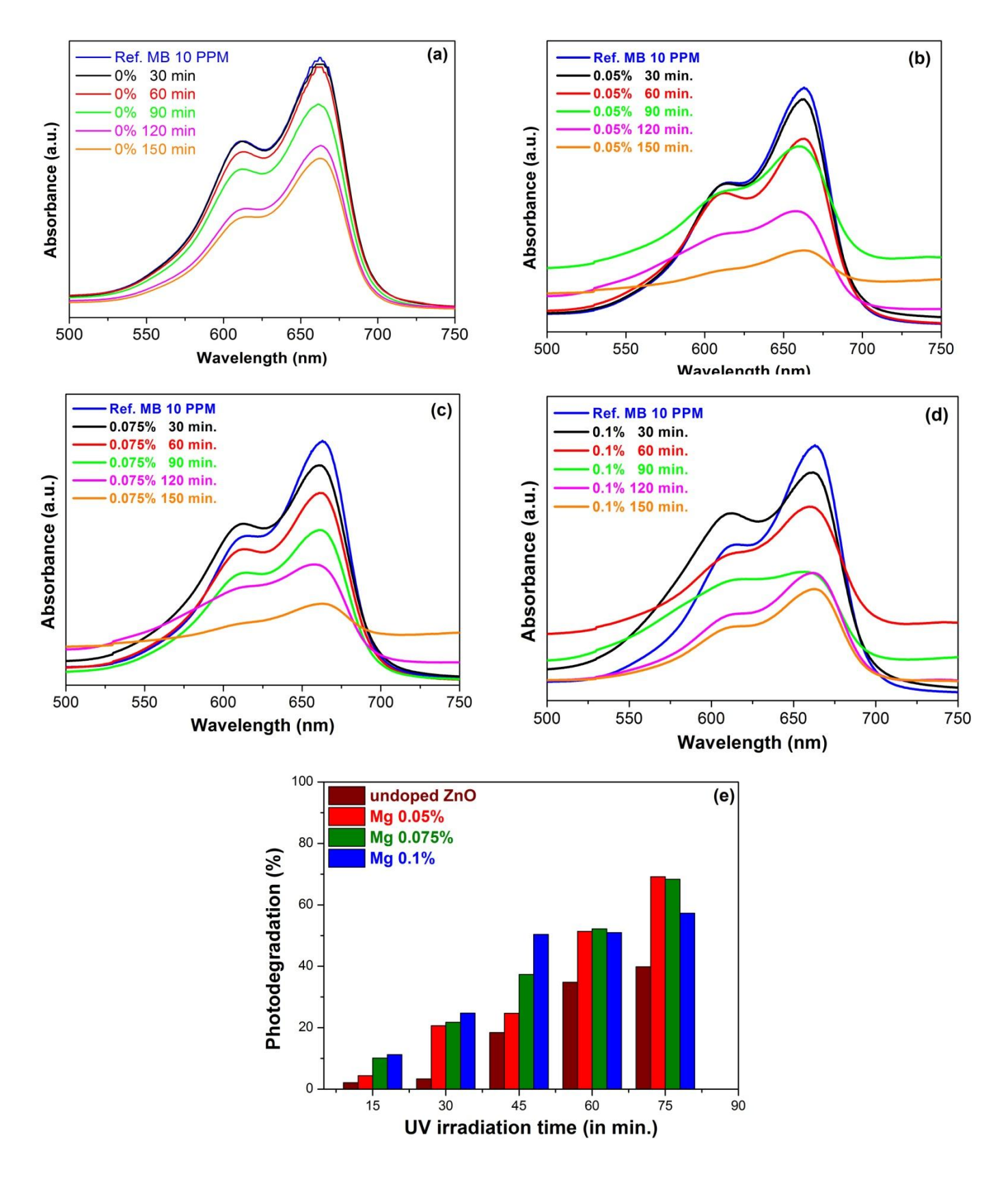


Fig.5.7: MB dye degradation of (a) pure (b) 0.05, (c) 0.075, (d) 0.1 mol.% Mg-doped ZnO nanoparticles (MB dye:10 ppm, catalyst dose:10 mg, pH=6) and (e) effect of irradiation time of UV on MB photo-degradation.

0.05, 0.075 and 0.1 mol.% Mg-doped ZnO nanoparticles. It can be seen that maximum degradation (92%) of MO dye was achieved for Mg (0.1%)-doped ZnO nanoparticles in 75 min. It should be noted that MO was degraded more faster than MB in the presence of the Mg-dopant. The possible photocatalytic degradation mechanism of MB and MO on Mg-doped ZnO nanoparticles under UV-visible light irradiation can be explained from the equation 2 to 7. During the catalytic process, photons can excite electrons in the valence band (VB) to be moved up to the conduct band (CB) and generate the same amount of electron-hole pair (e- and h⁺). The photo-excited electrons will be transferred from ZnO to Mg nanoparticles under the potential energy.

$$ZnO + h\gamma$$
 \longrightarrow $ZnO (h^{+}_{VB} + e^{-}_{CB})$... (2)

$$ZnO(e_{CB}^-) + Mg \longrightarrow ZnO + Mg(e_{CB}^-)$$
 ... (3)

$$Mg (e_{CB}) + O_2 \longrightarrow O_2 + Mg \qquad ... (4)$$

$$ZnO(h^{+}_{VB}) + H_2O \longrightarrow ZnO + H^{+} + OH$$
 ... (5)

$$(\cdot O_2^- + \cdot OH) + dye (MB \text{ or } MO) \longrightarrow degradation products ... (6)$$

$$(\cdot O_2^- + \cdot OH) + degradation products \longrightarrow CO_2 + H_2O$$
 ... (7)

The photocatalytic activity is effective thereby preventing the recombination between electrons and holes on the surface of ZnO. Afterwards, the electron on Mg dopant can produce the $\cdot O_2^-$ superoxide radical, while the holes in the VB can react with H_2O_2 to produce $\cdot OH$ hydroxyl radical [28]. These free radicals can degrade organic compounds to CO_2 and H_2O [21]. Till now, many studies have proven that electrons can transfer from Mg to the CB of ZnO. Then, they are scavenged by adsorbed O_2 molecules to yield superoxide radical anions $(\cdot O_2^-)$ to degrade dye molecules [28]. Therefore, the photocatalytic activity will be enhanced.

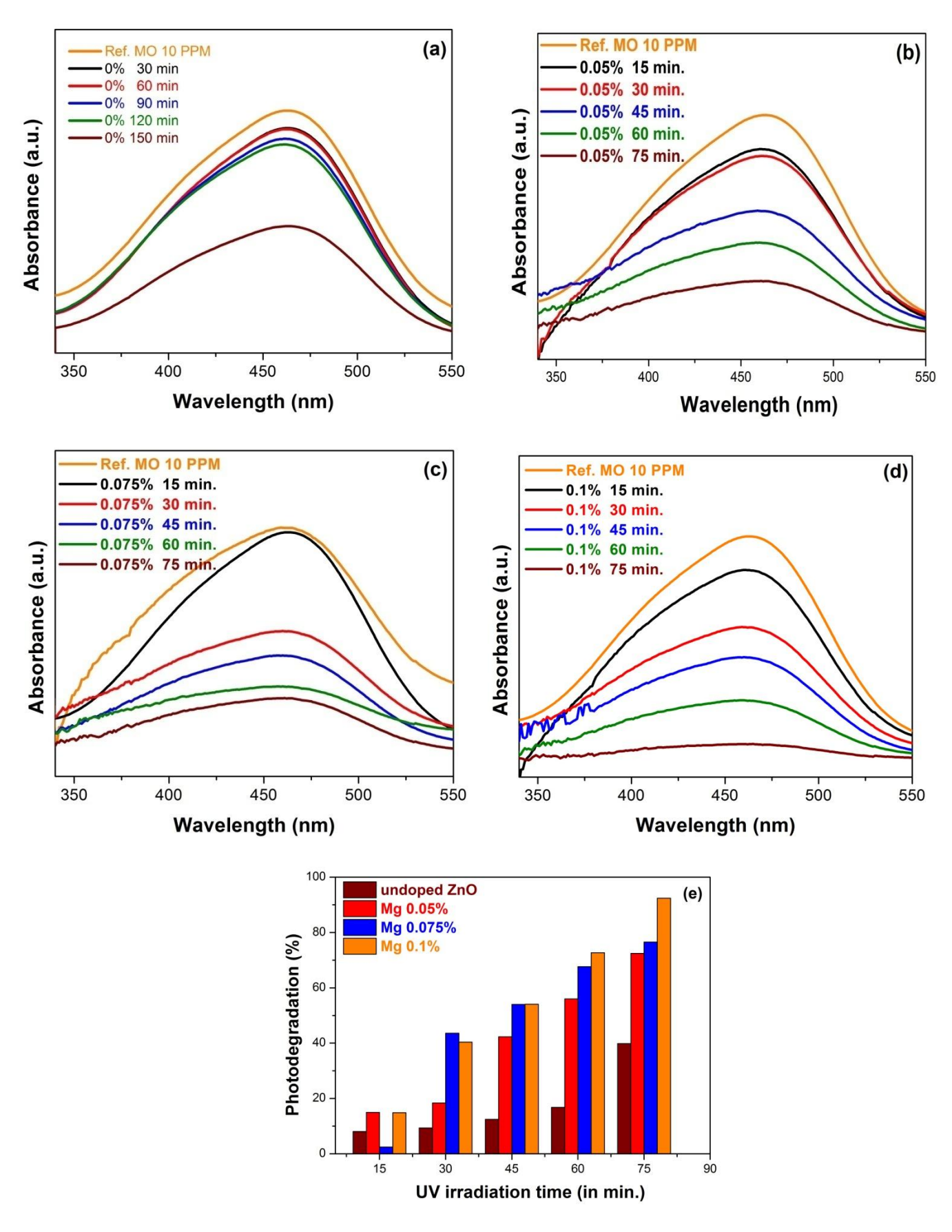


Fig.5.8: MO dye degradation of (a) pure (b) 0.05, (c) 0.075, (d) 0.1 mol.% Mg-doped ZnO nanoparticles (MB dye:10 ppm, catalyst dose:10 mg, pH=6) and (e) effect of irradiation time of UV on MO photo-degradation

5.4 Conclusion

Pure and different % of Mg doped ZnO nanoparticles were prepared by using simple co-precipitation method. All the prepared samples are characterized by using various techniques like X-ray diffraction technique, scanning electron microscope and UV-Vis spectroscopy analysis. The XRD result shows that when the doping concentration increases the particle size decreases. From the optical absorbance spectra, it should be noted that the band gap decreases with the dopant concentration. The effect of Mg doping on structural, optical and photocatalytic degradation of MB and MO have been investigated. It has been observed that 0.1% Mg doping the performance at higher pH values.

References

- [1] M. Swaminathan, N. Shobana, J. Sep. Pure. Techn. 56(2007) 101–107.
- [2] H. Tong , X. Tao, D. Wu, X. Zhang, D. Li, L. Zhang, J. Alloys Comp. 586(2014) 274–278.
- [3] A. Akyol, M. Bayramo glu, J. Haz. Mat. B124 (2005) 241–246.
- [4] K. Haga, T. Suzuki, Y. Kashiwaba, H. Watanabe, B.P. Zhang, Y. Segawa, Thin Sol. Films 433 (2003) 131–134.
- [5] J. H. Lee, K.H. Ko, B. O. Park, J. Cryst. Growth 247(2003) 119–125.
- [6] X. Jiang, F. L. Wong, M. K. Fung, S. T. Lee, Appl. Phys. Lett. 83(2003) 1875– 1877.
- [7] N. Audebrand, J. P. Auffredic, D. Louër, Chem. Mat. 10(1) (1998) 2450–2461.
- [8] S. Shi, Y. Yang, J. Xu, L. Li, X. Zhang, G. H. Hue, Z. M. Dang, J. Alloys Comp. 576(2013) 59–65.
- [9] B. Karthikeyan, C. S. Suchand Sandeep, T. Pandiyarajan, P. Venkatesan, R. Philip, Appl. Phys. Lett. 95 (2009) 023118.
- [10] B. Vinitha, K. Manzoor, R. S. Ajimsha, P. M. Aneeshs, and M. K. Jayaraj, Syn. Reactiv. Inorg. Met- Org. Nano-Met. Chem. 38(2008)126–131.
- [11] D.I. Suh, S.Y. Lee, T.H. Kim, J.M. Chun, E.K. Suh, O.B. Yang, S.K.Lee, Chem. Phys. Lett. 442 (2007) 348–353.
- [12] R. Yousefi, A. KhorsandZak, F. Sheini, Ceram. Inter. 39 (2013) 1371–1377.
- [13] N. M. Ganesan, N. Muthukumarasamy, R. Balasundaraprabhu, T. S. Senthil, Optoelectro. Adv. Mat. Rapid Commun. 8(5-6) (2014) 581–586.

- [14] J. Li, C. Hu, Y. Zhou, M. Li, F.Xue, H. Li, J. Health Sci. 55(4) (2009) 619–624.
- [15] B. K Körbahti, K. Artut, C. Geçgel, A. Özer, Chem. Eng. J. 173(3) 2011 677–688.
- [16] S. Jagadhesan, V. Senthilnathan, T. S. Senthil, J. Optoelectron Adv. Mat. 20(2008) 188–195.
- [17] D. Balarak, M. Baniasadi, K. Chandrika, Int. J. Life Sci. Pharma Res. 10(1) (2020) 17–22.
- [18] A. A Ashkarran, A. Irajizad, S. M. Mahdavi, M. M. Ahadian, Mat. Chem. Phys. 118(1) (2009) 6–8.
- [19] S. Saravanan, M. Silambarasan, T. Soga, Japanese J. Appl. Phys. 53 (11S) (2014) 11RF01.
- [20] I. Udom, Y. Zhang, M. K. Ram, E. K. Stefanakos, A. F. Hepp, R. Elzein, R. Schlaf, D. Y. Goswami, Thin Sol. Films 564 (2014); 258–263.
- [21] S. Y. Pung, W. P. Lee, A. Aziz, Int. J. Inorg. Chem. 2012 (2012) 1–9.
- [22] M. M. Mehedi Hassan, W. Khan, A. Azam A, A. H. Naqvi, J. Ind. Eng. Chem.21 (2015) 283–291.
- [23] A. E. Jiménez-González, J. A. S. Soto Urueta, R. Suárez-Parra, J. Cryst. Growth.192(3-4) (1998) 430–438.
- [24] D. Ramimoghadam, M. Z. B. Hussein, Y. H. Taufiq-Yap, Chem. Cent. J. 7(1)71(2013) 1–10.
- [25] K. Saoud, R. Alsoubaihi, N. Bensalah, T. Bora, M. Bertino, J. Dutta, Mat. Res. Bull.63 (2015)134–140.

- [26] M. Srivastava, A. K. Ojha, S. Chaubey, P. K. Sharma, A. C. Pandey, J. Alloys Comp. 494(1-2) (2010) 275–284.
- [27] S. Abed, H. Bougharraf, K. Bouchouit, Z. Sofiani, B. Derkowska-Zielinska, M.
 S. Aida, B. Sahraoui, Superlatti. Microstruct. 85(2015) 370–378
- [28] M. Mittal, M. Sharma, O. P. Pandey, Sol. Energy 110 (2014) 386–97.

CHAPTER – VI

CHAPTER - VI

Highly Enhanced Photocatalytic Degradation of Co-doped ZnO (Fe,Ag) Nanoparticles

6.1 Introduction

Pollution occurs when chemical substance release into the environment. The three major types of pollutions are air, soil and water pollution. Among them, water pollution causes severe environmental destruction and leads to risk for our health. Industrial effluents contain cosmetics, textile, leather, paint, paper, plastics and pesticide wastages discharged into water are the major source of pollution and also they are non-biodegradable [1]. Dyes such as methylene blue (MB: C₁₆H₁₈N₃SCl) and methyl orange (MO: C₁₄H₁₄N₃NaO₃S) are harmful to the environment even if they are at low concentration [2, 3]. Wastewater treatment becomes very attractive research to convert the hazardous organic dye into harmless chemicals. Therefore, several methods, such as advanced oxidation process (AOP), electro-peroxone, coagulation and photocatalysis have been employed to improve the dye degradation of toxic organic pollutants [4-9]. Among them, photocatalysis has emerged as an important degradation technology using semiconductors for the wastewater treatment [10].

The previously reports revealed that the semiconductor photocatalysts such as Bi₂O₃, Fe₂O₃, TiO₂ and ZnO exhibit excellent photocatalytic activity under UV-light irradiation [11-14], among these semiconductor photocatalysts, ZnO and TiO₂ have been investigated due to their wide bandgap, absence of toxicity and high chemical stability [15-18]. ZnO is a promising alternative to TiO₂ photocatalyst due to their similar band gap [19, 20]. ZnO also have unique physical, chemical, optical and

electronic properties as well as for wide range of applications including UV detectors, solar cells, gas sensors and photocatalysis [21-25]. ZnO exhibits excellent performance compared with TiO_2 under UV light (~3 to 5% of solar spectra) for the photocatalytic degradation of organic dyes in aqueous solution [26].

However, ZnO have several drawbacks such as a rapid recombination of photogenerated electron and hole-pairs which decreases the photocatalytic efficiency and limited the absorption in the visible range [27]. Therefore, numerous modification methods were proposed to overcome these drawbacks and to enhance the efficiency of the photocatalytic activity of ZnO for a large-scale usage, including combination with other metal oxide nanoparticles and element doping with a heteroatom [28, 29]. Compared with the above methods, doping with transition metals into the ZnO lattice easily modifies the electronic energy band structure of ZnO. Doping of transition metals with ZnO nanoparticles acts as trap sites by capturing the photogenerated electrons or holes and restrains their recombination with enhanced photocatalytic activity [30].

The presence of two kinds of atoms (Co-doping) into ZnO surface can be efficiently captured by photogenerated electrons from the conduction band. Co-doping of transition metals with ZnO has been significantly enhances their photocatalytic activity by capturing more electrons. Different transition or noble metals such as Pt, Fe, Ag and Au could facilitate the electron transfer by trapping the photoinduced charge carriers and enhances the photocatalytic efficiency [31-33]. Among these Ag and Fe seems to be the most effective dopants for tuning the electronic and optical properties of ZnO [34]. Recently, a variety of Ag or Fe₂O₃ doped ZnO nanostructures

were reported for photocatalytic applications [35-38]. However, only few reports on Ag co-doped Fe-ZnO nanoparticles for photocatalytic activity. The performance of Ag co-doped Fe-ZnO photocatalyst have been found to most effective than the single-element doping.

There are various methods were employed to synthesis the pure and doped ZnO nanoparticles among them hydrothermal, combustion, sol—gel, microwave synthesis, pulsed laser deposition and co-precipitation method are important [39-44]. Compared with all other methods, co-precipitation method is an efficient way to synthesize the ZnO nanoparticles. The advantages of this method are simple, inexpensive, non-toxic, and easy to operate experimental conditions and uses only water as solvent.

The chapter deals, a successful attempt for the synthesis of the Ag-Fe co-doped ZnO nanoparticles (AFZ) with different mole ratios by the co-precipitation method. Various characterizations such as XRD, SEM with EDX, UV–Vis absorption spectra, FT-IR and I-V characteristics were used to characterize the structural, optical and electrical properties of the prepared AFZ nanoparticles. The influence of optimized parameters including the initial pH, dye concentration, dosage of photocatalyst and degradation efficiency was investigated. AFZ photocatalysts exhibits the higher photocatalytic activity for the degradation of organic dyes (MB and MO) under UV light irradiation. In addition, a possible mechanism of the photocatalytic activity was also discussed in detail.

6.2 Synthesis of Pure ZnO, Co-Doped Ag, Fe-ZnO (ZnO-Fe_n-Ag_x, N \approx 0.075%, X \approx 0.01, 0.02 and 0.03%) Nanoparticles

Pure ZnO and Ag co-doped Fe-ZnO nanoparticles with various mol. % ($x \approx 0.01, 0.02$, and 0.03) were synthesized by using co-precipitation method.

6.2.1 Materials

Analytical Reagent (AR) grade zinc nitrate hexahydrate [Zn(NO₃)₂.6H₂O], silver nitrate Ag(NO₃)₂, ferric nitrate nonahydrate [Fe(NO₃)₂.9H₂O], laboratory reagent (LR) grade methylene blue (MB), methyl orange (MO), and sodium hydroxide [NaOH] were obtained from Alfa Aesar chemicals, India Limited and used without further purification. Deionized water (DW) was used to prepare all the experimental solutions.

6.2.2 Preparation of Pure ZnO Nanoparticles

Pure ZnO nanoparticle was prepared by using the following procedure [45]. In a typical synthesis process, 5 g of Zn(NO₃)₂·6H₂O was added to 10 ml of DW and 4 g of NaOH in 50 ml of DW was added drop wise into the solution until the pH of the solution reached into 11. By using the magnetic stirrer the solution was stirred and heated to 60 °C for 1h. After cooling in to room temperature, the formed precipitate-solution was centrifuged and washed three times with DW and ethanol and dried at 100 °C for 2h under vacuum oven. Finally, the collected white powder was annealed at 450 °C for 1h in a muffle furnace.

6.2.3 Preparation of co-doped Ag, Fe-ZnO (ZnO-Fe_n-Ag_x, $n \approx 0.075\%$, $x \approx 0.01$, 0.02 and 0.03%) Nanoparticles

Ag co-doped Fe-ZnO nanoparticles were prepared by using DW as solvent with the required molar ratio. 1 g (0.075 mol %) of Fe(NO₃)₂.9H₂O was combined

with the $Zn(NO_3)_2.6H_2O$ solution. With this mixture solution (FZ), various mol.% of $(x \approx 0.01, 0.02, \text{ and } 0.03)$ Ag $(NO_3)_2.6H_2O$ were dissolved into 15 ml distilled water. Subsequently, 4g NaOH was added in 50 ml of DW, this solution was added drop wise in to the dopant metal mixture solution under continuous stirring up to 2h. The obtained solid precipitates (denoted as AFZ-1, AFZ-2 and AFZ-3, respectively) were centrifuged and washed three times with DW and ethanol and finally dried at 150 °C for 5h under vacuum. The obtained materials were calcinated in a muffle furnace at 450 °C for 1hour. A systematic diagram of synthesizing pure and Ag co-doped Fe-ZnO nanoparticle was depicted in Fig.6.1.

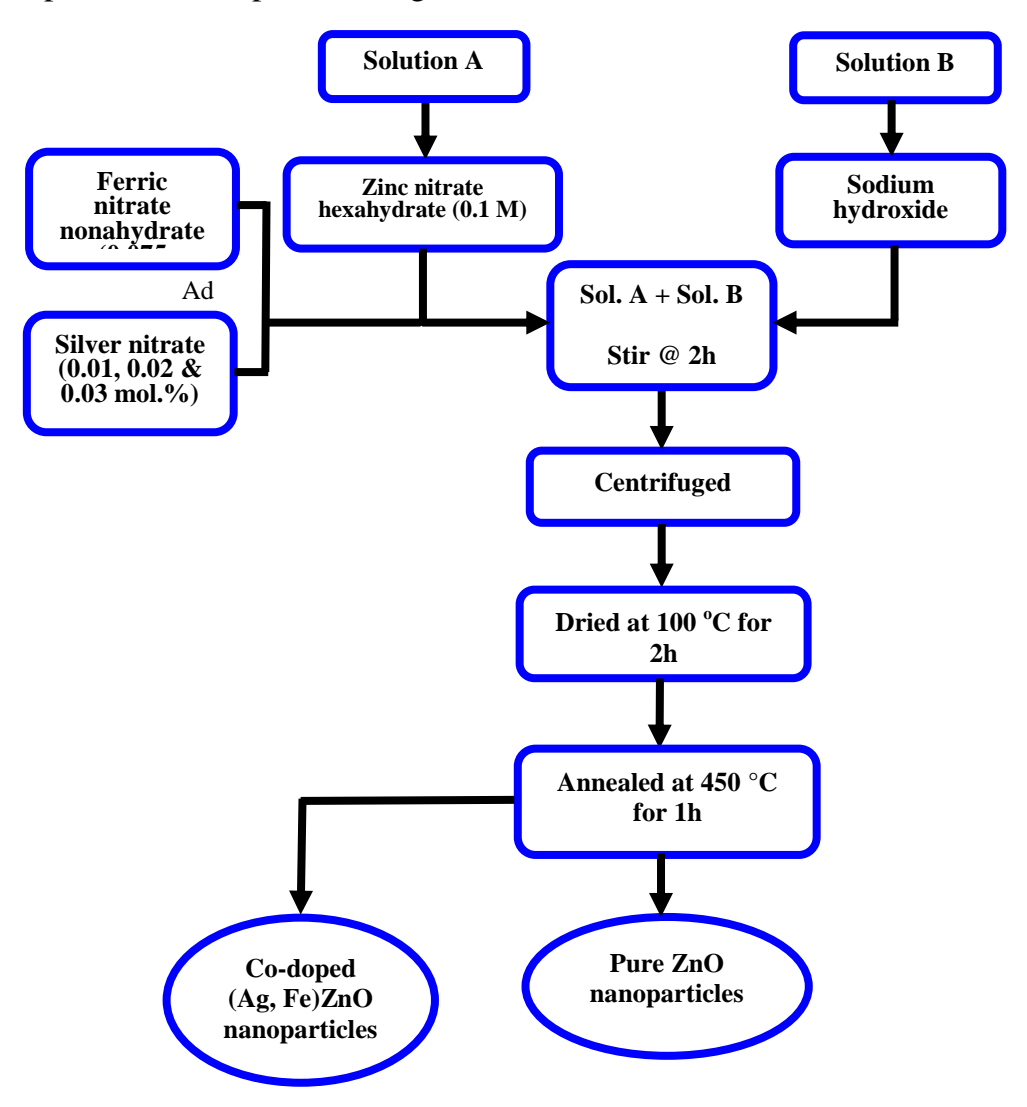


Fig.6.1: Schematic diagram of synthesizing the pure and Ag co-doped Fe-ZnO nanoparticles

6.3 Characterization techniques of Pure ZnO and Co-Doped (Ag, Fe) Zno Nanoparticles

The prepared Pure and co-doped (Ag,Fe) ZnO nanoparticles have been characterized by using XRD, SEM, EDX, UV-Visible, FTIR and I-V studies. The obtained results are given in the following section as follows.

6.3.1 XRD Analysis

The prepared nanoparticles were determined by powder X-ray diffractometer (X'PERT PRO MPD) using CuK α radiation ($\lambda = 0.15405$ nm) operated at 40 kV voltage and 30 mA current with a scanning rate of 2° per min21.XRD technique was used to characterize the crystalline phase of the as-synthesized nanoparticles. XRD patterns of the pure ZnO, AFZ-1, AFZ-2 and AFZ-3 nanoparticles are shown in Fig. 6.2 (a). All the diffraction peaks in the XRD patterns confirm the single crystalline phase with a hexagonal wurtzite structure of ZnO (JCPDS No. 36-1451, space group P6₃mc) [46]. There is no characteristic diffraction peak corresponding to Ag, Fe or any other metal impurity phases. Due to the low concentration of Ag and Fe, the peaks corresponds to the dopant might be too low [47]. Fig.6.2(b) shows a magnified view of the primary peaks present at 31.8° (100), 34.3° (002) and 36.3° (101), there is a gradual shift towards a higher angle specially in the AFZ-1, AFZ-2 and AFZ-3 nanoparticles [48]. This probably occurs due to the difference in ionic radius between the metals (Ag⁺ ≈ 1.22 Å, Fe³⁺ ≈ 0.68 Å and Zn²⁺ ≈ 0.74 Å), which indicates that the very little distortion in the crystal lattice can be caused by dopant ions, Ag^+ and Fe^{3+} ions are homogeneously distributed (substitution mechanism) in the Zn^{2+} ions matrix [49]. The intensity and width of the peaks decreases with increasing concentration of Ag. This result suggests a change in lattice parameters (i.e. a and c), volume and reduced average crystallite size (D) of the hexagonal wurtzite ZnO phase, they are presented in Table 5.1. The average crystallite size (D) of pure ZnO, AFZ-1, AFZ-2 and AFZ-3 nanoparticles have been determined by using Debye-Scherrer equation and they are found to be 23, 18, 14 and 12 nm, respectively [50]. According to this result, the doping of AFZ with ZnO matrix was confirmed, the obtained results are also similar to the previous reported literatures [31-33].

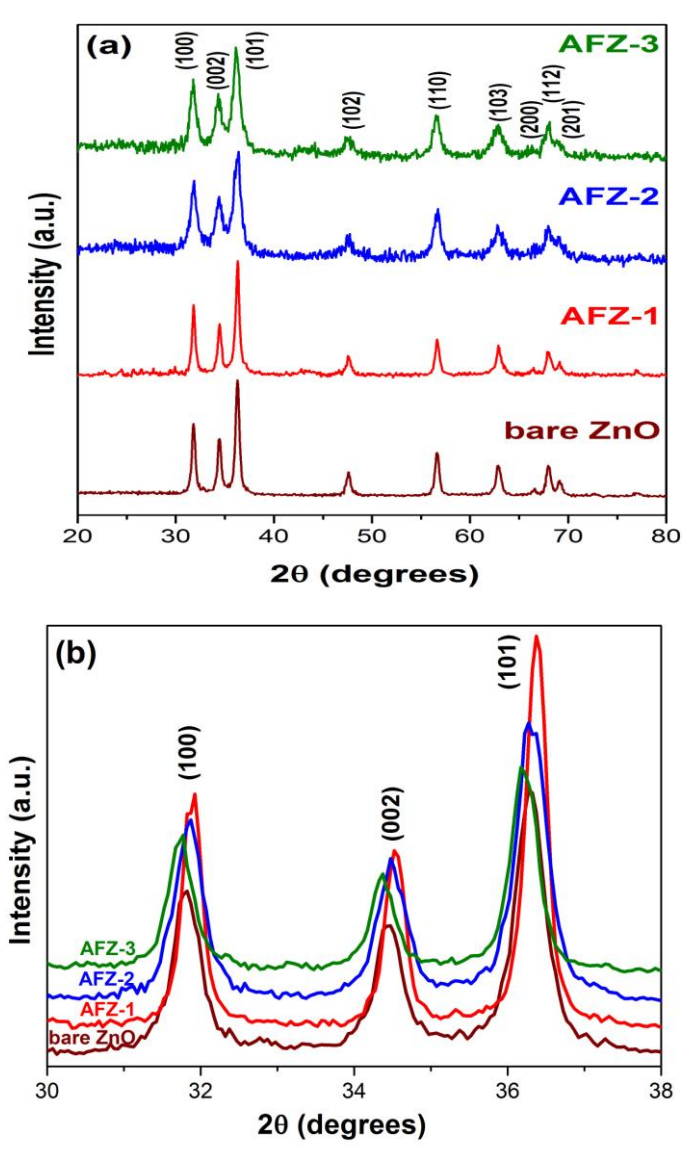


Fig.6.2: (a) XRD patterns of pure ZnO and AFZ-1, AFZ-2 and AFZ-3 nanoparticles (b) expanded view of primary XRD patterns

Table 6.1 The structural parameters for pure and AFZ nanoparticles

Ag co-doping Fe Concentration (mol.%)	Hkl	a[Å]	a[Å]	c/a	V (Å ³)	Crystallite size (nm)
ZnO	(100) (002) (101)	3.2482	5.2065	1.6028	47.5717	23
ZnO-Fe _{0.075} -Ag _{0.01}	(100) (002) (101)	3.2555	5.2174	1.6026	47.8858	18
ZnO-Fe _{0.075} -Ag _{0.02}	(100) (002) (101)	3.2562	5.2183	1.6025	47.9147	14
ZnO-Fe _{0.075} -Ag _{0.03}	(100) (002) (101)	3.2580	5.2208	1.6024	47.9907	12

6.3.2 SEM Analysis

The particle size and morphological features of the samples were observed by scanning electron microscope (SEM-JEOL JS-6390) with energy dispersive X-ray spectrometer (EDX). The surface morphology and structure of the pure ZnO, AFZ-1, AFZ-2 and AFZ-3 nanoparticles are given in the Fig.6.3. The Fig.6.3 (a) shows the presence of irregular and spherical nanoparticles with smooth surface. With the increase of the Ag dopant, the surface of the AFZ-1 nanoparticles became rough, and is shown in Fig.6.3 (b). From the Fig.6.3(c-d) it should be noted that the morphology of AFZ-2 and AFZ-3 nanoparticles are slightly agglomerated. This reveals that the Ag and Fe incorporated in to ZnO surface, and shows an aggregated form. The average diameter of spheres is around ~38-66 nm. The obtained results are good consistent

with the result of XRD results. Sabry et al. [32] found a similar behavior on Ag and Fe₂O₃ co-doped ZnO nanostructure.

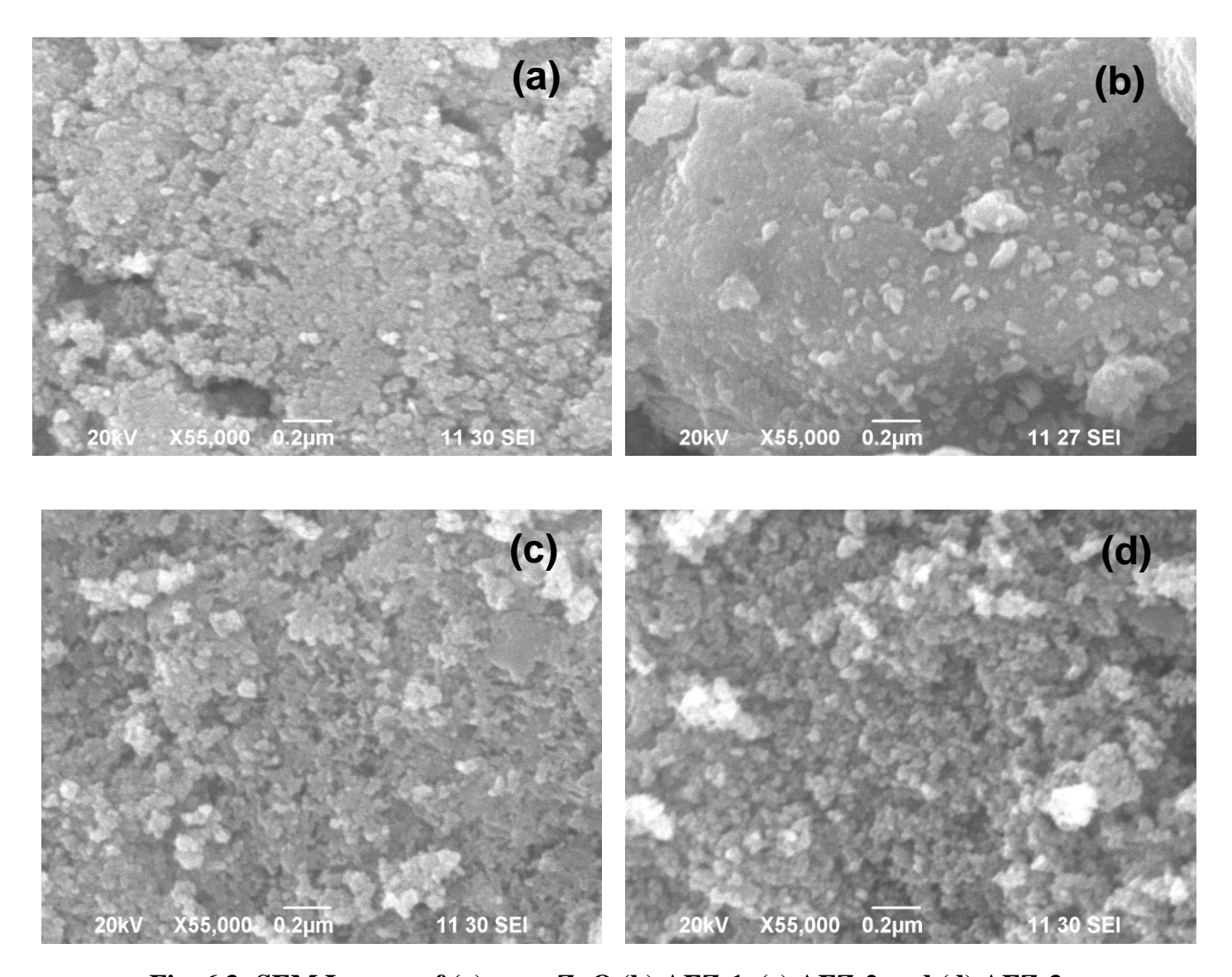


Fig. 6.3: SEM Images of (a) pure ZnO (b) AFZ-1, (c) AFZ-2 and (d) AFZ-3 nanoparticles

6.3.3 EDX Analysis

The chemical composition of as-prepared nanoparticles has been analyzed by X-Ray photometer. The EDX of pure ZnO, AFZ-1, AFZ-2 and AFZ-3 nanoparticles are shown in Fig.6.4. Typical EDX spectra of pure ZnO show the presence of zinc (Zn), and oxygen (O) [Fig.6.4 (a)]. As shown in Fig.6.4 (b-d), the EDX pattern of

AFZ nanoparticles further include deposited metals elements such as of silver (Ag), iron (Fe) together with zinc (Zn) and oxygen (O), respectively. The results of the elemental analysis investigated the homogeneous distribution of dopant metal nanoparticles in the ZnO lattice. The obtained EDX data are listed in Table 6.2.

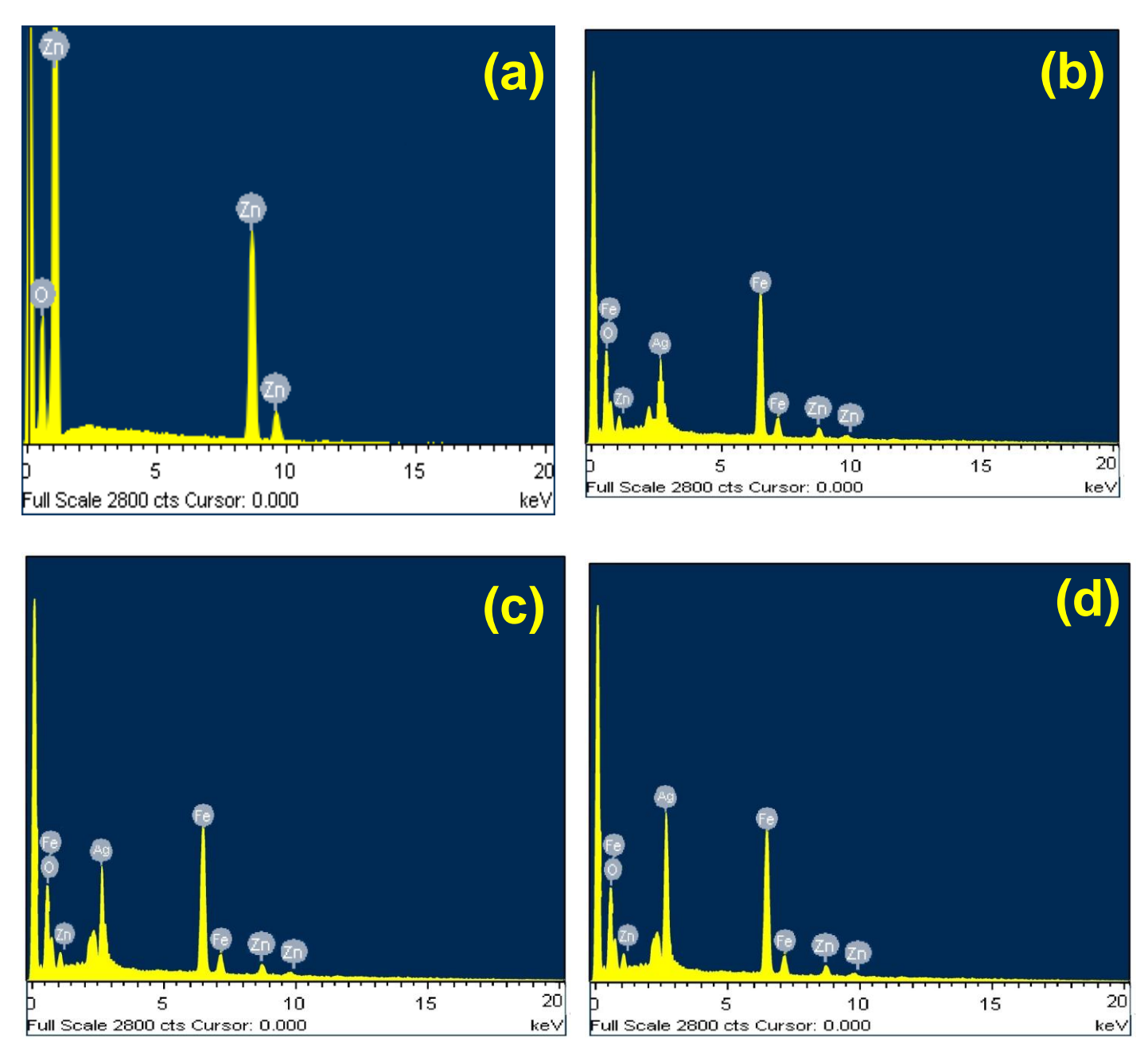


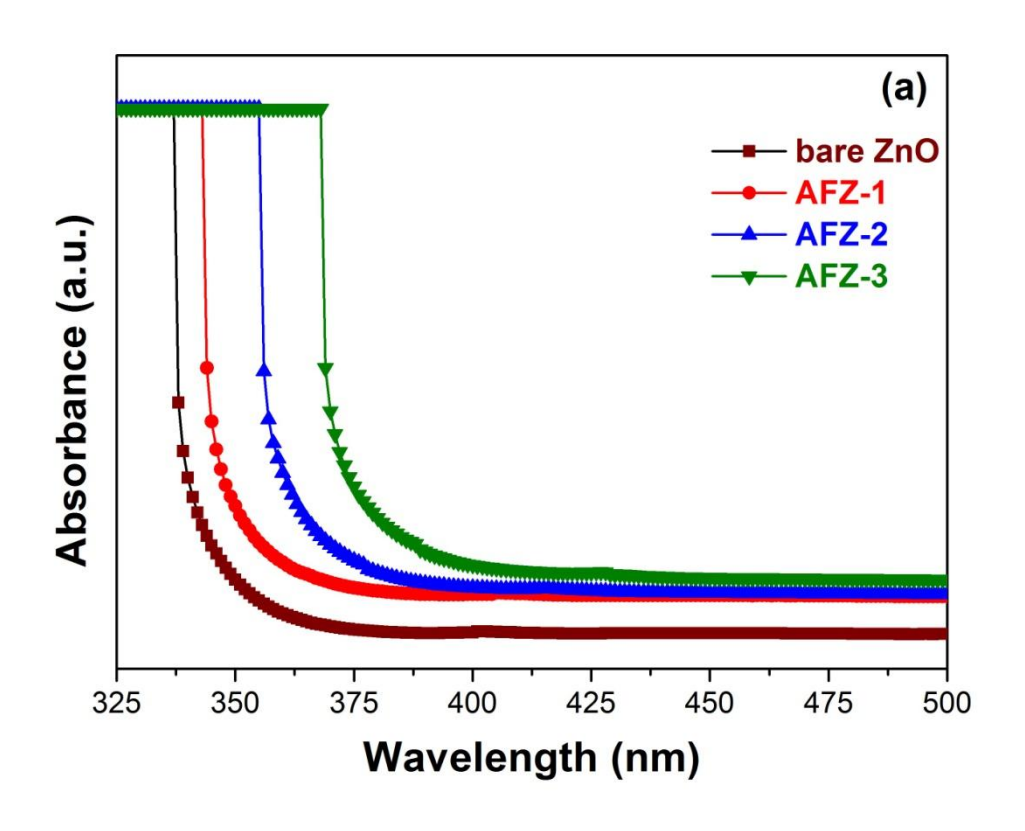
Fig. 6.4: EDX Images of (a) pure ZnO (b) AFZ-1, (c) AFZ-2 and (d) AFZ-3 nanoparticles

Table 6.2 Phase Composition of pure and AFZ nanoparticles

g .	Atomic (%)						
Samples	0	Zn	Fe	Ag			
ZnO	51.26	45.74	1	-			
AFZ-1	70.17	12.35	10.99	6.49			
AFZ-2	70.15	10.30	10.95	8.60			
AFZ-3	69.24	8.76	10.98	11.02			

6.3.4 UV-Vis Absorption Analysis

The optical absorption property is vital analysis for photocatalytic activity of the as-synthesized nanoparticles and it was investigated by UV-visible absorption spectra using UV-Vis double-beam spectrophotometer (Systronics: AU-2707) at room temperature. UV–Vis absorption spectra and the plot of (αhv)² versus hv of pure ZnO, AFZ-1, AFZ-2 and AFZ-3 nanoparticles are depicted in Fig.6.5, respectively. As shown in Fig.6.5 (a), the absorption spectra of pure ZnO show the absorption edge around ~340 nm. After co-doping, AFZ-1, AFZ-2 and AFZ-3 nanoparticles shows shift in the absorption edge from 370 to 390 nm. The bandgap energy of the photocatalysts were calculated from Fig.6.5 (b) [51]. The bandgap values of the samples are 3.65, 3.57, 3.46 and 3.33 for pure ZnO, AFZ-1, AFZ-2 and AFZ-3 nanoparticles, respectively. The observed shift of AFZ nanoparticles may be attributed to incorporation of Ag/Fe into ZnO lattice and reduces the bandgap of the material.



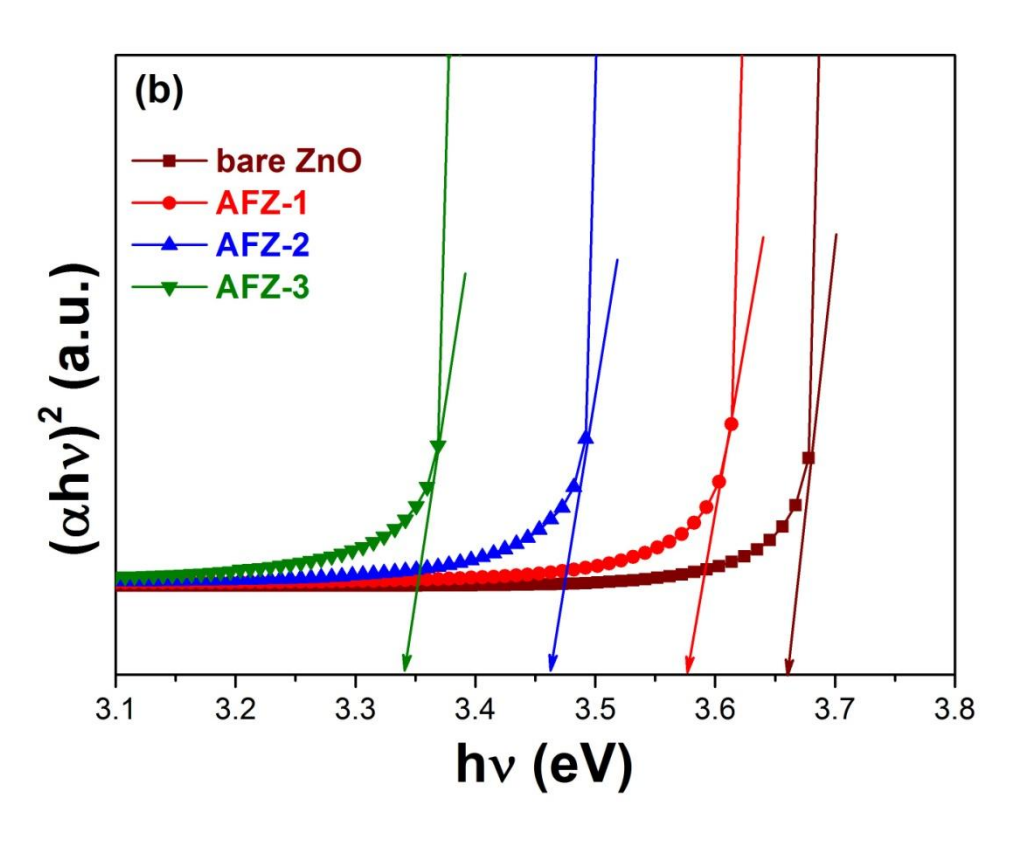


Fig.6.5: (a) UV-Vis Absorbance Spectra of bare and AFZ Photocatalysts, (b) The Plot of $(\alpha h v)^2$ vs. Photoenergy

6.3.5 FT-IR Analysis

The chemical characteristic functional groups of prepared nanoparticles have been characterized by FT-IR analysis. FT-IR spectra of the pure ZnO and AFZ-3 nanoparticles recorded by using a FTIR Spectrometer (JASCO FTIR-410) in the range 400–4000 cm-1with a resolution of 4 cm-1 at room temperature using KBr disc at room temperature in the range of 4000–400 cm⁻¹ were presented in Fig.6.6. FT-IR spectra of the pure ZnO nanoparticles shows broad absorption peaks at 3441 and 1625 cm⁻¹, corresponding to O-H stretching and O-H bending vibration of the water molecule [52] respectively. In fact, FT-IR spectra of AFZ-3 nanoparticles shows the vibration peaks at 3543 and 1622 cm⁻¹ shifts from high to lower wave number. FT-IR spectra of the pure ZnO nanoparticles shows prominent peak at 455 cm⁻¹ could be assigned to the metal–oxygen stretching modes and confirms the formation of ZnO and M/ZnO [53].

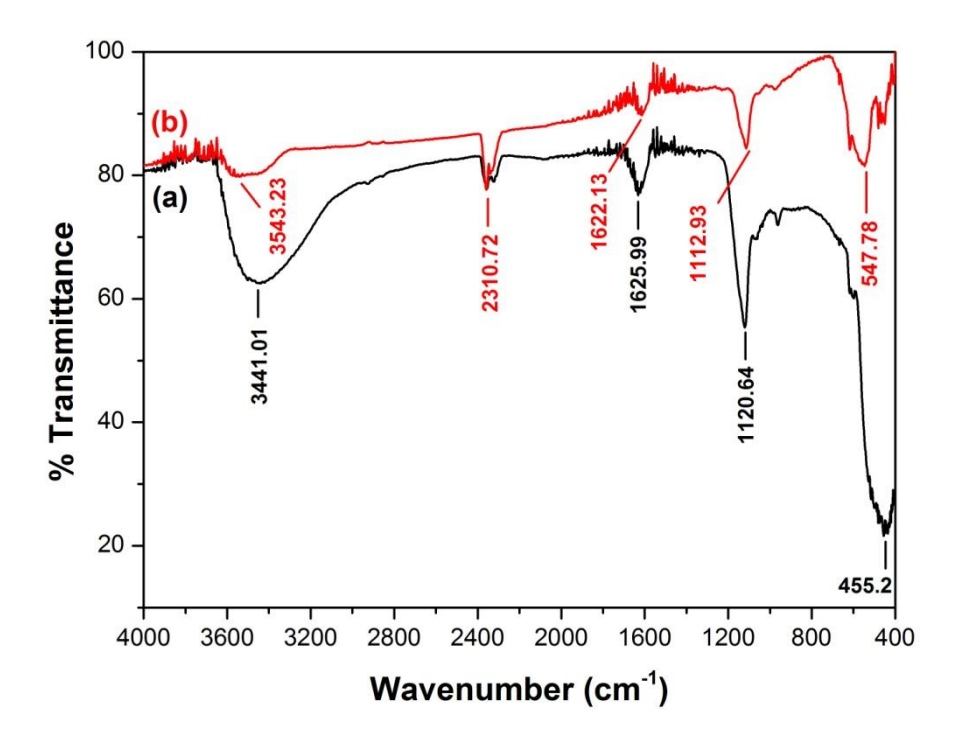
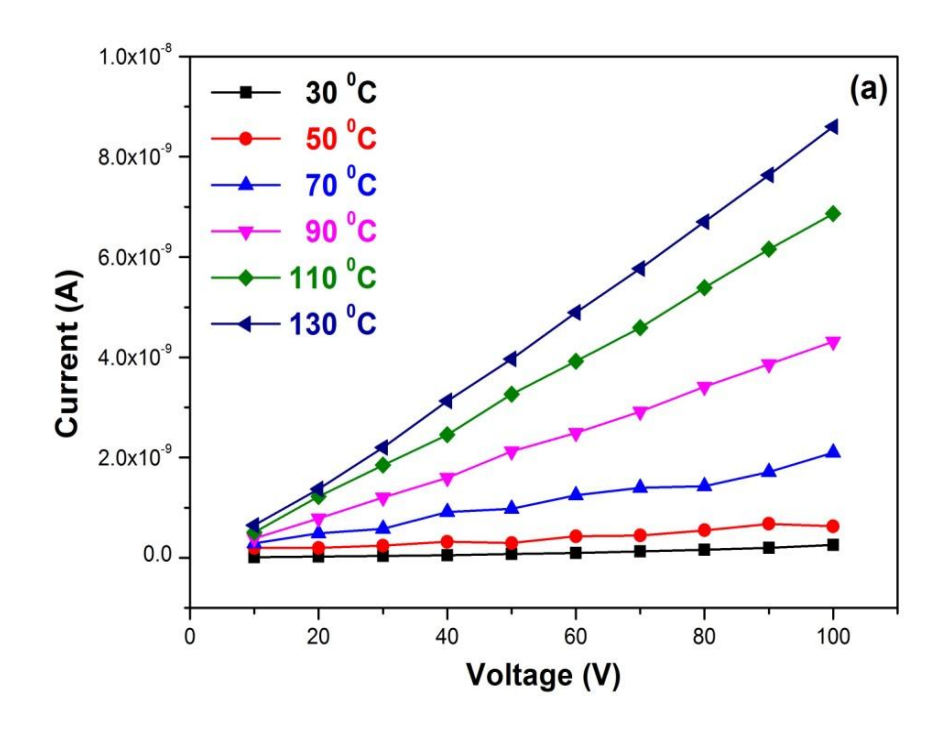


Fig.6.6: FT-IR spectra of (a) pure ZnO and (b) AFZ-3 nanoparticles

FT-IR spectra of the AFZ-3 nanoparticles absorption peak at 455 cm⁻¹ shifted to 547 cm⁻¹, respectively and the intensity of the M-O stretching was also weakened and no additional peaks are present indicating the absence of Ag and Fe bands. It clearly proves that the presence of co-dopants and changing of bonding energy of Zn-O stretching vibrations [54]. The weak intensity peak appeared at 2310 cm⁻¹ which corresponds to the absorption of atmospheric CO₂ on the metal cations surface [55]. The absorption peaks appeared at 1120 and 1112 cm⁻¹ assigned to the sulfate group, respectively [56].

6.3.6 I-V Characteristics

The Electrical characteristics of prepared nanoparticles have been investigated by using a Keithley electrometer 2400 model. I-V curves of pure ZnO and AFZ-3 nanoparticles are presented in Fig.6.7. The electrical conductivity of pure ZnO and AFZ-3 nanoparticles has been determined in the temperature range from 30 to 130 °C, respectively. It can be noticed that the variation of voltage with current of the both photocatalysts increase with increase of temperature. The estimated electrical conductivity of AFZ-3 nanoparticles increases compared with the value of Pure ZnO (from 10⁻⁹ to 10⁻⁶ S/cm). The increase of electrical conductivity of the AFZ-3 nanoparticles indicates the increase of charge carrier's mobility [57].



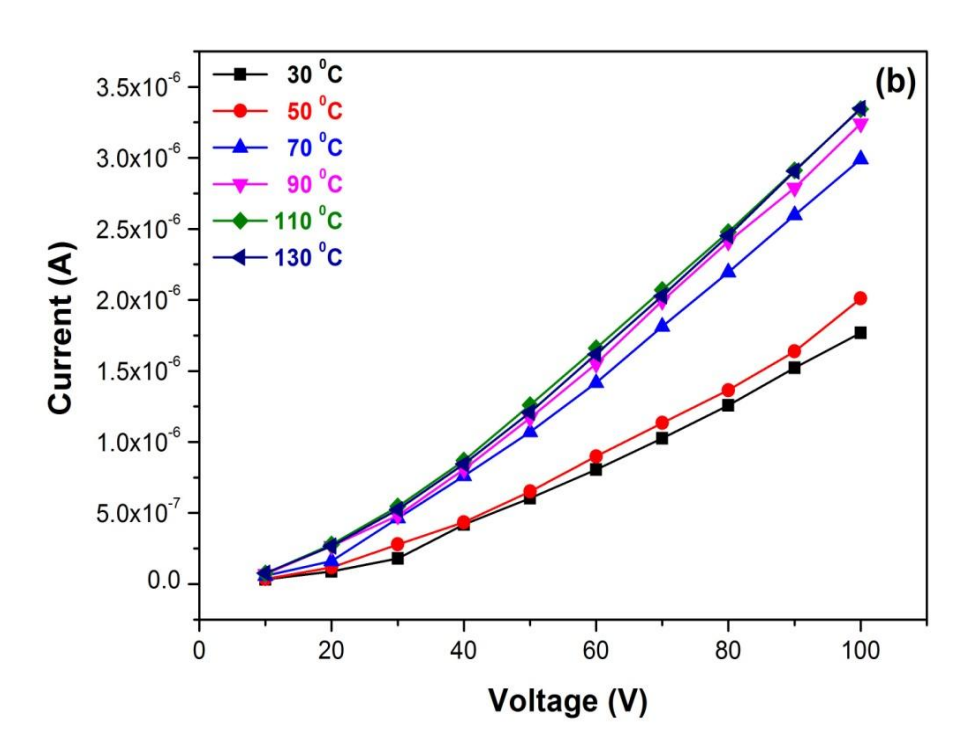


Fig.6.7: I-V characteristics of (a) Pure ZnO and (b) AFZ-3 nanoparticles

6.3.7 Photocatalytic Activity

The photocatalytic activities of the samples were evaluated by monitoring the time-dependent photodegradation of organic dyes including MB and MO solution under UV-light irradiation (8W Philips). In a typical experiment, 0.2g of photocatalysts were dissolved into beaker containing 25 ml of 0.1 g/l MB and MO dye solution at various pH (2, 4, and 6) in dark room for 30 min. Next, the dye solutions with photocatalysts were illumination with UV light irradiation from 0 to 150 min. at room temperature. The samples were taken out 2 ml of aliquot solution at regular time intervals (30 min.) and monitored via UV-visible spectroscopy to evaluate the degraded of MB and MO dye. The optical absorption peak of MB and MO dye-solution were measured by a double beam UV-Vis spectrophotometer at the wavelength range of \sim 664 and 464 nm (λ_{max}), respectively.

6.3.7.1. Influence of optimized parameters

The photocatalytic activity of pure ZnO, AFZ-1, AFZ-2 and AFZ-3 nanoparticles were evaluated using the photocatalytic degradation of MB and MO in aqueous solutions under UV light irradiation. The effect of various initial dye concentrations for the degradation of MB and MO on pure ZnO was investigated out by varying dye concentrations from 10 to 30 ppm. The effect of initial pH on the MB and MO degradation was carried out by varying the solution pH from 2 to 6. The effect of catalyst dosage on degradation of MB and MO under UV light was investigated out by varying the catalyst amount from 10 to 30 mg. The photocatalytic degradation strongly depends on the dye concentrations, solution pH and catalyst dosage. Fig.6.8 (a-c) depicts the optimized parameters values are found to be pH = 6, 20 mg and 10 ppm, respectively.

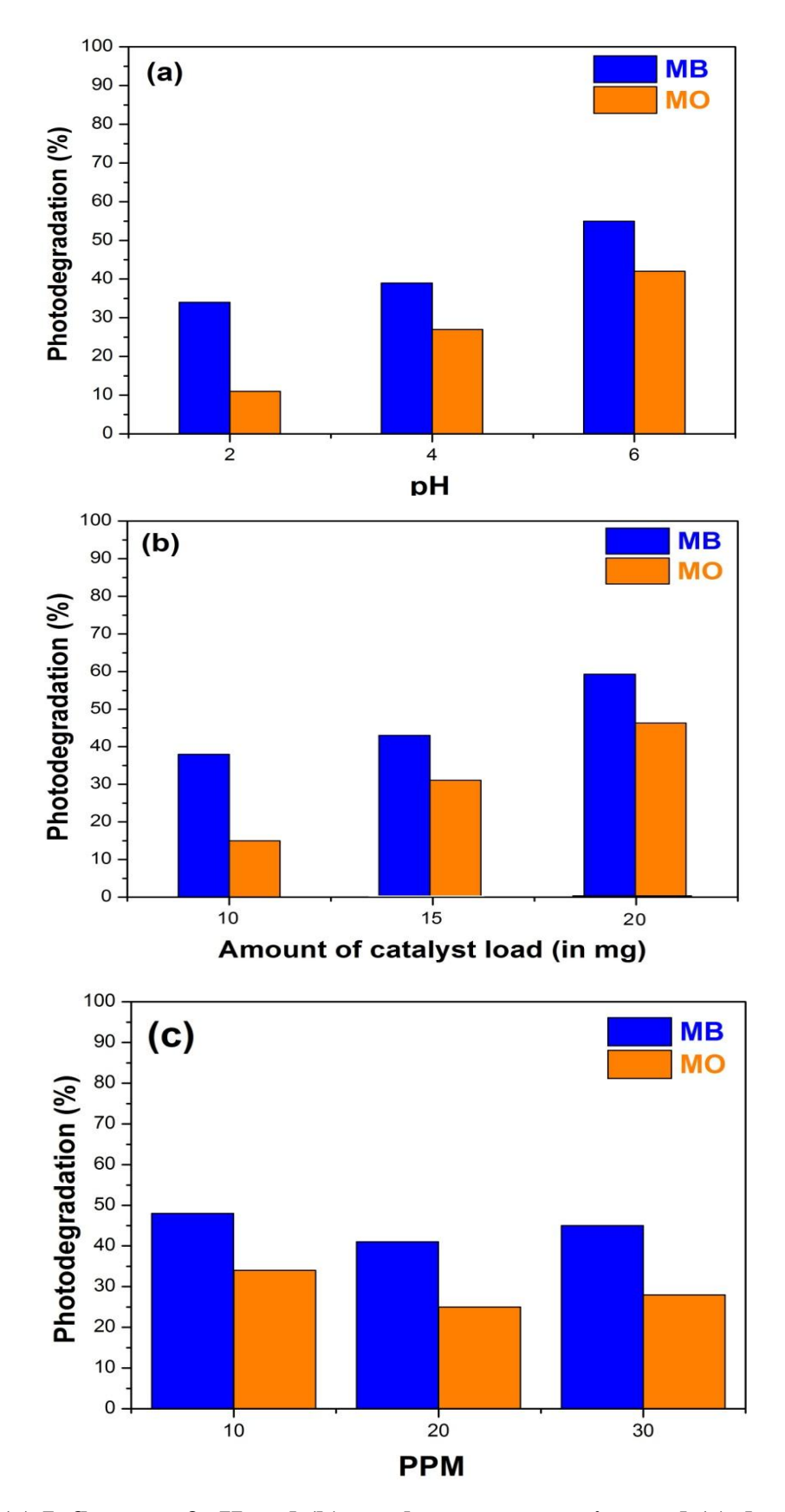
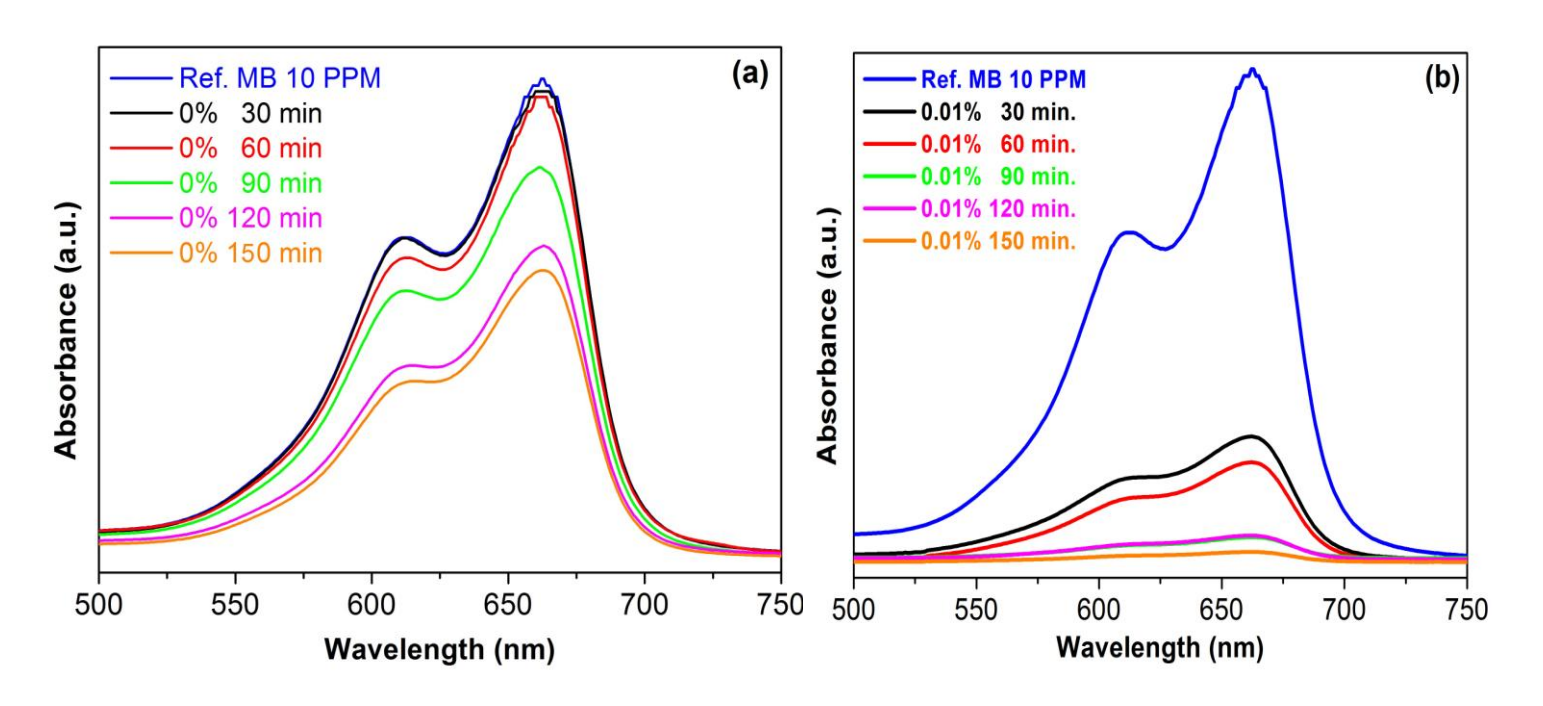


Fig.6.8: (a) Influence of pH and (b) catalyst concentration and (c) dye PPM on the photodegradation of MB and MO

6.3.7.2 Photocatalytic performance of MB

MB degradation was used to evaluate the photocatalytic activity of the pure ZnO, AFZ-1, AFZ-2 and AFZ-3 nanoparticles. The time-dependent absorbance spectra of the MB dye solution under UV light irradiation in the presence of pure ZnO, AFZ-1, AFZ-2 and AFZ-3 nanoparticles are displayed in Fig.5.9 (a–d).

The absorption characteristics of MB dye at ~664 nm decreases gradually with increased UV irradiation time. It is clear that all AFZ nanoparticles possess higher photocatalytic activities compare to pure ZnO. It depicts the Fig.5.9 (e) MB degraded as function of irradiation time with UV light. MB degradation efficiency of pure ZnO, AFZ-1, AFZ-2 and AFZ-3 nanoparticles reached 38, 96, 98 and 99% after 150 min. at pH=6. However, Ag / Fe ions co-doped into ZnO site and its photocatalytic performance higher than that of Pure ZnO.



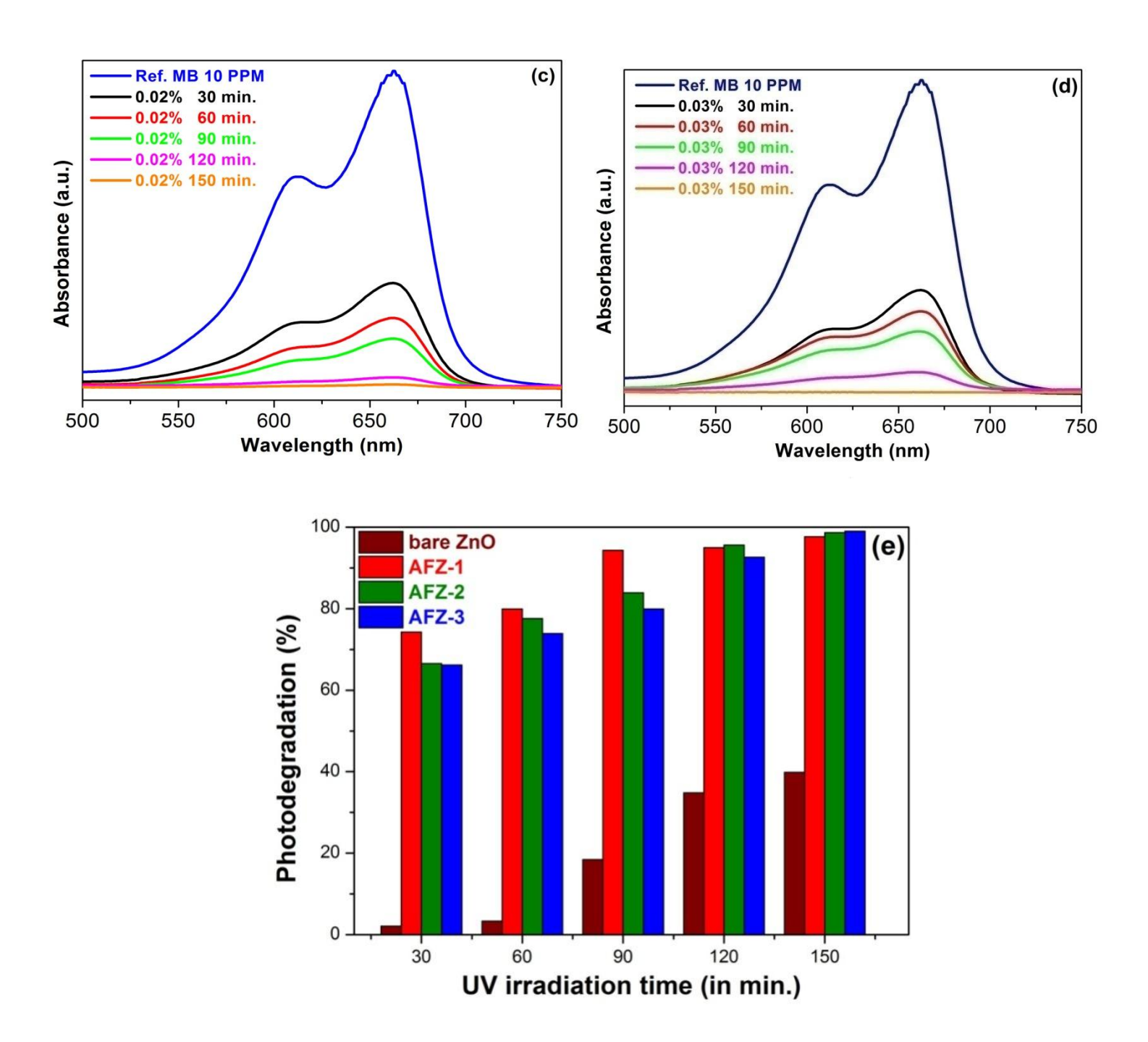
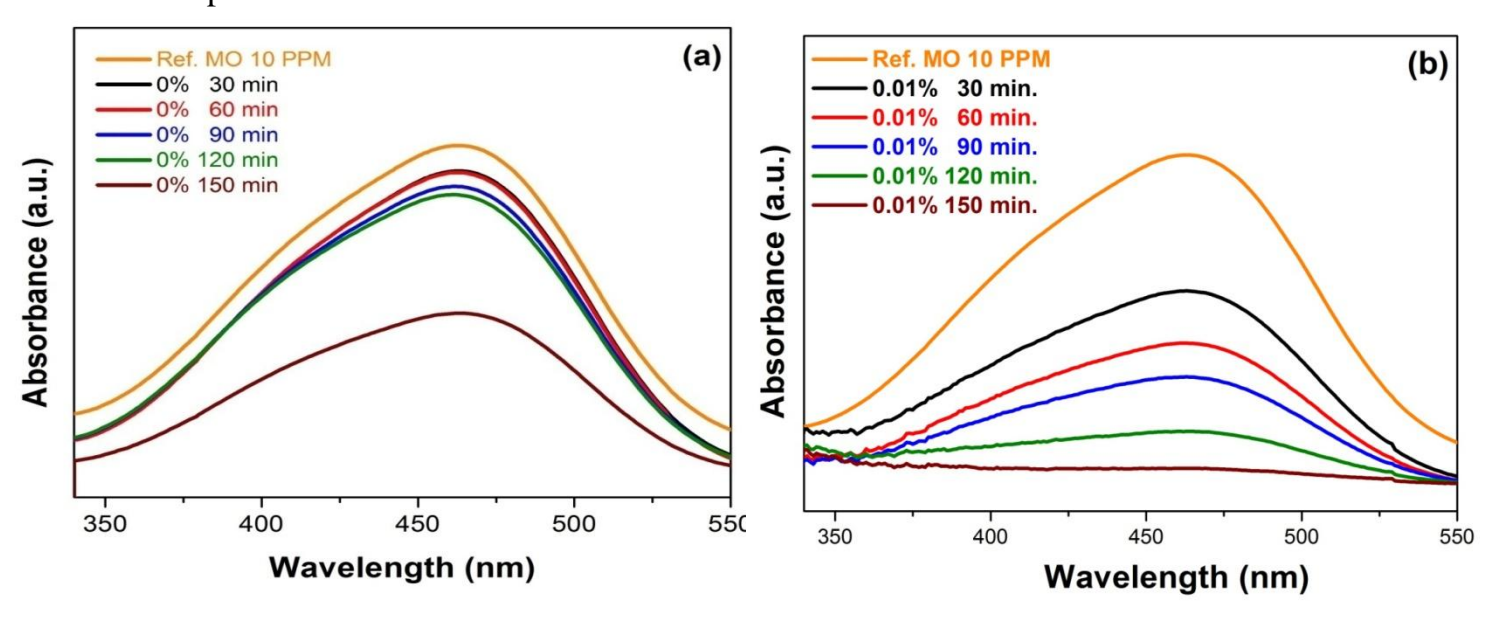


Fig. 6.9: UV-visible spectra of MB (dye conc.=10 ppm, pH = 6 and catalyst dosage =20 mg) at different time intervals in presence of (a) Pure ZnO (b) AFZ-1, (c) AFZ-2, and (d) AFZ-3 nanoparticles and (e) comparison of photocatalytic efficiency of MB

6.4 Photocatalytic performance of MO

The variation of UV-visible absorption spectra of aqueous MO dye solution as a function of irradiation time through the photodegradation of pure ZnO, AFZ-1, AFZ-2 and AFZ-3 nanoparticles are shown in Fig.6.10 (a-d). From the UV-visible absorption spectra it can be seen that the intensity of the absorption peak MO decreases when the irradiation time increases from 0 to 150 min. The characteristic absorption peak of MO dye (~454 nm) has been monitored as a function of UV light irradiation time, is shown in Fig.6.10 (e). MO degradation efficiency of pure ZnO, AFZ-1, AFZ-2 and AFZ-3 nanoparticles reached 39, 96, 90 and 94% after 150 min. at pH=6. Among our catalysts, the AFZ-1 showed the best performance with the MO degradation efficiency enhanced by the optimized parameters under UV light irradiation. Overall, MB degraded faster than MO in the presence of the AFZ nanoparticles.



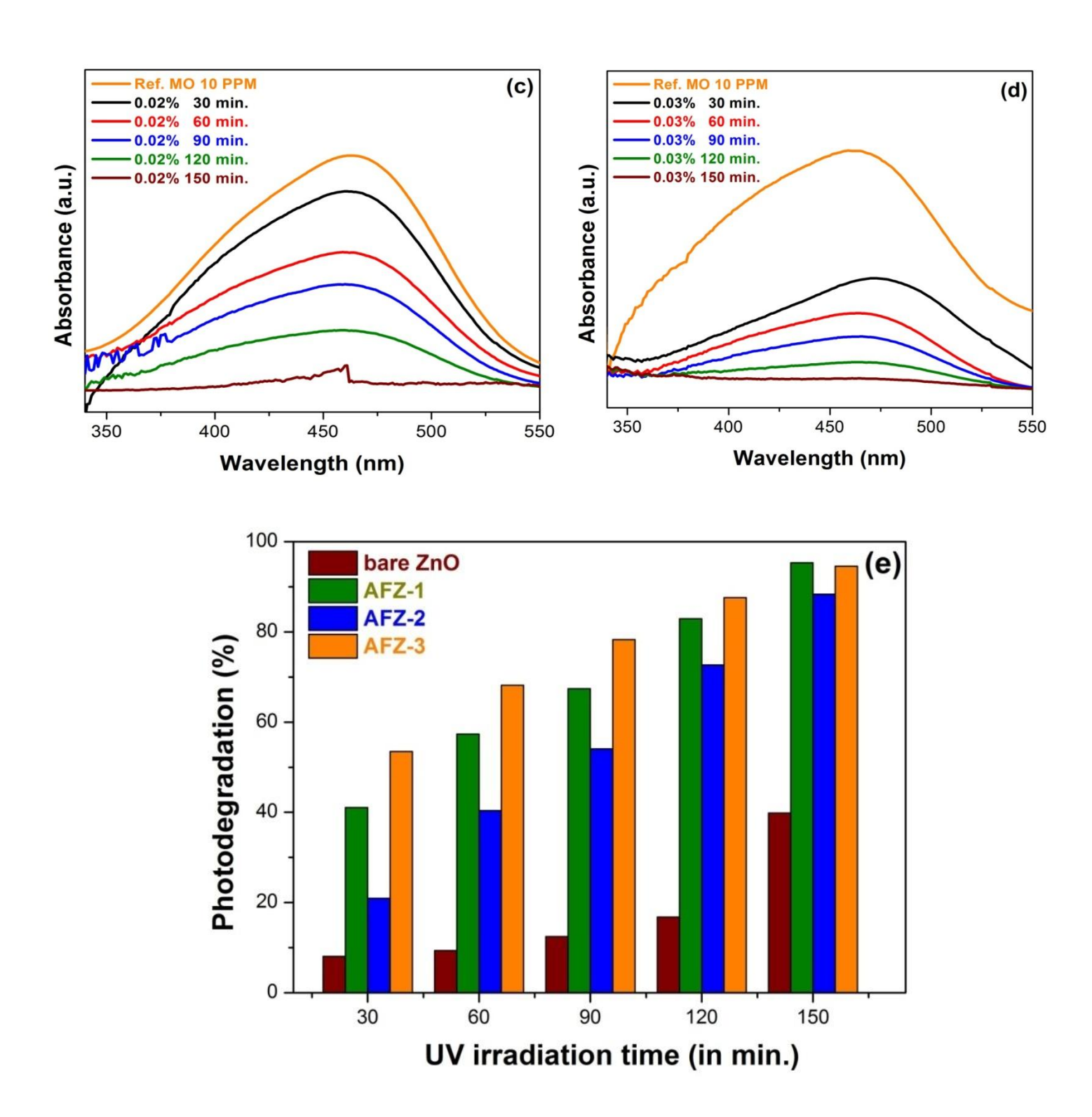


Fig. 6.10: UV-visible Spectra of MO (dye conc.=10 ppm, pH = 6 and catalyst dosage=20 mg) at Different Time Intervals in Presence of (a) Pure ZnO (b) AFZ-1, (c) AFZ-2, and (d) AFZ-3 nanoparticles and (e) Comparison of Photocatalytic Efficiency of MO

6.5 Degradation Mechanism of MB and MO

A possible photocatalytic mechanism of the as-prepared AFZ photocatalysts under UV irradiation were proposed and schematically illustrated in Fig.6.11. The enhanced photocatalytic process can be explained as follows: Initially, the adsorption of the dye molecules (MB and MO) onto the doped ZnO surface. Irradiation of dye (MB and MO) adsorbed on ZnO surface with UV light leads to the electron–hole pairs (e¯ and h¯) generation (equation (2)). The excited state of dye* would inject electrons into the conduction band (CB) of pure ZnO participate in the photo–reaction process. The Ag^+/Fe^{3+} ions trap electrons and convert into Ag^0/Fe^{2+} . The presence of Ag^0/Fe^{2+} ions less stable so it reacts with the oxygen molecules (O₂), thereby reducing to form superoxide radical anion (\cdot O₂ $^-$) (eqn. (4)). The Fe^{3+} ions located in the valence band (VB) of ZnO reacts with surface hydroxyl group (OH $^-$) to produce hydroxyl radical (\cdot OH). The highly reactive superoxide radical anion (\cdot O₂ $^-$) and hydroxyl radical (\cdot OH) react with dye adsorbed on ZnO lead to the degradation of dye solution.

The possible degradation of dye can be summarized by the following equations

$$Dye + hv \longrightarrow Dye^* + e^- \longrightarrow Dye + \cdot \dots (1)$$

co-doped ZnO + hv
$$\longrightarrow$$
 $e^-_{CB} + h^+_{VB}$... (2)

$$Ag^{+}/Fe^{3+} + e^{-} \longrightarrow Ag^{0}/Fe^{2+}$$
 [electron trap] ... (3)

$$Ag^0/Fe^{2+} + O_2 \longrightarrow Ag^+/Fe^{3+} + \cdot O_2^-$$
 [electron release] ... (4)

$$(h^+_{VB}) + H_2O \longrightarrow H^+ + \cdot OH$$
 ... (5)

$$H_2O_2 + e^- \longrightarrow OH + OH^-$$
 ... (6)

$$(\cdot O_2^- + \cdot OH) + dye (MB \text{ or } MO) \longrightarrow degradation products ... (7)$$

$$(\cdot O_2^- + \cdot OH) + degradation products \longrightarrow CO_2 + H_2O \dots (8)$$

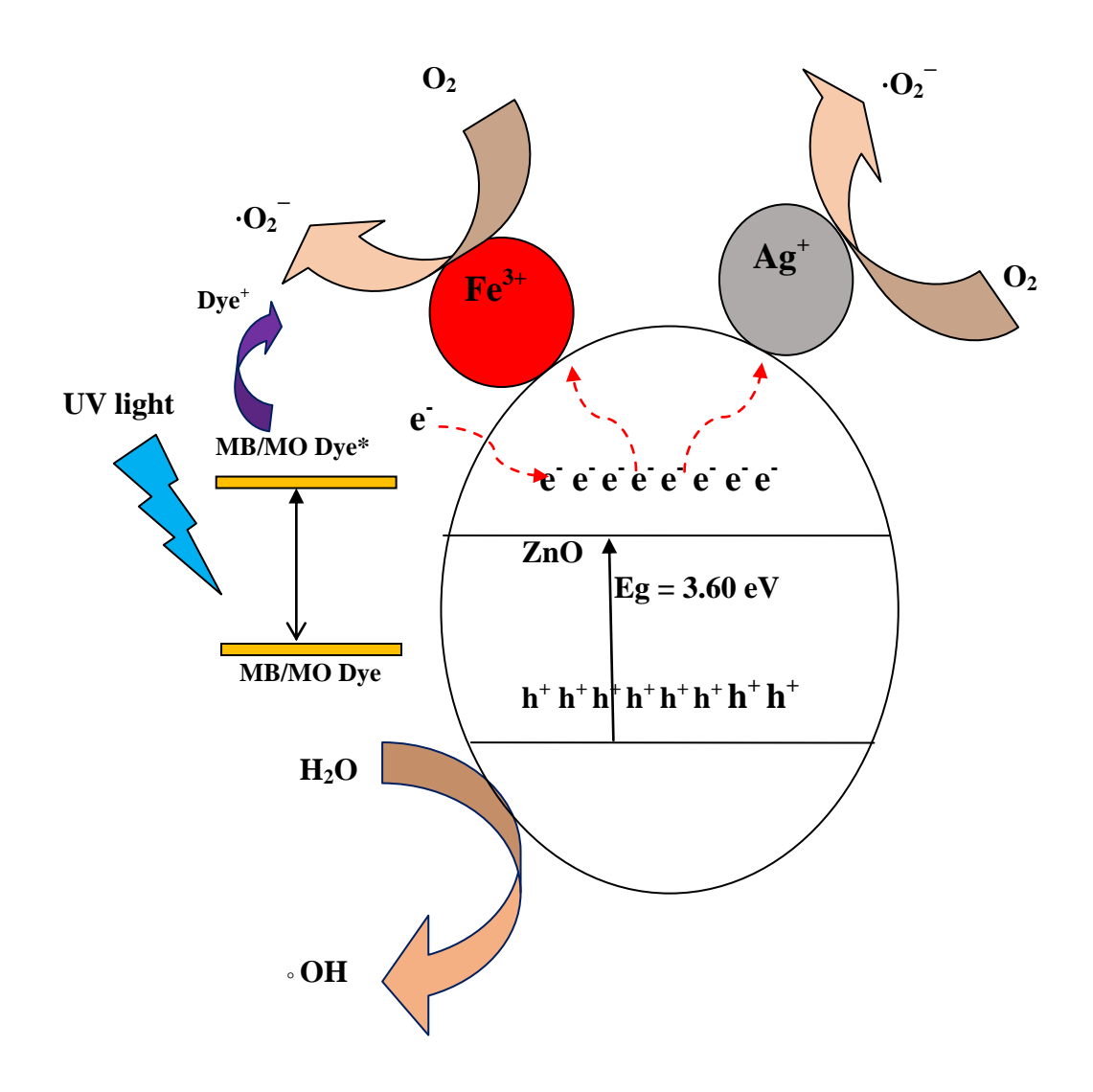


Fig.6.11: Photodegradation mechanism of the MB and MO dye in the presence AFZ photocatalysts

The photocatalytic activity of pure and AFZ photocatalysts were studied by measuring the photocatalytic degradation of dye (MB and MO) under UV light irradiation. AFZ-3 photocatalyst degrades MB up to 98% photodegradation efficiency after 150 min. and AFZ-1 photocatalyst degrades MO up to 93% photodegradation efficiency after 150 min. Saravanan *et al.* prepared Cd doped ZnO by a hydrothermal method with enhanced visible light photocatalytic activity as compared to pure ZnO,

degrading 95% methylene blue dye in 6h under visible light irradiation [58]. Zhang et al. reported that Fe doped ZnO nanowires much better than that of P25 degrades methylene orange up to 60% in 300 mins. [59]. Jayachitra *et al.* synthesised (Ag, Mg) co-doped ZnO by co-precipitation method under UV light irradiation with enhanced photocatalytic activity as compared to pure ZnO, degrading 82% of MB dye in 5h (pH=6) [60]. Based on the above results, novel AFZ photocatalysts have played a vital role in the degradation of MB and MO dyes from wastewater.

6.6. Conclusion

Pure and various concentrations of co-doped Ag, Fe ZnO nanoparticles were prepared by simple co-precipitation method. The synthesized samples are annealed at 450°C for 1 hr and they are characterized by using X-ray diffraction technique, scanning electron microscope and UV-Vis spectroscopy analysis. The XRD result clearly shows that the dopant concentration changes the average crystallite size. The optical absorbance spectra reveal that the band gap decreases with increase of dopant concentration. The effect of dopant, pH values, UV light irradiation time and dosage concentration was evaluated for photocatalytic decolourization of MB and MO. It has been observed that 0.075% Ag co-doped Fe-ZnO nanoparticles shows better catalytic activity at higher pH values.

References

- [1] M. Mahnoodi, M. Armani, N. Y. Lymaee and K. Gharanjig, J. Hazard. Mater. 145 (2007) 65–71.
- [2] M.A. Rauf, M. A. Meetani, A. Khaleel and A. Ahmed, Chem. Eng. Journal, 157 (2010) 373–378.
- [3] D. Lucaci, Duta A. Env. Eng.Mngt Journal, 9-10 (2011) 1255–1262.
- [4] Y. Wang, Water Research, 34 (2000) 990–994.
- [5] Y. S. Wong, T. T. Teng, S. A. Ong, N. Morad and M. Rafatullah, RSC Advances, 4 (2014) 64659–64667.
- [6] X. Chen and S. S. Mao, Chemical Reviews, 107 (2007) 2891–2959.
- [7] V. K. Saharan, A. B. Pandit, P. S. Satish Kumar and S. Anandan, Ind. Eng. Chem. Research, 51 (2012) 1981–1989.
- [8] B. Bakheet, S. Yuan, Z. Li, H. Wang, J. Zuo, S. Komarneni and Y. Wang, Water Research, 47 (2013) 6234–6243.
- [9] V. Murali, S. A. Ong, L. N. Ho and Y. S. Wong, Bioresource Technology, 143 (2013) 104–111.
- [10] M. N. Chong, B. K. Jin, C. W. K. Chow, C. Saint, Water Research, 44, (2010) 2997–3027.
- [11] C. Wang, C. Shao, Y. Liu and X. Li, Inorganic Chemistry, 48,(2009) 1105–1113.
- [12] I. K. Konstantinou, and T. A. Albanis, Applied Catalysis B: Environmental, 49 (2004) 1–14.
- [13] A. K. L. Sajjad, S. Shmaila, B. Z. Tian, F. Chen and J. L. Zhang, J.Hazard.Mater.177 (2010) 781–791.

- [14] D. Neena, A. H. Shah, K. Deshmukh, H. Ahmad, D. J. Fu, K. K. Kondamareddy, P. Kumar, R. K. Dwivedi and V. Sing, The European Physical Journal D, 70 (2016) 1–7.
- [13] A. Khodja, T. Sehili, J. Pilichowski and P. Boule, J.Photochem. Photobio. A: Chemistry", 141 (2001) 231–239.
- [14] B. Cao and W. Cai, J. Phys. Chem.C, 112 (2008), 680–685.
 R. Saravanan, Mohammad Mansoo Khan, Vinod Kumar Gupta, E. Mosquera,
 F. Gracia, V. Narayanang and A. Stephen, RSC Advances, 5 (2015) 34645–34651.
- [15] R Saravanan, N Karthikeyan, V. K. Gupta, E. Thirumal, P. Thangadurai, V. Narayanan, A. Stephen, Mater. Sci. Eng. C, 33 (2013) 2235–2244.
- [16] F. Peng, H. Wang, H. Yu and S. Chen, Mater.Resear. Bulletin, 41 (2006) 2123–2129.
- [17] C. Hariharan, Applied Catalysis A: General, 304, (2006) 55–61.
 S. Sahoo, S. K. Barik, A. P. S. Gaur, M. Correa, G. Singh, R. K. Katiyar, V. S.
 Puli, J. Liriano and R. S. Katiyar, ECS J.Solid-State Sci.Tech. 6 (2012) 140–143.
- [18] R. Murugan, T. Woods, P. Fleming, D. Sullivan, S. Ramakrishna, P. R. B, Materials Letters, 128 (2014) 404–407.
- [19] Q. F. Zhang, C.S. Dandeneau, X. Y. Zhou, G. Z. Cao, Advanced Materials, 41 (2009) 4087 – 4108.
- [20] J.J. Qi, H. Zhang, S. N. Lu, X. Li, M. X. Xu, Y. Zhang, J.Nano.mater. 2015(2015) 1–6.
- [21] S. He, X. Zou, Z. Sun, G. Teng, Materials Letters, 91 (2013) 258–260.

- [22] Okorn Mekasuwandumrong, Pongsapak Pawinrat, Piyasan Praserthdam, Joongjai Panpranot, Chem. Eng. Journal, 164 (2010) 77–84.
- [23] H. Zeng, W. Cai, P. Liu, X. Xu, H. Zhou, C. Klingshirn and H. Kalt, ACS Nano. 2 (2008) 1661–1670.
- [24] Wang Cun, Zhao Jincai, Wang Xinming, Mai Bixian, Sheng Guoying, Peng Ping'an, Fu Jiamo, Applied Catalysis B: Environmental, 39 (2002) 269–279.
- [25] Y. Qiu, H. Fan, G. Tan, M. Yang, X. Yang and S. Yang, Materials Letters, vol. 131 (2014) 64–66.
- [26] M. A. Barakat, H. Schaeffer, G. Hayes and S. Ismat-Shah, Applied Catalysis B: Environmental, 57 (2004) 23–30.
- [27] S. Sakthivel, M. V. Shankar, M. Palanichamy, B. Arabindoo, D. W. Bahnemann and V. Murugesan, Water Research, 38 (2004) 3001–3008.
- [28] Raad S. Sabry, Wisam J. Aziz and Muntadher I. Rahmah, Materials Technology, 35 (2020) 326–334.
- [29] H. Tran, K. Chiang, J. Scott and R. Amal, Photochemical & Photobiological Sciences, 4 (2005) 565–567.
- [30] T. M. Hammad, J. K. Salem and R. G. Harrison, Applied Nanosci, 3 (2013)133–139.
- [31] Z. N. Kayani, E. Abbas, Z. Saddiqe and S. Riaz, Materials Science in Semiconductor Processing, 88 (2018) 109–119.
- [32] E. Rokhsat and A. Khayatian, Inorganic and Nano-Metal Chemistry, 48 (2018) 203–209.
- [33] Z. Li, Y. Zhang, Y. Zhang, S. Chen and Q. Ren, Ferroelectrics, 526 (2018) 152–160.

- [34] H. Aby, A. Kshirsagar, P. Khanna, J. Mater. Sci. Nanotech. 4 (2018) 1–13.
- [35] A. Moulahi, F. Sediri, Ceramics International, 1 (2014) 943–950.
- [36] N.L. Tarwal, P.R. Jadhav, S.A. Vanalakar, S.S. Kalagi, R.C. Pawar, J.S. Shaikh, Powder Technology, 208, (2011) 185–188.
- [37] T. Ivanova, A. Harizanova, Materials Letters, 64 (2010) 1147–1149.
- [38] N.P. Herring, L.S. Panchakarla and M.S. El-Shall, Langmuir, 30 (2014) 2230–2240.
- [39] M. Naouar, I. Ka, M. Gaidi, H. Alawadhi, B. Bessais and M.A. El Khakani, Materials Research Bulletin, 57 (2014) 47–51.
- [40] A. Rahmati, A.B. Sirgani, M. Molaei, M. Karimipour, The European Physical Journal Plus, 129 (2014) 1–7.
- [41] M. Senthilkumar and C. Arunagiri, J. Mate. Sci : Mater. Electron. 13 (2015) 1–11.
- [42] A. A. Ashkarran, A. Irajizad, S.M. Mahdavi, M.M. Ahadian, Mater. Chem. Phy.118 (2009) 6–8.
- [43] B. Subash, B. Krishnakumar, M. Swaminathan, and M. Shanthi, Langmuir, 29 (2013) 939–949.
- [44] B. Cullity and S. Stock "Elements of X-ray diffraction", Third ed. Upper Saddle River (NJ): Prentice Hall, (2001).
- [45] T. Pandiyarajan, R. Udayabhaskar, B. Karthikeyan, Applied Physics A, 107 (2012) 411–419.
- [46] S. Kuriakose, V. Choudhary, B. Satpati, Physical Chemistry Chemical Physics, 16 (2014)17560–17568.

- [47] W. Li, Q. Ma, X. Wang, X.S. Chu, F. Wang, X.C. Wang, C.Y. Wang, J. Mater.
 Chem. A, 8 (2020) 19533–19543.
- [48] Amalia Mesaros, Cristina D. Ghitulica, Mihaela Popa, Raluca Mereu, Adriana Popa, Traian Petrisor Jr., Mihai Gabor, Adrian Ionut Cadis, Bogdan S. Vasile, Ceramics International, 40 (2014) 2835–2846.
- [49] H. Mardani, M. Forouzani, M. Ziari and P. Biparva, Spectrochimica Acta Part A: Mole. Spectro. 141 (2015) 27–33.
- [50] P. Solek, "Techincká Mechanika II", 1st edn. Slovenská technická univerzita v Bratislave, Nakladatel'stvo STU, Bratislava (Technical Mechanics II) in Slovak language, (2009).
- [51] C. K. Ghosh, S. R. Popuri, T. U. Mahesh and K. K. Chattopadhyay, J.Sol-Gel Sci.Tech. 52 (2009) 75–81.
- [52] C. Liu, D. Meng, H. Pang, X. Wua, J. Xie, X. Yu, L. Chen and X. Liu, J.Magnet. Magnetic. Mater. 324 (2012) 3356–3360.
- [53] S. Abed, H. Bougharraf, K. Bouchouit, Z. Sofiani, B. Derkowska-Zielinska, M.S. Aida, B. Sahraoui, Superlattices and Microstructures, 85 (2015) 370– 378.
- [53] R. Saravanan, H. Shankar, T. Prakash, V. Narayanan and A. Stephen, Mater.Chem. Phy. 125 (2011) 277–280.
- [54] Y. Zhang, M. K. Ram, E. K. Stefanalkos and D. Y. Goswami, Surface and Coatings Technology, 217 (2013) 119–123.
- [55] R. Jeyachitra, V. Senthilnathan, T. S. Senthil, J. Advance. Chem. 13, (2014) 5891–5902.

SUMMARY AND SUGGESTIONS FOR FUTURE WORK

Summary and Suggestions for Future Work

Summary

In the present work, ZnO-Fe_x, ZnO-Ag_x ,ZnO-Mg_x ($x \approx 0$, 0.05, 0.075 and 0.1 mol.%) nanoparticles and Ag (0.01, 0.02, 0.03%) co-doped Fe-ZnO nanoparticles were effectively synthesized by simple co-precipitation method. All the prepared samples are annealed at 450 °C for 1 hour. The pure and Fe, Ag, Mg-doped ZnO and Ag co-doped Fe-ZnO nanoparticles are characterized by XRD, SEM, EDX, FTIR, UV-Visible absorbance and electrical studies. The photocatalytic activity of the prepared samples is investigated.

The structural properties of the prepared pure, Fe, Ag, Mg-doped and Ag codoped Fe-ZnO nanoparticles have been studied using X-ray diffraction (XRD) analysis. XRD patterns reveals that the all the crystal phases are hexagonal wurtzite structure of ZnO. The average crystalline size was reduced by adding the concentration of 0.05, 0.075 and 0.1% Fe content in the ZnO nanoparticles. The low intensity of pure ZnO was slowly increased with increase of Fe, Ag and Mg (0.05, 0.075 and 0.1%) concentration. The average crystalline sizes are varied from ~23 to 12 nm for Fe, Ag and Mg-doped ZnO nanoparticles. The XRD pattern of the prepared co-doped ZnO (Fe, Ag) nanoparticles are well matched with standard JCPDS card. Also, there is no characteristic diffraction peak corresponding to Ag, Fe, Mg or any metal impurity phases. The obtained result confirms that the Fe³⁺, Ag⁺, Mg²⁺ ions effectively substitute into the ZnO lattice structure.

The surface morphology of Fe, Ag and Mg (0.05, 0.075, and 0.1%)-doped ZnO, Ag (0.01%, 0.02% & 0.03%) co-doped Fe-ZnO nanoparticles were determined

by using Scanning Electron Microscopy (SEM). Pure ZnO nanoparticles have irregular spherical morphology and Fe-doped ZnO nanoparticles shows variation in the surface structure. The SEM image of Ag (0.05, 0.075 and 0.1 mol. %) doped ZnO nanoparticles exhibit a worm, irregular square and spherical morphology. The images of Ag co-doped Fe-ZnO indicate that the spherical structure composed of nanoparticles is slightly agglomerated due to increase of dopants.

The chemical composition was investigated by using the Energy Dispersive X-ray spectroscopy (EDX) analysis. EDX spectrum displays that pure ZnO nanocrystals has a composition of Zn - 49.5 at% and O - 50.5 at%. EDX spectra of Fe-doped ZnO nanoparticles mainly contains ZnO, and Fe elements with a composition of Zn-59.56%, O-22.23% and Fe-18.21%. The EDX image of Ag-doped ZnO nanoparticles mainly contains Zn, Ag and O elements with a composition of Zn - 44.2 at%, O - 51.5 at% and Ag - 4.2 at%. Co-doped Ag (0.03%) Fe (0.075%)-ZnO nanoparticles contains Ag, Fe, Zn and O elements with a composition of Ag – 11.02 at%, Fe – 10.98 at%, Zn - 8.76 at% and O - 69.24 at%.

The chemical groups of the pure and doped ZnO were investigated by using FT-IR spectral analysis. From the FT-IR spectrum of pure and Fe (0.1 %)-doped ZnO nanoparticles, the broad absorption peaks at 3452, 3446, 1626 and 1591 cm⁻¹ corresponds to O H stretching and –OH bending vibration of the adsorbed H₂O molecules. The absorption peaks at 428 and 449 cm⁻¹ correspond to stretching mode of Zn–O bonding in pure and Fe (0.1 %)-doped ZnO nanoparticles. The absorption peaks of Fe (0.1 %)-doped ZnO nanoparticles have a small shift towards the lower wave number and it is due to the change in bond length and substitution of Fe³⁺ ions

instead of ZnO matrix. FT-IR spectra of 0.1 mol. % Fe-doped ZnO shows that the minor shift observed at 601 cm⁻¹ ascribed to Fe-O stretch.

The Functional group of pure and Mg (0.01%) doped ZnO is analysed by FTIR spectrum. It exhibits several well-defined absorption bands at 1122, 1120 and 920 cm⁻¹ and they are attributed to sulphate and C=C bonds, respectively. The absorption peaks appear at 400 and 550 cm⁻¹ were assigned to the metal–oxygen (M–O) stretching mode and the absorbance peak noticed in the spectra around 455 and 453 cm⁻¹ corresponds to the presence of Zn–O and Mg-O stretching bond, respectively.

In Ag (0.1%)-doped ZnO nanoparticles the peak at 2380 cm⁻¹ denotes the existence of C-H band. The peaks at 1122 and 920 cm⁻¹ was ascribed to the sulfate and C=C bonds. The small stretch observed at 455 cm⁻¹ corresponds to the Zn-O bending vibration. But the peak at 430 cm⁻¹ only establishes in the Ag (0.1%)-doped ZnO nanoparticles is characteristic of an Ag–O stretching bond. FT-IR peaks at 3441, 3543, 1625 and 1622 cm⁻¹ are ascribed to O–H stretching vibration and –OH bending vibration of the water molecule in the pure and Ag (0.03%) co-doped Fe (0.075%)-ZnO nanoparticles. The absorption peak at 2310 cm⁻¹ is due to the CO₂ on the metal cations surface.

The optical absorption properties of pure, Fe, Ag, Mg (0.05, 0.075, and 0.1%)-doped ZnO, co-doped Ag (0.01%, 0.02% & 0.03%) Fe-ZnO nanoparticles have been investigated by UV-Vis absorbance spectrophotometer. The band gap energy for Fe, Ag, Mg (0.05, 0.075, and 0.1%)-doped ZnO nanoparticles decreases with increase of (Fe, Ag & Mg)-doping concentrations. In co-doped Ag (0.01%, 0.02% & 0.03%) Fe-

ZnO nanoparticles the absorption edge shifted towards higher wavelength with increase of Ag concentrations. The decrease of band gap from 3.60 to 3.27 eV is due to the incorporation of Ag/Fe/Mg into ZnO lattice.

The electrical properties of pure, Fe, Ag, Mg (0.1%)-doped ZnO and Ag (0.03%) co-doped Fe-ZnO nanoparticles have been characterized using I-V analysis. The pure and Fe, Ag, Mg (0.1%)-doped ZnO nanoparticles taken under varying temperatures of 30, 50, 70, 90, 110 and 130 °C. The electrical conductivity value increases by increasing temperature. The electrical conductivity of Ag (0.03%) co-doped Fe-ZnO nanoparticles increased from the value of pure ZnO (from 10⁻⁹ to 10⁻⁶ S/cm). This result indicates that the increase in the charge carrier's mobility.

The photocatalytic activity of the pure and Fe-doped ZnO was evaluated by the degradation of MB and MO under UV light irradiation. The photodegradation was maximum at pH=6 and catalyst concentration=10 mg for the all the samples such as pure, Fe, Ag, Mg (0.05, 0.075, and 0.1%)-doped ZnO nanoparticles. The result reveals that the Fe, Ag, Mg (0.05, 0.075, and 0.1%)-doped ZnO shows higher photocatalytic activity than that of pure ZnO. Fe (0.075%)-doped ZnO shows enhanced photocatalytic activity with a degradation efficiency of 68% for MB and 55% for MO (pH 6) dye at 150 min. Mg (0.075%)-doped ZnO shows enhanced photocatalytic activity with a degradation efficiency of 68% for MB (pH 6) dye at 150 min.

Ag, (0.1%)-doped ZnO shows enhanced photocatalytic activity with a degradation efficiency of 98% for MB. Ag (0.075%)-doped ZnO shows enhanced photocatalytic activity with a degradation efficiency of 92% for MO (pH 6) dye at 75

min. Mg (0.01%)-doped ZnO shows enhanced photocatalytic activity with a degradation efficiency of 92% for MO (pH 6) dye at 75 min.

At pH=6, Ag (0.01%, 0.02% & 0.03%) co-doped Fe-ZnO nanoparticles shows enhanced dye degradation compared with pure ZnO. MB degradation efficiency of pure, Ag (0.01%, 0.02% & 0.03%) co-doped Fe-ZnO nanoparticles reached 38, 96, 98 and 99% after 150 min. MO degradation efficiency of pure, Ag (0.01%, 0.02% & 0.03%) co-doped Fe-ZnO nanoparticles reached 39, 96, 90 and 94% after 150 min.

Suggestion for Future Work

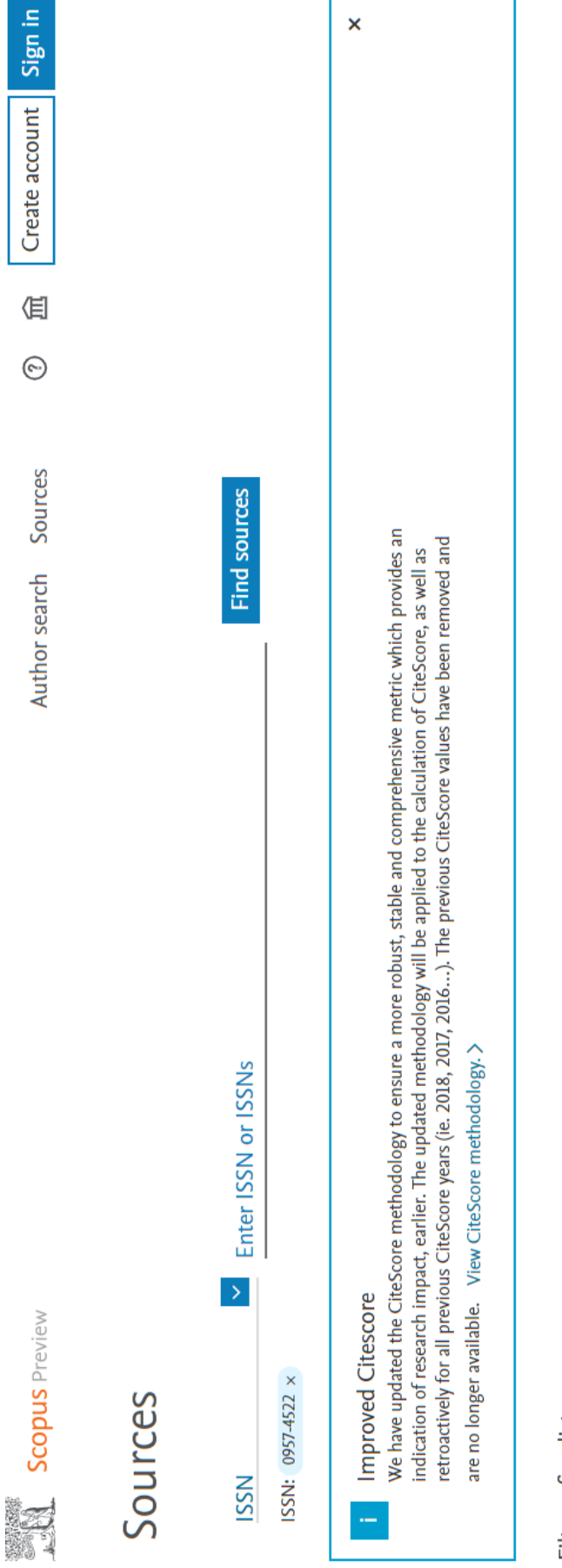
- Characterization of synthesized (Fe, Ag, Mg) doped and co-doped (Ag, Fe) ZnO nanoparticles particles will be performed by various techniques such as HRTEM, XPS, AFM, BET, etc.
- To evaluate the photocatalytic activity of other synthetic dyes like azo dye, rhodamine-B under UV/solar irradiation, etc.,
- Evaluation and performance studies of the co-doped (Ag, Fe) ZnO nanoparticles used as photocatalyst for removal of heavy metals from industrial effluent and antibacterial applications.
- ➤ In future, optimization of co-doped (Ag, Fe) ZnO nanoparticles for energy making such as hydrogen production application through water splitting.

LIST OF PUBLICATIONS

LIST OF PUBLICATIONS

Paper Published:

- Senthil Kumar M, Arunagiri C, 2021, "Efficient photocatalytic degradation of organic dyes using Fe doped ZnO nanoparticles", Journal of Materials Science: Materials in Electronics, Volume 32, Pages: 17925–17935.
- Senthil Kumar M, Arunagiri C, 2021, "Efficient photocatalytic degradation of organic dyes with Ag doped ZnO nanoparticles under UV light irradiation", International Journal of Life Science and Pharma Research, ijlpr 2021:DOI 10.22376 / ijbbs / Ipr.2022.12.1.L1-10.
- 3. **Senthil Kumar M, Arunagiri**, 2021 "Highly Enhanced Photocatalytic Degradation of Ag Co-doped Fe-ZnO Nanoparticles", (Communicated)



×





Efficient photocatalytic degradation of organic dyes using Fe-doped ZnO nanoparticles

M. Senthil Kumar¹ o and C. Arunagiri^{2,*}

Received: 9 March 2021 Accepted: 2 June 2021 Published online: 12 June 2021

© The Author(s), under exclusive licence to Springer Science+Business Media, LLC, part of Springer Nature 2021

ABSTRACT

 $ZnO-Fe_x$ (x=0,0.05,0.075, and 0.1 M) nanoparticles based photocatalysts are successfully synthesized by co-precipitation method. The synthesized nanoparticles are characterized using X-ray diffraction, scanning electron microscopy with energy-dispersive X-ray spectroscopy, and UV-visible double beam spectroscopy techniques. The prepared catalysts and its photocatalytic activity were evaluated by methylene blue and methyl orange dye under UV light irradiation. The effect of various photocatalyst parameters such as pH, catalyst dosage, and initial dye concentration on the photodegradation was examined in detail.

1 Introduction

In recent years, many hazardous organic pollutants, such as toxic dyes and organic residuals released into the atmosphere from several industries [1, 2]. The degradation and full-mineralization process are vicious, because of merged structure of organic dyes. Among these organic dyes, methylene blue (MB:C₁₆-H₁₈N₃SCl) and methyl orange (MO: C₁₄H₁₄N₃NaO₃S) are the most important dyes which are used in textile industries and very harmful to human. Because they cause increased heart rates, cyanosis, shock, sickness, injuries to tissue and various skin infections. They also highly harmful to the atmosphere, which then poses a threat to the health of cattle's and animals [3]. Industrial wastewater treatment and recycling are fundamental objectives to secure the worldwide biological system and improve the environment's quality. Various techniques have been extensively utilized to suppress pollutants from contaminated water sources [4, 5]. Among them, photocatalysis has emerged to be a promising way to control the massive scale's current environmental pollution. The photocatalysts with semiconducting nanostructures have concerned much more attention due to their exceptional physico-chemical properties in the photocatalytic reaction [6–8].

Many researchers recently developed various photocatalysts using metal oxide semiconductor nanoparticles, including Bi_2O_3 , TiO_2 , ZnO, and WO_3 . Among these transition metal oxides, zinc oxide (ZnO) is found very sensible in the photocatalytic method due to their wide-bandgap, non-toxicity, and high photosensitivity [9–11]. ZnO is a wide-bandgap semiconductor with a direct energy bandgap ($E_g \approx 3.37$ eV) [12]. ZnO nanoparticles are especially

Address correspondence to E-mail: arunasuba03@gmail.com



¹ Department of Physics, Srinivasan College of Arts and Science, Perambalur 621212, India

²PG& Research Department of Physics, Periyar EVR College, Bharathidasan University, Tiruchirappalli 620023, India

attractive for many interesting nanotechnology applications such as transparent conductive coatings [13], photoanodes for dye-sensitized solar cells (DSSCs) [14], gas sensors [15], and electro-photo luminescent materials [16]. Unfortunately, ZnO can only absorb UV light [17], and photocatalytic degradation efficiency was confined by the electron-hole charge carriers, low-adsorption, and low-reusability. To rectify this problem, numerous reports focused on doping ZnO with transition metal (Fe, Co, Mn) ions [18], non-metal (N, C, S) ions [19], and noble metals loading (Ag, Au, Pd) [20] have been carried out. Wu et al. reported that compared with pure ZnO nanoparticles, ZnO-based materials are potential photocatalysts, that can be used as the scaffold or the coating layer in various heterostructures [21-23].

Various techniques for the synthesis of pure ZnO and Fe-doped ZnO nanoparticles are reported in the literature: hydrothermal method [24], combustion [25], and sol–gel method [26]. Among these synthesis methods, co-precipitation [27] is a flexible method for synthesizing the ZnO nanoparticles due to its low-cost, and easy to operate.

Several studies have been reported that the doping of ZnO with transition metal ions for visible light photocatalysts [28, 29]. It has been discovered that 2% Fe-doped ZnO nanoparticles degraded the methyl orange dye up to 80.8% within 210 min under sunlight irradiation. The Fe-doped ZnO degrades MB in 4 h in sunlight [30]. Zhang et al. investigated that Fe/ZnO nanowires' utilization is superior to P25 against MO [31]. Abbad et al. synthesized a Fe-doped ZnO nanoparticle and degraded 2-chlorophenol under solar irradiation. The most significant photocatalytic action was accomplished with the optimized dopant centralization of 0.5 wt% Fe because of the small crystallite size and low bandgap with a low oxidation–reduction potential [32].

In the present work, we reported the various properties of an efficient Fe-doped ZnO nanoparticles for photocatalytic reaction. The effect various dopant concentration on structural, morphological, optical, and electrical properties of ZnO nanoparticles was investigated. Furthermore, we investigated the photocatalytic degradation of MB and MO dye under UV light irradiation.

2 Experimental

2.1 Preparation

Fe-doped ZnO (ZnO–Fe_x) nanoparticles were synthesized using various mol.% ($x \approx 0$, 0.05, 0.075, and 0.1) using co-precipitation method. The chemicals such as zinc nitrate hexahydrate [Zn(NO₃)₂·6H₂O], ferric nitrate nonahydrate [Fe(NO₃)₂·9H₂O] and sodium hydroxide [NaOH] used in the present study are of analytical grade obtained from Alfa Aesar chemicals, India.

To synthesis pure ZnO nanoparticles, 10 g of $Zn(NO_3)_2 \cdot 6H_2O$ was dissolved into 20 mL of deionized water (DW) and in parallel 8 g of NaOH was added drop wise in 100 mL water under continuous stirring until to reach pH 11. Then the above solution was heated in a vacuum oven at 100 °C for 2 h [12]. The obtained precipitates were centrifuged, washed three times with DW and ethanol; finally it was dried at 100 °C for 4 h. The collected precipitates were calcined at 450 °C for 1 h. To synthesis, various concentrations of Fe-doped ZnO nanoparticles, such as Fe = 0.05, 0.075, and 0.1 mol.%, 0.68 to 3.4 g of Fe(NO₃)₂·9H₂O was added into the reaction mixture.

2.2 Characterization techniques

XRD patterns of the samples were recorded using a mini desktop X-ray diffractometer (X'PERT PRO MPD) operated at an accelerating potential of 40 kV and 30 mA filament current with CuKα radiation of wavelength 1.5406 Å with a scanning rate of 3/min. (from $2\theta = 10$ to 80 °C). The surface morphology and particles size of the samples were characterized by scanning electron microscope (SEM-JEOL JS-6390) with energy dispersive X-ray spectrometer (EDS). UV-visible absorbance spectra of the samples were measured with a Systronics: AU-2707 double-beam spectrophotometer the absorption in 190–1000 nm. Fourier transform infrared (FT-IR) spectra of the samples were analyzed by JASCO FTIR-410 spectrometer in the range 400–4000 cm⁻¹. The current–voltage (*I–V*) characteristic curves were recorded using the Keithley electrometer 2400 model.

2.3 Photocatalytic degradation test

The photocatalytic activity of the samples was evaluated by the degradation of MB and MO under UV



light irradiation (8 W Philips). 20 mg of ZnO–Fe_x photocatalysts were dissolved in 20 mL aqueous MB and MO dye solution at various pH (2, 4, and 6). The dye solutions with ZnO–Fe_x photocatalysts were exposed to UV light from 0 to 180 min. at room temperature. Every 30 min, sampling out 2 ml of dye solution collected from samples for photocatalytic degradation test. The photocatalytic degradation of MB and MO was observed λ_{max} at \sim 664 and 464 nm respectively using a UV–visible spectrophotometer in the wavelength range 200–800 nm.

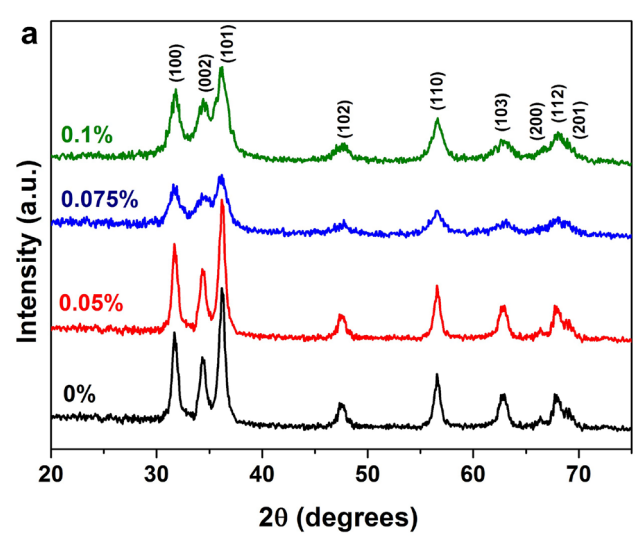
3 Results and discussion

3.1 X-ray diffraction (XRD)

Figure 1a shows the powder XRD characteristic patterns of ZnO-Fe_x ($x \approx 0$, 0.05, 0.075, 0.1%) nanoparticles. All the XRD diffraction peaks are indexed to the hexagonal wurtzite structure of crystalline ZnO, further confirmed from the standard ICPDS No. 36-1451 (a = 0.325 nm and c = 0.5207 nm) [33, 34]. There are no characteristic peaks of Fe phases, or its oxides were not detected in the samples. Figure 1b reveals that the magnification of primary peak at 31.8 (100), 34.3 (002), and 36.3° (101), it shows a minor shift in the 0.05, 0.075, and 0.1% Fe-doped ZnO. The ionic radii of Fe^{3+} and Zn^{2+} are different ($Fe^{3+} = 0.68 \text{ Å}$ and $Zn^{2+} = 0.74 \text{ Å}$). This result suggests that the Fe ions substitute into the ZnO lattice [35]. The average crystallite sizes (D) of the ZnO-Fe_x was determined from the Debye-Scherrer equation (Eq. 1) [36].

$$D = \frac{0.9\lambda}{\beta \cos \theta} \tag{1}$$

where λ is the incident of diffraction angle, β is the full width half maximum of the peak (FWHM), θ is the wavelength of the X-rays (1.5406 Å), respectively. The lattice parameters and average crystalline size of the samples are listed in Table 1. The average crystallite size (D) of ZnO–Fe_x calculated from XRD data are 23, 21, 16 and 12 nm, respectively. Furthermore, the increasing Fe content reduces the lattice parameters and average crystallite size. Previous reports reported by Jeyachitra et al. [12] in Fe-doped ZnO nanoparticles, Srinivasan et al. [37] in Mn-doped ZnO and Nahm et al. [38] in V₂O₅-doped ZnO ceramics are also similar to the obtained results.



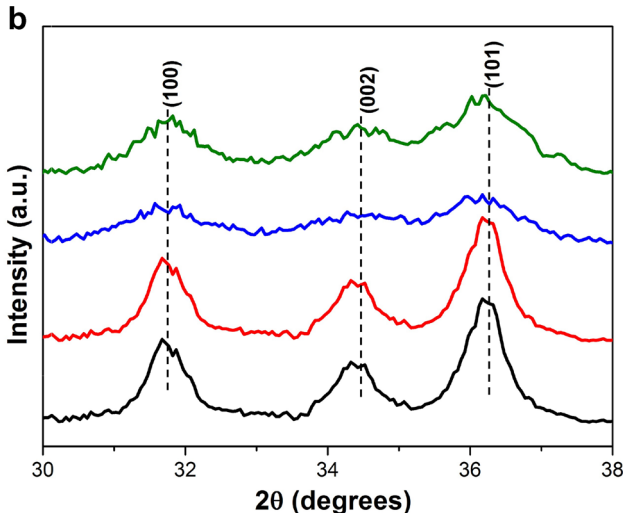


Fig. 1 XRD patterns of **a** undoped ZnO and Fe-doped ZnO nanoparticles **b** Fe concentration dependent shift in primary diffraction peaks

3.2 SEM analysis

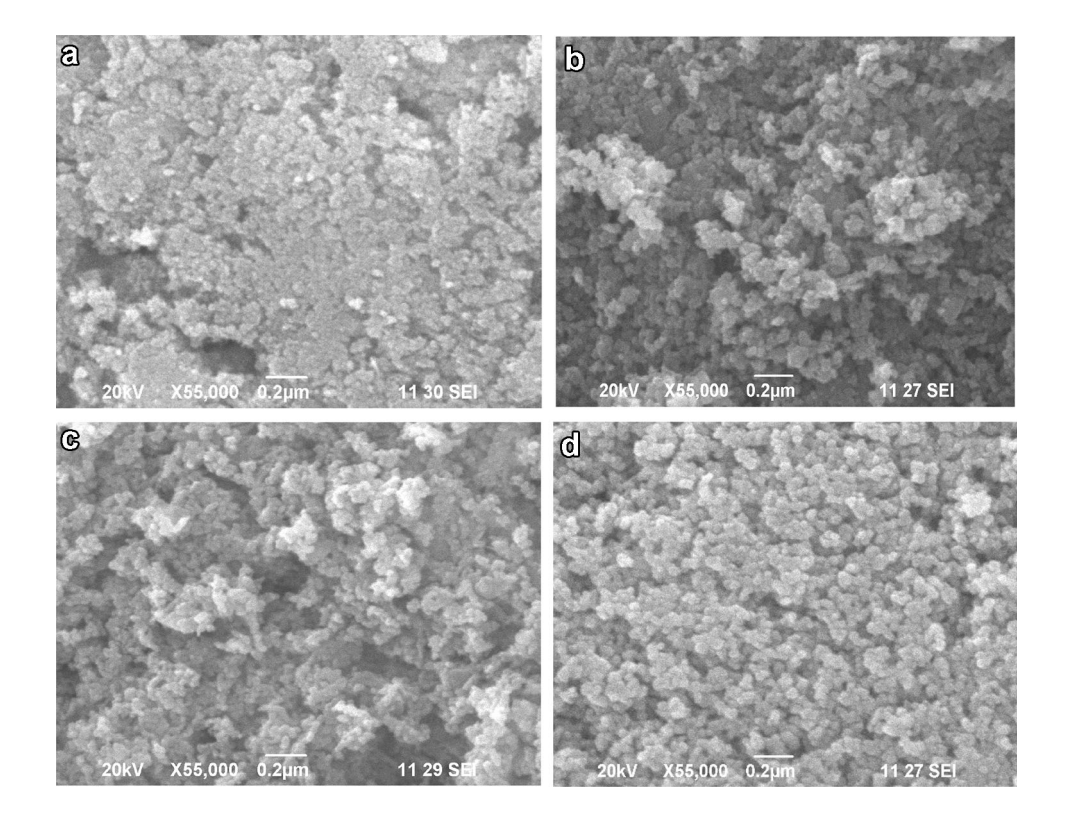
The surface morphologies of ZnO–Fe_x ($x \approx 0$, 0.05, 0.075, and 0.1 mol.%) nanoparticles are shown in Fig. 2a–d. Fig. 2a shows the surface morphology of undoped ZnO with crystallite size of ~ 42 –68 nm. Interestingly, when the Fe concentration was 0.05 mol.%, the ZnO nanoparticles are turned and it is shown in Fig. 2b. Figure 2c, d show turning of needle and spherical like structures due to the doping of 0.075 to 0.1 mol.% of Fe-dopants in ZnO nanoparticles. Compared with undoped ZnO, 0.1 mol.% of Fe-doped ZnO shows more information on the surface. The images clearly exposed that the surface morphology changed with the addition of Fe



Table 1 The lattice parameters and average crystallite size of ZnO–Fe_x nanoparticles

Fe Doping Concentration (mol.%)	hkl	2θ (degree)	a [Å]	c [Å]	Crystallite size (nm)
ZnO	(100)	31.77	3.24	5.20	23
	(002)	34.40			
	(101)	36.30			
ZnO-Fe _{0.05}	(100)	31.81	3.25	5.21	21
	(002)	34.23			
	(101)	36.37			
ZnO-Fe _{0.075}	(100)	31.71	3.25	5.20	16
	(002)	34.43			
	(101)	36.17			
ZnO–Fe _{0.1}	(100)	31.81	3.24	5.20	12
	(002)	34.23			
	(101)	36.23			

Fig. 2 SEM images of a undoped ZnO b 0.05, c 0.075 and d 0.1 mol.% Fedoped ZnO nanoparticles



concentration, the agglomerated particles breaks and pores were created and then finally reduced into spherical nanoparticles. It can also be noticed that the size and morphology of $ZnO{\rm -Fe}_{\rm x}$ nanoparticles enhanced with the dopant concentration.

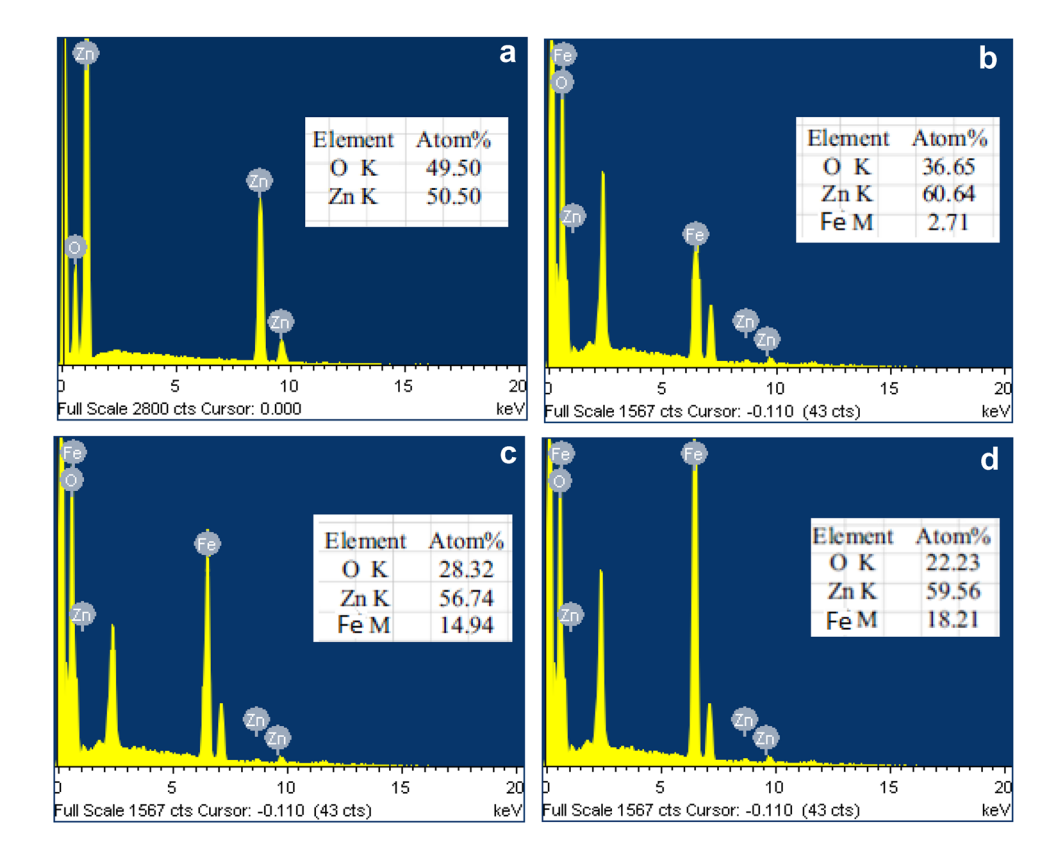
3.3 EDX analysis

EDX analysis (Fig. 3a–d) was used to investigate the chemical composition of ZnO–Fe_x ($x \approx 0$, 0.05, 0.075 and 0.1 mol.%) nanoparticles. EDX spectrum of undoped ZnO shows the existence of characteristic

peaks of oxygen (O) and zinc (Zn) elements (Fig. 3a). The atomic percentage of these elements found to be 49.5 and 50.5%, respectively. Figure 3b–d show the EDX spectra of Fe-doped ZnO nanoparticles also include elements such as O, Zn and Fe, respectively. The inset of EDX image ZnO–Fe $_{\rm x}$ nanoparticles data was given in table format. The measured Fe concentration of 0.05, 0.075 and 0.1 mol.%, are about 2.71, 14.94, and 18.21%, respectively. The observed atomic percentage values almost match well with the samples.



Fig. 3 EDX images of a undoped ZnO **b** 0.05, **c** 0.075 and **d** 0.1 mol.% Fedoped ZnO nanoparticles



3.4 UV-Vis spectral studies

UV-absorption spectra of ZnO–Fe_x ($x \approx 0$, 0.05, 0.075 & 0.1 mol.%) nanoparticles are shown in Fig. 4a–d. The absorption edge is shifted towards a higher wavelength region, which means that the bandgap decreases. The red-shift is due to the increase of crystallite size, and it was confirmed from the XRD results. The optical bandgap of ZnO and Fe-doped ZnO nanoparticles was calculated using the formula $E_{\rm g} = hc/\lambda$ [39]. The calculated optical bandgap values are 3.90, 3.89, 3.86 and 3.82 eV, which corresponds to undoped ZnO and 0.05, 0.075 & 0.1 mol.% Fe-doped ZnO nanoparticles. Similar result was also observed by Hassan et al. [40]. The substitute of Fe³⁺ with Zn²⁺ ion shares the oxygen with Zn atoms and reduces the bandgap.

3.5 FTIR analysis

FTIR spectra of ZnO–Fe_x ($x \approx 0$ and 0.1 mol.%) nanoparticles in the range 4000–400 cm⁻¹ are presented in Fig. 5a, b. The broad absorption band appearing in the range 3452–3446 cm⁻¹ corresponds to –OH stretching vibration, while the two peaks located at 1625 and 1591 cm⁻¹ is due to –OH bending

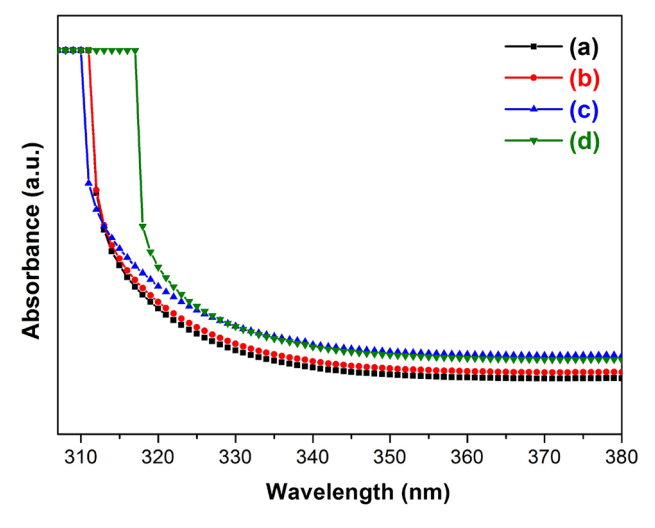


Fig. 4 UV–Vis absorbance spectra of **a** undoped ZnO **b** 0.05, **c** 0.075 and **d** 0.1 mol.% Fe-doped ZnO nanoparticles

vibration of the adsorbed H_2O molecules [41]. The band lower intensity absorbed around 2380 cm⁻¹ which corresponds to the symmetric and asymmetric C–H bond. Two weak absorption peaks at 428 and 449 cm⁻¹ for undoped and 0.1 mol.% Fe-doped ZnO sample may corresponds to Zn–O stretching mode. The absorption peaks located at 1120, 1122, and



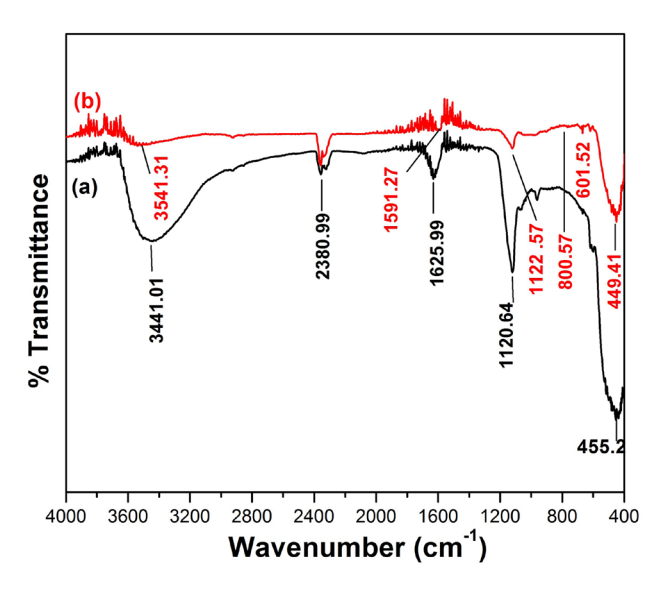


Fig. 5 FT-IR spectra of a undoped ZnO and b 0.1 mol.% Fedoped ZnO nanoparticles

800 cm⁻¹ attributed to the sulfate group, respectively [42]. Also, FTIR spectra of 0.1 mol.% Fe-doped ZnO shows that the small stretch observed at 601 cm⁻¹ corresponds to Fe-O stretch, as reported by Liu et al. [42]. Therefore, it might be due to Fe³⁺ ions substituted in Zn.

I–V characteristics

The *I–V* characteristics of ZnO–Fe_x ($x \approx 0$ and 0.1 mol.%) nanoparticles have been determined using Ag-paste for better electrical contact and the result is shown in Fig. 6a, b. From these curves, DC electrical conductivity measurement of ZnO-Fe_x ($x \approx 0$ and 0.1 mol.%) nanoparticles taken under varying temperatures of 30, 50, 70, 90, 110 and 130 °C (Increase of 20 °C). Thus, it increases the conductivity of 0.1 mol.% Fe-doped ZnO nanoparticles due to the increase in the mobility of charge carriers [43]. The remarkable increase in these samples conductivity may result in a higher advantage for optical device fabrication.

Photodegradation of MB and MO

3.7.1 Influence of pH

The adsorption of MB and MO dye molecules on undoped ZnO nanoparticles strongly depends on the solution's pH displayed in Fig. 7a. The influence of pH on the photodegradation of MB and MO dye was

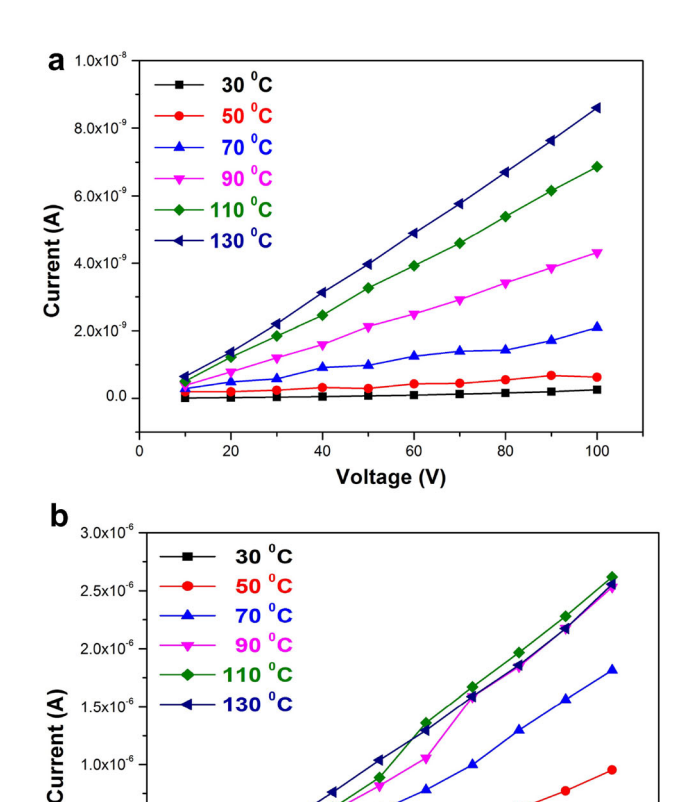


Fig. 6 I–V characteristics of a undoped ZnO and b 0.1 mol.% Fedoped ZnO nanoparticles

40

60

Voltage (V)

80

100

studied by varying the solution's pH from 2 to 6. The outcome shows that photodegradation was maximum in base medium. The degradation arrives at most extreme at pH 6 and decreases sensibly up to pH 2. Henceforth, the pH 6 was accepted as an ideal pH and utilized for additional investigation.

3.7.2 Influence of catalyst concentration

20

1.0x10

5.0x10

0.0

The influence of catalyst concentration on the photodegradation of MB and MO dye was verified using ZnO catalyst concentrations from 5 to 15 mg/30 ml in 10 ppm MB, and MO dye solution at pH 6 and it is displayed in Fig. 7b. The variation in photodegradation can be clarified by accessibility of several surface-active sites and UV light radiation into dye solution. The photodegradation reaches maximum at 10 mg/30 ml. The reduced photodegradation at higher catalyst concentration (15 mg/30 ml) may be



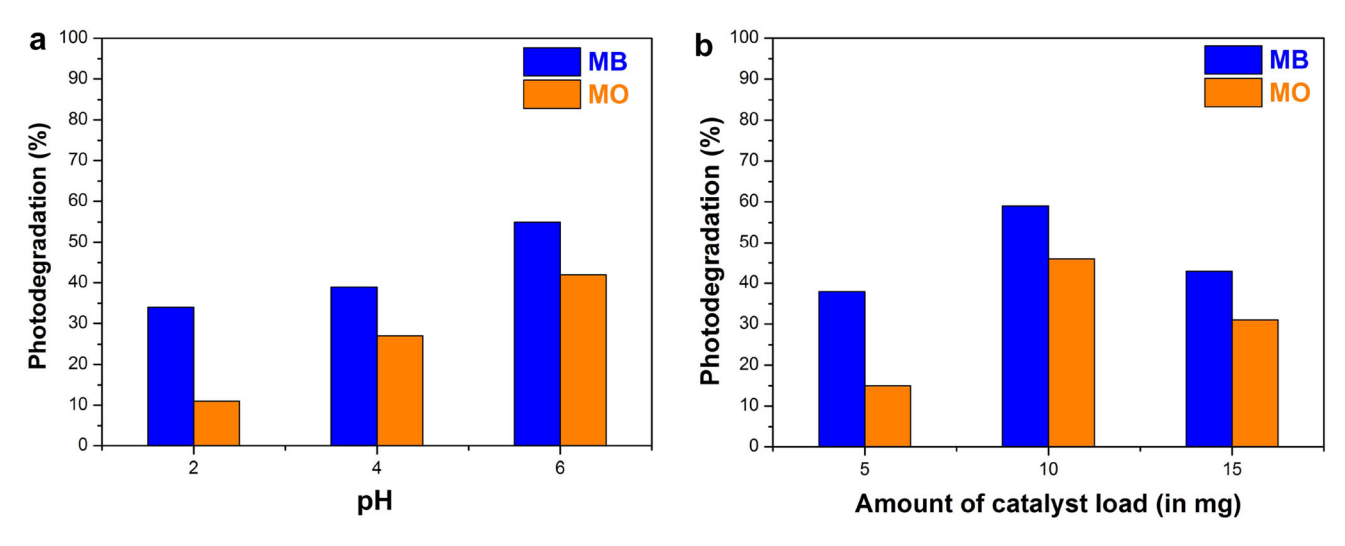


Fig. 7 a Influence of pH and b catalyst concentration on the photodegradation of MB and MO

due to ZnO nanoparticles aggregation increases the scattering effect [44]. Consequently, 10 mg/30 ml ZnO photocatalyst was expected as an ideal catalyst weight.

3.7.3 Influence of UV irradiation time of MB

The photocatalytic activity was carried out with MB concentration of 2.0 mM, catalyst concentration of 10 mg, pH 6 and irradiation time up to 150 min. Figure 8a–d show the variation in absorption spectra of MB illuminated to UV light for various irradiation times (0, 30, 60, 90, 120 and 150 min) in the presence of ZnO–Fe_x ($x \approx 0$, 0.05, 0.075, 0.1 mol.%) nanoparticles. The intensity of absorption peaks at 664 nm decreases gradually with irradiation time.

MB dye was degraded under UV light from 0 to 150 min. in the presence of ZnO-Fe_x ($x \approx 0$, 0.05, 0.075, 0.1 mol.%) nanoparticles and is shown in Fig. 8e. The result reveals that the Fe-doped ZnO shows higher photocatalytic activity than that of undoped ZnO. Fe (0.075%)-doped ZnO shows enhanced photocatalytic activity with a degradation efficiency of 68% for MB (pH 6) dye at 150 min. Fe (0.075%)-doped ZnO nanoparticles took less time to degrade the MB dye compared with other concentration of Fe. The reduction of photocatalytic activity at higher concentration Fe (0.1%)-doped ZnO may be due to photons' reduced path length [44]. Similar results are also observed by Suganthi and colleagues [45]. Another reason for the increase in the photocatalytic activity of Fe-doped ZnO nanoparticles, Fe ions substituted into ZnO surface may suppress the electron-hole pair recombination and enhance the dye degradation efficiency [46, 47].

3.7.4 Influence of UV irradiation time of MO

The photocatalytic activity was carried out with MO concentration of 3.0 mM, catalyst concentration of 10 mg, pH 6 and irradiation time up to 150 min. The variation in absorption spectra of MO showing to UV light for various irradiation times (0, 30, 60, 90, 120 and 150 min) in the presence of ZnO–Fe_x ($x \approx 0, 0.05, 0.075, 0.1 \text{ mol.}\%$) nanoparticles. The intensity of absorption peaks at 454 nm decreases gradually with the extension of irradiation time shown in Fig. 9a–d.

Figure 9e shows the MO dye degradation under UV light from 0 to 150 min. in the presence of ZnO– Fe_x ($x \approx 0, 0.05, 0.075, 0.1 mol.\%$) nanoparticles. The result reveals that the Fe (0.075%)-doped ZnO showed efficient photocatalytic activity with a degradation efficiency of 55% for MO (pH 6) dye at 150 min [48].

In this process, narrow semiconductors act as a sensitizer to improve the dye's photodegradation based on their electronic band structure. When the photocatalyst was illuminated with higher energy photons, it only allows the dye molecule oxidation [44]. We proposed a mechanism of $ZnO-Fe_x$ nanoparticles for efficient photocatalytic activity. It can be described as follows:

$$ZnO + h\gamma \rightarrow ZnO(h_{VR}^+ + e_{CR}^-)$$
 (2)



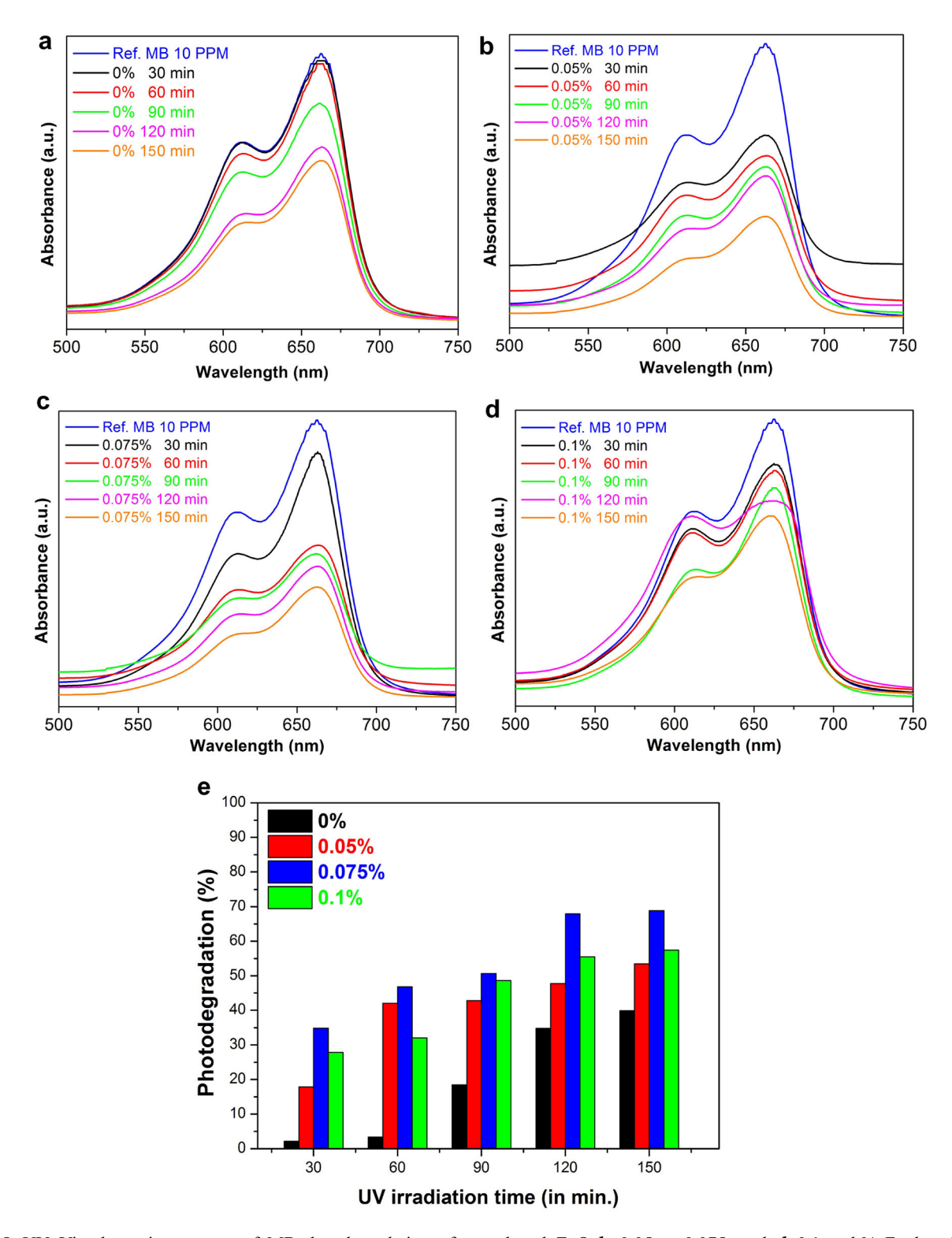


Fig. 8 UV-Vis absorption spectra of MB dye degradation of **a** undoped ZnO **b** 0.05, **c** 0.075, and **d** 0.1 mol.% Fe-doped ZnO nanoparticles and **e** influence on the photodegradation of MB



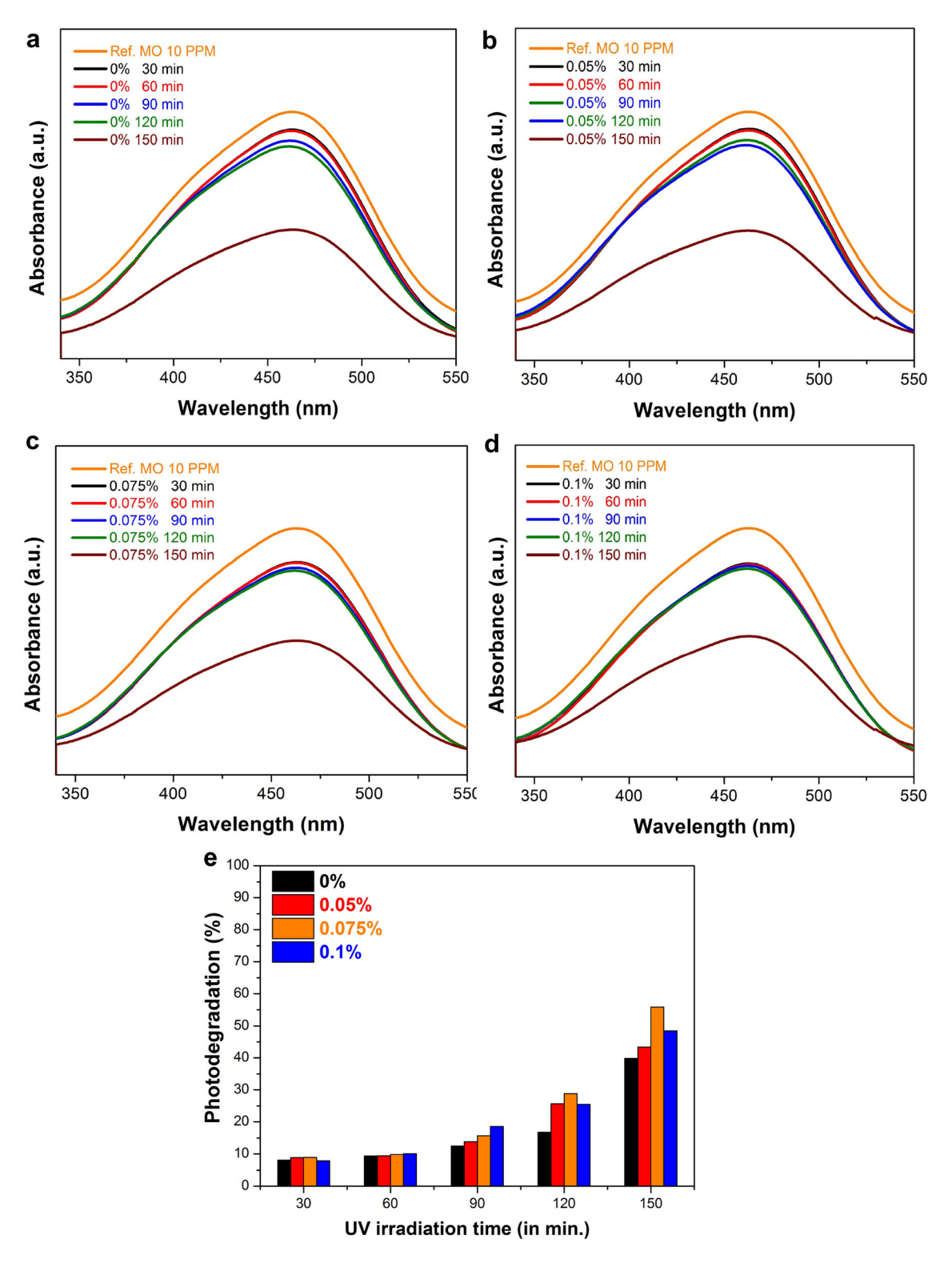


Fig. 9 UV-Vis absorption spectra of MO dye degradation of **a** undoped ZnO **b** 0.05, **c** 0.075, and **d** 0.1 mol.% Fe-doped ZnO nanoparticles and **e** influence on the photodegradation of MO



$$\left(h_{VB}^{+}\right) \,+\, dye \to dye_{VB}^{+} \to oxidation\, of\, dye\, molecule$$

When ZnO is illuminated by visible light, holes (h⁺_{VB}) and electrons (e⁻_{CB}) are generated and passed through from valence to conduction band. The photogenerated electrons and holes combine with Fe³⁺ ions, respectively.

$$Fe^{3+} + O_2 \rightarrow Fe^{5+} + O_2^{\circ} - (electron release)$$
 (4)

$$Fe^{3+} + OH^{-} \rightarrow Fe^{2+} + OH^{\circ}(hole \ release)$$
 (5)

$$OH^{\circ} + dye (MB \& MO) \rightarrow oxidation of dye molecule$$

(6)

These superoxide anions $(O_2^{\circ}-)$ and hydroxyl radicals (OH°) are strong oxidizing species, and it will degrade of MB and MO dye molecule (Eq. 6) [48]. From these results, novel Fe-doped ZnO nanoparticles have played a primary role in the degradation of organic dyes from wastewater.

4 Conclusion

In this paper, we reported the synthesis of ZnO-Fe_x $(x \approx 0, 0.05, 0.075 \& 0.1 \text{ mol.}\%)$ nanoparticles by coprecipitation method. The intensity of Fe-doped ZnO nanoparticles decreases due to the incorporation of Fe (0.05, 0.075 & 0.1 mol.%), confirmed by XRD. Doping of Fe modifies the morphology and crystallite size of ZnO nanoparticles and it was estimated to be ~ 42-68 nm. UV-Vis absorbance studies reveals that increasing of Fe concentration up to 0.1 mol.%, the bandgap decreases when compared with undoped ZnO. The maximum percentage of MB and MO photodegradation was achieved for the dosage concentration of 10 mg and irradiation time of 150 min at pH 6. Fe-doped ZnO nanoparticles may be used as an efficient photocatalyst to degrade the organic dyes under UV light.

References

- A. Nezamzadeh-Ejhieh, N. Moazzeni, J. Ind. Eng. Chem. 19, 1433–1442 (2013)
- M. Safari, M. Nikazar, M. Dadvar, J. Ind. Eng. Chem. 19, 1697–1702 (2013)

- 3. A. Arques, A.M. Amat, A. Garcia-Ripoll, R. Vicente, J. Hazard. Mater. **146**, 447 (2007)
- V.K. Gupta, D. Pathania, S. Agarwal, P. Singh, J. Hazard. Mater. 243, 179 (2012)
- B.K. Korbahti, K. Artut, C. Gecgel, A. Ozer, Chem. Eng. J. 173, 677 (2011)
- J.B. Joo, I. Lee, M. Dahl, G.D. Moon, F. Zaera, Y. Yin, Adv. Funct. Mater. 23, 4246–4254 (2013)
- 7. T.H. Yu, W.Y. Cheng, K.J. Chao, S.Y. Lu, Nanoscale 5, 7356 (2013)
- M. Lima, D. Fernandes, M. Silva, M. Baesso, A. Neto, G. de Morais et al., J. Sol–Gel Sci. Technol. 72, 301–309 (2014)
- 9. B. Cao, W. Cai, J. Phys. Chem. C 112, 680 (2008)
- R. Saravanan, M.M. Khan, V.K. Gupta, E. Mosquera, F. Gracia, V. Narayanan, A. Stephen, RSC Adv. 5, 34645–34651 (2015)
- R. Saravanan, N. Karthikeyan, V.K. Gupta, E. Thirumal, P. Thangadurai, V. Narayanan, A. Stephen, Mater. Sci. Eng., C 33, 2235–2244 (2013)
- R. Jeyachitra, V. Senthilnathan, T.S. Senthil, J Mater Sci. Mater Electron 29, 1189–1197 (2018)
- D. Rajesh, B. Varalakshmi, C.S. Sunandana, Phys. B 407, 4537–4539 (2012)
- M. Arshad, M.M. Ansari, A.S. Ahmed, P. Tripathi, S.S.Z. Ashraf, A.H. Naqvi, A. Azam, J. Lumin. 161, 275e280 (2015)
- L. Chow, O. Lupan, G. Chai, H. Khallaf, L.K. Ono, B.R. Cuenya, I.M. Tiginyan, V.V. Ursaki, V. Sontea, A. Schulte, Sens. Actuators A 189, 399–408 (2013)
- Y.X. Liua, Y.C. Liua, D.Z. Shena, G.Z. Zhonga, X.W. Fana, X.G. Konga, R. Muc, D.O. Hendersonc, J. Cryst. Growth 240, 152–156 (2002)
- T. Bak, J. Nowotny, M. Rekas, C. Sorrell, Int. J. Hydr. Energy 27, 991–1022 (2002)
- Z. Han, L. Ren, Z. Cui, C. Chen, H. Pan, J. Chen, Appl. Catal. B Environ. 126, 298 (2012)
- S.S. Shinde, C.H. Bhosale, K.Y. Rajundoped, J. Photochem. Photobiol. B 113, 70 (2012)
- Y. Min, K. Zhang, Y. Chen, Y. Zhang, W. Zhao, Sep. Purif. Technol. 92, 115 (2012)
- H. Wu, Z. Zheng, Y. Tang, N.M. Huang, R. Amal, H.N. Lim, Y.H. Ng, Pulsed electrodeposition of CdS on ZnO nanorods for highly sensitive photoelectrochemical sensing of copper (II) ions. Sustain. Mater. Technol. 18, e00075 (2018)
- H. Wu, Z. Zheng, C.Y. Toe, X. Wen, J.N. Hart, R. Amal, Y.H. Ng, J. Mater. Chem. A 8, 5638–5646 (2020)
- 23. H. Wu, T.H. Tan, R. Liu, H.-Y. Hsu, Y.H. Ng, Sol. RRL (2021). https://doi.org/10.1002/solr.202000423
- 24. A. Moulahi, F. Sediri, Ceram. Int. 40, 943-950 (2014)

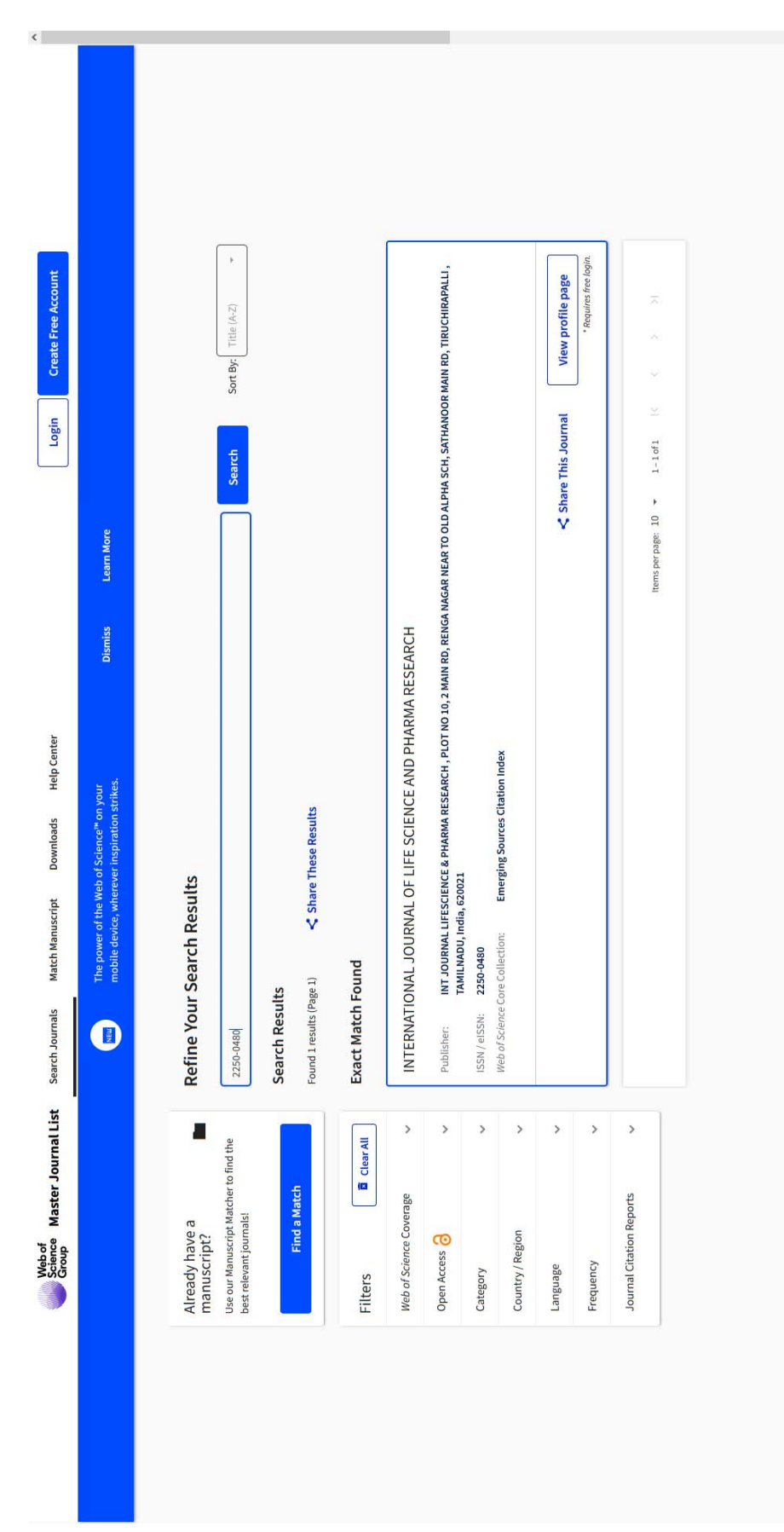


- N.L. Tarwal, P.R. Jadhav, S.A. Vanalakar, S.S. Kalagi, R.C. Pawar, J.S. Shaikh et al., Powder Technol. 208, 185–188 (2011)
- T. Ivanova, A. Harizanova, T. Koutzarova, B. Vertruyen, Mater. Lett. 64, 1147–1149 (2010)
- A. Rahmati, A.B. Sirgani, M. Molaei, M. Karimipour, Eur. Phys. J. Plus **129**, 7 (2014)
- 28. P. Malathy, K. Vignesh, M. Rajarajan, A. Suganthi, Ceram. Int. 40, 101 (2014)
- 29. B.M. Rajbongshi, S.K. Samdarshi, Appl. Catal. B: Environ. **144**, 435 (2014)
- 30. S. Dong, K. Xu, J. Liu, H. Cui, Phys. B 406, 3609 (2011)
- Y. Zhang, M.K. Ram, E.K. Stefanalkos, D.Y. Goswami, Surf. Coat. Technol. 217, 119 (2013)
- 32. M.M. Ba-Abbad, A.A.H. Kadhum, A. Mohamad, M.S. Takriff, K. Sopian, Chemosphere **91**, 1604–1611 (2013)
- 33. A.A. Ashkarran, A. Irajizad, S.M. Mahdavi, M.M. Ahadian, Mater. Chem. Phys. 118, 6–8 (2009)
- 34. J. Zhou, F. Zhao, Y. Wang, Y. Zhang, L. Yang, J. Lumin. **122–123**, 195–197 (2007)
- 35. S. Bai, T. Guo, Y. Zhao, J. Sun, D. Li, A. Chen et al., Sens. Actuators B Chem. **195**, 657–666 (2014)
- M. Nasir, S. Bagwasi, Y. Jiao, F. Chen, B. Tian, J. Zhang, Chem. Eng. J. 236, 388 (2014)
- 37. G. Srinivasan, J. Kumar, Cryst. Growth 310, 1841 (2008)
- 38. C.W. Nahm, J. Mater. Sci. Mater. Electron. 24, 70 (2013)

- 39. T.G. Venkatesh, Y.A. Nayaka, R. Viswanatha, C.C. Vidyasagar, B.K. Chethana, Power Tech. 225, 232–238 (2012)
- M.M. Hassan, W. Khan, A. Azam, A.H. Naqvi, J. Ind. Eng. Chem. 21, 283–291 (2015)
- A. Mesaros, C.D. Ghitulica, M. Popa, R. Mereu, A. Popa, T. Petrisor Jr., M. Gabor, A.I. Cadis, B.S. Vasile, Ceram. Int. 40, 2835–2846 (2014)
- 42. C. Liu, D. Meng, H. Pang, X. Wua, J. Xie, X. Yu, L. Chen, X. Liu, J. Magn. Magn. Mater. **324**, 3356 (2012)
- S. Abed, H. Bougharraf, K. Bouchouit, Z. Sofiani, B. Derkowska-Zielinska, M.S. Aida, B. Sahraoui, Superlattice Microstruct. 85, 370 (2015)
- 44. S.V. Elangovan, V. Chandramohan, N. Sivakumar, T.S. Senthil, Desalin. Water Treat. **57**, 9671–9678 (2016)
- K. Vignesh, M. Rajarajan, A. Suganthi, J. Ind. Eng. Chem. 20, 3826–3833 (2014)
- 46. W. Bousslama, H. Elhouichet, M. Ferid, Optik 134, 88 (2017)
- X. Yu, D. Meng, C. Li, U.K. Xu, J. Chen, C. Lu, Y. Wang, J. Mater. Sci. 25, 3920 (2014)
- 48. S.K. Kansal, M. Singh, D. Sud, J. Hazard. Mater. **141**, 581–590 (2007)

Publisher's Note Springer Nature remains neutral with regard to jurisdictional claims in published maps and institutional affiliations.







International Journal of Life science and Pharma Research ISSN 2250-0480

Research Article Nanomaterial



Efficient photocatalytic degradation of organic dyes with Ag doped ZnO nanoparticles under UV light irradiation

M. Senthil Kumar (D), C. Arunagiri^{2*}

Department of Physics, Srinivasan College of Arts and Science, (Affiliated to Bharathidasan University, Tiruchirapalli) Perambalur, Tamilnadu, India

²PG & Research Department of Physics, Periyar E.V.R College (Bharathidasan University, Tiruchirapalli), Tiruchirapalli, Tamilnadu,India

Abstract: Semiconductor based photocatalyst for degradation of cationic and anionic dye pollutants under UV light was demonstrated for wastewater treatment. In the present work, un-doped and Ag (mol% = 0, 0.05, 0.075 and 0.1)-doped ZnO nanoparticles were synthesized by co-precipitation method. X-ray diffraction (XRD) pattern confirms that the samples are found to be of highly crystalline hexagonal wurtzite structure. Scanning electron microscopy (SEM) image reveals that the morphology of the doped ZnO nanoparticles are highly affected by the addition of silver (Ag). Fourier transform infra-red (FTIR) and energy-dispersive spectra (EDS) demonstrates the presence of Ag in the ZnO lattice. UV–Vis absorption spectra shows that the Agdoped ZnO nanoparticles exhibit a red-shift with reduced bandgap energy compared with un-doped ZnO nanoparticles. Hence, our aim is to find the effect of Ag- doping in ZnO nanoparticles for the improvement of photocatalytic degradation. The photocatalytic activities of these Ag-doped nanoparticles were evaluated by measuring the rate of photo-degradation reaction of hazardous methylene blue (MB) and methyl orange (MO) dye under UV-light irradiation. Photocatalytic efficiency in the degradation of MB and MO dyes was compared with the efficiency of un-doped ZnO. The effects of various factors like solution pH, photocatalytic dosage and UV irradiation time with concentration of MB and MO on photocatalytic degradation were studied. It was found that cationic dyes shows better photo-degradation than the anionic dyes. The main objective of the present work was optimizing the various factor for better photocatalytic activity, complete mineralization and evaluating the photocatalytic-degradation mechanism.

Keywords:, Ag-Doping, Nanoparticles, Methylene Blue, Methyl Orange, Photocatalytic Degradation

*Corresponding Author

Citation

C. Arunagiri , PG & Research Department of Physics, Periyar E.V.R College (Bharathidasan University, Tiruchirapalli), Tiruchirapalli, Tamilnadu,India



Received On 06 September 2021
Revised On 30 November 2021
Accepted On 08 December 2021
Published On 05 January 2022

Funding This research did not receive any specific grant from any funding agencies in the public, commercial or not for profit sectors.

M. Senthil Kumar, C. Arunagiri, Efficient photocatalytic degradation of organic dyes with Ag doped ZnO nanoparticles under UV light irradiation.(2022).Int. J. Life Sci. Pharma Res.12(1), L1-10 http://dx.doi.org/10.22376/ijpbs/lpr.2022.12.1.L1-10

This article is under the CC BY- NC-ND Licence (https://creativecommons.org/licenses/by-nc-nd/4.0)

CC (I) (S) (E) BY NC ND

Copyright @ International Journal of Life Science and Pharma Research, available at www.ijlpr.com

Int J Life Sci Pharma Res., Volume 12., No 1 (January) 2022, pp L1-10

I. INTRODUCTION

Economically growing countries like India are facing environmental pollution due to industrial developments. In particular, industrial effluents discharged from cosmetics, textile, paper and paint industries contain high levels of organic contaminants including toxic chemicals and heavy metals¹. Untreated industrial effluents release into water system has become one of the most serious water pollutions that severely affect the ecosystem and human health. Appropriate treatment is essential for effective destruction of effluents before they are released into the ecosystem². There are several techniques available for the wastewater treatment such as activated carbon adsorption, chemical oxidation, coagulation, ion exchange, reverse osmosis, electrodialysis and advanced oxidation processes (AOP) have been found to be ineffective for the mineralization of toxic organic compounds³⁻⁷. Among them, photo-catalysis is an effective process that is used for heterogeneous photocatalytic degradation of organic effluents using a semiconductor as a photo-catalyst⁸. Many researchers are recently focused in conversion of organic dyes into harmless chemicals using photo-catalysts. ZnO is a versatile multifunctional wide band gap semiconductor like TiO₂ and it has numerous superior properties such as high electron transport, light sensitive, thermal and chemically stable, non-toxic and sustainable with hydrogen environment, 2,10 nanoparticles are effective photo-catalysts for degradation of toxic pollutants under UV irradiation. ZnO has better activity than TiO_2 for photocatalytic degradation of some organic dyes^{11,12}.The photocatalytic efficiency of ZnO nanoparticles mainly depends on the ability of electron-holes (e-/h+) pair formation under light illumination. However, the rapid recombination of photo-excited electron-holes (e⁻/h⁺), aggregation and low surface area of the bulk form are the main factors for the reduction of photocatalytic efficiency. Numerous methods, such as doping of metals and nonmetals, combining with different semiconductors are used to overcome these drawbacks. The metal (Ag) doping of ZnO is most efficient way to improve its photocatalytic efficiency, because metal doping accelerates the charge carrier separation and change its physical and chemical properties 13-²⁰. ZnO has been prepared by a variety of techniques such as hydrothermal method²¹, combustion²², and sol-gel method²³. Among these, co-precipitation²⁴ shows some advantages over the other methods. The present work explains the effect of various concentrations of Ag dopant on the structural and photocatalytic activity of ZnO nanoparticles. Furthermore, the samples were characterized by XRD, SEM, FTIR and UV-Vis spectrophotometer. To the best of our knowledge, this is the first report of application of Ag-doped ZnO nanoparticles for the degradation of cationic dye (methylene blue) and anionic dye (methyl orange) in water.

2. EXPERIMENTAL

2.1 MATERIALS AND METHODS

All the chemical used in the experiments are analytical grade and were used without further purification. Zinc nitrate hexahydrate $[Zn(NO_3)_2.6H_2O]$, silver nitrate $Ag(NO_3)$, methylene blue (MB), methyl orange (MO) and sodium

hydroxide [NaOH], were purchased from Alfa Aesar chemicals, India. Double distilled water (DDW) was used for all of the solutions.

2.2 Photo-catalyst Preparation

In a typical synthesis, 10 g of Zn (NO₃)₂ 6H₂O was dissolved into 20 ml of DDW. In another container, 8 g of NaOH in 100 ml DDW. Then NaOH added to the zinc nitrate solution. Both these solutions were added dropwise under continuous magnetic stirring until pH adjusted into 11. Then the above solution was heated in in a vacuum oven at 150 °C for Ih. Afterwards, white color precipitates were separated by centrifugation and washed twice with DDW followed by ethanol and dried at 100 °C for 3h. The dried participate was calcined at 450 °C for Ih and finally un-doped ZnO nanoparticles formed. For synthesis of Ag doped ZnO nanoparticles containing various concentrations (mol% = 0.05, 0.075 and 0.1) of silver nitrate dissolved in water were added to the zinc nitrate solution with stirring. The coprecipitation method was selected based on available literature as described above²⁴

2.3 Characterizations

The crystalline phases of un-doped and Ag-doped ZnO nanoparticles were determined by powder X-ray diffractometer (X'PERT PRO MPD) using CuKα radiation (λ = 0.15405 nm) operated at 40 kV voltage and 30 mA current with a scanning rate of 2° per min²¹. The particle size and morphological features of the samples were observed by scanning electron microscope (SEM-JEOL JS-6390) with energy dispersive X-ray spectrometer (EDX)²¹. Band gap energies of the samples were analysed from UV-visible spectra recorded UV-Vis double-beam using (Systronics: AU-2707). spectrophotometer Transform Infrared (FT-IR) spectra of prepared samples were recorded by using a FTIR Spectrometer (JASCO FTIR-410) in the range 400-4000 cm⁻¹ with a resolution of 4 cm⁻¹ at room temperature using KBr disc. Electrical characteristics (I-V) curve of the samples were carried out using a Keithley electrometer 2400 model

2.4 Evaluation of Photocatalytic activity

Photocatalytic activity of the un-doped and Ag-doped ZnO nanoparticles was evaluated for degradation of MB and MO dye solution under UV light irradiation. The photocatalytic procedure was conducted by adding 10 mg of photo-catalyst in 50 mL, 10 ppm of MB and MO dye solution. The reaction mixture was stirred for 30 min. under a dark to reach adsorption-desorption equilibrium. After that the dye solution was irradiated with an 8 W UV lamp was switched on. At different time intervals (0, 15, 30, 45, 60 and 75 min.) samples were taken out and centrifuged to separate the catalyst and then the supernatant was analysed in a UV-visible double beam spectrophotometer maximum wavelength (λmax) observed at ~664 and 464 nm to study the photocatalytic degradation. The photo-degradation efficiency (D%) of the MB and MO dye was calculated using the equation²⁵

 $(D\%) = [C-C_0/C_0] \times 100$

Where, C₀ and C are the initial and final degradation time of MB and MO (mg/L) dye solution used.

3. RESULT AND DISCUSSION

3.1 XRD Analysis

In order to investigate the crystal structure of un-doped ZnO and Ag doped ZnO nanoparticles were characterized by powder X-ray diffraction (PXRD) data. Fig. I(a) depicts the PXRD patterns of un-doped ZnO and Ag doped ZnO

nanoparticles with different concentrations of Ag, i.e. 0.05, 0.075 and 0.1%. The XRD pattern of all samples have strong diffraction peaks are assigned to (100), (002), (101), (102), (110), (103), (200), (112) and (201) planes of hexagonal wurtzite structure of ZnO in the Miller indices (JCPDS-36-1451) ²⁶. There is no extra peaks or other unidentified peaks corresponds to Ag or its oxide phases in the XRD pattern.

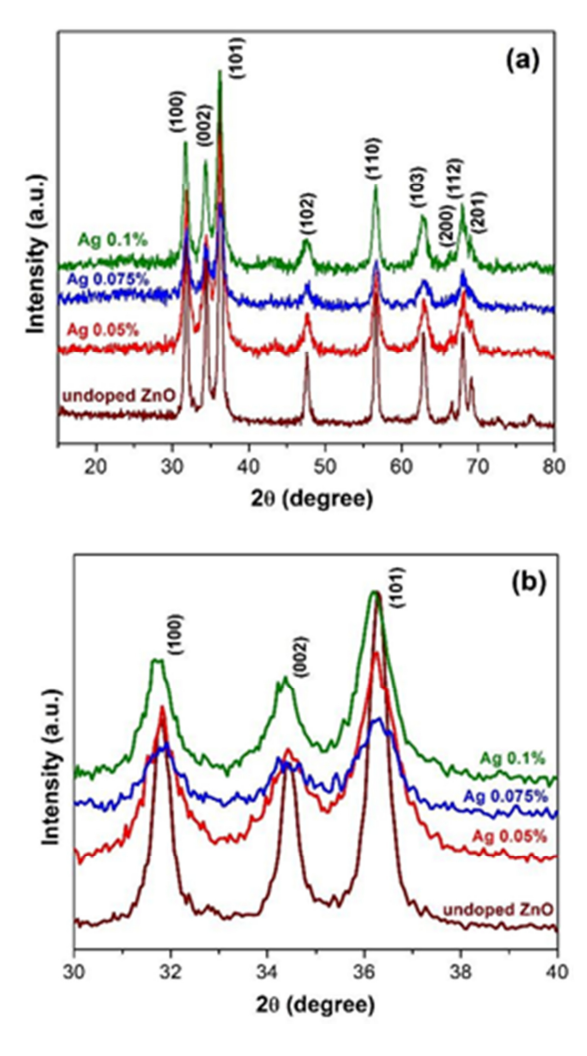


Fig. 1. (a) XRD patterns of un-doped and Ag-doped ZnO nanoparticles (b) expanded view of XRD patterns shift.

Table I. Lattice parameters and crystallite size of undoped and Ag-doped ZnO nanoparticles.								
Ag doping (mol%)	hkl	a[Å]	c[Å]	c/a	Average Crystallite Size (nm)			
ZnO	10 0 00 2 10 1	3.2555	5.2184	1.6029	23			
Ag _{0.05} Zn _{0.95} O	10 0 00 2 10	3.2562	5.2190	1.6028	20			

	I				
Ag _{0.075} Zn _{0.925} O	10 0 00 2 10	3.2584	5.2210	1.6023	19
$Ag_{0.1}Zn_{0.9}O$	10 0 00 2 10 1	3.2586	5.2240	1.6031	18

Fig. 1(b) shows a magnification of the peak at 31.8 (100), 34.3 (002) and 36.3° (101) were a slight peak shift to lower angles observed in the 0.05, 0.075, and 0.1% Ag-doped ZnO nanoparticles. This result confirms that Ag impurity has been successfully incorporated into the ZnO lattice structure. The lattice constants and average crystallite size of major XRD peaks calculated for different samples are listed in Table I. In our study, the effect of Ag doping on the average crystallite size (D) of was calculated for all samples by Debye-Scherrer's equation, and are found to be 23, 20, 19 and 18 nm, respectively²⁷. These results indicate that the D value in the Agdoped ZnO nanoparticles decreased as the doping concentration increased. Furthermore, the increasing Ag content decreases the lattice parameters and average crystallite size values. Other studies have found the same results were reported by Pal et al.28 in Codoped ZnO nanoparticles, Saravanan et al.29 in Ag-doped ZnO nanoparticles and Udom et al.30 in Ag-doped ZnO nanowires.

3.2 SEM with EDX Analysis

The surface morphology and chemical composition of the prepared samples were investigated by SEM with EDX. SEM images of undoped ZnO and Ag (0.05, 0.075 and 0.1 mol.%) doped ZnO nanoparticles are shown in Fig. 2(a-d). Fig. 2(a) shows the formation of irregular spherical morphology of the un-doped ZnO. From the Fig 2(b-d), it was precisely discovered that well prepared samples are in nanometer size and the surface morphology changes with the silver concentration. The variation of surface morphology with Ag dopant is due to the variation of number of nucleation sites²¹. The silver concentration reduces the particle size and it was confirmed from the XRD results. The obtained results are similar to the results reported by Pung et al³¹.

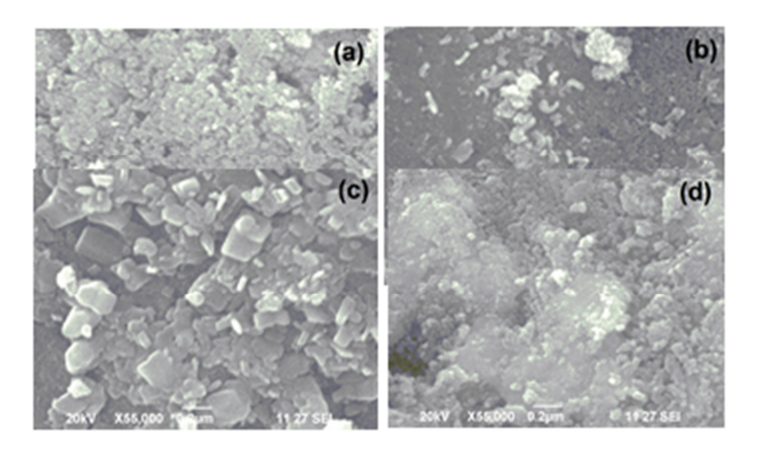
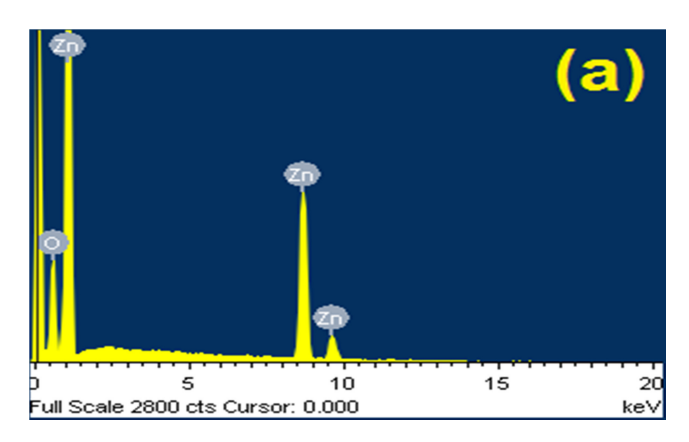


Fig. 2. SEM images of (a) undoped (b) 0.05, (c) 0.075 and (d) 0.1 mol.% Ag-doped ZnO nanoparticles.

The EDX spectra for un-doped ZnO and Ag (0.1%)-doped ZnO nanoparticles are shown in Fig. 3 (a, b). EDX spectrum of un-doped ZnO shows presence existence characteristic peaks of oxygen (O) and zinc (Zn) elements. The EDX pattern of Ag-doped nanoparticles also include elements such as existence of silver (Ag) together with Zn and O, indicating the successful doping of Ag in the ZnO matrix³¹.



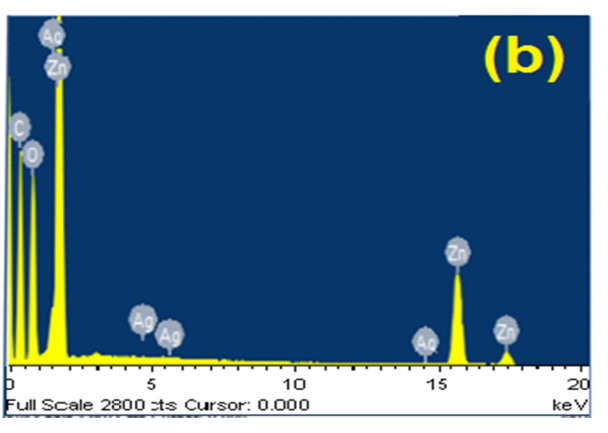


Fig. 3. EDX images of (a) un-doped and (b) 0.1 mol.% Ag-doped ZnO nanoparticles.

3.3 UV-Vis Analysis

In order to investigate the optical properties of un-doped ZnO and Ag (0.05, 0.075 and 0.1 mol.%) doped ZnO nanoparticles were investigated by UV-Vis. absorption spectroscopy. Fig. 4 (a-d) shows the UV-Vis absorption spectra of un-doped ZnO and Ag (0.05, 0.075 and 0.1 mol.%) doped ZnO nanoparticles. Un-doped ZnO has an absorption cut-off edge was observed around 370 nm. The

adsorption of Ag-doped ZnO nanoparticles was shifted to the longer wavelength from ZnO with the increase of the molar ratio of Ag (0.05, 0.075 and 0.1 mol.%). After Ag-doping display an additional hump absorption in the visible region observed at 373, 375 and 377 nm. The calculated optical band gap energies were 3.35, 3.33, 3.30 and 3.28 eV for un-doped ZnO and Ag-doped ZnO nanoparticles, respectively. According to some previous reports similar result was observed by Hassan et $al.^{32}$.

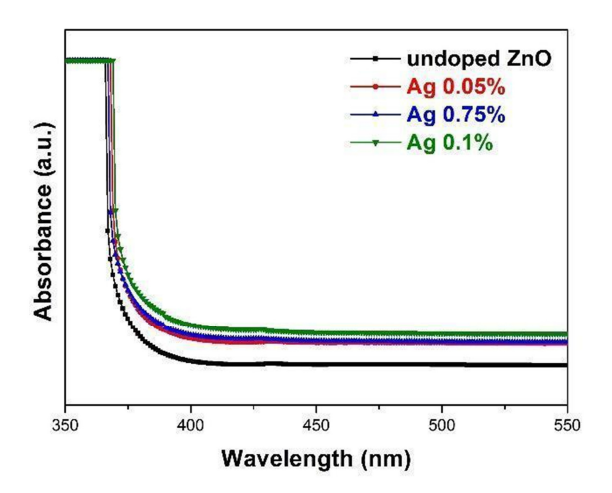


Fig. 4. UV-Vis absorbance spectra (a) un-doped (b) 0.05, (c) 0.075 and (d) 0.1 mol.% Ag-doped ZnO nanoparticles.

3.4 FT-IR Analysis

The FTIR spectra of un-doped ZnO and Ag (0.1%)-doped ZnO nanoparticles are presented in Fig. 5 (a, b). The absorption peaks present at 3441 and 1625 cm⁻¹ which corresponds to the -OH stretching and bending vibration of the water molecule³³.

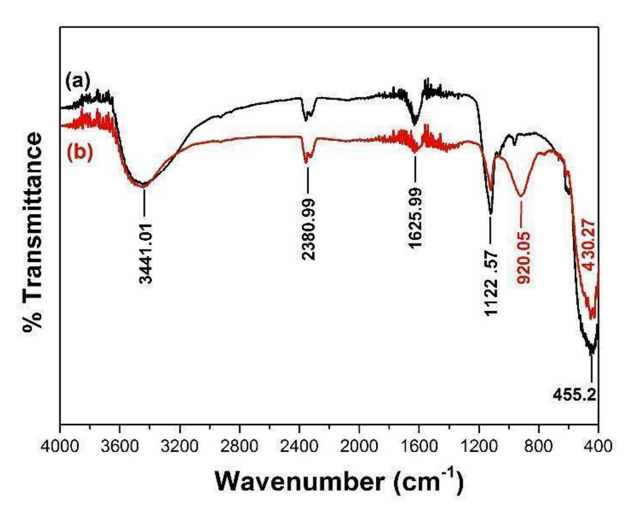


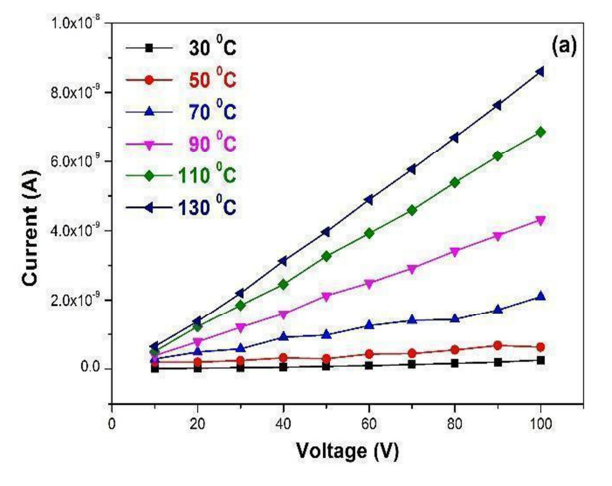
Fig. 5. FT-IR spectra of (a) un-doped and (b) 0.1 mol.% Ag-doped ZnO nanoparticles.

The band at 2380 cm⁻¹ corresponds to symmetric and asymmetric C–H bond³⁴. The observed FTIR spectrum exhibits several well-defined absorption bands at 1122 and 920 cm⁻¹ and they are attributed to sulphate and C=C bonds, respectively³⁵. The absorption peaks appears at 400 and 550

cm⁻¹ were assigned to the metal-oxygen (M-O) stretching mode³⁶ and the absorbance peak noticed in the spectra around 455 and 430 cm⁻¹ corresponds to the presence of Zn-O and Ag-O stretching bond, respectively.

3.5 I-V Characteristics

Electrical properties of un-doped ZnO and Ag (0.1%)-doped ZnO nanoparticles was measured by using the I-V characteristics and it is presented in Fig. 6 (a, b). From IV curves, electrical conductivity of un-doped ZnO and Ag (0.1%)-doped ZnO taken under varying temperatures from 30 to 130 °C.



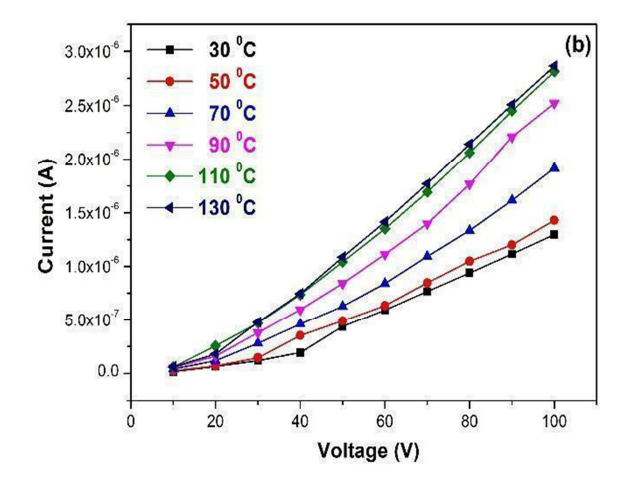


Fig. 6. I-V characteristics of (a) un-doped and (b) 0.1 mol.% Ag-doped ZnO nanoparticles.

This study reveals that (0.1%) Ag-doped ZnO nanoparticles shows better conductivity than the un-doped ZnO and it may due to the presence of more charge carrier's mobility³⁷.

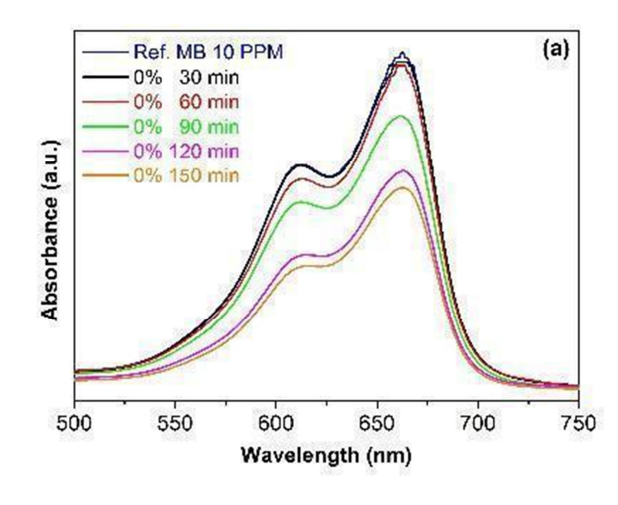
3.6 Photocatalytic Activity

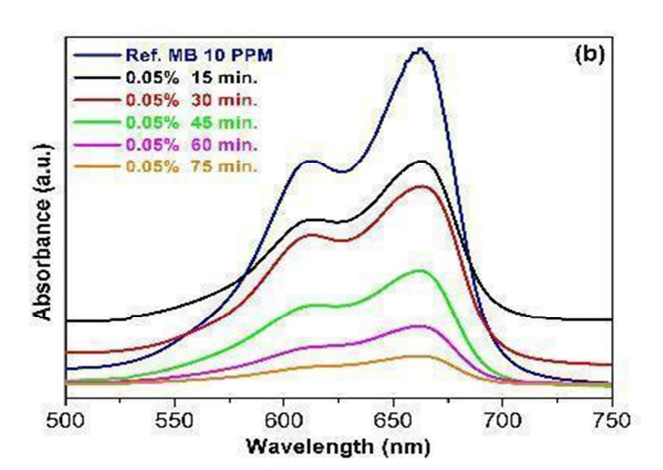
3.6.1 Optimized Factors to the Catalytic Activity

The photocatalytic degradation of un-doped ZnO and Ag-doped ZnO nanoparticles were selected for the evaluation of

photocatalytic activity under UV-visible light. In order to study the effect of the UV light on the degradation of MB and MO dye. The dyes were prepared in various concentrations like acidic, neutral and alkaline medium. The photocatalytic activity was carried out and optimised for un-doped ZnO catalyst with MB and MO dye concentration of 10 ppm, catalyst concentration of 10 mg, pH = 6 and UV irradiation time up to 150 min.

3.6.2 Impact of UV irradiation on Degradation of MB and





For the above mentioned conditions the photocatalytic degradation was carried out for Ag-doped ZnO nanoparticles. The Fig. 7(a-d) shows the comparative spectra of degradation of MB dye with un-doped ZnO and Ag (mol%

= 0.05, 0.075, 0.1)-doped ZnO nanoparticles with respect to time. The high intensity absorption peaks was observed at 664 nm for MB dye. It was observed that the degradation of MB dye increases with increase of dopant concentration²⁴.

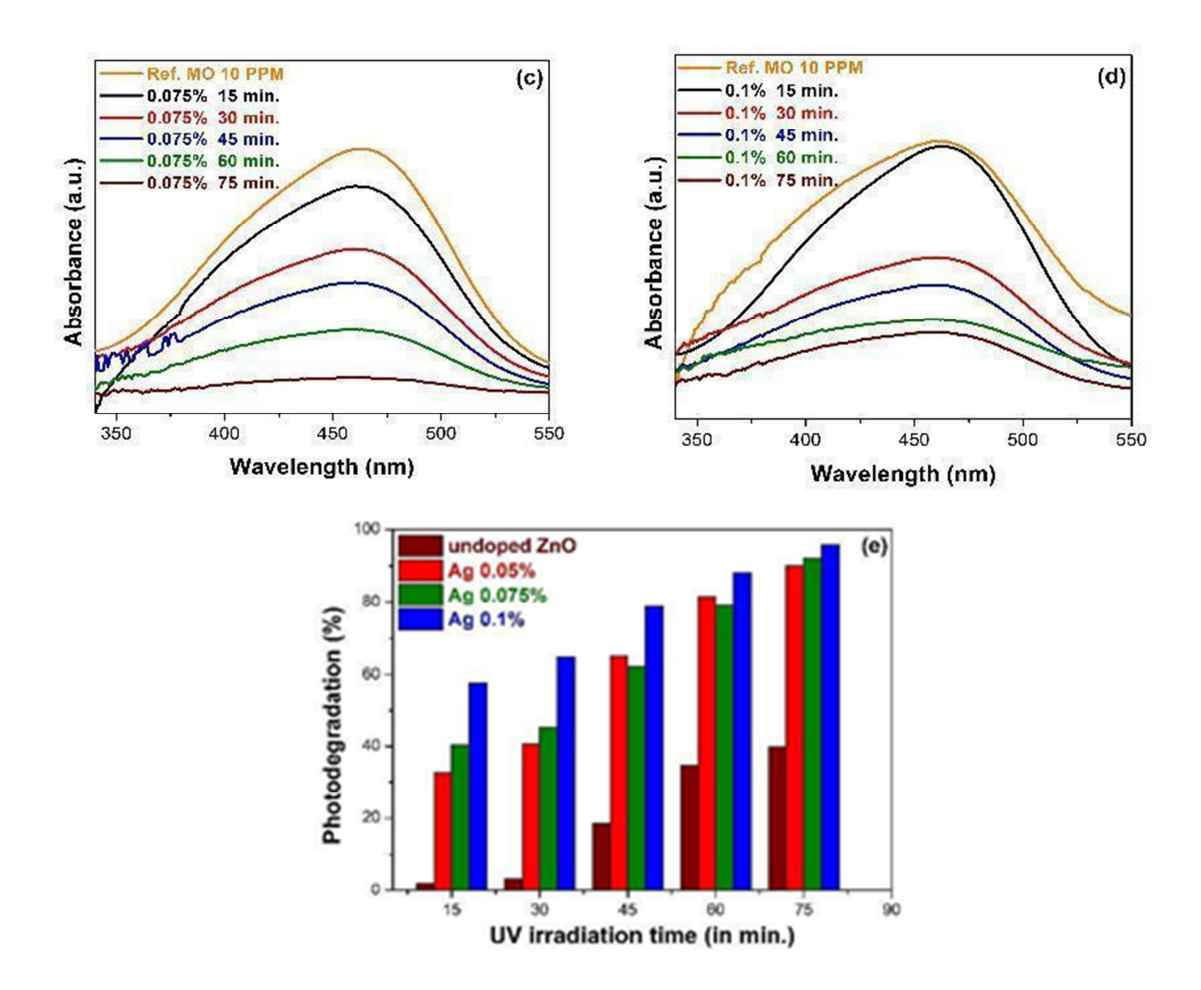


Fig. 7. MB dye degradation of (a) un-doped (b) 0.05, (c) 0.075, (d) 0.1 mol.% Ag-doped ZnO nanoparticles (MB dye:10 ppm, catalyst dose:10 mg, pH=6) and (e) effect of irradiation time of UV on MB photo-degradation.

The efficiency of un-doped and Ag-doped ZnO nanoparticles under UV light reaches 38, 90, 92 and 95% after 75 min light irradiation. Ag (0.1%)-doped ZnO nanoparticle shows the highest degradation efficiency of 95% under UV radiation for

MB dye, while under similar conditions, a much lower efficiency (38%) was observed for un-doped ZnO nanoparticles under visible light radiation²⁴.

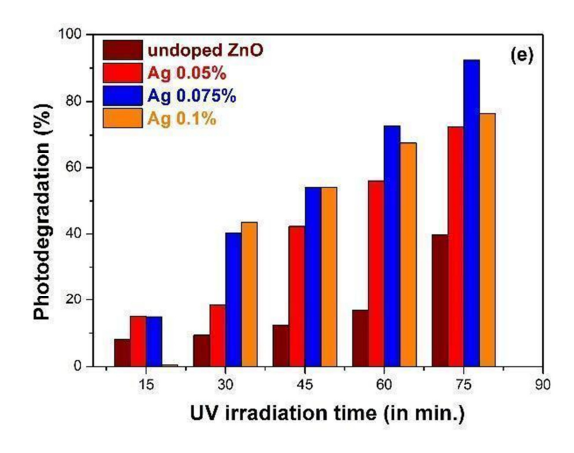


Fig. 8. MO dye degradation of (a) un-doped (b) 0.05, (c) 0.075, (d) 0.1 mol.% Ag-doped ZnO nanoparticles (MO dye:10 ppm,

catalyst dose:10 mg, pH=6) and (e) effect of irradiation time of UV on MO photo-degradation. The comparative spectra for degradation MO dye with un-doped ZnO and Ag (mol% = 0.05, 0.075, 0.1)-doped ZnO nanoparticles with respect to time was presented in Fig. 8(a-d). The high intensity absorption peaks of MO dye were observed at 464 nm. The effect of irradiation time of UV on MO

dye degradation is shown in Fig. 8 (e). The degradation efficiency increases with increase of dopant concentration and the obtained values are 36, 72, 92 and 76%, respectively for un-doped, 0.05, 0.075 and 0.1 mol.% Ag-doped ZnO nanoparticles. It can be seen that maximum degradation (92%) of MO dye was achieved for Ag (0.075%)-doped ZnO nanoparticles in 75 min. It should be noted

that MB was degraded more faster than MO in the presence of the Ag-dopant. The possible photocatalytic degradation mechanism of MB and MO on Ag-doped ZnO nanoparticles under UV-visible light irradiation can be explained from the equation I to 6. During the catalytic process, photons can excite electrons in the valence band (VB) to be moved up to the conduct band (CB) and generate the same amount of electron-hole pair (e- and h+). The photo-excited electrons will be transferred from ZnO to Ag nanoparticles under

the potential energy. The photocatalytic activity is effective thereby preventing the recombination between electrons and holes on the surface of ZnO. Afterwards, the electron on Ag nanoparticles can produce the O_2^- superoxideradical, while the holes in the VB can react with H_2O_2 to produce OH hydroxylradical³⁸. These free radicals can degrade organic compounds to CO_2 and $H_2O_3^{11}$

$$ZnO + h\gamma \longrightarrow ZnO(h^{+}_{VB} + e^{-}_{CB}) \qquad (1)$$

$$ZnO (e^{-}_{CB}) + Ag \longrightarrow ZnO + Ag (e^{-}_{CB}) \qquad (2)$$

$$Ag (e^{-}_{CB}) + O_{2} \longrightarrow O_{2}^{-} + Ag \qquad (3)$$

$$ZnO (h^{+}_{VB}) + H_{2}O \longrightarrow ZnO + H^{+} + OH \qquad (4)$$

$$(\cdot O_{2}^{-} + \cdot OH) + dye \longrightarrow degradation \qquad (5)$$

$$(MB \text{ or } MO) \qquad products$$

$$(\cdot O_{2}^{-} + \cdot OH) + degradation \longrightarrow CO_{2} + H_{2}O \qquad (6)$$

$$products$$

Products Till now, many studies have proven that electrons can transfer from Ag to the CB of ZnO. Then, they are scavenged by adsorbed O_2 molecules to yield superoxide radical anions (O_2) to degrade dye molecules³⁸. Therefore, the photocatalytic activity will be enhanced.

4. CONCLUSION

In summary, various mol% of Ag-doped ZnO nanoparticles was synthesized using co-precipitation method. The structural, morphological, optical and electrical properties as well as the photocatalytic activity under UV irradiation of the resultant samples were characterized by XRD, SEM with EDX, UV–Vis FT-IR and IV analysis. Doping of Ag modified the morphology and average crystallite size of ZnO nanoparticles. In photocatalytic activity, Ag-doped ZnO nanoparticles enhances the degradation of MB dye under UV irradiation than the degradation of MO dye. The optimum

reaction conditions for the degradation of MB and MO under UV-visible light irradiation of samples were pH= 6.0, catalyst dosage of 10 mg, and MB and MO concentration of 10 ppm. The possible mechanism of photocatalytic activity was studied and Ag enables the trapping of electrons in Ag-doped ZnO nanoparticles. Ag (0.1 mol%)-doped ZnO nanoparticles may be assumed as a promising photo-catalyst for the degradation of toxic organic effluents at room temperature.

5. AUTHOR CONTRIBUTION STATEMENT

Mr. Senthil Kumar, M conceptualized and gathered the data with regard to this work. Dr.Arunagiri, C analysed these data and supervised

6. CONFLICT OF INTEREST

Conflict of interest declared none.

7. REFERENCES

- Pereira RA, Pereira MFR, Alves MM, Pereira L. Carbon based materials as novel redox mediators for dye wastewater biodegradation. Appl Catal B. 2014;144:713-20. doi:10.1016/j.apcatb.2013.07.009.
- Umar A, Akhtar MS, Al-Hajry A, Al-Assiri MS, Dar GN, Saif Islam M. Enhanced photocatalytic degradation of harmful dye and phenyl hydrazine chemical sensing using ZnO nanourchins. Chem Eng J. 2015;262:588-96. doi:10.1016/j.cej.2014.09.111.
- 3. Gao B, Liu B, Chen T, Yue Qinyan. Effect of aging period on the characteristics and coagulation behavior of polyferric chloride and polyferric chloride–polyamine composite coagulant for synthetic dying wastewater treatment. J Hazard Mater. 2011; 187(1-3): 413-20. doi:10.1016/j.jhazmat.2011.01.044, PMID 21295910.
- 4. Szyguła A, Guibal E, AriñoPalacín MA, Ruiz M, Sastre AM. Removal of an anionic dye (Acid Blue 92) by coagulation–flocculation using chitosan. J Environ

- Manage. 2009;90(10):2979-86. doi:10.1016/j.jenvman.2009.04.002, PMID 19467769.
- Kim T-H, Park Chulhwan, Kim Sangyong. Water recycling from desalination and purification process of reactive dye manufacturing industry by combined membrane filtration. J Clean Prod. 2005;13(8):779-86. doi: 10.1016/j.jclepro.2004.02.044.
- Gupta VK, Pathania D, Agarwal S, Singh P. Adsorptional photocatalytic degradation of methylene blue onto pectin—CuS nanocomposite under Solar Light. J Hazard Mater. 2012;243:179-86. doi: 10.1016/j.jhazmat.2012.10.018, PMID 23122730.
- 7. Körbahti BK, Artut K, Geçgel C, Özer A. Electrochemical decolorization of textile dyes and removal of metal ions from textile dye and metal ion binary mixtures. Chem Eng J. 2011;173(3):677-88. doi: 10.1016/j.cej.2011.02.018.
- 8. Umar A, Akhtar MS, Al-Hajry A, Al-Assiri MS, Almehbad NY. Hydrothermally grown ZnO nanoflowers for environmental remediation and clean energy applications. Mater Res Bull. 2012;47(9):2407-14. doi: 10.1016/j.materresbull.2012.05.028.
- Jagadhesan S, Senthilkumar N, Senthilnathan V, Senthil TS. Sb doped ZnO nanostructures prepared via co precipitation approach for the enhancement of MB dye degradation. Mater Res Express. 2018;5(2):025040. doi: 10.1088/2053-1591/aaaf80.
- 10. Tu VA, Tuan VA. A facile and fast solution chemistry synthesis of porous ZnO nanoparticles for high efficiency photodegradation of tartrazine. Viet J Chem. 2018;56(2):214-9. doi: 10.1002/vjch.201800016.
- Shafaei A, Nikazar MM, Arami M. Photocatalytic degradation of terephthalic acid using titania and zinc oxide photocatalysts: comparative study. Desalination. 2010;252(1-3):8-16. doi: 10.1016/j.desal.2009.11.008.
- 12. Xie J, Li Y, Zhao W, Bian L, Wei Y. Simple fabrication and photocatalytic activity of ZnO particles with different morphologies. Powder Technology. 2011;207(1-3):140-4. doi: 10.1016/j.powtec.2010.10.019.
- Subash B, Krishnakumar B, Swaminathan M, Shanthi M. Synthesis and characterization of cerium-silver co-doped zinc oxide as a novel sunlight-driven photocatalyst for effective degradation of Reactive Red 120 dye. Mater Sci Semicond Process. 2013;16(4):1070-8. doi: 10.1016/j.mssp.2013.04.001.
- Araújo ES, da Costa BP, Oliveira RAP, Libardi J, Faia PM, de Oliveira HP. TiO2/ZnO hierarchical hetero nanostructures: synthesis, characterization and application as photocatalysts. J Environ Chem Eng. 2016;4(3):2820-9. doi: 10.1016/j.jece.2016.05.021.
- Neelakanta Reddy I, Venkata Reddy Ch, Shim J, Akkinepally B, Cho M, Yoo K, Kim D. Excellent visible-light driven photocatalyst of (Al, Ni) codoped ZnO structures for organic dye degradation. Cat Today. 2018;340:277-85.
- 16. Bera A, Basak D. Photoluminescence and photoconductivity of ZnS-coated ZnO nanowires. ACS Appl Mater Interfaces. 2010;2(2):408-12. doi: 10.1021/am900686c, PMID 20356186.
- 17. Li BX, Wang YF. Facile synthesis and photocatalytic activity of ZnO-CuO nanocomposite. Superlattices

- and Microstructures. 2010;47(5):615-23. doi: 10.1016/j.spmi.2010.02.005.
- Lei YZ, Zhao GH, Liu MC, Zhang ZN, Tong XL, Cao TC. Fabrication, characterization, and photoelectrocatalytic application of ZnO nanorods grafted on vertically aligned TiO2 nanotubes. J Phys Chem C. 2009;113(44):19067-76. doi: 10.1021/jp9071179.
- Zhang ZY, Shao CL, Li XH, Wang CH, Zhang MY, Liu YC. Electrospun nanofibers of p-type NiO/n-type ZnO heterojunctions with enhanced photocatalytic activity. ACS Appl Mater Interfaces. 2010;2(10):2915-23. doi: 10.1021/am100618h, PMID 20936796.
- Wang Q, Geng BY, Wang SZ. ZnO/Au hybrid nanoarchitectures: wet-chemical synthesis and structurally enhanced photocatalytic performance. Environ Sci Technol. 2009;43(23):8968-73. doi: 10.1021/es902568h, PMID 19943674.
- Sriharan N, Muthukumarasamy N, Thambidurai M, Senthil TS. Importance of ZnO nanorods prepared from hydrothermal method for various dyes degradation. J Optoelectron Adv Mater. 2017;19(9-10):634-40.
- Tarwal NL, Jadhav PR, Vanalakar SA, Kalagi SS, Pawar RC, Shaikh JS, Mali SS, Dalavi DS, Shinde PS, Patil PS. Photoluminescence of zinc oxide nanopowders synthesized by a combustion method. Powder Technol. 2011;208(1):185-8. doi: 10.1016/j.powtec.2010.12.017.
- 23. Alireza Samadi Tabrizi. Investigating various factors to increase the strength of alumina nano-fibers using sol-gel method. Int J Life Sci Pharma Res. 2016;6(4):1-11.
- Jagadhesan S, Senthilnathan V, Senthil TS. Studies on Diamond like Sn doped ZnO nanostructures prepared via co-precipitation approach for improving photo-catalytic application. J Optoelectron Adv Mater. 2018;20:188-95.
- 25. Davoud Balarak, Marzieh Baniasadi, Kethineni Chandrika. Investigating the efficiency of zirconium oxide nanoparticles in removal ofciprofoxacin from aqueous environments. Int J Life Sci Pharma Res., 2020;10(1):17-22.
- Ashkarran AA, Irajizad A, Mahdavi SM, Ahadian MM.
 ZnO nanoparticles prepared by electrical arc discharge method in water. Mater Chem Phys. 2009;118(1):6-8. doi: 10.1016/j.matchemphys.2009.07.002.
- Nasir M, Bagwasi S, Jiao Y, Chen F, Tian B, Zhang J. Characterization and activity of the Ce and N codoped TiO2 prepared through hydrothermal method. Chem Eng J. 2014;236:388-97. doi: 10.1016/j.cej.2013.09.095.
- 28. Pal B, Giri PK. Defect mediated magnetic interaction and high Tc ferromagnetism in Co doped ZnO nanoparticles. J Nanosci Nanotechnol. 2011;11(10):9167-74. doi: 10.1166/jnn.2011.4293, PMID 22400318.
- Saravanan S, Silambarasan M, Soga T. Structural, morphological and optical studies of Ag-doped ZnO nanoparticles synthesized by simple solution combustion method. Jpn J Appl Phys. 2014;53(11S). doi: 10.7567/JJAP.53.11RF01.

- Udom I, Zhang Y, Ram MK, Stefanakos EK, Hepp AF, Elzein R, Schlaf R, Goswami DY. A simple photolytic reactor employing Ag-doped ZnO nanowires for water purification. Thin Solid Films. 2014;564:258-63. doi: 10.1016/j.tsf.2014.05.057.
- 31. Pung SY, Lee WP, Aziz A. Kinetic study of organic dye degradation using ZnO particles with different morphologies as a photocatalyst. Int J Inorg Chem. 2012;2012:1-9:Article ID 608183. doi: 10.1155/2012/608183.
- 32. Mehedi Hassan MM, Khan W, Azam A, Naqvi AH. Influence of Cr incorporation on structural, dielectric and optical properties of ZnO nanoparticles. J Ind Eng Chem. 2015;21:283-91. doi: 10.1016/j.jiec.2014.01.047.
- 33. Jiménez-González AE, Soto Urueta JAS, Suárez-Parra R. Optical and electrical characteristics of aluminum-doped ZnO thin films prepared by sol–gel technique. J Cryst Growth. 1998;192(3-4):430-8. doi: 10.1016/S0022-0248(98)00422-9.
- 34. Ramimoghadam D, Hussein MZB, Taufiq-Yap YH. Synthesis and characterization of ZnO nanostructures using palm olein as biotemplate. Chem Cent J. 2013;7(1):71. doi: 10.1186/1752-153X-7-71, PMID 23601826.

- Saoud K, Alsoubaihi R, Bensalah N, Bora T, Bertino M, Dutta J. Synthesis of supported silver nanospheres on zinc oxide nanorods for visible light photocatalytic applications. Mater Res Bull. 2015;63:134-40. doi: 10.1016/j.materresbull.2014.12.001.
- Srivastava M, Ojha AK, Chaubey S, Sharma PK, Pandey AC. Influence of calcinations temperature on physical properties of the nanocomposites containing spinel and CuO phases. J Alloys Compd. 2010;494(1-2):275-84. doi: 10.1016/j.jallcom.2010.01.008.
- Abed S, Bougharraf H, Bouchouit K, Sofiani Z, Derkowska-Zielinska B, Aida MS, Sahraoui B. Influence of Bi doping on the electrical and optical properties of ZnO thin films. Superlattices Microstruct. 2015;85:370-8. doi: 10.1016/j.spmi.2015.06.008.
- 38. Mittal M, Sharma M, Pandey OP. UV–visible light induced photocatalytic studies of Cu doped ZnO nanoparticles prepared by co-precipitation method. Sol Energy. 2014;110:386-97. doi: 10.1016/j.solener.2014.09.026.